Kinetic models for protein adsorption on porous cylindrical particles.

Onugha, Leonard C

KINETIC MODELS FOR PROTEIN ADSORPTION ON POROUS CYLINDRICAL PARTICLES

By

Leonard C. Onugha

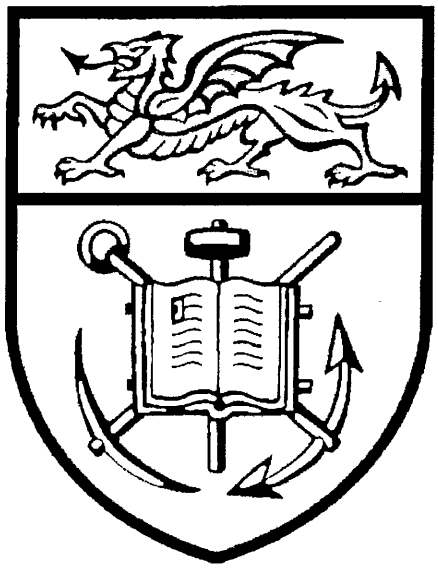

A Thesis Submitted to the University of Wales for the Degree of Doctor of Philosophy

Department of Chemical Engineering
University of Wales Swansea
Singleton Park
Swansea SA2 8PP, United Kingdom

September 2002

DECLARATION

This work has not previously been accepted in substance for any degree and is not being concurrently submitted in candidature for any degree.

Signed ..... (candidate)

Date 23-09-02

STATEMENT 1

This thesis is the result of my own investigations, except where otherwise stated.

Other sources are acknowledged by footnotes giving explicit references. A bibliography is appended.

Signed ..... (candidate)

Date 23-09-02

STATEMENT 2

I hereby give consent for my thesis, if accepted, to be available for photocopying and for inter-library loan, and for the title and summary to be made available to outside organisations.

Signed ..... (candidate)

Date 23-09-02

ACKNOWLEDGMENT

I would like to express my profound gratitude to my supervisor, Dr John R. Conder for his guidance, valuable time and suggestions covering the scope of this study. My sincere gratitude also goes to Dr Margaret Watson, Dr H. N. S. Yousef, and Mrs Diana Philips for their help with debugging the computer program. I would like to thank Whatman UK for the gift of the adsorbent used in this study.

I would like to thank my parents and siblings for their financial and moral support. My thanks are also for my friends for their encouragement and kind gestures.

Finally, I would like to thank Joanna and René for all that matter most.

Dedicated to the glory of God and the effect of a vision (Je:12 ^{23b})

SUMMARY

Most chromatographic purification techniques for macromolecules (biopolymers) operate on the principles of adsorption. The rate of the adsorption process depends on mass transfer kinetics. Previous models of the adsorption kinetics have assumed that the adsorbent/packing particles used are spherical.

Adsorbents which are fibrous or consist of rod-like particles offer potential advantages over the spherical particles. Whatman UK Ltd. market a semi-rigid cellulosic range of chromatographic adsorbents for macromolecule separation (Express-Ion) which are of this type, i.e. may be likened in shape to cylinders. The major aim of this study is to develop detailed kinetic models for the pore diffusion and mass transfer processes governing the adsorption kinetics of proteins that will predict the concentration-time profiles for the adsorption in both stirred tank and packed column modes of operation using semi-rigid cylindrical adsorbents.

The models have been developed to allow for particle size distribution within adsorbent samples, and for the delay and mixing that occurs in the flow line of the equipment.

The stirred cell model constructed has been validated by fitting theoretical data to experimental curves obtained for the adsorption of bovine serum albumin on the anion exchanger Express-Ion D. This system was characterised by determining adsorption isotherms and the physical parameters of the adsorbent. The effects of varying the protein concentration, effective pore diffusivity, liquid film mass transfer coefficient, particle dispersity, number of particle size groups, stirrer speed, and the equilibrium isotherm parameters on the adsorption profiles has been studied. A packed bed variant model has also been constructed and used to predict the effect of process parameters on the breakthrough curve in a packed bed (chromatographic) mode, and to study the effects of particle geometry on the adsorption process.

LIST OF TABLES

LIST OF FIGURES

Chapter 2

Chapter 3

Chapter 6

Appendix A

Appendix B

NOMENCLATURE

A	Cross sectional area of packed bed column	(m^2)
A	Total external surface area	(m^2)
A_{ap}	Total external surface area of all particles	(m^2)
A_P	Total external area of particles	(m^2)
a	Specific external surface area	(m^2/cm^3)
a	Hard sphere radius	(nm)
C	Concentration of protein in liquid phase	(g/l)
C^*	Equilibrium concentration in the liquid phase	(g/l)
C_f	Final protein concentration	(g/l)
C_i	Point concentration of protein in the liquid inside the pores	(g/l)
C_L	Bulk liquid protein concentration	(g/l)
C_o	Initial protein concentration (stirred cell) Feed concentration (packed bed)	(g/l)
C_S	Protein concentration on the particle external surface at pore entrance	(g/l)
D	Hindered diffusion coefficient	(m^2/s)
D_{AB}	Diffusion coefficient in free solution	(m^2/s)
D_e	Effective diffusivity	(m^2/s)
D_p	Effective pore diffusivity	(m^2/s)
D_h	Effective homogenous diffusion coefficient	(m^2/s)
d	Particle diameter	(m)
d_L	Linear (length) diameter	(m)

d_S	Surface diameter	(m)
d_{NL}	Number – Linear mean diameter (Number – length mean diameter)	(m)
d_{NS}	Number – surface mean diameter	(m)
d_{LS}	Linear-surface mean diameter (Length – surface mean diameter)	(m)
f_i	Number distribution	
f_L	Linear (Length) distribution function	
f_s	Surface distribution function	
g	Reciprocal time constant	(s^{-1})
g	Gravitational constant (9.81 m s^{-2})	(m/s^2)
G	$= \frac{(1-\varepsilon)}{\varepsilon_k}\frac{S_k}{S} q_m K_d$	
H	Time step (computer program)	
I	Counter for position within pore (computer program)	
k_1	Forward reaction rate constant for surface reaction	(l/g.s)
k_2	Reverse reaction rate constant for surface reaction	(s^{-1})
K_d,	Distribution coefficientt	(g/l)
K_D	Dissociation constant	(g/l)
k_f	Liquid film mass transfer coefficient	(m/s)
K_j	Constant	($= R_{j,s}/R_{j,l}$)
L	Counter denoting particle centre (computer program)	
LL	Counter denoting particle surface (computer program)	
M	Molar volume	(cm^3/mol)

N	Counter denoting bulk liquid (computer program)	
NN	Counter denoting mobile phase (computer program)	
N_A	Avogadro's number (6.022×10^{23})	(atoms/g-at wt)
N_A	Flux of protein inside the pores	(g/m^2s)
N_j	Total number of particle size bands	
N_{sh}	Modified sherwood number	
n	Total number of mesh points (stirred cell)	
n_j	Number of nodes in size group j	
q	Concentration of protein on adsorbent	(g/g_{solid})
q_i	Point concentration of protein on the solid surface inside the pore	(g/g_{solid})
q_m	Maximum binding capacity of protein on the adsorbent (Langmuir isotherm constant)	(g/g_{solid})
r	Radial distance from the centre of the particle	(m)
R	Average particle radius	(m)
Re	Reynold's number ($Re = \rho ud/\mu$)	
R_m	Rate of mass depletion	(g/ls)
$R_{j,s}$	Surface mean radius	(m)
R_{LS}	Linear (length) – surface radius	(m)
S	Surface area (BET measurements)	(m^2/g)
Sc	Schmidt number ($Sc = \mu/\rho D_{AB}$)	
Sh	Sherwood number ($Sh = k_L R/D\varepsilon$)	
T	Temperature	(°K)
t	Elapsed time	(s)

t_o	Delay time in sampling line	(s)
t_R	Residence time in mixing chamber	(s)
U	Interstitial velocity	(m/s)
u	Superficial velocity	(m/s)
V	Volume	(l)
V_{ap}	Total volume of all particles	(cm^3)
V_L	Volume of liquid (stirred cell)	(cm^3)
V_o	Volume at standard temperature and pressure (22 400)	(cm^3/mol)
V_p	Volume of pores per unit mass of particles	(cm^3/g)
V_s	Solid volume of particles excluding the pore space (stirred cell)	(cm^3/g)
V_s	Volume of gas adsorbed at saturation pressure (BJH)	(m^3)
W	Dimensionless concentration of protein in liquid	
X_T	column length	(m)
Z	Dimensionless radial distance	
ε	Particle porosity	
ε_b	Bed voidage	
ϕ	Particle porosity	
λ	Ratio of solute radius to pore radius	
μ	Liquid viscosity	(cP)
ν	Specific volume	(g/cm^3)
ρ	Density	(kg/m^3)
ρ_s	True solid density	(kg/m^3)
ρ_p	Particle density	(kg/m^3)
τ	Dimensionless time	

ω	Dimensionless concentration

Suffix

i	counter for position within pore
j	counter for particle size band
M	number of particle size bands
n	denotes the particle surface
x	number of sections in the packed bed

CHAPTER 1

INTRODUCTION & LITERATURE REVIEW

1.1 INTRODUCTION

The need for purified proteins and other macromolecules both for food and medicines has continued to grow significantly over the last few decades. The core part of the protein extraction and purification process is the downstream section where the extracted mixture of proteins, in large liquid volumes, is separated and the individual proteins are purified. The operations sequence through which a bioreactor broth must pass for a highly purified protein product is typically as follows:

1. *Removal of particulates (insolubles).* By filtration, centrifugation, and/or settling/sedimentation/decanting.
2. *Primary isolation.* Through solvent extraction, sorption, precipitation and ultrafiltration.
3. *Purification.* Approaches include fractional precipitation, many kinds of chromatography and adsorption.
4. *Final product isolation.* The processes here include centrifugation and subsequent drying of crystallised product, drum or spray drying, freeze drying (lyophilisation), or organic solvent removal.

The protein undergoes differing levels of purification depending on the intended final factory product and subsequent consumer use.

The product yields from downstream processing of large molecules is ordinarily very small, so the process of boosting yields lead to the large costs involved in the downstream process compared to the other stages of production, such as fermentation. The purification process, which follows protein (biomolecular) separation/isolation as part of the downstream process, accounts for between 40 and 90% of the total operating cost when compared with the fermentation, particulate-removal and the final product isolation

stages. The final product is required in an adequate yield, with high purity, maximum productivity, minimum loss of expensive adsorbents, and the shortest operating time since throughputs depend on the rates of adsorption and desorption of the protein on the surface of the adsorbent. Careful thought is required therefore for the overall planning of the processing scheme including rigorous optimisation steps for the process to be economically viable. Weatherley [1] has studied, in detail, the necessary objectives that have to be achieved for a project of this nature to be viable. Proteins can be denatured and/or destroyed with ease, so there is also a need for separation techniques, with mild processing conditions that minimise the damage or destruction of the proteins structure and function and still give maximum yield such as chromatographic separations (selective adsorption).

Chromatographic separation or selective adsorption techniques can selectively isolate proteins from broths and are also good methods of purification, liquid chromatography being particularly effective in the final stages of downstream processing where large molecules such as proteins are concerned. Selective adsorption techniques specifically recover between 75 and 95% of a desired product from a batch, in a minimum number of process steps.

A large surface area is required for the mass transfer processes involved in selective adsorption. This requirement is met either by using very small particles of a few micrometers in diameter or particles with a porous structure with large internal surface area. The kinetics of protein adsorption are slow since large molecules have low diffusivities. It is necessary to understand the mass transfer kinetics that govern the adsorption process in order to determine the kinetic coefficients needed to predict the performance of the chromatographic separation process. Therefore, to obtain accurate process predictions and design optimisation, a mathematical model able to simulate the adsorption/mass transfer kinetics of the system and predict its performance has to be constructed.

1.2 BACKGROUND TO THIS STUDY

The origin of the chromatographic technique has been widely discussed [2, 3]. Several chromatographic techniques have been deployed in the purification of proteins and in many cases more than one method has been used in the downstream process. The fact that most macromolecules are extracted from a liquid broth makes liquid chromatography the method of choice for selective adsorption of proteins. The chromatographic/ selective adsorption techniques used for protein separation and their application are shown in Table 1-1 summarised by Katz *et. al.* [4] Detailed discussion on the factors that determine the use of specific chromatographic techniques for different separation processes can be found elsewhere [(5 – 12)].

Method	Interaction	Application
Affinity (AF)	Biospecific (very strong)	Proteins and Enzymes
Hydrophobic interaction (HIC)	Dispersive interactions Salt gradients	Proteins Polysaccharides
Ion Exchange (IEX)	Electrostatic interactions Buffers	Proteins and peptides Nucleic acids Polysaccharides
Reversed Phase (RPC)	Dispersive interactions Aqueous/organic	Proteins, peptides Amino acids Nucleic acids, Enzymes
Size Exclusion (SEC)	Separation by molecular size. No molecular interactions	Peptides and Proteins Polysaccharides

TABLE 1-1: Chromatographic methods used for protein separation [4]

Adsorbents employed in the chromatographic purification of proteins are numerous, and in many cases more than one has been used in downstream processing. The available types of adsorbent are classified either by their adsorption chemistry or their solid phase matrix. A classification based on chemistry is summarised in the Table 1-1. The distinguishing characteristics of protein molecules on adsorbent surfaces, which differentiate one adsorption type from another, have been thoroughly reviewed [4, 13 and

14] and the principal factors that determine the proteins' behaviour at solid surfaces can are summarised under three headings;

- **Protein characteristics:** Isoelectric points, net charge and charge distribution, size, structure and stability in solution, placement and nature of hydrophobic patches.
- **Solution characteristics:** pH, temperature, ionic strength, solute types and concentrations, hydrodynamics.
- **Solid/surface characteristics:** Composition, chemical and energetic heterogeneity, topography, electrochemical potential, hydrophilic/hydrophobic balance, and temperature. The surface characteristics describe the properties of the adsorption sites on the particles, regardless of whether the sites are located on the surface of the pores within the particles or on the external surfaces of the particles.

Materials used for selective adsorption of proteins must be preferably hydrophilic since proteins are more stable in aqueous environments [15]. The particles will be highly porous for adsorption capacity and diffusion kinetics requirements to be satisfied because proteins are large molecules. This makes the sizes as well as the number of pores of great importance. The particles should be preferably rigid and incompressible to perform favourably under high operating pressure and flowrate, giving correspondingly rapid separations. The particles should be made from chemically inert materials so that they are insoluble and will not react except in the specific way for which they have been chosen.

For separations involving high pressure drops with varying salt concentration and pH during the operations, rigid adsorbents such as macroporous silica and polyacrylamides are preferred over soft adsorbents such as dextran and agarose because they do not swell or contract as operating conditions change and tolerate higher pressure drops when packed into a column. The rigid adsorbents also allow higher process throughputs, longer column life with more easily characterised structure, shape, particle size and pore size.

Some naturally occurring and synthetic materials with fibrous structures (felts, cloths, yarns and assemblies of rod-shaped particles) have been employed as adsorbents and ion-exchangers in modern liquid chromatography in place of the more traditional spherical or equi-axed packing particles. Semi-rigid fibrous ion exchangers have found application in water conditioning (demineralisation, softening) and waste water treatment for pollutant control. These fibrous ion exchangers have also been used in new applications where the processes involved favour the physical structure of the materials [16]. The Whatman Company markets a cellulosic range of chromatographic adsorbents for protein separation. The Whatman adsorbents consist of rod-like microgranules of non-uniform diameters in the range 15 – 30 μm and length of 100 – 200 μm, such as the Express-Ion D anion exchange material used in this work.

Fibrous packings have been shown to have some important advantages over bead-like or equi-axed particles. They are more stable mechanically down to small particle diameters and high liquid velocities which are less limited by the onset of fluidisation. For increased throughputs, fibrous packings have a clear advantage over 'spherical' (bead-like and equi-axed) particles since the rate of adsorption, which controls the throughputs, may be very sensitive to liquid velocity and, especially, particle diameter and surface area [16, 17 and 18]. Petruzzelli et al [16] believe that fibrous polymers of diameter 20 – 50 μm such as Express Ion D are mechanically equivalent to 100 – 500 μm bead-like particles. These workers suggested that the fibrous polymers studied gave much improved kinetics over the bead-like particles.

Wikström and Larsson [19] developed a novel support using non-porous quartz fibre with a mean diameter of 0.5 μm, and successfully used the support for large-scale affinity purification of an enzyme. They demonstrated that large volumes of dilute solution from crude extracts could be processed rapidly using these fibrous particles. This also showed that it is possible to use fibrous particles of much smaller sizes than those currently used in analytical chromatography (3 μm) for large-scale affinity purification. The small fibre diameter allowed non-porous particles to have good surface area and capacity combined with high mass transfer rates since pore diffusion is then not a limiting factor.

Beaver [20] used a bundle of hexagonally close-packed fibres aligned parallel to each other and to the axis of the column thus achieving a small reduction in the analysis time, a reduction in the voidage to 0.09 (Appendix A1) and an increase in column capacity. The flow channels created are equivalent to a bundle of longitudinal capillaries which gives much less form drag than with spherical or equi-axed particles or with fibres aligned across the flow. This in turn leads to lower column pressure drops and greater bed stability. However, the effect of axial dispersion could be substantially high as to reduce the efficiency of such a system if the bundles are not perfectly aligned.

Rao *et al.* [21] have discussed the effective diffusivity in structures developed with bundles of collagen fibres that occur as part of a complex structural organisation in leather and animal skins. The structure of adsorbents is an important parameter in the theoretical modelling of the kinetics of protein adsorption since the rates of mass transfer, pore diffusion, and film mass transfer are closely related to the structure of the particles. Generally, smaller particles with wide pores will result in faster adsorption because of their large surface areas and less resistance to the protein diffusion.

Over the past fifteen years, several kinetic models that predict concentration-time profiles for the adsorption of protein under either stirred cell, packed bed or both conditions of operation have been developed. The models usually operate on the principles of solving a set of coupled ordinary differential equations and produce theoretical concentration-time profiles that can be fitted to experimental data. The fitting is usually done by adjusting one of the parameters in the model, either the liquid film mass transfer coefficient or the effective diffusivity. Some authors have studied the effect of several pore sizes and/or particle sizes of the adsorbent. There have also been more recent detailed kinetic models developed at Swansea which took into consideration a pore volume distribution [3], and a polydisperse system of particles [17]. However, only spherical adsorbent particles have been used in these studies and the models developed.

Kinetic studies of macromolecule adsorption usually fall into one of the following categories:

1. Simple rate equation models [7, 22, 23 and 24]
2. Pulse technique models [25, 26 and 27]
3. Differential bed models [3, 28, 29 and 30]
4. Comprehensive rate equation models [3, 5, 17, 18, 31, 32, 33, and 34]

Mathematical models developed through these methods differ from each other in the principal simplification used. Hayek [18] has described and compared of all the methods, including their merits and demerits. A summary of methods is listed in Table 1-2, which is an updated form of Hayek's original work.

The present work employs the comprehensive rate equations method. Comprehensive rate equation models combine diffusion equations for the transfer of solute through the intraparticle pore space with rate equations for mass transfer through the external liquid film. The length of the adsorption column is not restricted and the models, additionally, allow for multistage kinetics [17, 28]. Two particularly important simplifications are, first, the number of kinetic stages considered to control the overall adsorption process and, second, the extent to which the equilibrium isotherm is simplified. While analytical solutions may be obtained for some isothermal, single component systems with linear isotherms and single resistances (one step ''lumped parameter mass transfer'') as in Chase et al. [32], the more complex systems involving non-linear isotherms and multi-stage kinetics usually require numerical (computational) solutions [17, 32].

TABLE 1-2: Summary of the methods for studying adsorption kinetics (*STR: stirred tank study; P.B.: Packed bed study)

Method	Study by	Kinetic stages	Operation*	Determination of kinetics constant	Dependence on equilibrium isotherm?	Notes on the model, and the dorminant kinetic stage.
1. Simple rate equations	Sajonz *et al.* (7)	Single lumped	P. B.	By fitting the model to experimental curve. ''Numerical solution''.	Yes	Mass transfer was dominant.
	Kaczmarski *et al.* (22)					
	Graham & Fook (23)	Film and Pore	STR	By slope of degree of conversion curves. ''Direct solution''	Yes	Changed from Liquid film to particle diffusion control according to the shape of the equilibrium curve.
	Tsou & Graham (24)	Film and pore rate of particle shrinkage	STR	By slope of degree of conversion curves. ''Direct soultion''	Yes	
2. Pulse techniques	Arnold, Blanch & Wilkie (25)	Several stages of peak spreading ''film, particle and axial dispersion	P.B.	Liquid film: from correlation, particle diffusion and axial dispersion from slope and intercept of HETP plot. ''Direct solution''.	Yes, unless conditions were chosen carefully to eliminate the effect	Particle diffusion was dominant
	Schneider & Smith (26)	Film, pore reaction, and dispersion	P.B.	Reaction: from plot of first moment. Liquid film: from correlation. Others: from plot of second moment ''Direct solution''	Yes, linear isotherm is required	(Applied on gases) Particle diffusion , Liquid film may be significant according to the flow rate.
	Venkatesh *et al.* (27)	Film (with steric mass action)	P. B.	By fitting the model to experimental curve. ''Numerical solution''.	Yes (linear isotherm required).	Model fitted curves rather well: solution scheme is a good method development tool.
3. Differential bed methods	Ashmead (3)	Film and pore	P.B.	Estimated from the slope and intercept of the regression line of the plot of the overall coefficients. ''Direct solution''.	Yes	Particle diffusion was dominant.
	Leaver & Conder (28)	Single step ''lumped	P. B.	By fitting the model to experimental curve. ''Analytical solution''.	No	Single step model fitted the results poorly, pore diffusion model was better. However, it was suggested that a model of liquid film and pore diffusion may give better description of kinetics.
		Pore diffusion	P. B.	By fitting the model to experimental curve. ''Numerical solution.''	No	

3. Differential bed methods	Hayek (29)	Liquid film and Particle	P.B.	By splitting the limiting overall coefficient to film and particle components using a plot of the overall coefficients and the slope at equilibrium curve ''Direct solution''.	Yes, but using small steps of concentrations eliminates the effect.	Particle diffusion was dominant.
	Fernandez *et al.* (30)	Film and pore	P.B.	Fitting the model to experimental curve. ''Numerical solution''.	No	Particle diffusion was dominant
4. Comprehensive rate equations methods	Chang & Lenhoff (5)	Film and Pore	STR	By fitting the model to experimental curve. ''Direct solution''.	No	Particle diffusion was dominant
	Horstmann & Chase (31)	Film, pore and surface reactions	STR and P.B.	Liquid film: from correlation. Others: by fitting the model to experimental curves. ''Expensive Numerical'' solution.	No	Model of Liquid film and particle diffusion was most appropriate. The particle diffusion stage was dominant. Reaction step was very fast.
		Film and pore		Liquid film: from correlations. Particle diffusion by fitting to experimental ''Moderate numerical work''.		
	Skidmore, Horstmann & Chase (32)	Single ''lumped		By fitting to experimental curve ''Analytical solution''	No	Liquid film and particle diffusion model was more appropriate to fit the results. Particle diffusion stage was more dominant.
		Film and pore		Film: from correlation Particle: by fitting to experimental curves ''Moderate numerical work''		
	Conder & Hayek (33, 34)	Two step (Film and Pore)	STR and P.B.	Film: from correlation Particle: by fitting to experimental curves. ''Moderate numerical work''.	No	Particle diffusion was dominant

1.3 LITERATURE REVIEW

1.3.1 Introduction

In this Section a brief review of work carried out previously in this area of research is presented. Only the models employed in studying the kinetics of protein adsorption developed using the comprehensive rate equations methods are discussed. This Section also looks at the shape of the equilibrium isotherm, the adsorbent porosity, and the film mass transfer coefficient, important parameters used in the models that have been tested.

1.3.2 Comprehensive Rate Equation Models

Comprehensive rate equation models are based on writing diffusion equations for the transfer of solute through the intra-particle pore space and rate equations for mass transfer through the external liquid film. They can allow for one stage or multistage kinetics, and the number of kinetic steps assumed in their development constitutes the main difference between them. In single component mass transfer systems such as the adsorption of a protein from the bulk liquid to the porous particles, the adsorption process may be modelled as taking place in one or all of the following steps:

1. Mass transfer of protein across the extra-particle boundary layer or liquid film to the external surface of the adsorbent particles.

2. Diffusion (transport) of protein molecules through the pores inside the particles, that is the intra-particle diffusion process.

3. Reaction of protein with the adsorbing sites at the solid phase surface (protein-adsorbent interactions).

4. Lastly, diffusion in the sorbed phase along the solid surface (surface diffusion).

In the one step models (the homogeneous diffusion or lumped parameter approach) a single mass transfer resistance to the adsorption process is assumed. This approach employs models that use mass transfer coefficients rather than diffusion coefficients in modelling the diffusion. The mass transfer coefficients assume a rate coefficient that is a function of the mobile phase concentration [7]. The theory of the lumped parameter method is that the large concentration differential across the liquid film boundary layer around the particles is the sole driving force for the adsorption process, and that the solutions far from the boundaries are well mixed. These models, which usually have analytical solutions, are useful for diffusion across phase boundaries [28, 32] and (as a linear driving force model) only have a physical meaning when strong adsorption occurs, and surface diffusion controls intra-particle transport [35]. Due to this assumption, the mass transfer coefficient is found to be a function of the mobile phase concentration [7], thereby complicating its determination because the data directly accessible from a given breakthrough curve are averages of the rate coefficients during the experiment. Other workers have reported poor theoretical results that did not fit the experiments as well as taking a two-step model [28, 32].

A two-step model assumes that the process of protein adsorption occurs in two major steps involving external mass transfer in the one step and intra-particle diffusion in the other. They usually presuppose that the reaction of protein with the adsorbing sites at the solid phase surface (protein-adsorbent interactions) and the sorbed phase diffusion along the solid surface (surface diffusion) proceed at a fast enough rate to constitute no significant resistance to the overall process of adsorption. Various workers [3, 9, 17, 18, 31, 36, and 37] have carried out both theoretical and experimental analysis of the protein adsorption process using two-step models. The resulting mathematical models require numerical solutions [5, 9, 12, 18, 31 and 38].

Two variants of the two-step model can be constructed. The first kind of two step models is developed such that diffusion is assumed to take place in the liquid-filled pores, accompanied by adsorption on the bounding pore walls (a 'pore diffusion model'). It is described by a diffusion equation involving two separate concentration parameters, one

for the concentration of protein in the pores and another for the adsorbed protein concentration [5]. Weaver and Carta amongst others found a pore diffusion two-step model adequate, for the comparison of macroporous and gel-composite media, in protein adsorption studies on cation exchangers [12].

Chang and Lenhoff [5] also developed a second type of two step model, the homogenous diffusion model, in which they assumed that all protein within the particle (free or adsorbed) is lumped into the single quantity q (the total protein concentration), a function of the radial position and time. The adsorbent particle was treated as a homogeneous medium instead of being differentiated into liquid-filled pores and intervening solid. They assumed that the diffusion within the particle was governed by the gradient in the total protein concentration q. The effective homogenous diffusion coefficient D_h (homogenous diffusion model) was typically smaller than the effective pore diffusivity D_p or D_e (pore diffusion model), and they attributed this to the concentrating effect of adsorption. The homogenous diffusion model led to protein concentrations in the pores that were lower than the concentration of protein adsorbed. The concentration gradient for the protein adsorbed was also higher than the concentration gradient for the protein in the pores.

Both models (homogenous diffusion and pore diffusion) described the protein uptake data equally well, leading the workers [5] to conclude that two-step models should be capable of predicting protein adsorption processes well. Some questions remained unanswered with regards to the physical mechanisms of coupled diffusion and adsorption.

A third category of model can be developed by including the reaction of protein at the solid surface as a third step in the model of the adsorption process. This added resistance leads to models that require very tedious computational numerical solutions, and consume excessive amounts of computer time with very little improvement, if any, compared with the two-step result [17, 31]. Li [17] showed that the introduction of the third step did not improve the model but increased the computational time. She stated

that the three-step model did not improve the fitting, notably poorer in the initial part of the simulation curve than that of a monodisperse two-step model for the myoglobin-Bakerbond cation exchanger CBX system. This meant that the surface reaction resistance (k_1) should not be introduced for modelling the experimental system investigated. Li also pointed out that a larger value of the effective diffusivity was required to compensate for the introduction of k_1 in fitting the experimental data. She [17] also demonstrated that in the case of hydrophobic hi-propyl HIC systems, the three-step model again did not fit results well. When a polydisperse two-step model was used, the fit improved. Although the improvement was less for the stirred cell cationic CBX systems, it substantially improved the simulation results in the packed bed mode.

Other researchers [31] have demonstrated, using immunoglobulin G (MW ~ 150,000) on Sepharose particles, that the reaction step is fast enough for any resistance given by this step to be ignored. Accurate approximations based on the conclusion of an insignificant resistance to the adsorption process by the reaction step have been made within reason by various authors: Hayek [18] successfully studied the ion exchange and hydrophobic interaction adsorption profiles of BSA; Skidmore and Chase [32] modelled two-component protein adsorption on cation exchanger S Sepharose FF; McCoy and Liapis [9] theoretically validated the argument. The same theory has been successfully applied to the adsorption of BSA (MW ~ 67,000) on rigid porous particles (Bakerbond CBX and weak anion exchanger Bioprep WAX.) [3]. The conclusion here is therefore that the first two steps, the mass transfer of protein (across the liquid film) to the external surface of the adsorbent particles and the diffusion of protein molecules through the pores inside the particles, alone control the kinetics of the adsorption of protein (assuming no axial dispersion occurs).

1.3.3 Equilibrium Isotherm

The equilibrium isotherm is a plot that relates the protein concentration on the solid phase to the residual liquid concentration in the pores when a system of a protein solution in

contact with a solid adsorbent medium at constant temperature reaches equilibrium. When the surface reaction step is not rate-determining, there is direct local equilibrium between the liquid (mobile) phase and solid (stationary) phase, neglecting mass transfer resistances [17]. The reason an isotherm can exist is due to competitive adsorption of protein solute and the salt ions within the solution [39]. Leaver demonstrated that the quantity of protein adsorbed depends on the quantity of protein presented to the medium, the greater adsorption occurring with the system of the greater initial protein concentration. The protein adsorbs in preference to the salt ions if the relative protein concentration is increased, leading to a higher equilibrium solid phase concentration. Various isotherm forms or equations have been used to interpret the experimental results (adsorption isotherms) from protein adsorption processes. Broad discussion on the merits and demerits of the various isotherm types can be found elsewhere [39, 40].

The more commonly used isotherm equations include the Linear, Rectangular, Freundlich, BET and Langmuir. Earlier adsorption studies involved the use of a linear type equation. The linear isotherms did not give good fits to the whole adsorption process, and in most cases were only able to predict the behaviour of the breakthrough profile at the start of the process. A rectangular approximation to the adsorption isotherm has been derived and tested by other researchers. The rectangular isotherm could only predict adsorption profiles with very steep starts and also the results of those adsorption processes at equilibrium. This problem of a rectangular isotherm meant that the results in the curved section of the adsorption isotherm, which frequently is the range desired for adsorption experiments, could not be accurately determined. The predicted results from both linear and rectangular isotherms fitted experimental data poorly.

The Freundlich equation is most useful for dilute solutions over small concentration ranges, but previous workers [39] reported a less than satisfactory fit when the Freundlich form was applied to BSA adsorption on DEAE cellulose adsorbents. The isotherm equation of Brunauer, Emmett and Teller (BET), derived for multi-layer adsorption, describes a curve with a different shape than usual for protein adsorption. There is also the added difficulty of having to resolve three constants with this isotherm form.

A fifth isotherm form, the Langmuir equilibrium isotherm, based on single layer adsorption of solute molecules (originally gases) that are not free to move on the surface of the adsorbent has been used in the adsorption studies carried out by most of the previous workers in this area [31, 32, 38] and more recently [3, 5, 11, and 41]. The Langmuir isotherm form gives a much better interpretation of experimental results than the linear and rectangular forms. The Langmuir isotherm form gives good fits to experimental data for chromatographic columns with fast rates, such as those for analysing small samples of small molecules [42]. It gives a good general location of the concentration profiles of a chromatographic system.

Chang and Lenhoff [5] have demonstrated that this isotherm form works even better if a third parameter, akin to the Freundlich form, is introduced with the adsorption equilibrium constant. However, the Langmuir form gives better correlation coefficients [43] but should only be considered an empirical fit useful for design purposes due to the theoretical assumptions used in its development [39]. The maximum capacity of the adsorbents for a protein can be obtained from the equilibrium isotherm for the system (buffer, pH et.c.). The isotherm affects the kinetics of the process and therefore enters the kinetic equations.

Experimental results have shown that certain conditions affect the adsorption isotherm a great deal. Li [17] observed that the pI value of protein materials had a great effect on the adsorption isotherms obtained for the ion exchange adsorption of Myoglobin on CBX. The different fractions of Myoglobin used gave different adsorption isotherms, which resulted in different retardation (breakthrough) times in packed bed operation. She concluded that an adjustment of the pH would reduce the differences in adsorption capacity of some Myoglobin (Mb) fractions with certain pI values, and thus decrease the differences in the breakthrough times.

In the same study [17], it was pointed out that the buffer used for the experiments affected the rate of adsorption and thus the isotherm. It was concluded that different

adsorption media required different buffer solutions, with different salt concentrations and viscosity, for a Langmuir isotherm with relatively high adsorption capacity for the system to be obtained.

Hayek [18] stated that high salt concentration increases the hydrophobicity at the adsorbent surface and the protein, and may result in attraction between the protein molecules themselves leading to low diffusivity. Protein molecular aggregation that occurs in solution could also have an effect on the shape of the adsorption isotherm. The size of the hydration sphere surrounding the protein molecule may also be a contributory factor to the low diffusivity. Evidence of the aggregation of protein molecules was obtained by the measurement of molecular size variations in different buffers using a photon correlation spectrometer. The results obtained for the measurement of BSA for evidence of molecular aggregation [18] showed that the average molecular size of BSA in 2 M $(NH_4)_2SO_4$ buffer (pH = 7.0) was three times larger than that in 0.01 M NaH_2PO_4 buffer (pH = 5.7). The concentration of BSA in both solutions was 5 g/l, giving clear evidence of the molecular aggregation of BSA in high salt concentration solutions. In addition, it was found that the solution of BSA in 2 M $(NH_4)_2SO_4$ buffer became colloidal (cloudy) within twenty-four hours after preparation, while a solution in 0.01 M $(NH_4)_2SO_4$ buffer was still stable (remained clear) even after ten days. Li [17] acknowledges this as a valid argument.

1.3.4 Porosity

The porosity of the adsorbent studied in the present work is a crucial parameter in the model for the simulation of the adsorption process. Several methods have been used to measure the pore volume and pore size distribution. The porosity of the adsorbent particles has been determined from the results. The methods include, nitrogen adsorption, mercury porosimetry and size exclusion chromatography. Hagel [44] gives a description of the various analytical techniques for characterising pore structure in size exclusion chromatography matrices. Electron microscopy is used to characterise porous beads of silica and glass. Gas adsorption techniques, using the equation of Brunauer *et*

al., are limited by reliability questions such as the inability of a nitrogen molecule to enter the smaller pores and the possibility of capillary condensation in pores less than 50 –100 nm. Mercury porosimetry should not be employed alone due to uncertainty with the data but in complement to the gas adsorption technique especially for adsorbents with a large pore diameter. Hagel concluded that pore size characteristics from size exclusion techniques were in reasonable agreement with those determined by capillary condensation and mercury porosimetry on porous silica.

The nitrogen adsorption method of Barrett, Joyner and Halender [45], the theory of which is a combination of Brunauer, Emmett, and Teller (BET) multilayer adsorption and capillary condensation [46], is most frequently used. The method involves the relationship between nitrogen desorption isotherms at liquid temperatures and the distribution of pore volume and area. The distribution of pore volume and area were determined in each case with respect to pore radii whilst assuming an equilibrium between the gas and adsorbed phase during the desorption. This method requires that the adsorbents be dried at appropriate temperatures prior to measurements since the presence of moisture might affect the adsorption results. The Express Ion D adsorbents studied are preswollen and as such drying them might damage the structure rendering any results obtained in this way irrelevent or misleading without a second measurement on an undried sample using another method such as Mercury porosimetry.

Dullen [47] suggests a density method for porosity that depends on the determination of the bulk density of the adsorbent and the density of the solids in the sample, in this case cellulose. Since the mass of a porous medium resides entirely in the solids matrix, it follows that by the definition of porosity ϕ, the value of the bulk density ρ_B, divided by the solid density ρ_S, subtracted from unity gives the total porosity of the adsorbent (Equation 1.1).

$$\phi = \frac{\rho_B}{\rho_S} - 1 \qquad (1.1)$$

The value of porosity obtained by this method, 0.93, lies in the range given by Horstman and Chase [31] for porous cellulose adsorbents Sepharose and Superose. The calculated porosity value from the porosimetry and BET measurements was used in this study.

1.3.5 Film Mass Transfer Coefficient

The film mass transfer parameter k_f is also very important for the simulation of the adsorption process. The method and procedure used to estimate this parameter is discussed in detail in Chapter 2. It is often considered that k_f is not rate determining [3, 18] so that varying this parameter does not alter the shape of the adsorption profile. Li [17] showed that this is not always the case as some sensitivity of the rate of adsorption to k_f can be observed when the protein is of a low molecular weight (e.g Myoglobin) and the adsorbent particle is relatively small as well (e.g Bakerbond CBX). For adsorbents with wide pores, say 300 Å, it appears that the liquid film mass transfer coefficient k_f would at least be jointly rate determining with the pore effective diffusivity D_e if the hard sphere radius of the protein molecule is around 10 Å (small protein e.g Myoglobin, Mb,). If the hard sphere radius of the protein is around 30Å, such as for Bovine Serum Albumin (BSA), then the liquid film mass transfer coefficient is unlikely to be rate determining.

Li split the mass transfer parameter into two parameters k_f and k_{fc}, where k_{fc} is the calculated film mass transfer coefficient such that $k_f/k_{fc} = 1$, would represent the film mass transfer parameter for the system involved. She reported that the fit of simulated breakthrough curves to experimental data was further improved by adopting $k_f/k_{fc} = 2$ compared with the case of $k_f/k_{fc} = 1$.

Li concluded that since the semi-empirical correlations used to determine the film mass transfer coefficient originate from correlations for small molecules, they may not be fully applicable to the Mb-Bakerbond wide pore CBX and the wide pore Hi-propyl HIC systems that involve macro bio-molecules and relatively small adsorbent particles.

1.3.6 Effective Pore Diffusivity

The effective diffusivity in most protein adsorption studies is determined by fitting the model predictions for the concentration profile in stirred cell adsorption with experimental results. This is because with the film mass transfer coefficient determined as described in the last section, and the assumption that only film mass transfer and pore diffusion are the prevailing steps, the only unknown parameter in the concentration-time uptake in a stirred cell is the effective diffusivity.

A comparison of the values of effective pore diffusivity from various studies [18] revealed no consistent pattern in the data even after the effects of viscosity and molecular weights differences of the different protein solution systems have been normalised (by calculating the ratio of the pore to free solution diffusion coefficients). One thing is clear at this time. The diffusion coefficient is greatly affected by the system characteristics such as the partricle specifications and protein size.

Hence the correct value of the effective diffusivity can be determined by varying it in the model prediction until a good fit to the experimental data is obtained. The effective diffusivity in the packed bed simulation is adopted as the same value as determined from the modelling of the stirred cell adsorption. Previous studies [31, 35, 48, 49, etc.] have demonstrated that for a given adsorption system, the (pore) effective diffusivity D_e, which characterises the intraparticle diffusion, should be applicable to both the stirred cell and the packed bed operational modes since the mass transfer within the particles should be independent of the operation mode. The implication of this is that the effective diffusivity estimated from the data obtained from batch experiments in a stirred cell should be applicable to the packed bed models. Successfully fitting these packed bed models to experimental data using the diffusivity values from the stirred cell models would then validate the newly developed stirred cell model.

Batch experiments (stirred cell) are easier to perform, faster, and less expensive when compared to column experiments (packed beds). Also, the numerical solution of the batch model uses less computational time than that required for the solution of the

column models. Experiments using different particle sizes and different initial concentrations for a stirred cell system and different flow rates for a packed bed system can also be employed to provide additional validation of a new model.

1.4 PURPOSE AND SCOPE OF THE RESEARCH

The major aim of this study is to simulate the diffusional and mass transfer processes governing the adsorption kinetics of proteins and by so doing develop detailed kinetic models for predicting the adsorption of protein on rigid cylindrical adsorbents. The purification section of a downstream process consumes a major part of the entire production capital as earlier mentioned because of the cost of adsorbents and the small yield of saleable product, particularly where high levels of purity are required. Against this backdrop, a detailed kinetic model that would enable initial process design and prediction of the effect(s) of varying the operation conditions is very important.

Of the various models developed to predict the protein adsorption process the more successful ones have been the models developed using a size distribution (polydispersity). The polydispersity models are more accurate than their monodisperse (uniform adsorbent particle size) counterparts because chromatographic adsorbents usually display a wide range of particle sizes, thereby limiting the accuracy of the monodispersity models. Secondly, the polydispersity models are constructed with enough flexibility to accommodate monodisperse situations too. The simulated breakthrough profiles [17] obtained using a size distribution (polydisperse) model were a better representation of experimental data than the simulated profiles [9, 18, 31] obtained assuming a uniform adsorbent particle size (monodisperse). The present research goes back to previous work done with monodisperse, spherical particles of uniform pore size, particularly by Hayek [18] and Horstmann and Chase [31], in order first to develop monodisperse cylindrical kinetic models. These monodisperse cylindrical models are then further developed to a polydisperse form along the lines of the work done on spherical particles by Li [17].

The present work is then split into two parts. In the first part, the cylindrical stirred cell models have been used to simulate the adsorption process of the protein Bovine Serum Albumin (BSA) in a stirred cell and the curves obtained were then fitted to the experimental results obtained for Express Ion D (cylindrical adsorbents). In the second part of this work the packed bed model has been used to predict the adsorption process of the proteins Bovine Serum Albumin (BSA) and Myoglobin (Mb) in packed bed systems with the effective diffusivities obtained from previous stirred cell experiments [17, 18].

The effect of varying the number of assumed particle size groups on the theoretical adsorption profiles has been studied. The changes to the shape of the adsorption curves when the effective pore diffusivity and liquid film mass transfer coefficient were varied were also studied. The result of the latter test revealed that the diffusion coefficient was jointly rate controlling with the liquid film mass transfer coefficient. The concentration-time profiles obtained from these predictions were then compared with those obtained experimentally for spherical particles [17 and 18] to study the effects of particle geometry on the protein adsorption process. The models are intended to provide a basis for scale-up and process predictions for both analytical and large scale processes.

1.5 OUTLINE OF THIS THESIS

The thesis is divided into seven chapters. Following the introduction and literature review of the main subject of this work, the theoretical models and their numerical solutions for macromolecule adsorption on porous particles are developed in Chapter 2. The models derived and modified include stirred cell and packed bed models for cylindrical adsorbents assuming adsorbent particles are polydisperse. Chapter 3 describes the protein and adsorbent materials investigated. Also described are the experimental set-ups for conducting stirred cell operations and experimental methods for protein concentration monitoring and adsorption isotherms. In Chapter 4, the specification of the materials, such as the particle size and size distribution of the adsorbents, the particle porosity and density, the properties of buffers, and the

experimental results of the adsorption isotherm for Bovine Serum Albumin-Express Ion D (EID) system is presented. The experimental and simulation results for the BSA adsorption on EID particles in stirred cell and packed bed modes are presented in Chapter 5 and 6, respectively. Finally, the conclusions drawn and recommendations for future work are presented in Chapter 7.

CHAPTER 2

MODEL DEVELOPMENT

2.1 INTRODUCTION

In the last chapter, the general validity of mathematical models for studying the adsorption kinetics of macromolecules was explained. In this chapter, a model based on cylindrical particles will be built along similar lines. Some of the major assumptions governing the process will be stated and then the model will be developed. The construction of a computer implementable form of the model will also be discussed.

The chapter begins with a recap of the formation of a simple two-step, stirred-cell, cylindrical particles model [50] in which it is assumed that a monodisperse system of particles is involved. This treatment shows the basic construction of the model more clearly than when the complication of polydispersity is introduced subsequently. We then proceed to the development of stirred cell and packed bed models that allow for particle size distribution (polydispersity). The models discussed allows for the effect of delay and mixing in the apparatus.

2.2 BASIC ASSUMPTIONS OF A TWO STEP MODEL

In all the previous work reported in the literature [3, 17, 18] a model was developed for a spherical particle whose outer surface is almost entirely covered with pore openings through which a flux is passing. The previous spherical models are a good starting point for analyses of this kind because a cylindrical particle's cross-sectional outer surface resembles that of a spherical particle on a head-on planar perspective and because spherical models have been successfully validated. Using this basis for a cylindrical particle, a set of differential equations are introduced that take into account the two mass transfer resistances, first for the pore diffusion with boundary conditions at the particle centre and the particle surface, and secondly for the extra-particle transport process. The

following sections explain the rationale behind some other assumptions necessary for the development of any two-step model in general and that for cylindrical particles in particular.

2.2.1 Assumptions of Large Pore Surface Area and Infinite Length

The external surface of a porous adsorbent is assumed to be small in comparison with the very large total available internal surface of the pores. Consider the following table showing three available pore sizes of the Whatman Partisil BioPrep (40/300 WAX) adsorbents and their corresponding surface area and pore volumes (spherical silica-based particles).

Mean Pore Size, Å	Surface Area, m^2/g	Pore Volume, cm^3/g
75	485	0.76
150	300	1.1
300	275	1.8

TABLE 2-1: Pore Size of Partsil BioPrep Media

Whatman recommends that a mean pore size of 300 Å be used for macromolecules (MW 50,000 to 500,000) within our range of interest e.g. Bovine Serum Albumin estimated molecular weight (MW) 66,500 [18]. For the 300 Å media, Whatman states that the total available pore surface area is 275 m^2/g (confirmed by BET studies [18]) and that the pore volume is 1.8 cm^3/g. The total surface area of a sphere with a pore diameter of 300Å and particle diameter of 40 μm (such as the ones used by Hayek [18]) is only about 0.135 m^2/g. The assumption that the pore surface area is very much larger than the external surface area is therefore well justified for wide pore silica media commonly used for separating proteins, and so is likely to be true for other wide pore soft gel or rigid media used for the same purpose.

The particles that have motivated this present study are rod-shaped fibrous materials that can be likened in shape to cylinders. These cylindrical particles have an average pore

diameter of 9.5 μm (9.5×10^4 Å) and pore volume of 1.1 cm^3/g. Pictures obtained by optical microscopes of the cylindrical particles in question show their lengths to be usually many times (greater than six times) the measurement of their diameters (Figure 2-1). The actual observed diameters of the particles are non-uniform along the length of individual particles and the diameters (along a particle) are at some points barely a tenth of the length. Overall, they have a particle diameter range of 7 - 40 μm and their length is between 40 and 600 μm. Such particles can be adequately treated for modelling purposes as being of infinite length, i.e. protein adsorption through the ends is negligible. It will therefore be assumed that no end effects or longitudinal diffusion occur.

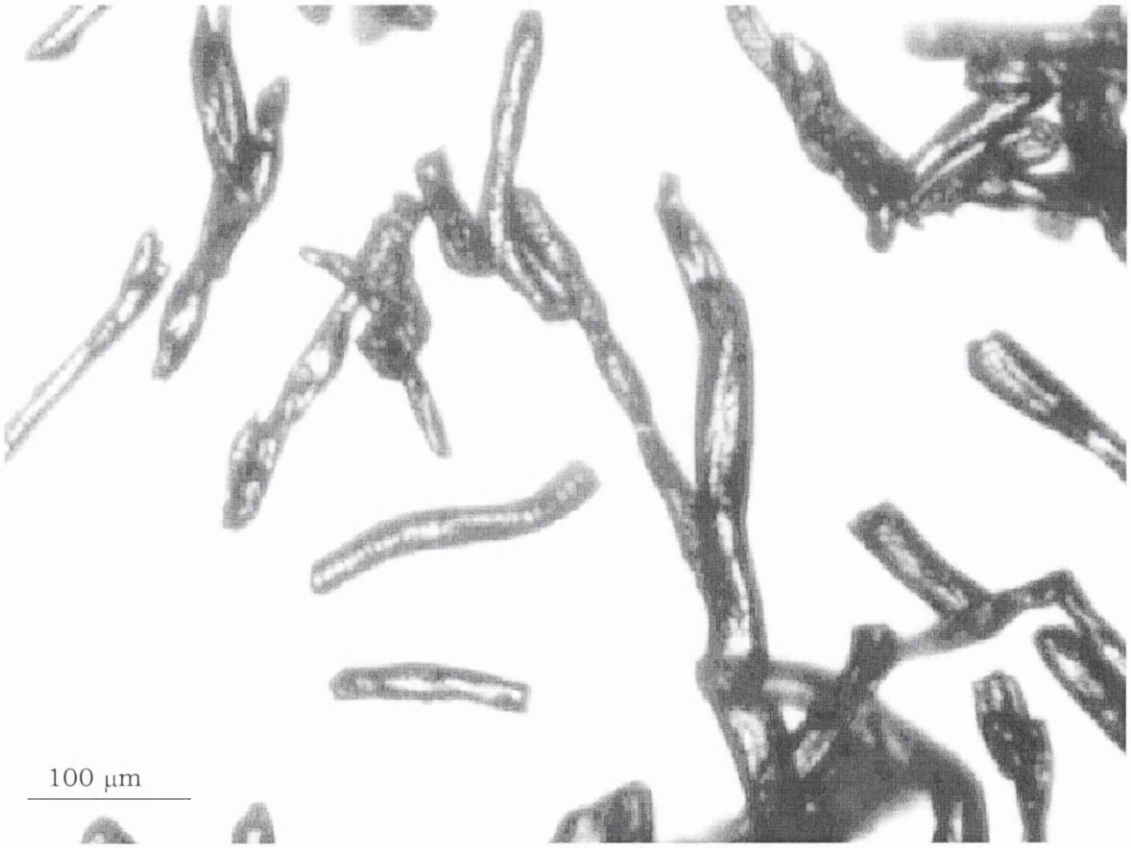

FIGURE 2-1: *Sample micrograph showing a cross section of Express-Ion D particles.*

2.2.2 Assumptions of Particle Size and Density

The particles are polydisperse in nature but will be assumed to be uniform in density, with the ligands evenly distributed throughout the interior surface of the adsorbent particles. The particle size in this case is the distance of intraparticle diffusion of the protein molecules within the adsorbent. This assumption is frequently discussed in the literature.

Although fairly monodisperse spherical particulate adsorbents are now available, most commercial adsorbents are polydisperse. For example, researchers [3, 17, and 18] using laser light scattering have reported a wide particle size distribution for the brand of spherical particles they studied. A model [18], which did not take this polydispersity into consideration, gave reasonably good fits to experimental data, which compare satisfactorily with the results of modified versions of this model [3, 17] that allowed for polydispersity. However, Li [17] has been able to show using a polydisperse model that the value of the fitted effective diffusivity does not always vary with the initial protein concentration as previously accepted. She fitted her modified models almost perfectly to experimental data but still had a residual lack of fit attributed to the assumptions in their development. The monodispersity model [18] consumes much less computational time and is also less complex. Optical micrographs of the cylindrical particles that have motivated the present study show that the particles are of varying sizes too. Despite the evidence above, the assumption of monodispersity will initially be adopted for developing the simpler monodisperse model and subsequently dropped as progress is made towards the more complex but accurate polydisperse models.

The assumption of an even distribution of ligands throughout the interior surface of the adsorbent particles comes from a few literature sources [51, 52]. The assumption is that the surfaces are evenly charged and that there is no reason why the protein molecules should prefer one point on the pore surface to the other. This assumption is not necessarily always true, depending on the adsorbent concerned.

2.2.3 Assumption of Uniform Pore Sizes and Porosity

The particles will be assumed to be of uniform pore size, pore volume and porosity. The pores in the adsorbents can be randomly oriented within the particles. This model uses the effective diffusivity as the curve fitting parameter to experimental data. For a uniform pore size model it is assumed that the pores, whether straight and cylindrical or tortuous and intersecting, are of the same diameter with the resulting structural effect on the diffusion rate hidden in the experimentally fitted effective diffusion coefficient. In constructing a non-uniform porosity model it is assumed that the diffusion of a solute through a porous solid occurs in pores of different sizes within it. The pores can then be assigned different values of tortuosity to account for the different pore sizes [3].

Comparisons of Bassam Hayek's uniform porosity model [18] and the non-uniform pore size model of Simon Ashmead [3] suggests that they both give good fits to experimental data when the effective diffusivity is used to fit the curves.

When the tortuosity component of the non-uniform porosity model [3] was used as curve fitting parameter however, the results were not as satisfactory as those obtained using the diffusivity without consideration for non-uniformity of pore sizes. The computational requirement of the non-uniform porosity model is also vast.

The results therefore do not suggest any great error if the uniform porosity model is used.

2.2.4 Outline of a Two-Step model

A two-step model presupposes that for a process of adsorption taking place in a stirred tank or packed bed, resistances to external film mass transfer and to pore diffusion are the controlling steps of the process. Any resistance to the surface reaction can be neglected. The process is assumed to proceed as follows: considering one adsorbent particle, as in Figure (2-2).

1. Protein molecules diffuse across the liquid film to the external surface of the adsorbent particles (a).

2. The molecules are then transported by diffusion into the particles through the liquid in the pores (intra-particle diffusion) until protein reaches a free adsorbent site (b).

3. The protein then reacts quickly with the adsorbing sites at the surface of the solid phase.

4. Surface diffusion (particle surface), in the sorbed phase, is assumed to be too slow to be significant in comparison with the parallel transport mechanism of diffusion through the liquid in the pore.

5. The reactions at the surface are reversible and of the second order, i.e.

$$\frac{\partial q}{\partial t} = k_1 C(q_m - q) - k_2 q \tag{2.1}$$

At equilibrium Equation 2.1 can be rearranged to give the Langmuir relation 2.2, which is the isotherm employed for modelling this adsorption process.

$$q = \frac{q_m C}{K_d + C} \tag{2.2}$$

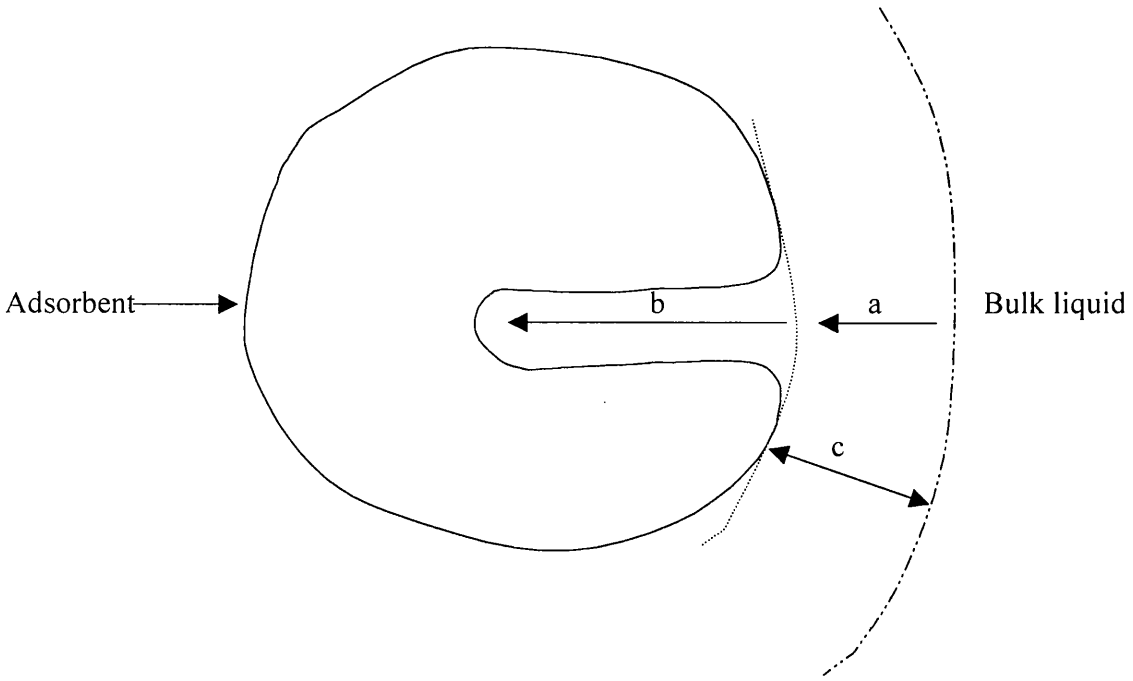

FIGURE 2-2: *Schematic diagram showing the two mass-transfer steps associated with one schematic pore (the arrows (a) and (b) indicate the direction of the adsorption process and (c) is the liquid film around the particle).*

2.3 CONSTRUCTION OF A MONODISPERSE STIRRED CELL MODEL

All the assumptions made so far for the general case of two-step models apply to a monodisperse model. However, as discussed in Section 2.2.2, the assumption of monodispersity will now be made for all the adsorbent particles for simplicity in developing a monodisperse model.

1. Equation of protein diffusion inside the pores

We take a cylindrical shell of a particle of thickness Δr, as shown in Figure 2-3(b). The shell is intersected by pores, through which a flux N_A of protein is passing, Figure 2-3(a).

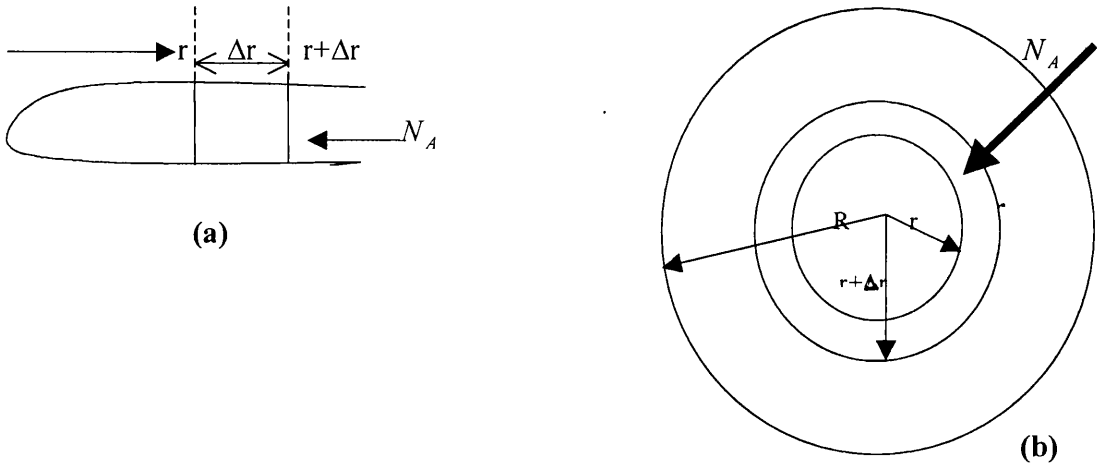

FIGURE 2-3: *Schematic diagrams showing (a) a pore within the cylindrical shell and the direction of flux, and (b) an adsorbent particle.*

Cylindrical pores with uniform cross section approximate the pores in the adsorbent particles. Taking a mass balance across the shell,

$$N_A\big|_{r+\Delta r}\,\varepsilon 2\pi(r+\Delta r)l - N_A\big|_{r}\,\varepsilon 2\pi rl - (1-\varepsilon)2\pi rl\Delta r\frac{\partial q}{\partial t} = \varepsilon 2\pi rl\Delta r\frac{\partial C}{\partial t} \qquad (2.3)$$

Dividing Equation 2.3 by $2\pi l$ gives:

$$N_A\big|_{r+\Delta r}\,\varepsilon(r+\Delta r) - N_A\big|_r\,\varepsilon r - (1-\varepsilon)r\Delta r\frac{\partial q}{\partial t} = \varepsilon r\Delta r\frac{\partial C}{\partial t}$$

Dividing this equation by $r\Delta r$ and taking limits as $\Delta r \to 0$ [see Figure 2-2)] gives,

$$\frac{\varepsilon}{r}\frac{\partial}{\partial r}(N_A r) = (1-\varepsilon)\frac{\partial q}{\partial t} + \varepsilon\frac{\partial C}{\partial t} \tag{2.4}$$

Introducing Fick's first law for the flux,

$$N_A = -D\frac{\partial C}{\partial r} \tag{2.5a}$$

in which D is the diffusion coefficient and the negative sign indicates that flux is in the same direction as increasing r. Since flux in the case of adsorption is in the opposite direction to increasing r, the negative sign cancels, giving

$$N_A = D\frac{\partial C}{\partial r} \tag{2.5b}$$

Substituting for N_A in Equation 2.4 by Equation 2.5b and expanding the left hand side gives the equation of diffusion inside the pores:

$$D\varepsilon\left(\frac{\partial^2 C}{\partial r^2} + \frac{1}{r}\frac{\partial C}{\partial r}\right) = (1-\varepsilon)\frac{\partial q}{\partial t} + \varepsilon\frac{\partial C}{\partial t} \tag{2.6}$$

2. *Rate of change of protein concentration in the bulk liquid*

In stirred cell mode, the equation for the rate of change of protein concentration in the bulk liquid can be determined by writing a mass balance over an increment of time Δt. Thus,

$$C_L V_L\big|_t - C_L V_L\big|_{t+\Delta t} = k_f(C_L - C_S)A_P\Delta t \tag{2.7}$$

Dividing by Δt and taking the limit as $\Delta t \to 0$

$$-V_L\frac{\partial C_L}{\partial t} = K_f(C_L - C_S)A_P \tag{2.8}$$

The area of all particles A_P is defined as:

A_P = Total surface area of all particles

= number of particles × area of one particle

$$= \frac{Volume\ of\ all\ particles}{Volume\ of\ one\ particle} \times \text{area of one particle} \quad \text{(neglecting end effects)}$$

$$= \frac{V_S}{\pi R^2 l} 2\pi Rl = 2\frac{V_S}{R} \tag{2.9}$$

Where V_S is the volume of all particles including the volume of pores, and R is the particle radius.

Substituting for A_P in Equation 2.8 by Equation 2.9 gives the equation for the rate of change of protein concentration in the bulk liquid,

$$\frac{\partial C_L}{\partial t} = -\frac{2V_S}{V_L R} k_f (C_L - C_S) \tag{2.10}$$

3. *Concentration-time profile C(t)*

To predict the concentration-time profile C(t), the system of two Equations 2.6 and 2.10 are solved numerically by a finite difference method to give Equation 2.11. The solution runs from the centre of the particle to the bulk liquid, at each step of time, calculating a new concentration at each node.

$$\frac{dC_i}{dt} = \frac{D(K_d + C_i)^2}{(K_d + C_i)^2 + G} \frac{1}{(\Delta r)^2} \left[\frac{2i-1}{2i-2} C_{i+1} - 2C_i + \frac{2i-3}{2i-2} C_{i-1} \right] \tag{2.11}$$

4. *Equations for particle centre and surface*

To derive the equations for the rate of diffusion at the centre of the particles $i = 1$ and at the surface of the particles $i = n$, boundary conditions are considered as follows:

A) At the centre of the particles,

$$\frac{\partial C}{\partial r} = 0 \qquad \text{at } r = 0,\ i = 1 \tag{2.12}$$

leading to Equation 2.13

$$\frac{dC_1}{dt} = \frac{4}{B}\left[\frac{C_2 - C_1}{(\Delta r)^2}\right] \tag{2.13}$$

B) At the surface of the particles,

$$\varepsilon D \frac{\partial C_i}{\partial r}\Big|_{r=R} = k_f (C_L - C_i)\Big|_{r=R} \qquad \text{at } r = R,\ i = n \tag{2.14}$$

The boundary condition, Equation 2.14 is used to relate the concentration in the bulk liquid to that at the external surface at the pore entrance.

5. *Dimensionless form of equations for stirred tank model*

We define: dimensionless concentration $W = C/C_O$

dimensionless time $\tau = t\,D/R^2$

dimensionless radius $Z = r/R$

where, C_O is the initial liquid concentration at time zero.

1. For $i = 1$ (particle centre), from Equation 2.13,

$$\frac{dW_1}{d\tau} = \frac{4F}{(\Delta Z)^2}(W_2 - W_1) \tag{2.15}$$

where $F = \dfrac{C_O^{\,2}(\dfrac{K_d}{C_O} + W_i)^2}{C_O^{\,2}(\dfrac{K_d}{C_O} + W_i)^2 + G}$ and $G = q_m K_d (1-\varepsilon)/\varepsilon$.

2. For $i = 2$ to $i = n-1$ (interior nodes), from Equation 2.6,

$$\frac{dW_i}{d\tau} = \frac{F}{(\Delta Z)^2}\left(\frac{2i-1}{2i-2}W_{i+1} - 2W_i + \frac{2i-3}{2i-2}W_{i-1}\right) \tag{2.16}$$

3. For $i = n$ (surface of particle),

$$\frac{dW_i}{d\tau} = \frac{2F}{(\Delta Z)^2}\left[\frac{2n-1}{2n-2}N_{Sh}\Delta Z W_{n+1} - \left(1 + \frac{2n-1}{2n-2}N_{Sh}\Delta Z\right)W_n + W_{n-1}\right] \tag{2.17}$$

where the modified Sherwood number $N_{Sh} = k_f R/D\varepsilon$

4. For $i = n+1$ (bulk liquid), from Equation 2.10,

$$\frac{dW_i}{d\tau} = -2N_{Sh}\varepsilon\frac{V_S}{V_L}(W_{n+1} - W_n) \tag{2.18}$$

2.4 CONSTRUCTION OF THE POLYDISPERSE STIRRED CELL MODEL

The cylindrical particles investigated in this study, Whatman Express-Ion D (nominal size 30 μm), have a wide particle size range both in terms of their diameters and their lengths. Since the assumption has already been made (Section 2.2.1) that the particles are all of infinite length compared to their diameter, the particle size distribution in this work is based on the particle diameters. A model is developed in this section to describe the adsorption process in polydisperse (non-uniform diameter) cylindrical particle systems. The present polydisperse model is constructed based on the same assumptions of a two step model: that the external film mass transfer and pore diffusion are the rate determining steps in the adsorption process, taking the resistance posed by the surface reaction to be insignificant (negligible).

Assuming that the particles are rigid cylinders with a size distribution, the particles can then be divided into a number of size groups based on their diameter. In reality the size groups are based on the varying particle diameters measured at different points along the length of each individual particle (as seen in micrographs obtained by an optical microscope, Figures 2-4) by data processing software MOCHA (A Jandel Scientific product).

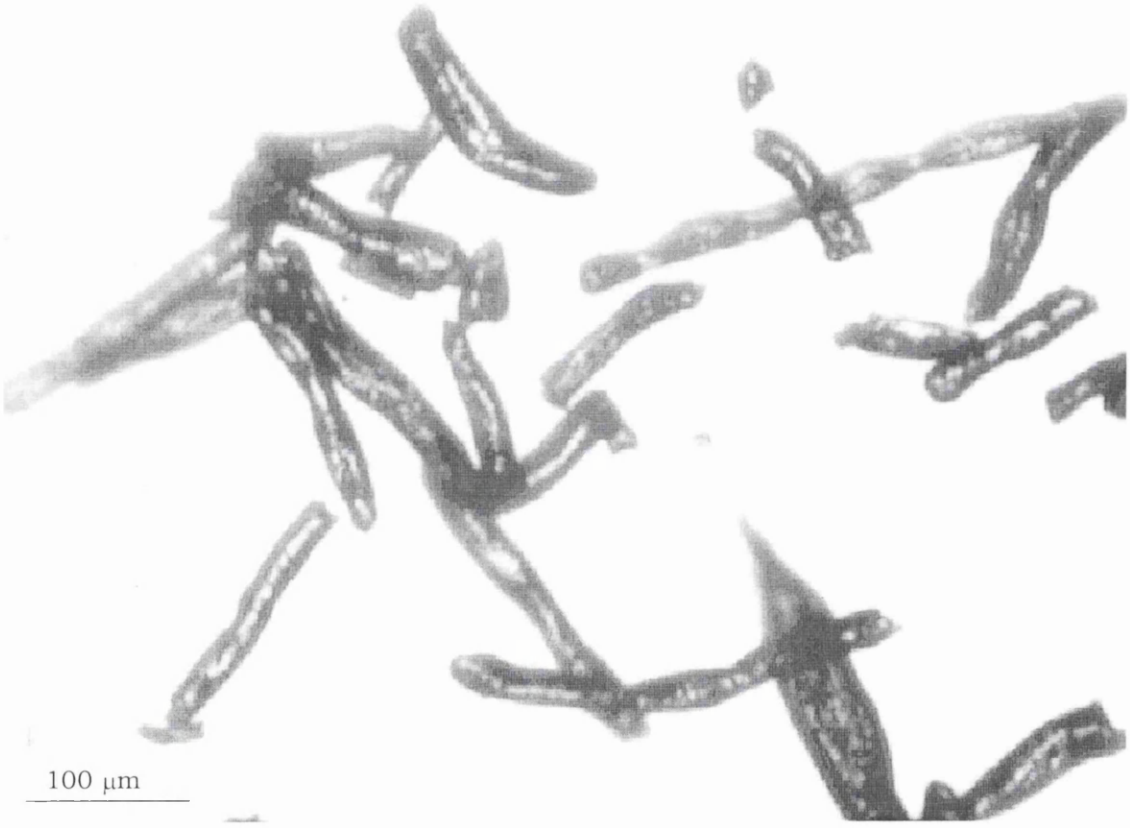

FIGURE 2-4: *Sample micrograph showing a cross section of Express-Ion D particles.*

The points were kept as close together as possible to ensure consistency in the measurement. The diameter is allowed to vary along a single particle as well as between particles. No distinction is drawn since the assumption of infinite length relative to

diameter effectively treats all particles as part of a single continuous filament of infinite length. The size of particles in each group can be represented by a suitable mean diameter. A single effective pore diffusivity value is assumed based on a uniform pore size for all particles in the sorption.

2.4.1 Particle Size and Distribution

1. Particle Size Distributions

The particle size distributions can be presented in various ways including surface, length and number distributions. Each type is represented by a corresponding distribution function. These three types of distribution are defined as follows:

Surface distribution: size distribution expressed as a proportion of the total surface area of all particles.

$$f_s = \frac{n(d)d^2}{\int n(d)d^2} = \frac{N_j d_j^2}{\sum_{j=1}^{M} N_j d_j^2}$$

Length distribution: size distribution expressed as a proportion of the total diameter of all particles.

$$f_L = \frac{n(d)d}{\int n(d)d} = \frac{N_j d_j}{\sum_{j=1}^{M} N_j d_j}$$

Number distribution: size distribution expressed as a proportion of the total number of all particles.

$$f_1 = \frac{n(d)}{\int n(d)} = \frac{N_j}{\sum_{j=1}^{M} N_j}$$

where M is the number of size groups, d_j is the average diameter of particles in size group j and N_j is the number of particles in size group j.

2. *Mean particle diameters for the size groups*

As discussed in Section 2.3, diameter is allowed to vary along a single particle as well as between particles. These diameters are then grouped. The size of particles in each group can be represented by a suitable mean diameter that represents the set of individual sizes in the group. The mean diameters represent the groups in an uncomplicated and succinct manner, and make it easier to understand the set. The diameters are average values, measures of the central tendency unaffected by the relatively few extreme values in the tails of the distribution.

By dividing the adsorbent particles into small intervals of size δx the particle sizes can be expressed mathematically (assuming that the particles all have the same shape and that x_1, x_2, ..., represent the diameters). If the number of particles in these group intervals are δN_1, δN_2,..., respectively, then the aggregate length, surface and volume of the particles in each group are $x\delta N$, $x^2\delta N$ and $x^3\delta N$. The total length, surface and volume for the adsorbent system are obtained by the summation of these expressions. The mathematical expressions for some of the mean diameters more commonly used in the characterisation of irregular shaped adsorbent particles are shown in Table 2-1 [53].

Since we are assuming infinite length for the particles, we have no need to determine the length of the cylindrical particles and hence cannot express the diameters in terms of a volume mean. This leaves us with the parameter called the length-mean diameter. To prevent ambiguity with the use of the term 'length' we will now rename the length-mean diameter as linear-mean diameter, and use this parameter to represent the cross-sectional diameter of the particles.

Mean diameters	Mathematical Expression
Number- Length	$d_{NL} = \frac{\sum \delta L}{\sum \delta N} = \frac{\sum d\delta N}{\sum \delta N} = \sum f_i d$
Number-surface	$d_{NS} = \sqrt{\frac{\sum \delta S}{\sum \delta N}} = \sqrt{\frac{\sum d^2 \delta N}{\sum \delta N}} = \sqrt{\sum f_i d^2}$
Number-volume	$d_{NV} = \sqrt[3]{\frac{\sum \delta V}{\sum \delta N}} = \sqrt[3]{\frac{\sum d^3 \delta N}{\sum \delta N}} = \sqrt[3]{\sum f_i d^3}$
Length-Surface	$d_{LS} = \frac{\sum \delta S}{\sum \delta L} = \frac{\sum d^2 \delta N}{\sum d\delta N} = \sum f_L d$

TABLE 2-2: *Definitions of the various mean diameters.*

These definitions may be applied either to a complete system of particles made up of groups of particles having diameters, or to one such group within which there is some spread of diameters.

2.5 DEVELOPMENT OF A STIRRED CELL MODEL FOR POLYDISPERSE SYSTEM

2.5.1 Equation for Protein Diffusion inside the Pores

For the purpose of developing a two-step polydisperse model for adsorption in a stirred cell, the basic assumptions are as described in Section 2.2. As in the monodisperse case, we consider a stirred cell operation where the porous particles are fully suspended in the protein solution by mechanical stirring. The concentration of the bulk liquid phase is uniform throughout the cell. However, the adsorbent particles are now divided into a number of size groups based on their size distribution. The size of the particles in each group is represented in terms of mean diameters.

For a particle size group j containing N_j particles, consider the lth particle, Figure 2-3(b), with radius R_l, ($l = 1, 2,\ldots,N_j$). If we take the cylindrical inner shell, thickness Δr, of this

*l*th particle at a point $r = r_i$. Let us assume that the point r_i is along a pore of the particle, Figure 2-3(a), (where i is the counter denoting position within the pore). The mass balance on the *l*th particle represents the contribution it has made to the overall adsorption for a particular size group j. Summation for all particles over all particle size groups provides the total amount of protein adsorbed in a given time period. Taking a mass balance on the shell of the of the *l*th particle, Equation 2.3 becomes

Rate mass in – Rate mass out – Rate mass adsorbed = Rate mass accummulation

$$N_A\big|_{r_i+\Delta r}\varepsilon 2\pi(r_i+\Delta r)l - N_A\big|_{r_i}\varepsilon 2\pi r_i l - (1-\varepsilon)2\pi r_i l\Delta r\frac{\partial q_i}{\partial t} = \varepsilon 2\pi r_i l\Delta r\frac{\partial C_i}{\partial t} \qquad (2.19)$$

where ε is the porosity of the particles and N_A the mass flux at r_i. The mass balance for the group is given by the summation over all the particles N_j, in the size group j, Equation 2.20.

$$\sum_{l=1}^{N_j} N_A\big|_{r_i+\Delta r}\varepsilon 2\pi(r_i+\Delta r)l - \sum_{l=1}^{N_j} N_A\big|_{r_i}\varepsilon 2\pi r_i l - \sum_{l=1}^{N_j}\frac{\partial q_i}{\partial t}(1-\varepsilon)2\pi r_i l\Delta r = \sum_{l=1}^{N_j}\frac{\partial C_i}{\partial t}\varepsilon 2\pi r_i l\Delta r \qquad (2.20)$$

Dividing through Equation 2.20 by $2\pi l$ gives

$$\sum_{l=1}^{N_j}\varepsilon\left[N_A\big|_{r_i+\Delta r}(r_i+\Delta r) - N_A\big|_{r_i} r_i\right] - \sum_{l=1}^{N_j}\frac{\partial q_i}{\partial t}(1-\varepsilon)r_i\Delta r = \sum_{l=1}^{N_j}\varepsilon\frac{\partial C_i}{\partial t}r_i\Delta r \qquad (2.21)$$

by the definition of the increment in $N_A r_i$

$$\sum_{l=1}^{N_j}\varepsilon\,\Delta(N_A r_i) - \sum_{l=1}^{N_j}\frac{\partial q_i}{\partial t}(1-\varepsilon)r_i\Delta r = \sum_{l=1}^{N_j}\varepsilon\frac{\partial C_i}{\partial t}r_i\Delta r \qquad (2.22)$$

Replacing the mass flux N_A, solid concentration q_i, and liquid concentration C_i with the corresponding average values N_{Aj}, q_j, and C_j within the *jth* particle size group and rewriting Equation (2.21) gives

$$\varepsilon\,\Delta(N_{Aj}\sum_{l=1}^{N_j} r_i) - (1-\varepsilon)\frac{\partial q_j}{\partial t}(\sum_{l=1}^{N_j} r_i)\Delta r = \varepsilon\frac{\partial C_j}{\partial t}(\sum_{l=1}^{N_j} r_i)\Delta r \qquad (2.23)$$

Let us recall that the point r_i is along a pore of the particle, Figure 2-3(a), i being the counter denoting position within the pore. We add to the last sentence that the pore is split into a number of nodes n_l. Let us also define the thickness Δr as the separation between two such nodes along the pore, such that $\Delta r = R_l / n_l$, and $r_i = n_{l,i}\Delta r$ (i.e. $\Delta r = r_i / n_{l,i}$). It now means that n_l and $n_{l,i}$ are the number of fractions or nodes for R_l and r_i respectively.

If n_l is constant whatever the particle size (for computational reasons), so that the distance between nodes will be different depending on particle size, then r_i will be proportional to R_l (and $\Delta r \propto R_l$). Therefore r_i will vary with l in proportion to the radius of the lth particle i.e., $r_i = (n_{l,i}/n_l)R_l$ ($l = 1, 2, \ldots, N_j$).

Since r_i is be proportional to R_l, we can define the linear-mean radii as:

$$\frac{\sum_{l=1}^{N_j} R_l}{N_j} = R_{j,L} \tag{2.24}$$

and surface-mean radii within size group j as

$$\frac{\sum_{l=1}^{N_j} R_l^2}{N_j} = R_{j,S}^2 \tag{2.25}$$

respectively. Consequently,

$$\frac{\sum_{l=1}^{N_j} r_i}{N_j} = r_{j,L} \tag{2.27}$$

and

$$\frac{\sum_{l=1}^{N_j} r_i^2}{N_j} = r_{j,S}^2 \tag{2.28}$$

Dividing Equation 2.23 by N_j, and substituting Equations 2.27 and 2.28 in 2.23, to allow for size, gives

$$\varepsilon\,(N_{Aj}\partial r_{j,L} + r_{j,L}\partial N_{Aj}) - (1-\varepsilon)\frac{\partial q_j}{\partial t} r_{j,S}\partial r_{j,S} = \varepsilon\frac{\partial C_j}{\partial t} r_{j,S}\partial r_{j,S} \tag{2.29}$$

By dividing through Equation 2.29 by $r_{j,L}\partial r_{j,L}$, it can be written in terms of the linear and surface mean radii as

$$\varepsilon\left(\frac{N_{Aj}}{r_{j,L}} + \frac{\partial N_{Aj}}{\partial r_{j,L}}\right) - (1-\varepsilon)\frac{\partial q_j}{\partial t}\frac{r_{j,S}\partial r_{j,S}}{r_{j,L}\partial r_{j,L}} = \varepsilon\frac{\partial C_j}{\partial t}\frac{r_{j,S}\partial r_{j,S}}{r_{j,L}\partial r_{j,L}} \tag{2.30}$$

For a particle size group j the ratio of particle radii $R_{j,S}/R_{j,L}$ is a constant independent of particle size, and can be denoted by a constant K_j such that

$$\frac{R_{j,S}}{R_{j,L}} = \frac{r_{j,S}}{r_{j,L}} = \frac{\partial r_{j,S}}{\partial r_{j,L}} = K_j \tag{2.31}$$

Substituting Equation 2.31 into 2.30

$$\varepsilon\left(\frac{N_{Aj}}{r_{j,L}} + \frac{\partial N_{Aj}}{\partial r_{j,L}}\right) - (1-\varepsilon)\frac{\partial q_j}{\partial t} K_j^2 = \varepsilon\frac{\partial C_j}{\partial t} K_j^2 \tag{2.32}$$

Introducing Fick's law, Equation 2.33, into Equation 2.32, and noting that the diffusion occurs in the opposite direction to particle radius,

$$N_{A,j} = D\frac{\partial C_j}{\partial r_{j,L}} \tag{2.33}$$

dividing through by ε and rearranging gives

$$D\left(\frac{\partial^2 C_j}{\partial r_{j,L}^2} + \frac{\partial C_j}{r_{j,L}\partial r_{j,L}}\right) = \frac{(1-\varepsilon)K_j^2}{\varepsilon}\frac{\partial q_j}{\partial t} + K_j^2\frac{\partial C_j}{\partial t} \tag{2.34}$$

Assuming the surface reaction is instantaneous and (reversible) second order [Equations 2.1 and 2.2], the reaction term can be expressed as

$$\frac{\partial q_j}{\partial t} = \frac{\partial q_j}{\partial C_j}\frac{\partial C_j}{\partial t} = \frac{q_m K_d}{(K_d + C_j)^2}\frac{\partial C_j}{\partial t} \tag{2.35}$$

Substituting Equation 2.35 into 2.36 gives

$$\frac{\partial C_j}{\partial t}\left[1 + \frac{(1-\varepsilon)}{\varepsilon}\frac{q_m K_d}{(K_d + C_j)^2}\right]K_j^2 = D\left(\frac{\partial^2 C_j}{\partial r_{j,L}^2} + \frac{\partial C_j}{r_{j,L}\partial r_{j,L}}\right) \tag{2.36}$$

Equation 2.36 is the desired equation describing the process of diffusion inside the pores for cylindrical particles with known size distribution (cylindrical polydisperse system). Equation 2.36 is applicable to both the stirred cell and the packed bed modes of operation. It is worth noting that in the case where $K_j \equiv 1$, Equation 2.36 becomes identical to Equation 2.6 derived for cylindrical particles with uniform size distribution (cylindrical monodisperse system).

2.5.2 Equation for Rate of Change of Bulk Liquid Concentration

Assuming that the bulk liquid concentration is uniform throughout the stirred cell, the mass balance for this bulk liquid phase, can be written as

Loss of mass from liquid in cell = Mass transferred to particles per unit time

$$C_L V_L\Big|_t - C_L V_L\Big|_{t+\Delta t} = \sum_{j=1}^{M} k_{f,j}\left(C_L - C_{n,j}\right)A_j \Delta t \tag{2.37}$$

Dividing by Δt and taking limits as $\Delta t \to 0$

$$-V_L\frac{dC_L}{dt} = \sum_{j=1}^{M} k_{f,j}\left(C_L - C_{n,j}\right)A_j \tag{2.38}$$

where C_{nj} is the concentration at the external surface of particles in size group j

k_{Lj} is the mass transfer coefficient for particles in size group j

A_j is the total surface area of particles in size group j

A_j is determined from the surface distribution function f_s according to the following relationship

$$A_j = f_s A_{ap}$$

Where A_{ap} is the total external surface area of all particles, defined as

$$A_{ap} = N 2\pi R_{NS}^2 l = \frac{V_{ap}}{\pi R_S^2 l} 2\pi R_L l = \frac{2V_{ap} R_L}{R_S^2} = \frac{2V_{ap}}{R_{LS}} \tag{2.39}$$

and R_{LS} is the linear-mean surface radius of all particles defined as

$$R_{LS} = \frac{R_S^2}{R_L}$$

to allow for the size of the adsorbent particles. The linear-mean surface radius can be obtained from the particle size distribution measurement through the corresponding diameter. A_j can be written as

$$A_j = f_S \frac{V_{ap}}{R_{LS}} \tag{2.40}$$

With A_j derived and expressed as in Equation 2.40 above, it is unnecessary to calculate the linear-surface mean radius $R_{j,LS}$ in each size group. Substituting Equation 2.40 into 2.38 and rearranging gives

$$\frac{dC_L}{dt} = -\frac{2V_{ap}}{V_L} \sum_{j=1}^{M} k_{f,j} \left(C_L - C_{n,j}\right) \frac{f_S}{R_{LS}} \tag{2.41}$$

Equation 2.41 is the differential equation that describes the rate of change of concentration in the bulk liquid for cylindrical polydisperse systems.

2.5.3 Finite Difference Forms of the Stirred Cell Equations

The set of equations that comprise the cylindrical polydisperse stirred cell model was solved numerically using a finite difference method. The mesh analysis of the solution and the development of finite difference forms for the model are given in this section.

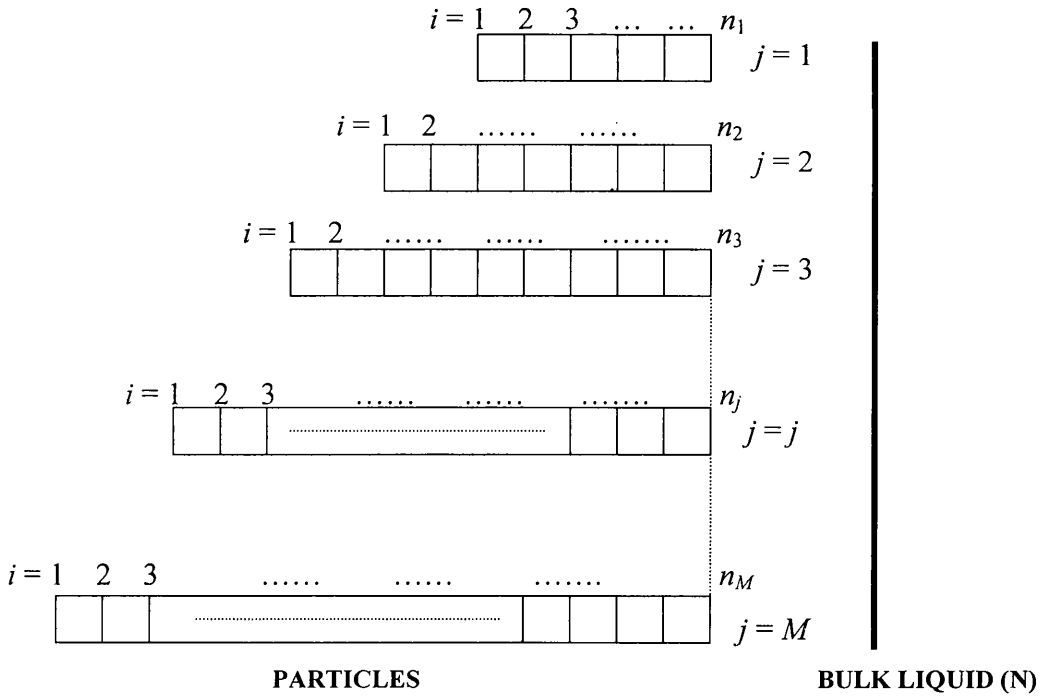

FIGURE 2-5: *Illustrative description of the mesh construction for stirred cell model.*

1. Stirred Cell Mesh Analysis

Figure 2-5 depicts the complete mesh construction for solving the stirred cell model. The mesh analysis allows for varying pore lengths in different particle size groups. The indices j and i stand for the size group and the points along the pores in each size group respectively, while Δr_j represents the step length between nodes along the pores and which varies between different size groups.

The distance between nodes Δr_j is given by

$$\Delta r_j = \frac{R_j}{(n_j - 1)} \tag{2.42}$$

where R_j is the surface mean radius of particles in size group j ($R_j = R_{j,s}$), n_j is the number of nodes along the pores of particles in size group j, and $n_j - 1$ is the number of steps along the pores of particles in size group j ($n_j - 1 = n_l$).

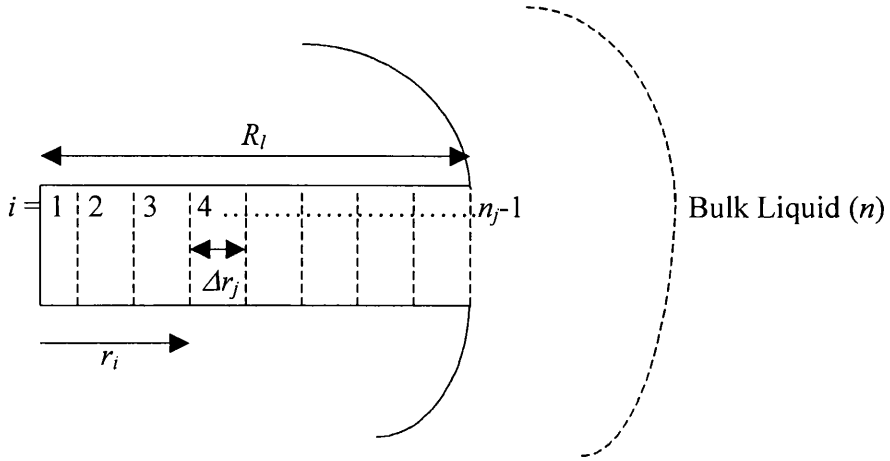

FIGURE 2-6: *Schematic diagram of a pore mesh layout inside a particle.*

The total number of mesh points is

$$n = 1 + \sum_{j=1}^{M} n_j \tag{2.43}$$

where n_j is constant for all particle size groups so that Δr_j varies with j. The value of n should now be equal to the total number of the finite difference equations, developed by conversion from the differential equations, which will be solved for the model at each time step.

2. Finite Difference Forms of the Stirred Cell Model

The following second order finite difference formulae, Equations 2.44 and 2.45 are introduced into Equation 2.36 to obtain the solution of the diffusion equation at various nodes along the pores.

$$\frac{\partial C_j}{\partial r_j} = \frac{C_{i+1,j} - C_{i-1,j}}{2\Delta r_j} \tag{2.44}$$

$$\frac{\partial^2 C_j}{\partial r_j^2} = \frac{C_{i+1,j} - 2C_{i,j} + C_{i-1,j}}{(\Delta r_j)^2} \tag{2.45}$$

The differential form of Equation 2.36 for protein diffusion inside the pores becomes

$$\frac{\partial C_{i,j}}{\partial t}\left[1 + \frac{G}{(K_d + C_j)^2}\right] K_j^2 = D\left(\frac{C_{i+1,j} - 2C_{i,j} + C_{i-1,j}}{(\Delta r_j)^2} + \frac{1}{r_{i,j}}\frac{C_{i+1,j} - C_{i-1,j}}{2\Delta r_j}\right) \tag{2.46}$$

where $G = \left(\frac{1-\varepsilon}{\varepsilon}\right) q_m K_d$

$i = 2, 3, \ldots, n_j - 1,\ j = 1, 2, 3, \ldots, M$

Let $r_{i,j} = (i-1)\Delta r_j$, so that the right hand side of Equation 2.46 can be rewritten

$$\frac{D}{(\Delta r_j)^2}\left(\frac{2r\left(C_{i+1,j} - 2C_{i,j} + C_{i-1,j}\right)}{2(i-1)\Delta r_j} + \frac{\Delta r_j (C_{i+1,j} - C_{i-1,j})}{2(i-1)\Delta r_j}\right)$$

Expanding the brackets above gives

$$\frac{D}{(\Delta r_j)^2}\left(\frac{\left[(2i\Delta r_j - 2\Delta r_j)C_{i+1,j} + C_{i+1,j}\Delta r_j\right]}{2i\Delta r_j - 2\Delta r_j}\right.$$

$$\left. - \frac{\left[2(2i\Delta r_j - 2\Delta r_j)C_{i,j}\right] + \left[(2i\Delta r_j - 2\Delta r_j)C_{i-1,j} - C_{i-1,j}\Delta r_j\right]}{2i\Delta r_j - 2\Delta r_j}\right)$$

The expression above can then be rearranged to give

$$\frac{D}{(\Delta r_j)^2}\left[\frac{2i-1}{2i-2}C_{i+1,j} - 2C_{i,j} + \frac{2i-3}{2i-2}C_{i-1,j}\right]$$

Combining both sides of Equation 2.46 now gives

$$\frac{dC_{i,j}}{dt} = \frac{1}{K_j^2}\left[\frac{D(K_d + C_{i,j})^2}{(K_d + C_{i,j})^2 + G}\right]\frac{1}{(\Delta r_j)^2}\left[\frac{2i-1}{2i-2}C_{i+1,j} - 2C_{i,j} + \frac{2i-3}{2i-2}C_{i-1,j}\right] \tag{2.47}$$

Equation 2.47 is the finite difference form of Equation 2.36 that describes the protein diffusion inside the pores.

3. Boundary Conditions

Equation 2.47 describes only the diffusion process at the interior nodes of the pores. It is necessary to introduce boundary conditions to get the solution of the differential equations for points at the centres of particles (where $i = 1$) and at the surfaces of particles (where $i = n_j$).

(1) At the centres of particles, $i = 1$

When $r_j \rightarrow 0$, ($j = 1, 2, \ldots, M$) it follows that at $r_j = 0$, $\frac{1}{r_j}$ is indeterminate. Using the MacLaurin series expansion gives

$$\left.\frac{\partial C_j}{\partial r_j}\right|_{r=0} = r_j \frac{\partial^2 C_j}{\partial r_j^2} \tag{2.48}$$

Substituting Equation 2.48 into Equation 2.35

$$\frac{\partial C_j}{\partial t}\left[1+\frac{(1-\varepsilon)}{\varepsilon}\frac{q_m K_d}{(K_d+C_j)^2}\right]K_j^2 = 2D\frac{\partial^2 C_j}{\partial r_j^2} \tag{2.49}$$

At the particle center ($i = 1$)

$$\frac{\partial^2 C_j}{\partial r_j^2} = \frac{C_{2,j} - 2C_{1,j} + C_{0,j}}{(\Delta r_j)^2} = \frac{2(C_{2,j} - C_{1,j})}{(\Delta r_j)^2} \tag{2.50}$$

Substituting Equation 2.50 into Equation 2.49 and rearranging the terms gives

$$\frac{dC_{1,j}}{dt} = \frac{4}{K_j^2}\left[\frac{D(K_d + C_{i,j})^2}{(K_d + C_{i,j})^2 + G}\right]\frac{(C_{2,j} - C_{1,j})}{(\Delta r_j)^2} \tag{2.51}$$

Equation 2.51 is the equation for the points at the centre of the particles.

(2) At the surface of the particles, $i = n_j$ ($j = 1, 2, \ldots, M$)

The mass balance equation at the surface of the particles is

$$\frac{\partial C_{n,j}}{\partial r_j} = \frac{k_{f,j}}{D\varepsilon}\left(C_L - C_{n,j}\right) \tag{2.52}$$

Equation 2.52 can be written in finite difference form as

$$\frac{C_{n+1,j} - C_{n-1,j}}{2\Delta r_j} = \frac{k_{f,j}}{D\varepsilon}\left(C_L - C_{n,j}\right) \tag{2.53}$$

From where $C_{n+1,j}$ can be isolated and expressed as

$$C_{n+1,j} = \frac{2\Delta r_j k_{f,j}}{D\varepsilon}\left(C_L - C_{n,j}\right) + C_{n-1,j} \tag{2.54}$$

The term $C_{n+1,j}$ represents an arbitrary concentration at a point within the liquid film a distance Δr_j from the particle surface.

The difference between $C_{n+1,j}$ and C_L (the concentration at the liquid film boundary) can be illustrated using a schematic representation of the concentration profile through the liquid film boundary into the pore Figure 2-7.

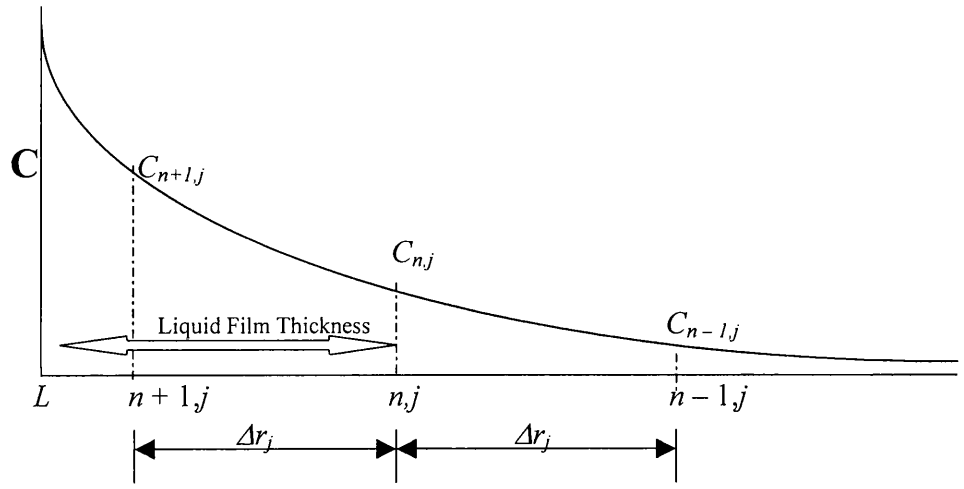

FIGURE 2-7: *Schematic diagram of the surface boundary condition.*

Substituting Equation 2.54 into Equation 2.47 gives

$$\frac{dC_{n,j}}{dt} = \frac{1}{K_j^2}\left[\frac{D(K_d + C_{n,j})^2}{(K_d + C_{n,j})^2 + G}\right]\frac{2}{(\Delta r_j)^2}\left[\frac{2n-1}{2n-2}\frac{k_{f,j}\Delta r_j}{D\varepsilon}C_L - \left(\frac{2n-1}{2n-2}\frac{k_{f,j}\Delta r_j}{D\varepsilon} + 1\right)C_{n,j} + C_{n-1,j}\right] \quad (2.55)$$

Equation 2.55 describes the diffusion process at the points on the particle surfaces. It is the fourth of the equations that makes up the polydisperse model for stirred cells, the others being Equations 2.41, 2.47 and 2.51.

4. Dimensionless Forms of the Polydisperse Stirred Cell Equations

We define: dimensionless concentration $W_{i,j} = C_{i,j}/C_O$

dimensionless time $\tau = t\,D/R_{LS}^2$

dimensionless radius $Z_j = r_j/R_{LS}$

The overall linear-surface mean radius R_{LS}, is used instead of the group equivalent R_j to define the dimensionless distance Z_j, and the dimensionless time τ, in order to solve the ordinary differential equations computationally using NAG routines. Complexities would otherwise arise if R_j is used instead, due to the creation of more dimensionless time variables, making the ODEs impossible to solve using the current NAG routines. Also the definition of the dimensionless variables does not affect the final solutions of the corresponding ODEs and hence the accuracy of the model.

The dimensionless forms of Equations 2.41, 2.47, 2.51, and 2.55 can be written as follows:

1. For $i = 1$ (particle centre), from Equation 2.51,

$$\frac{dW_{n,J}}{d\tau} = \frac{4F}{K_j^2}\frac{(W_{2,j} - W_{1,j})}{(\Delta Z_j)^2} \tag{2.56}$$

where $F = \dfrac{C_O{}^2(\dfrac{K_d}{C_O} + W_{i,j})^2}{C_O{}^2(\dfrac{K_d}{C_O} + W_{i,j})^2 + G}$ and $G = q_m K_d (1-\varepsilon)/\varepsilon$.

2. For $i = 2$ to $i = n_j - 1$ (interior nodes), from Equation 2.47,

$$\frac{dW_{i,j}}{d\tau} = \frac{1}{K_j^2}\frac{F}{(\Delta Z_j)^2}\left(\frac{2i-1}{2i-2}W_{i+1,j} - 2W_{i,j} + \frac{2i-3}{2i-2}W_{i-1,j}\right) \tag{2.57}$$

3. For $i = n_j$ (surface of particle), from Equation 2.55,

$$\frac{dW_{n,j}}{d\tau} = \frac{2}{K_j^2}\frac{F}{(\Delta Z_j)^2}\left[\frac{2n-1}{2n-2}N_{Sh,j}\Delta Z_j W_L - \left(\frac{2n-1}{2n-2}N_{Sh,j}\Delta Z_j + 1\right)W_{n,j} + W_{n-1,j}\right] \tag{2.58}$$

where the modified Sherwood number $N_{Sh,j} = k_{f,j} R_{LS}/D\varepsilon$

4. For $i = n_j + 1 = L$ (bulk liquid), from Equation (2.41),

$$\frac{dW_L}{d\tau} = -2\frac{V_{ap}}{V_L}\varepsilon\sum_{j=1}^{M} N_{Sh,j}(W_L - W_{n,j})f_L \tag{2.59}$$

Where j = 1, 2, 3, …. , M, stands for the number of particle size groups.

The model developed is used to describe the adsorption process by predicting the concentration profile of the bulk liquid in the stirred cell. However, in practice, the adsorption process is determined by monitoring the concentration profile by means of a UV detector connected to the sampling loop.

2.5.4 Delay and Mixing Effect

Experimental observations [48] reveal that the concentration profile monitored by the UV detector fixed in the sampling loop (as arranged for the present study) is different from the predicted concentration profile due to the time delay and mixing that occurs as liquid is carried from the stirred cell through a filter and the sampling line to the UV detector. If the adsorption kinetics of a system is fast, the delay and mixing effect is undetected but it becomes significant if the adsorption kinetics of the system is slow.

The effect is defined mathematically as

$$C(t) = \int_{R=0}^{R=\infty} C(t - t_0 - t_R) g e^{-gt} dt_R \tag{2.60}$$

where t is the time (s), t_o is the delay constant (s) in the sampling loop, t_R the residence time in the mixing chamber, C the concentration (kg/m^3) of protein in the bulk liquid and g the reciprocal time constant (s^{-1}) for the mixing. Equation 2.60 can also be expressed in the following finite difference form

$$C_{i+1} = C_i + 0.5\Delta t g(C_{st,i} - C_i + C_{st,i+1} - C^O_{i+1}) \tag{2.61}$$

where i is the number of the time step and Δt the length of one time step. Equation 2.61 was introduced to the data processing package (EXCEL), to modify the results predicted by the model, to account for the effect of mixing and delay in the sampling loop. The delay time t_o was subtracted from the experimental results.

The stirred cell rig used for the present study is the same one used by previous workers [48]. Conder *et al.* [48] showed that the values of t_o and g for the rig could be determined experimentally at the operational flowrate (3.8 ml/min for this study). This was done by measuring the response profile of the UV detector to a step change of known concentration in the stirred tank. t_o was directly obtained from the measured profile and g by fitting Equation 2.60 to the experimental points.

2.6 Development of a Packed Bed Model for Polydisperse System

The process of adsorption in a packed bed is conceptualised as the transfer of solute (adsorbate) from a flowing liquid stream (mobile phase) to adsorbents particles as the fluid passes through a pre-packed bed of the adsorbent (stationary phase). The solute concentration in the mobile phase fed to the bed inlet is sufficiently small, but constant, such that the solute exchange with the stationary packing phase does not alter total bulk-fluid concentration, and thus mobile phase superficial velocity through the bed. If the bed is initially free of any adsorbed material when the feed is introduced at the inlet, the output of the bed will initially contain no adsorbed material or the concentration will be zero. However, the bed will continue to adsorb material, and the level of adsorbate in the output will increase until it is finally equal to the inlet feed concentration. As this occurs, a concentration-time profile develops in the output. This concentration-time profile is called a breakthrough curve. Models developed for predicting the packed bed mode of operation usually predict the breakthrough curve.

Several authors [17, 18, 31, 54) have produced mathematical models that predict the breakthrough curves produced when a constant concentration step is introduced to a packed bed of rigid spherical adsorbents (usually in a chromatographic column). The greater accuracy of polydisperse models over monodisperse models has also been established [3]. This section describes the development of a model that in contrast to previous models considers a packed bed of cylindrical, semi-rigid particles. The cases of both monodisperse and polydisperse particles are analysed sine neither has previously been treated.

As in the stirred cell case, we consider the two resistances of the liquid film and particle diffusion to govern the rate of the adsorption process. We assume further that:

- The bed is of constant voidage ε_b
- The interstitial velocity is constant
- The particles are cylindrical and of uniform size (in the first instance) and density.

- The surface reaction is fast, and at equilibrium, the relation is given by a Langmuir isotherm.
- Axial dispersion in the bed is neglected.

1. Continuity Equation of the Mobile Phase (monodisperse model)

Consider the fixed bed in Figure 2-8, of a cross sectional area A, length X_r and bed voidage ε_b.

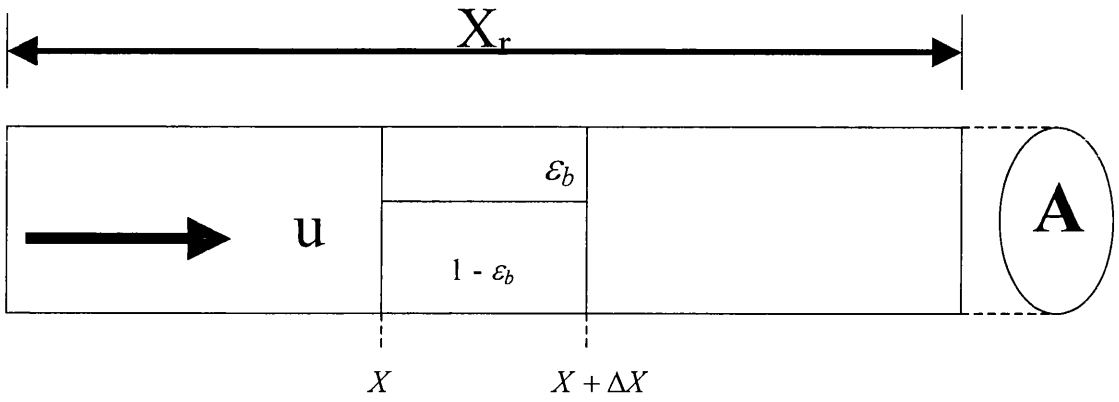

FIGURE 2-8: *Schematic diagram of a packed bed showing the continuity equation derivation.*

Taking a short element of thickness ΔX, through which a mobile phase is flowing at an interstitial velocity u, the continuity equation for the liquid phase can be written as

$$\textit{Rate of Mass IN} - \textit{Rate of Mass OUT} - \textit{Rate of Mass Transfer} = \textit{Rate of Accumulation} \quad (2.62)$$

$$N_L|_x A\varepsilon_b + CU|_x A\varepsilon_b - \left(N_L|_x + \frac{\partial N_L}{\partial X}\Delta X\right)A\varepsilon_b - \left(CU|_x + \frac{\partial CU}{\partial X}\Delta X\right)A\varepsilon_b - R_m = A\Delta X\varepsilon_b \frac{\partial C}{\partial t} \quad (2.63)$$

where N_L is the longitudinal flux of protein, $N_L = -D_L\,\partial C/\partial X$

D_L is the longitudinal diffusion coefficient (axial dispersion coefficient)

R_m is the rate of mass depletion from mobile phase to solid phase in element ΔX of bed.

Rearranging equation 2.63 gives

$$-\frac{\partial N_L}{\partial X}-\frac{\partial CU}{\partial X}-\frac{\Delta R_m}{A\varepsilon_b \Delta X}=\frac{\partial C}{\partial t} \tag{2.64}$$

Now, the axial dispersion term can be expressed as

$$\frac{\partial N_L}{\partial X}=\frac{\partial}{\partial X}\left(-D_L\frac{\partial C}{\partial X}\right)=D_L\frac{\partial^2 C}{\partial X^2} \tag{2.65}$$

and since the velocity is assumed constant

$$\frac{\partial CU}{\partial X}=U\frac{\partial C}{\partial X} \tag{2.66}$$

Substituting equations 2.66 and 2.65 into 2.64

$$D_L\frac{\partial^2 C}{\partial X^2}-U\frac{\partial C}{\partial X}-\frac{R_m}{A\varepsilon_b \Delta X}=\frac{\partial C}{\partial t} \tag{2.67}$$

The rate of mass depletion R_m is given by

R_m = *rate of mass transfer across the liquid film per unit area of particles* × *Area of particles*

= $k_f\,(C\text{-}C_s)\,A_{ap}$

where k_f is the liquid film mass transfer coefficient and C_s is the liquid concentration at the pore entrance.

Now A_{ap} the external surface area of all particles in $A\Delta X$ is given by

A_{aP} = Area of one particle × Number of particles

$$= 2\pi Rl \times \text{(Volume of adsorbent /Volume of one particle)} \tag{2.68}$$

$$= 2\pi Rl \times \frac{(1-\varepsilon_b)A\Delta X}{\pi R^2 l} \tag{2.69}$$

or

$$A_{aP} = \frac{2}{R}(1-\varepsilon_b)A\Delta X \tag{2.70}$$

and R_m becomes

$$\Delta R_m = k_f (C - C_s)\frac{2}{R}(1-\varepsilon_b)A\Delta X \tag{2.71}$$

Substituting equation 2.71 in 2.64 and rearranging gives the equation of rate of change of concentration in the mobile phase.

$$D_L \frac{\partial^2 C}{\partial X^2} - U\frac{\partial C}{\partial X} - \frac{2}{R}\frac{(1-\varepsilon_b)}{\varepsilon_b}K_f(C - C_S) = \frac{\partial C}{\partial t} \tag{2.72}$$

and assuming the axial dispersion is negligible, $D_L\,\partial^2 C/\partial X^2 = 0$, the equation becomes

$$-U\frac{\partial C}{\partial X} - \frac{2}{R}\frac{(1-\varepsilon_b)}{\varepsilon_b}K_f(C - C_S) = \frac{\partial C}{\partial t} \tag{2.73}$$

2. Equation of Protein Diffusion inside the Pores

This is identical to Equation 2.6 of the stirred cell model

$$D\varepsilon\left(\frac{\partial^2 C}{\partial r^2} + \frac{1}{r}\frac{\partial C}{\partial r}\right) = (1-\varepsilon)\frac{\partial q}{\partial t} + \varepsilon\frac{\partial C}{\partial t} \tag{2.74}$$

Furthermore, it has the same treatment for $(\partial q/\partial t)$ and the same finite difference form as Equation 2.6.

3. Predicting a Breakthrough Curve

The conversion of Equation 2.74 to finite difference form, that gives the rate of change of concentration at any point inside the pores, is identical to that for a stirred cell. However, in contrast to the stirred cell case, the system of equations for the complete set of nodes for a packed bed involves distances along the bed as variables, as well as the distances along the pore. In developing the equation for the point concentrations inside the pore for a stirred cell, we took $r = (i-1)\Delta r$, where i = 1, 2, 3, ... , and set the node counter so that i = 1 denoted the centre of a particle. For a packed bed (Figure 2-9), the counter i goes from i = 1, at the centre of a particle of the first section of the column, to i=N, at the

mobile phase node of the last section in the column, by repeatedly moving from the centre of the particle to the mobile phase of each section. The centre of a particle in each section will be denoted by $i = L$ where the index L will be a multiple of the number of pore sections N_y (including the mobile phase as the last section at the end of the pore).

Thus for a packed bed the particle radial distance r from the centre of the particle is equal to $(i-L)\Delta r$ and accordingly the equation for point concentration along the pores is

$$\frac{\partial C_i}{\partial t} = \frac{D(K_d + C_i)^2}{(K_d + C_i)^2 + G}\left(\frac{1}{(\Delta r)^2}\right)\left[\frac{i-L+0.5}{i-L}C_{i+1} - 2C_i + \frac{i-L-0.5}{i-L}C_{i-1}\right] \qquad (2.75)$$

which is equivalent to Equation 2.11 for the stirred cell and runs from the centre to the surface of the particles of each section in the bed.

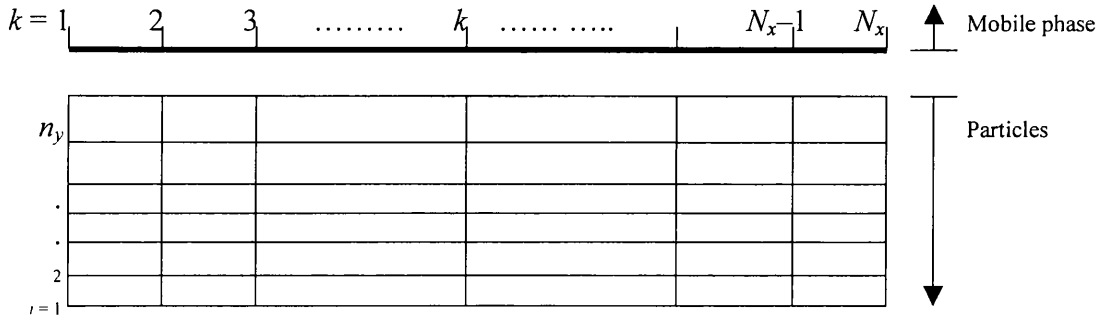

FIGURE 2-9: *Mesh construction for monodisperse packed bed model.*

The equation of the rate of change of concentration in the mobile phase, Equation 2.75 is to work on the upper nodes of the packed bed mesh. Introducing a backward difference formula for $\partial C/\partial X$ as

$$\frac{\partial C}{\partial X} = \frac{C_k - C_{k-1}}{\Delta X} \qquad (2.76)$$

in which k is the increment index along the length of the bed, as in Figure 2-9. Substituting Equation 2.76 in equation 2.73 and rearranging gives

$$\frac{dC}{dt} = \frac{U}{\Delta X}(C_{k-1} - C_k) - \frac{2}{R}\frac{(1-\varepsilon_b)}{\varepsilon_b} k_f (C_k - C_s) \tag{2.77}$$

Equation 2.77 is solved numerically for the bulk liquid concentration along the bed together with the equations for the point concentrations at the adjacent particles to give the concentration profile at the outlet of the column.

4. Boundary Conditions

The boundary conditions for the packed bed model are similar to the boundary conditions for the stirred cell model, and they are therefore treated identically. The solution of the equation for the boundary conditions finally gives, for the packed bed at the centre of the particles,

$$\frac{dC_i}{dt} = \frac{D(K_d + C_i)^2}{(K_d + C_i)^2 + G} \frac{4}{(\Delta r)^2}[C_{i+1} - C_i] \tag{2.78}$$

and at the surface of the particles,

$$\frac{dC_i}{dt} = \frac{D(K_d + C_i)^2}{(K_d + C_i)^2 + G} \frac{2}{(\Delta r)^2}\left[\frac{i - L + 0.5}{i - L}\frac{K_f}{D\varepsilon}\Delta r C_{i+1} - (1 + \frac{i - L + 0.5}{i - L}\frac{K_f}{D\varepsilon}\Delta r)C_i + C_{i-1}\right] \tag{2.79}$$

which is the finite element equivalent of Equation 2.17 for the stirred cell model where L=1.

2.6.1 Continuity Equation of the Mobile Phase (Polydisperse model)

Up until this point it has been assumed that the particles packed in the column are of uniform size in order to simplify the process of developing the packed bed equations. The rate of mass depletion from the mobile phase to the solid phase in the element of bed ΔX was expressed as

$$R_m = k_f (C\text{-}C_s) A_{ap}$$

and A_{ap} defined for cylindrical uniformly sized particles as

$$A_{ap} = \frac{2}{R}(1-\varepsilon_b)A\Delta X$$

For a system where the pre-packed adsorbent particles in the bed have a wide size distribution such as the particles in the present study, a size distribution function has to be included in the derivation of R_m since k_f, C_s, and A_{ap} are all independent of the particle size.

Consider an element $A\Delta X$ packed with polydisperse particles. As in the stirred cell case, the particles can be divided into M size groups so that in each group the particles have a narrow size distribution and are uniform in size relative to particles in the same group. R_m can be written in the form

$$R_m = \sum_{j=1}^{M} k_{f,j}(C - C_{s,j})A_j \tag{2.80}$$

where k_{fj} is the film mass transfer coefficient for particles in size group j,

$C_{s,j}$ is the protein concentration at the pore entrance of the particles in size group j,

C is the mobile phase protein concentration in the element $A\Delta X$

Aj is the total external surface area of particles in size group j, and

$$A_j = f_{s,j}A_{ap} \tag{2.81}$$

where $f_{s,j}$ is the particle surface distribution function which represents the proportion of the surface area for particles in size group j. Let V_{ap} represent the total volume of particles in the element $A\Delta X$, defined as

$$V_{ap} = A\Delta X(1-\varepsilon_b) \tag{2.82}$$

A_{ap} can now be defined in terms of the number-linear mean diameter d_{NL}, the number-surface mean diameter d_{NS}, and V_{ap} as

$$A_{ap} = N(\pi d_{NSl}) = \frac{V_{ap}}{\frac{\pi}{4} d_{NS}^2 l} \pi d_{NL} l = \frac{4V_{ap}}{\frac{d_{NS}^2}{d_{NL}}} \tag{2.83}$$

Using linear-surface mean diameter d_{LS} to replace (d^2_{NS}/d_{NL}), Equation 2.83 can then be rewritten

$$A_{ap} = \frac{4V_{ap}}{d_{LS}} \tag{2.84}$$

Substituting Equation 2.82 and 2.84 into 2.81 gives

$$A_j = f_{s,j} \frac{4A\Delta X(1-\varepsilon_b)}{d_{LS}} \tag{2.85}$$

and substituting Equation 2.85 into Equation 2.80, R_m becomes

$$R_m = \frac{4A\Delta X(1-\varepsilon_b)}{d_{LS}} \sum_{j=1}^{M} k_{f,j}(C - C_{s,j}) f_{s,j} \tag{2.86}$$

Now, substituting Equation 2.86 into Equation 2.67, we have

$$D_L \frac{\partial^2 C}{\partial X^2} - U \frac{\partial C}{\partial X} - \frac{1-\varepsilon_b}{\varepsilon_b} \frac{4}{d_{LS}} \sum_{j=1}^{M} k_{f,j}(C - C_{s,j}) f_{s,j} = \frac{\partial C}{\partial t} \tag{2.87}$$

The correlations of Arnold et al. [25] and Liapis [35] can be used to evaluate the axial dispersion term D_L. Their calculations for separations in a packed bed of spherical particles at low Reynolds numbers suggest that the effect of the mass transfer mechanism of axial dispersion can be safely neglected in modelling such systems. The results of Heeter and Liapis [41] uphold the argument for the neglect of axial dispersion in mathematical models of most chromatographic systems involving the adsorption of proteins with long columns. Therefore neglecting the axial dispersion term gives

$$\frac{\partial C}{\partial t} = -U \frac{\partial C}{\partial X} - \frac{1-\varepsilon_b}{\varepsilon_b} \frac{4}{d_{LS}} \sum_{j=1}^{M} k_{f,j}(C - C_{s,j}) f_{s,j} \tag{2.88}$$

Equation 2.88 is the equation for the rate of change of concentration in the mobile phase (continuity equation) for a packed bed of polydisperse particles.

2.6.2 Equation of Protein Diffusion inside the Pores (Polydisperse model)

The equation for protein diffusion within the pores is the same as Equation 2.36 for the stirred cell model.

$$\frac{\partial C_j}{\partial t}\left[1+\frac{(1-\varepsilon)}{\varepsilon}\frac{q_m K_d}{(K_d+C_j)^2}\right]K_j^2 = D\left(\frac{\partial^2 C_j}{\partial r_j^2}+\frac{1}{r_j}\frac{\partial C_j}{\partial r_j}\right) \tag{2.89}$$

2.6.3 Finite Difference Forms of the Packed Bed Equations

The set of equations that make up the cylindrical polydisperse packed bed model was solved numerically using a finite difference method. The two-dimensional mesh analysis for the solution of the packed bed model and the development of finite difference forms for the model are given in this section.

1. Packed Bed Mesh Analysis

Figure 2-10 depicts the complete mesh construction for solving the packed bed model. The mesh analysis in contrast to the stirred cell mesh involves numbering the nodes in the axial direction of the bed as well as along the pores of particles in different particle size groups. The bed is divided into N_x sections and the index k represents the sections (k = 1,2,...,N_x) along the bed. The end result is such that each section can be treated as an independent stirred cell within the bed. The index j (j = 1,2,3,....,M) represents the individual size groups, where the polydisperse particles are divided into M size groups. The size of particles in each group is denoted by a mean diameter. Δr_j represents the step length between nodes along the pores in size group j, and is given as

$$\Delta r_j = \frac{R_j}{(n_j-1)}$$

where n_j is the number of nodes in size group j, and R_j is the average radius of particles in the group.

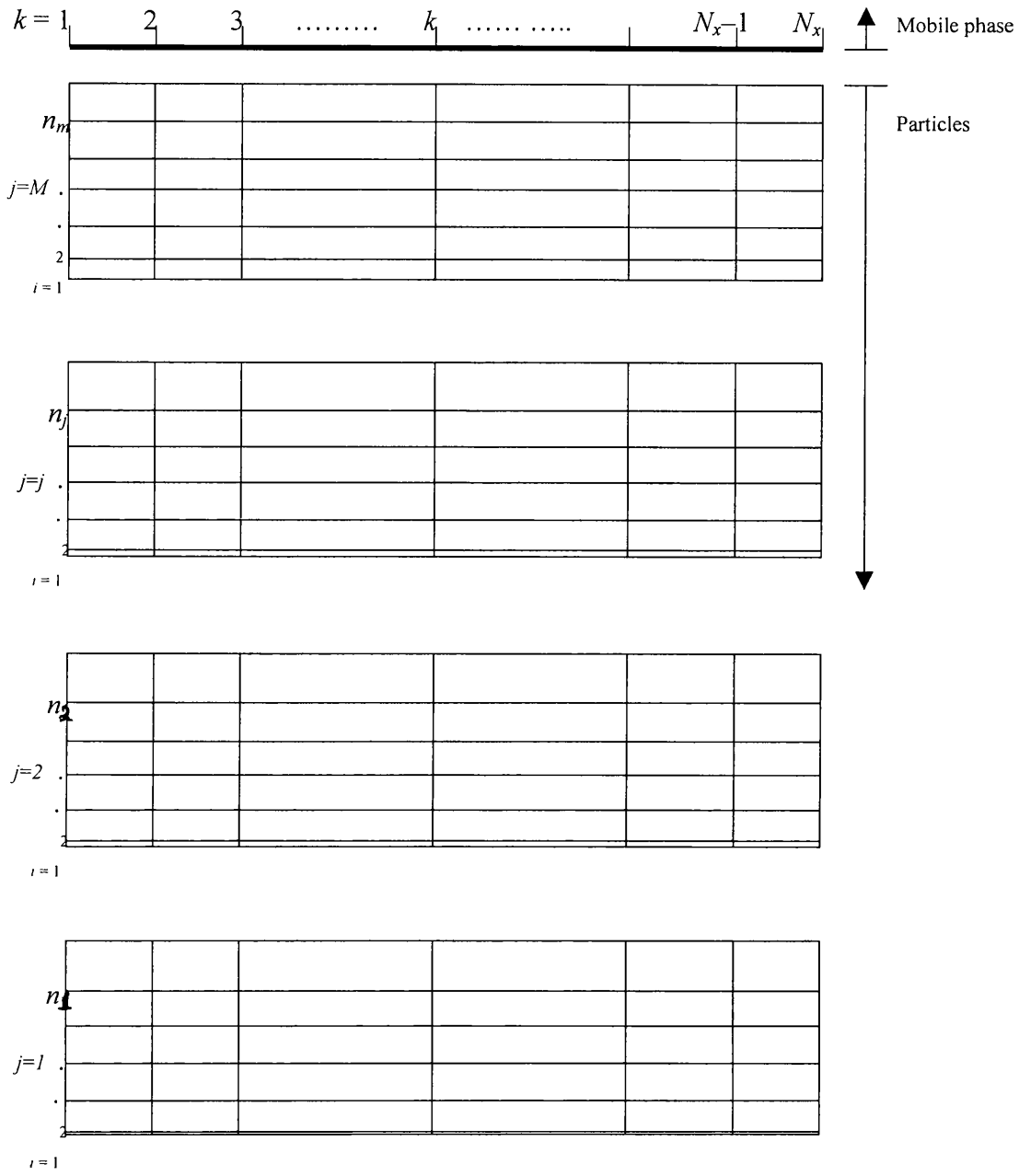

FIGURE 2-10: *Mesh construction for polydisperse packed bed model.*

The step length between nodes is constant for all size groups. The number of steps (points) along the pores in each size group is different. The groups with larger mean diameters have greater numbers of pore mesh points than the groups with smaller mean

diameters. The index i (i = 1,2,3....,n_j), denotes the points along the pores in each size group. $C_{i,j,k}$ stands for the point concentration for the mesh point (i,j,k), the concentration in the ith section of size group j in the kth section of the bed. The mobile phase concentration in section k is denoted as C_k. N_m is the total number of mesh points for the whole bed i.e. the number of finite difference equations to be set up, and is calculated as

$$N_m = \left(1 + \sum_{j=1}^{M} n_j\right).N_X$$

2. *Finite Difference Forms of the Packed Bed Model*

The continuity equation for the mobile phase, Equation 2.88, is converted to a finite difference form by introducing the backward difference formula

$$\frac{\partial C}{\partial X} = \frac{C_k - C_{k-1}}{\Delta X} \tag{2.90}$$

Substituting Equation 2.90 into 2.88 and rearranging gives

$$\frac{dC_k}{dt} = \frac{U}{\Delta X}(C_{k-1} - C_k) - \frac{2(1-\varepsilon_b)}{R_{LS}\varepsilon_b}\sum_{j=1}^{M} k_{f,j}(C_k - C_{N_j,j,k})f_{s,j} \tag{2.91}$$

where $C_{Nj,j,k}$ is the surface point concentration of particles in size group j, and bed division k. For the interior nodes ($1< i <N_j$-1), the treatment of the packed bed equation is similar to that for the stirred cell and is given as

$$\frac{dC_{i,j,k}}{dt} = \frac{1}{K_j^2}\left[\frac{D(K_d + C_{i,j,k})^2}{(K_d + C_{i,j,k})^2 + G}\right]\frac{1}{(\Delta r_j)^2}\left[\frac{2i-1}{2i-2}C_{i+1,j,k} - 2C_{i,j,k} + \frac{2i-3}{2i-2}C_{i-1,j,k}\right] \tag{2.92}$$

The equation for the centre of the particles (i = 1) is

$$\frac{dC_{1,j,k}}{dt} = \frac{4}{K_j^2}\left[\frac{D(K_d + C_{i,j,k})^2}{(K_d + C_{i,j,k})^2 + G}\right]\frac{(C_{2,j,k} - C_{1,j,k})}{(\Delta r_j)^2} \tag{2.93}$$

For the surface points, ($I = N_j$), the finite difference equation is

$$\frac{dC_{N_j,j,k}}{dt} = \frac{2B}{K_j^2}\frac{1}{(\Delta r_j)^2}\left[\frac{2N_j-1}{2N_j-2}\frac{k_f \Delta r_j}{D\varepsilon}C_k - \left(1+\frac{2N_j-1}{2N_j-2}\frac{k_f \Delta r_j}{D\varepsilon}\right)C_{N_j,j,k} + C_{N_j-1,j,k}\right] \quad (2.94)$$

where $B = \dfrac{D(K_d + C_{N_j,j,k})^2}{(K_d + C_{N_j,j,k})^2 + G}$

$C_k = C_{Nj+1,j,k}$ = bulk liquid concentration of the mobile phase in bed division k, (j = 1,2,3,.....M) and (k = 1,2,3,....N_x).

2.6.4 Dimensionless Forms of the Packed Bed Equations

In order to obtain the relevant dimensionless forms of the packed bed equations, we define the following dimensionless variables:

concentration $W = C/C_O$; time $\tau = t\,D/R_{LS}^2$; radius $Z_j = r_j/R_{LS}$; and bed length $X_k = X/X_T$

where C_o is the initial concentration at inlet of the bed, and R_{LS} is the length-surface mean radius.

The dimensionless form of the mobile phase continuity equation (2.91) is given as

$$\frac{dW_k}{d\tau} = \frac{R_{LS}^2 U}{X_T D}\frac{(W_{k-1} - W_k)}{\Delta X_k} - 2\varepsilon\frac{(1-\varepsilon_b)}{\varepsilon_b}\sum_{j=1}^{M} N_{Sh,j}(W_k - W_{N_j,j,k})f_{s,j} \quad (2.95)$$

The equation for the diffusion at the centre of the particles i = 1, is

$$\frac{dW_{1,j,k}}{d\tau} = \frac{4F}{K_j^2}\frac{(W_{2,j,k} - W_{1,j,k})}{(\Delta Z_j)^2} \quad (2.96)$$

The dimensionless form of the equation for the intraparticle nodes $1 < i < N_j$, is

$$\frac{dW_{i,j,k}}{d\tau} = \frac{1}{K_j^2}\frac{F}{(\Delta Z_j)^2}\left(\frac{2i-1}{2i-2}W_{i+1,j,k} - 2W_{i,j,k} + \frac{2i-3}{2i-2}W_{i-1,j,k}\right) \quad (2.97)$$

and the equation for the points at the surface of the particles $i = N_j$, is

$$\frac{dW_{N_j,j,k}}{d\tau} = \frac{2}{K_j^2}\frac{F}{(\Delta Z_j)^2}\left[\frac{2N_j-1}{2N_j-2}N_{Sh,j}\Delta Z_j W_k - \left(\frac{2N_j-1}{2N_j-2}N_{Sh,j}\Delta Z_j + 1\right)W_{N_j,j,k} + W_{N_j-1,j,k}\right] \tag{2.98}$$

where $F = \dfrac{C_O{}^2(\frac{K_d}{C_O} + W_{i,j,k})^2}{C_O{}^2(\frac{K_d}{C_O} + W_{i,j,k})^2 + G}$ and $G = q_m K_d (1-\varepsilon)/\varepsilon$.

2.6.5 Delay and Mixing Effect

The concentration profile for the packed bed model, formerly treated as an instantaneous profile following the introduction of concentration a step at the inlet [18, 35], has rather been shown to actually build up over a period of time [48]. This has been attributed to the spreading process that occurs in the connecting tube between the sample inlet point, at one end of the tube, and the point where the tube is connected to the column (the other end of the tube). The modified boundary condition for a perfectly sharp inlet profile for the adsorption process suggested by Conder et al. [48] is

$$C(0,t>0) = C_0\{1-\exp[-g(t-t_0)]\} \tag{2.99}$$

where t is the time (s), t_o is the delay constant (s) in the sampling loop, C the concentration (kg/m^3) of protein in the bulk liquid and g the reciprocal time constant (s^{-1}) for the mixing. Equation 2.99 can also be expressed in the following form for desorption operations

$$C(0,t>0) = C_0\{\exp[-g(t-t_0)]\} \tag{2.100}$$

The computer program developed for the solution of the packed model presented in this chapter allows for a non-sharp profile.

2.7 THE LIQUID FILM MASS TRANSFER COEFFICIENTS

2.7.1 Stirred Cell

The form of the liquid film mass coefficient used for predicting the adsorption process depends on the shape and diameter of the particles involved. Few correlations that can estimate the liquid film transfer coefficient to cylinders in stirred tanks are available in the literature [55-58]. We derived Equation 2.101 to estimate the film mass transfer coefficient for a single cylindrical particle (in the size range of small catalyst particles or micro organisms). The equation was obtained from the mass transfer (molecular diffusion) coefficient at stagnant conditions and a correlation developed from experimental data obtained for mass transfer from single cylinders when the flow is perpendicular to the cylinder plotted by Geankoplis [55].

$$k_f = \frac{D_{AB}}{d_{LS}}\left[2 + 0.6\left(\frac{\rho u d_{LS}}{\mu}\right)^{0.513}\left(\frac{\mu}{\rho D_{AB}}\right)^{\frac{1}{3}}\right] \qquad (2.101)$$

where k_f is the liquid film mass transfer coefficient and d_{LS} is the length-surface mean diameter for the particles in size group j. ρ is the liquid density, μ the liquid viscosity, and D_{AB} the diffusion coefficient in free solution.

On expansion, the first term on the right hand side of the equation is the mass transfer (molecular diffusion) coefficient at stagnant conditions. The second term is a correlation derived from experimental data obtained for mass transfer from single cylinders when the flow is perpendicular to the cylinder. Of great value to this research are that the cylinders for which the experimental data was obtained [55] are infinitely long and mass transfer to their ends is not considered. The derivation of this semi-empirical correlation [Equation 2.101] is as follows.

Geankoplis [55] gives the molecular diffusion term at stagnant conditions in a dilute solution as $\frac{2D_{AB}}{d}$ ignoring the effects of natural convection that would increase the value of this term if present.

Data from several sources were plotted [55] for Schmidt's number 1000 to 3000 and a Reynolds number range of 50 to 50,000. Geankoplis expressed the result in terms of a dimensionless mass transfer factor J_D as

$$J_D = 0.6\,\mathrm{Re}^{-0.487} = Sh \Big/ \left(\mathrm{Re}.Sc^{\frac{1}{3}}\right) \tag{2.102}$$

Rearranging the Equation 2.102 for k_f gives

$$\frac{k_f d}{D_{AB}} = 0.6\,\mathrm{Re}^{-0.487}\,\mathrm{Re}.Sc^{\frac{1}{3}} \tag{2.103}$$

Where $Sh = k_f d/D_{AB}$, $\mathrm{Re} = \rho u d/\mu$ and $Sc = \mu/\rho D_{AB}$. The relevant velocity, u, in a stirred tank is the terminal settling velocity and d is the linear-surface mean diameter d_{LS}.

Equation 2.103 becomes

$$\frac{k_f d_{LS}}{D_{AB}} = 0.6\left(\frac{\rho u d_{LS}}{\mu}\right)^{0.513}\left(\frac{\mu}{\rho D_{AB}}\right)^{\frac{1}{3}} \tag{2.104}$$

Hence,

$$k_f = \frac{D_{AB}}{d_{LS}}\left[0.6\left(\frac{\rho u d_{LS}}{\mu}\right)^{0.513}\left(\frac{\mu}{\rho D_{AB}}\right)^{\frac{1}{3}}\right] \tag{2.105}$$

Adding the term of molecular diffusion at stagnant conditions to Equation 2.105 gives the liquid film mass transfer coefficient for a cylindrical particle in a stirred cell, which is can be reduced to give Equation 2.101.

$$k_f = \frac{2D_{AB}}{d_{LS}} + \frac{D_{AB}}{d_{LS}}\left[0.6\left(\frac{\rho u d_{LS}}{\mu}\right)^{0.513}\left(\frac{\mu}{\rho D_{AB}}\right)^{\frac{1}{3}}\right] \qquad (2.106)$$

2.7.2 Packed Bed

The equation for the liquid film mass transfer coefficient, for cylindrical particles in packed bed operation, is determined using the following correlation [59] for spherical particles in a packed bed

$$Sh_j = 2 + 1.45\,\mathrm{Re}_j^{1/2}\,Sc^{1/3} \qquad (2.107)$$

Where $Sh_j = k_{fj}d_{LS,j}/D_{AB}$, $\mathrm{Re}_j = \rho u d_{LS,j}/\mu$ and $Sc = \mu/\rho D_{AB}$.

Foo and Rice highlighted the advantages of this correlation in their review of this and other correlations [60]. They showed that it lies in a mean position (between the other estimates proposed) at low Reynolds numbers, and unlike other correlations reaches an asymptotic value of $Sh = 2$, which is the molecular diffusion term expected theoretically at stagnant conditions. The correlation is recommended for Re < 100, which is of practical importance since the Reynolds number of all systems that have been (different particle types and flowrates) range from 0.010 to 0.134. Geankoplis [55] suggests that the following adjustments could be made to Equation 2.107 to obtain an estimate for a bed of cylinders

$$Sh_j = 2 + \left(0.79 \times 1.45\,\mathrm{Re}_j^{1/2}\,Sc^{1/3}\right)$$

where the diameter of the cylinders being investigated replaces that of the spheres (in Re_j and Sh_j) in the above equation. The required mass transfer coefficient can therefore be estimated from Equation 2.108.

$$k_{f,j} = \frac{D_{AB}}{d_{LS,j}}\left[2 + 0.11\left(\frac{\rho u d_{LS,j}}{\mu}\right)^{\frac{1}{2}}\left(\frac{\mu}{\rho D_{AB}}\right)^{\frac{1}{3}}\right] \tag{2.108}$$

The molecular diffusivity in free solution D_{AB}, can be estimated from Polson's semi-empirical equation for biological solutes with molecular weight above 1000 [61], modified by Geankoplis [55] to account for different temperatures in dilute aqueous solutions,

$$D_{AB} = \frac{9.40 \times 10^{-15} T}{\mu (M_A)^{1/3}} \tag{2.109}$$

where M_A is the molecular weight of the large molecule A (protein) and T is the temperature in Kelvin units.

2.8 Effective Diffusivity and other Parameters Used in the Model

The reason for the procedure involved in determining the effective pore diffusivity has been discussed in Section (1.3.6). The effective diffusivity of the protein within the pore of the adsorbent particles was determined by comparing the concentration profiles predicted by the stirred cell model with the experimental results obtained. The effective diffusivity was determined by varying its value in the model until a good fit to the experimental data was obtained. This value obtained from the stirred cell operation was then adopted in the packed bed simulations since the diffusion coefficients are independent of operation mode.

The procedure for obtaining the parameters characterising the adsorption isotherm, q_m and K_D is described in Chapter 4 with sample calculations. They were obtained from the adsorbent isotherm experiments.

The particle size distribution and other size related data are determined from particle size measurements. The size measurement results and the methods of calculation used to determine the length-surface mean diameter $d_{LS,j}$ are also given in Chapter 4. The parameters related to the experimental operating conditions are obtained from the

experimental set-up. The main parameters involved in the models are summarised in Table 2-3.

Parameters	Notations	Determination
K_{fj} (S.C.)*	Film mass transfer coefficient	Equation (2.97)
K_{fj} (P.B.)**	Film mass transfer coefficient	Equation (2.99)
D_e (S.C.)	Effective diffusivity	Best fit to experimental data
D_e (P.B.)	Effective diffusivity	Same value as S.C. for same adsorbent
C_0	Initial protein concentration	Experimental operation condition
C_f	Protein feed concentration	Experimental operation condition
q_m	Langmuir isotherm constant	Isotherm experiment
K_D	Dissociation constant	Isotherm experiment
ε	Adsorbent porosity	Pore size measurement (BJH method)
f_L	Length distribution function	Size distribution measurement
f_S	Surface distribution function	Size distribution measurement
d_{LSj}	Length-surface mean diameter	Size distribution measurement

* stirred cell mode; ** packed bed mode

TABLE 2-3: *Parameters used in the models.*

2.9 NUMERICAL SOLUTIONS OF THE STIRRED CELL AND PACKED BED EQUATIONS

The differential equations obtained in Section (2.5) and (2.6) were obtained by partially discretising the original partial differential equations with respect to distance alone, keeping rather than discretising the partial differential with respect to time. The resulting forms of the differential equations have been solved using a package subroutine [Numerical Algorithm Group (NAG) D02EJF] that solves the equations as a set of ordinary differential equations.

The methods of solving ordinary differential equations numerically used here are well developed [3, 17, 18, and 31]. An alternative solution scheme using explicit differential equations has been described elsewhere [50], for cylindrical particles and extensively discussed by Hayek [18] for spherical particles. The solution using ordinary differential

equations is more suitable for the present study as it uses less computer time and is more stable.

The NAG subroutine employed (D02EJF) has been used previously for different adsorbents in stirred cell predictions [18]. An alternative package subroutine to NAG's D02EJF, the HSL (formerly the Harwell Subroutine Library) DC03, can also be used to solve the model equations. However, the DC03 is not as user-friendly as the NAG subroutine, and requires a lot more user prompts and inputs to run efficiently. The NAG subroutines deal with nonlinearity efficiently and handle stiff equations such as these rather well. A stiff system of differential equations is a system that contains equations whose solutions have both fast and slow dynamic response terms. The NAG subroutine optimises the time interval by using Gear's backward differentiation formula, with a variable step, variable order technique, thus saving computational time.

2.9.1 Stirred Cell and Packed Bed Computer Program Format

The computer program for solving the system of ordinary differential equations describing the stirred cell adsorption process uses the subroutine D02EJF from the 32-bit NAG library of subroutines compatible with a Fortran 95 (version 2.0) compiler loaded onto a Dell PC in the laboratory.

The NAG subroutine developers suggested the notation used in developing the computer program (Appendix B). In the program, X is the dimensionless time, $F(I)$ is the rate of change of dimensionless concentration Y at node I and N is the number of equations.

The computer programs (Appendix B1, B2 and B3) consist of a main program and the subroutine DO2EJF, which carries out the solution. DO2EJF integrates the stiff system of first-order ordinary differential equations over the given interval and returns the solution at points specified by the user, if desired.

The program comprises two parts, a main program and a set of subroutines. The main program defines the system to be solved, inputs the data and parameters and sets the initial conditions. It then calls the subroutine DO2EJF and transfers the input information to it. DO2EJF calls the function subroutine FCN, where the model equations to be solved are stored internally. The subroutine OUT called by FCN at the end of each solution cycle (time step) prints out desired results at intermediate points. The number of intermediate points at which OUT is to be called are determined by the value given to a parameter K in the program.

An external subroutine DO2EJY called by D02EJF starts the solution. D02EJY calculates the Jacobian matrix, and works out both the stability limits and the step size of the dimensionless time X at which the new solution $Y(I)$ will be determined. When DO2EJF has calculated the solution *Y(I)* with the specified step length of X, it calls DO2EJY to define a new step length of X and the solution proceeds in the same form from $X = 0$ to $X = XEND$. The program stops when X reaches *XEND*.

2.9.2 Stirred Cell Program Development

The schematic representation of the pattern employed by the program for the solution of the stirred cell model is shown as a mesh in Figure 2-11. Consider an adsorbent particle, as in Figure 2-12, with n_1 divisions of its pore depth and representing the particles in size group 1. The counter follows the increments of the index I, from the centre of the particles $I = 1$, to the surface $I = n_1$, then goes to the centres of the particles in size group 2, onto the surfaces and proceeds in like manner till the surfaces of the particles in size group M ($I = N_m$) and finally into the bulk liquid $I = N$, where $N_m = N - 1$. The values of I at each node are shown in Figure 2-11.

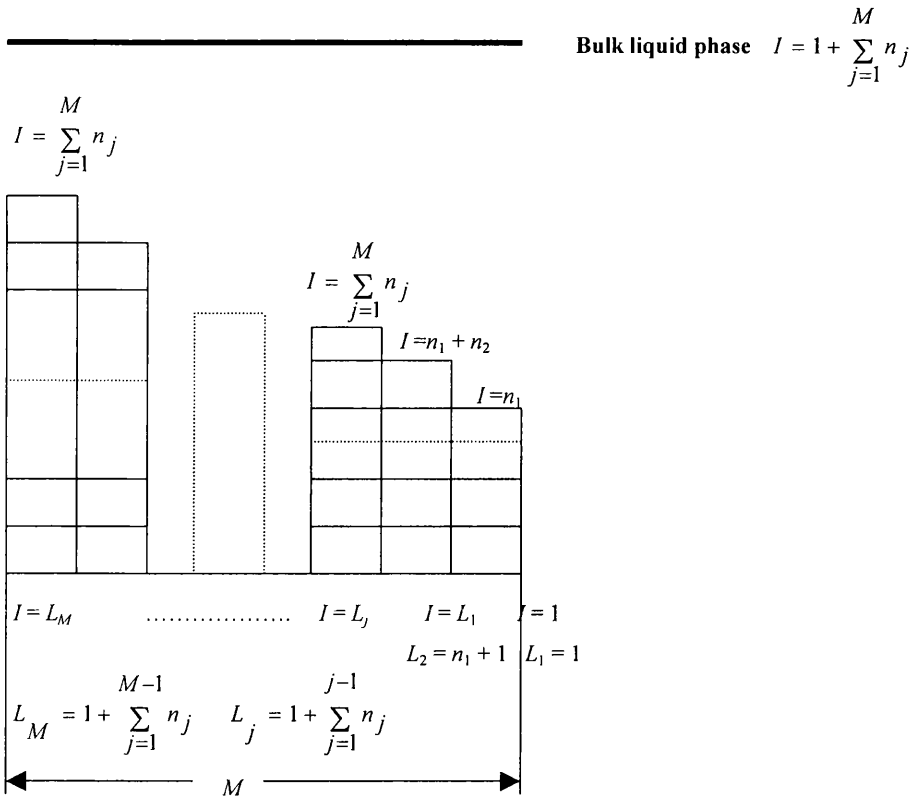

FIGURE 2-11: *Schematic representation of the mesh for solving the stirred cell model*

The counter L_j, is used to indicate the centres of particles in different size groups, j = 1, 2,..., M, where $L_1 = 1$ for size group 1, $L_2 = n_1+1$ for size group 2,....., $L_j = 1+\sum_{j=1}^{j-1} n_j$ for size group j, and so on.

Each node I has a differential equation that describes the rate of change $F(I)$ of the dimensionless concentration $Y(I)$ with dimensionless time X. Thus at the centre of the particles in size group j, $I = L_j$, we have the following Equation equivalent to Equation 2.56

$$F(I) = \frac{dY(I)}{dX} = \frac{4}{K_j^2}\frac{Q[Y(I)]}{(\Delta Z_j)^2}\left[Y(L_j+1) - Y(L_j)\right] \qquad (2.110)$$

At the nodes along the pores, $Lj < I < Lj+(nj-1)-1$, the program solves Equation (2.111) which is the equivalent of Equation 2.57

$$F(I) = \frac{1}{K_j^2}\frac{Q[Y(I)]}{(\Delta Z_j)^2}\left[\frac{2I-2L_j+1}{2I-2L_j}Y(I+1) - 2Y(I) + \frac{2I-2L_j-1}{2I-2L_j}Y(I-1)\right] \qquad (2.111)$$

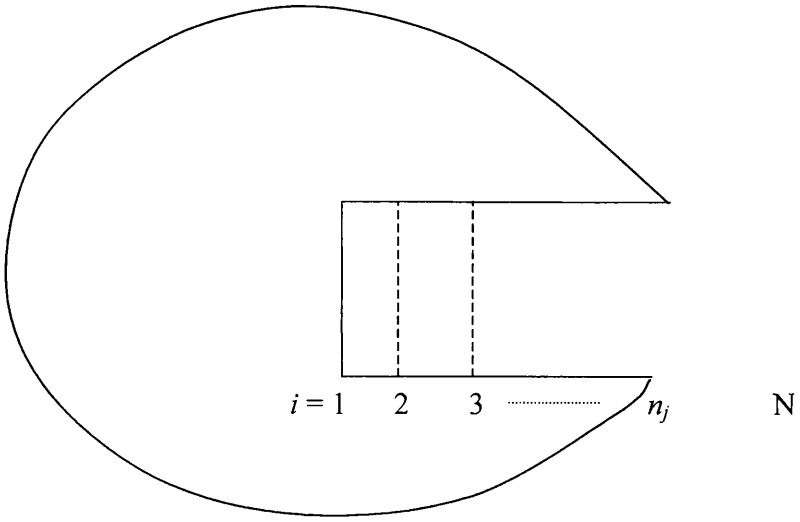

FIGURE 2-12: *Schematic representation of pore increment in a particle.*

At the surface of the particles, $I = L_j+n_j-1$, the differential equation solved [Equation 2.112] is equal to Equation 2.58

$$F(I) = \frac{1}{K_j^2}\frac{Q[Y(I)]}{(\Delta Z_j)^2}\left\{\left[\frac{2(2I-2L_j+1)}{2I-2L_j}N_{Sh,j}\Delta Z_j\right]Y(I+1) + \left[-2-2\frac{(2I-2L_j+1)}{2I-2L_j}N_{Sh,j}\Delta Z_j\right]Y(I) + 2Y(I-1)\right\} \qquad (2.112)$$

For the bulk liquid, at $I = 1+\sum_{j=1}^{M} n_j = N$, the differential equation is identical to Equation 2.59

$$F(I) = \frac{dY(N)}{dX} = -2VAL\varepsilon \sum_{j=1}^{M} N_{Sh,j}\left[Y(N) - Y\left(L_j + n_j - 1\right)\right] f_{L,j} \qquad (2.113)$$

where $VAL =$ Volume of all adsorbent particles/Volume of liquid $= V_{ap}/V_L$ (i.e. the solid to liquid ratio).

$$Q[Y(I)] = Q(S) = \frac{C_O^2\left(\frac{K_d}{C_O} + S\right)^2}{C_O^2\left(\frac{K_d}{C_O} + S\right)^2 + B}$$

Where $B = q_m K_d (1-\varepsilon)/\varepsilon$

Thus at each time step, N equations are solved to predict new concentrations at the nodes $I = 1$ to $I = N$. In the computer program, the expression $Q[Y(I)]$ appears in place of F in Equations 2.56 – 2.59 as the subroutine is pre-programmed with a different meaning of F.

2.9.3 Packed Bed Program Development

The schematic representation of the pattern employed by the program for the solution of the packed bed model is shown as a mesh in Figure 2-13. N_x is the number of divisions or nodes along the bed length. The number of particle size groups is M and thus the total number of nodes for the particles in each bed section is N_m. The solution scheme for the particles in each bed section is the same as that described for the stirred cell mode in Figure 2-12. The node at the centre of the particles in different size groups is labelled L_j and the system of differential equations to be solved at each time step, denoted by the counter I, runs from the centre of the particles in size group 1 (j = 1), bed section 1 (k = 1), to the surface of the particles in size group M as depicted in the diagram.

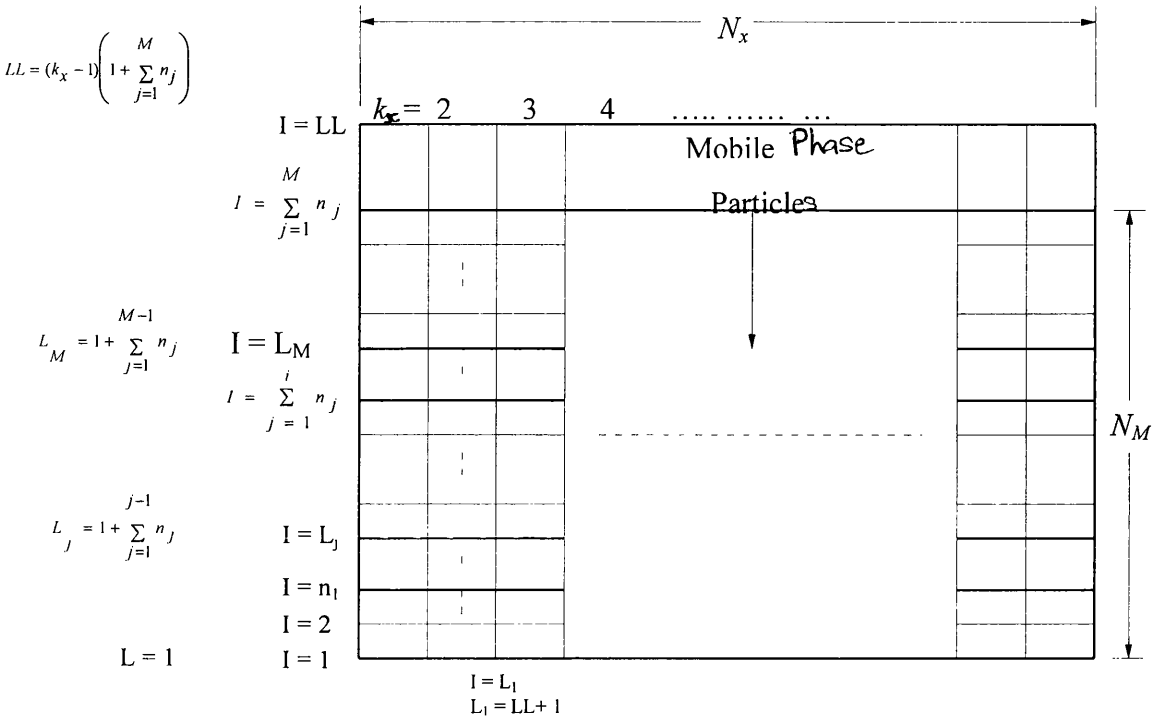

Figure 2-13: *Schematic representation of the mesh for solving the packed bed model.*

The equations describing the rate of change of concentration at the centre, interior nodes and surface of the particles are the same as those for the stirred cell mode viz:

At the centre of the particles in size group j, bed section k, $I = L_j$, we have

$$F(I) = \frac{dY(I)}{dX} = \frac{4}{K_j^2}\frac{Q[Y(I)]}{(\Delta Z_j)^2}\left[Y(L_j+1) - Y(L_j)\right] \tag{2.114}$$

At the nodes along the pores, $L_j < I < L_j + (n_j - 1) - 1$,

$$F(I) = \frac{1}{K_j^2}\frac{Q[Y(I)]}{(\Delta Z_j)^2}\left[\frac{2I - 2L_j + 1}{2I - 2L_j}Y(I+1) - 2Y(I) + \frac{2I - 2L_j - 1}{2I - 2L_j}Y(I-1)\right] \tag{2.115}$$

and at the surface of the particles, $I = L_j + n_j - 1$,

$$F(I)=\frac{1}{K_j^2}\frac{Q[Y(I)]}{(\Delta Z_j)^2}\left\{\left[\frac{2(2I-2L_j+1)}{2I-2L_j}N_{Sh,j}\Delta Z_j\right]Y(I+1)+\left[-2-2\frac{(2I-2L_j+1)}{2I-2L_j}N_{Sh,j}\Delta Z_j\right]Y(I)+2Y(I-1)\right\} \quad (2.116)$$

For the nodes in the mobile phase labelled LL, where $I=LL=(k_X-1)(1+\sum_{j=1}^{M}n_j)$, the differential equation to be solved is

$$F(I)=\frac{R_{LS}^2U}{X_TD}\frac{\left(Y(LL-N_m)-Y(I)\right)}{\Delta X_k}-2\varepsilon\frac{(1-\varepsilon_b)}{\varepsilon_b}\sum_{j=1}^{M}N_{Sh,j}\left(Y(I)-Y(L_j+n_j-1)\right)f_{L,j} \quad (2.117)$$

The packed bed model for particle size distribution involves a very large number of differential equations compared with that of the stirred cell. This is due to the fact that the total number of points calculated for each stirred cell simulation, for a particular adsorbent type per time step, is multiplied by the total number of bed sections in order to get the packed bed profile for the same adsorbent. This added complexity increases the computational requirement both in terms of computer memory capacity and CPU time.

The program for predicting concentration profile for the desorption of the packed bed, which is quite similar to the program for the packed bed adsorption but for the initial boundary conditions, is given in Appendix B3. For adsorption, the concentration profile at the bed inlet used is

$$\begin{cases}C=0.0 & t<t_0'\\ C=C_0 & t\geq t_0'\end{cases}$$

That is protein concentration is zero throughout the bed at time t = 0, for the adsorption program, where t_0' is the hold-up time needed for the flow from the sample inlet of the system to the bed inlet. For the desorption process, the concentration profile at the bed inlet used is

$$\begin{cases}C=C' & t<t_0'\\ C=0.0 & t\geq t_0'\end{cases}$$

where $C' \leq 1.0$, depending on whether the run was terminated before equilibrium was achieved in the adsorption phase or not, at time $t = 0$) (i.e. the bed is initially loaded with protein to some extent).

CHAPTER 3

MATERIALS, EQUIPMENT AND EXPERIMENTAL METHODS

3.1 INTRODUCTION

The objective of this chapter is to describe the materials, equipment and experimental methods used throughout this study of the protein adsorption kinetics on cyilindrical porous semi-rigid adsorbent particles. Experimentally, the major studies conducted included measurements of the adsorption equilibrium isotherm and the mass transfer kinetics in stirred cell configuration (batch operation). Adsorption isotherms characterise the equilibrium position of protein adsorption. The equilibrium study provides information for determining the optimum experimental conditions, such as the type and concentration of bonding phase buffer and pH range, for the proposed kinetic studies in batch (and packed bed) experiments. The experimental data on adsorption kinetics have been used to verify the models developed in Chapter 2. The measurements and measuring techniques, such as the particle size and size distribution, protein concentration, etc., are also described in this chapter.

3.2 MATERIALS

3.2.1 Adsorbates

The protein used in this study is Bovine Serum Albumin (BSA). BSA is extracted from the blood of cattle and is available in substantial quantities commercially. It is a large molecular weight (MW) protein (MW ~ 67000) [62], when compared to Myoglobin (Mb), molecular weight ~ 16890, with an isoelectric point at pH of 4.8 [62]. Molecular weight values of 66300 [18] and 66500 [3], and pH 4.7 - 4.9 at isoelectric point have also been successfully applied in previous kinetic studies using BSA.

The hard sphere radius of BSA can be approximated using the following molecular volume equations proposed by Cantor and Schimmel [51], for a completely isolated molecule:

$$V_h = \frac{M}{N_A} v \tag{3.1}$$

Where M is the molecular weight, N_A is the Avogadro's number (6.02×10^{23} molecules/g-mole) and v the specific volume (0.734 cm^3/g for BSA, [51]). Assuming that BSA is a spherical molecule then:

$$V_h = \frac{4}{3}\pi a^3 \tag{3.2}$$

Where a is the hard sphere radius.

Bowen and Williams [63] have given the hard sphere radius of BSA as 2.69 nm, and estimated its molecule hydrodynamic radius to be 3.2 nm. The later result appears to be in agreement with values from diffusivity measurements and that of Arnold *et al.* [25] about 3.6 nm (36 Å). A hard sphere radius of 3.2 nm as obtained by Bowen *et al.*, will be used throughout this study since it has been successfully applied previously [3 and 17].

Sigma Ltd supplied the BSA used in the present study, catalogue No A7638, and Lot No. 76F9302. The sample is a lyophilised powder, basically globulin free and of purity ≥ 99%. It is a further purified form of the fraction V powder of purity 96% (Sigma A4503) prepared by a modification of the Cohn method [64]. Its main properties are listed in Table 3-1.

3.2.2 Adsorbents

The adsorbents studied are semi-rigid porous (granular) particles supplied by the Whatman company. The process of manufacturing granular cellulose adsorbents have been well documented in by Edwards [65]. The method used by Whatman for the manufacture of DEAE cellulose is briefly explained. Cotton linters are treated with

concentrated sulphuric acid to remove the amorphous regions of the cellulose. This destroys the fibrous nature of the cellulose leaving a crystalline cellulose material. This acid degraded cellulose is then mercerised (steeped in caustic alkali – NaOH – solution) leading to enormous lateral swelling of the fibre and treated with epichlorohydrin to induce cross-linking. The material is then stirred and heated under reflux with an aqueous solution of N,N-diethyl 2-chloroethylamine hydrochloride (to encourage the swelling of the material). A pore forming material such as sodium sulphate or phospate is added before precipitating the material and washing it free of alkali.

The adsorbent materials, Express-ion exchanger D, are roughly cylindrical with average dimensions of between 100 - 150 μm length and 20 - 40 μm diameter, and are made of diethylaminoethyl (DEAE) reconstituted (derivatised) cellulose [Cellulose-O-$(CH_2)_2N(C_2H_5)_2$ (freebase form)]. Express-ion D is a pre-swollen microgranular weak anion exchanger of moderate binding strength in the pH range 3 to 9, and usually binds negatively charged proteins at pH above their pI (anion exchanger). It is more or less basic and has low salt content when dispersed in water. The manufacturers quote a BSA capacity of 0.37 g/dry g for Express-ion D with 0.01M buffer at pH 8.5, and a packing density of 0.24 dry g/ml of column. The particles are irregular in shape and therefore proffer a high surface area per unit weight. The real particle size and size distribution were measured by Microscopy, the method used is described in Section 3.2.8, and the main properties of the material are listed in Table 3-2. The manufacturer states that the material has been extensively de-fined during manufacture.

3.2.3 Buffer Solution

The process of protein adsorption onto an ion exchange medium is pH dependent making it necessary and important that the protein solution is at an optimal pH and ionic state. Once achieved, a constant pH is maintained with the aid of a buffer. The properties of the functional groups on both the protein and the ion exchangers may be affected by both the pH and the salt concentration of the buffer solutions used. Any particular ion exchanger - adsorption system, has a suitable working pH range within which the adsorption capacity is high. The buffer components are themselves charged species that

can interact with the protein and the ion exchanger resulting in a reduction of the binding capacity of the adsorbent. It is therefore necessary to exercise great care in the selection of buffer materials to eliminate any interaction with the adsorption system and to maintain optimum process conditions. The buffer used in this study has been chosen according to previous experimental work and the recommendations of the adsorbent manufacturers: 0.01 M Tris (hydroxymethyl)methylamine (AnalaR) [MERCK Prod No. 10315] solution, used with 1.2 g/l sodium chloride (AnalaR) and titrated to pH 7.5 with hydrochloric acid; and tested by trial adsorption experiments. The buffer solution was used in all dilutions/preparation of protein, slurry preparation, sample pre-equilibration, equilibrium isotherm studies and adsorption studies. The characteristics of the buffer used in the equilibrium and kinetic studies are given in Table 3-3, and the preference will be discussed in chapter 4.

The buffer was prepared by dissolving the salts in de-ionised water, which was produced in the Department by membrane filtration and reverse osmosis to remove solid particles and unwanted ionic species. The pH of the buffer solution was adjusted by titrating with hydrochloric acid and sodium hydroxide solutions. All experiments were performed with added traces of sodium chloride as described in the previous paragraph to control the adsorption as required, but not to stabilize the protein as in the case of experiments with Myoglobin [17].

Materials	Molecular Weight	pI	Ionic Groups	Molecular Size
BSA ≥ 99%	67000	4.8	$-COO^-$, $-NH_3^+$	14 × 4 × 4 nm

TABLE 3-1: *Properties of BSA.*

Name	Functional Groups	Specification	Working pH	Application
Express-ion D: 20 µm	$-CH_2CH_2COOH$	Weak anion exchanger	3 - 9	binds protein at pH_S above its pI; general protein & peptide purification; chromatofocusing with simple buffers

TABLE 3-2: *Properties of ion exchanger material.*

System	Buffer	Concentration	PH
BSA – Express-ion D	0.01 M Tris (hydroxymethyl)methylamine	0.01 M	7.5

TABLE 3-3: *Buffer.*

3.2.4 Preparation of BSA Solutions of Desired pH

The 0.01M Tris buffer solution has very weak buffering effect in ion exchange systems especially at pH values below 6.0. The pH necessary for optimum adsorption for BSA and Express-ion D as in the present study is 7.5. However, when dissolving BSA in the buffer solution at pH 7.5, a slight decrease in the pH of the system was observed. The observed decrease in pH varies with changes in the BSA concentration, generally the higher the concentration the greater the pH decrease. The decrease however was monitored for the protein concentrations used in this study and observed not to significantly lower the pH of the solutions as to required special preparation techniques other than to dissolve the protein directly in the required volume of buffer solution.

3.2.5 Determination of the Adsorbent Dry Weight

The dry weight of the Whatman Express-ion D cellulose anion exchange media was determined by drying a 2 g pre-swollen sample at 60 °C until a constant weight. A low temperature was used to avoid any decomposition of the sample. The moisture content of the sample was determined to be 65.3% of the pre-swollen sample weight agreeing with 65.6% independently obtained by Micromeritics (U.K. Ltd) and agreeing, roughly, with the value of 67.1% quoted by the adsorbent manufacturer. This gives the sample dry weight as 0.35 g/g-swollen ion-exchanger.

3.2.6 Adsorbent Sample Pre-equilibration

All adsorbent samples used in this study were pre-equilibrated with buffer before use, to ensure uniform adsorption behaviour for both the adsorption and isotherm studies. A

sample of the pre-swollen adsorbent was dispersed in an initial 0.2M buffer solution in a 1:5 w/v ratio, following the procedure Whatman advised. The resulting slurry was titrated with a 0.5M hydrochloric acid solution to pH 7.5 and allowed to settle for 2-3 hours.

The supernatant solution was removed almost to the level of the settled ion-exchanger and the slurry brought back to the initial volume by the addition of dilute buffer (0.01M Tris, pH 7.5 and 1.2 g/l NaCl), this being the buffer concentration required for the subsequent chromatography.

After dispersion and settling, the supernatant was removed as in the last paragraph and the slurry dispersed once more in dilute buffer. After the ion-exchanger had settled, the supernatant was removed down to the volume of the settled exchanger plus 20%.

3.2.7 Adsorbent Density Measurement

The true density (solid density) of the adsorbent was determined using a 25 ml density bottle and a sample of the adsorbent particles of about 1 g weight. The density bottle was weighed, filled with water, weighed again and then warmed on a water bath to 75°C for 2 hours and excess water wiped off. The bottle was then cooled down to 25°C, at which temperature the bottle (with contents) was again weighed. The bottle was cooled down to 25°C because this was the temperature at which the density measurement was to be taken. The volume of water left in the bottle is determined from the mass of water left in the bottle and the density of water at this temperature.

After emptying and drying the bottle, its weight was again measured and then 1 g of adsorbent particles put inside it. The density bottle with the adsorbent sample in it was filled with water and warmed to 75°C for 2 h on a water bath to promote the replacement of air by water in the pores of the particles. The bottle was then cooled down to 25°C and weighed with its contents. The density of the adsorbent is then determined by dividing the mass of adsorbent in the mixture by its volume. The mass of water in the

mixture is determined by subtracting the mass (1g) of adsorbent used from the total mass of the mixture. The volume of the adsorbent sample is determined by subtracting the volume of water in the bottle at this stage (determined from its density at 25°C and the mass of water in the mixture) from the volume of water left in the bottle after the original measurements with only water (as described in the previous paragraph).

This procedure assumes that the water diffuses into the pore spaces completely (as the temperature increase lowers the density of the water and the wetting angle), and thus the density measurement is the solid density. The result is given in Table 4-7.

3.2.8 Adsorbent Particle Size and Size Distribution Measurement

A Singer light optical microscope (Singer Instruments Ltd) was used to obtain micrographs of the particles. Image-analysis software 'MOCHA' (Jandel Scientific Ltd.) was used to determine the average diameter of the particles and to measure the diameter across a total of several hundred points closely and evenly spaced along the length of a hundred particles chosen for their clearity, from ten micrographs, in order to get an approximate representation of the adsorbent (Ion D). The particles were then divided into size groups based on their diameters, from which a representative linear-surface mean diameter was calculated for each group. The method used for determining the particle size distribution, through the optical microscope and MOCHA, could be described as an absolute method since the particles are actually observed and measured. Sample micrographs from which the particle size measurements were made are shown in Chapter 4.

3.2.9 Surface Area, Pore Volume and Pore Size Distribution Measurement

The surface area, pore volume and pore size distribution of the adsorbents were measured using liquid nitrogen adsorption and Mercury porosimetry by staff of Micromeritics UK Ltd and MCA Services Ltd respectively.

An intrusion run Micromeritics Autopore IV 9500 porosimeter was used for the mercury porosimetry. The equipment was degassed prior to running the tests but the sample was not pre-treated in order to prevent any form of denaturing. To ensure accuracy of the results obtain with these untreated pre-swollen adsorbents, the radius of the tiny pores within which condensation is likely to occur due to the vapour pressure defect [66] was predetermined to be well below our range of interest (less than 1.0 nm at 25 °C). The results of the test are compiled automatically by an attached data processing unit showing particle intrusion volume, total pore area, average pore diameter, and the median pore diameters (volume and area).

The method of porosimetry is based on the fact that a minimum pressure P is required to force mercury through a pore entrance. This is given by theYoung and Laplace equation (Equation 3.3) for circular pores.

$$P = \frac{2\gamma \cos\theta}{r} \tag{3.3}$$

γ is the surface tension of mercury, r is the pore radius and θ the angle of contact. To determine the pore volume distribution, the cumulative volumes of mercury entering the sample as the pressure is increased is obtained. The pressure is increased in steps and is converted to pore radii using the above equation [53].

The sample is usually evacuated first and then immersed in mercury. Pressure is applied and the amount of mercury penetrating into the pores determined by the fall in the level of the interface between mercury and the hydraulic fluid, with correction made for compression of mercury and the distortion of the interface. It is necessary for the initial pressure to be as low as possible for maximum information because as the mercury is forced into smaller and smaller pores, as pressure is increased, problems such as the fracture of pores and the opening up of blind pores are more likely to occur. The method is not applicable to systems where mercury will come into contact with a metal with which it can form an amalgam. Glycerine can be used as an alternative to mercury in such cases.

The results of the intrusion study is summarised in Table 3-7 and the complete result is included in Appendix C1.

A Tristar 3000 surface area and porosimetry analyser (Micromeritics Ltd) apparatus was used for the nitrogen adsorption. A weighed sample of adsorbent which provided a surface area greater than 10 m^2/g was dried at 70°C under vacuum to a constant mass, re-weighed and the sample information entered into the computer. The analysis is fully automated and once the process is complete a detailed report containing a five point BET adsorption and desorption isotherms, and BJH adsorption and desorption pore size distributions is produced by an attached computer. Ashmead [3] summarised the essential elements of the BJH theory in his work. Allen [53] describes, in depth, the principles and procedures of the BET method of measurement. A brief description of some necessary points is given below.

The BET theory is a good foundation for describing the multiplayer adsorption of gases on solid surfaces. For the BET isotherm, the relation between the gas volume adsorbed and relative pressure is established as

$$V = \frac{V_m B p}{(p_s - p)(1 + (B-1)p/p_s)} \tag{3.4}$$

which transforms to the linear form

$$\frac{p}{V(p_s - p)} = \frac{1}{V_m B} + \left(\frac{B-1}{V_m B}\right)\frac{p}{p_s} \tag{3.5}$$

where V is the amount of gas adsorbed at pressure p, volume/g (solid).

V_m is the amount of gas adsorbed for monolayer formation

B is the constant at a given temperature, related to the heat of liquefaction and monolayer adsorption

P is the adsorption pressure

p_s is the saturation vapour pressure (SVP)

1. Surface Area

The experimental results of the nitrogen adsorption on porous particles can be plotted in terms of $p/V(p_s-p)$ as a function of p/p_s, which gives a linear relationship with a slope $(B-1)/V_mB$ and an intercept $1/VmB$. From the values of the slope and the intercept, V_m can be obtained and so the constant B. The surface area per unit mass of adsorbent S_w is then calculated using the following formula

$$S_w = \frac{V_m \sigma N_{AO}}{M_g} \tag{3.6}$$

where σ is the molecular area, $\sigma = 16.2$ Å^2 for N_2 at 77 K

M_g is the molar volume, $M_g = 22414$ cm^3/mol for N_2 at SVP

N_{AO} is Avogadro's Number, $N_{AO} = 6.02 \times 10^{23}$

Substituting the values in Equation 3.6, gives

$$S_w = 4.353 V_m \tag{3.7}$$

Note that the unit for V_m here is cm^3/g(solid) and for S_w is m^2/g(solid).

2. Pore Volume

If the amount of gas adsorbed on the external surface is small compared with the amount adsorbed in the pores, the pore volume is the volume of gas adsorbed at the saturation pressure. Pore volume is calculated using the following relationship

$$V_p = \frac{v_s M_w}{M_g \rho_c} \tag{3.8}$$

where v_s is the volume of gas adsorbed at the saturation pressure , cm^3/g(solid)

M_w is the molecular weight of gas, N_2, $M_w = 28.02$ g/mol

ρ_c is the density of condensed gas, for N_2, $\rho_c = 0.808$ g/cm^3

therefore for N_2 at SVP, we have

$$V_p = 1.547 \times 10^{-3} V_S \tag{3.9}$$

3. Pore Size

The average pore diameter can be estimated from the pore volume and the surface area of the pores once these have been determined. Considering the number of pores, n_p, and assuming that the pores are cylindrical in shape with an average diameter d_p and length L_p, the total volume and surface area of the pores are

$$V_p = \frac{1}{4}\pi d_p^2 L_p n_p \tag{3.10}$$

$$S_w = \pi d_P L_P n_P \tag{3.11}$$

Consequently the pore diameter is

$$d_p = 4\frac{V_p}{S_w} \tag{3.12}$$

The result of the particle pore measurement studies are summarised in Table 3-4 to 3-6 below. The complete result is included in Appendix C1.

Area	m^2/g
Single Point Surface Area at P/Po 0.17971225	0.3156
BET Surface Area	0.3979
BJH Adsorption Cumulative Surface Area of Pores between 1.7 and 300.0 nm Diameter	0.4289
BJH Desorption Cumulative Surface Area of Pores Between 1.7 and 300.0 nm Diameter	0.4591

TABLE 3-4: *Particle Surface Area.*

Volume	cm^3/g
Single Point Adsorption Total Pore Volume of Pores less than 148.6052 nm Diameter at P/Po 0.98680588	0.000788
BJH Adsorption Cumulative pore Volume of Pores between 1.7 and 300.0 nm Diameter	0.001066
BJH Desorption Cumulative Pore Volume of Pores between 1.7 and 300.0 nm Diameter	0.001065

TABLE 3-5: *Particle Pore Volume.*

Pore Size	nm
Adsorption Average Pore Diameter (4V/A by BET)	7.9180
BJH Adsorption Average Pore Diameter (4V/A)	9.9385
BJH Desorption Average Pore Diameter (4V/A)	9.2760

TABLE 3-6: *Particle Pore Size.*

Property	Express-Ion D
Total Intrusion Volume (cm^3/g)	1.083
Total Pore Area (m^2/g)	0.455
Median Pore Diameter (Volume) (μm)	60.089
Median Pore Diameter (Area) (μm)	0.0092
Average Pore Diameter (4V/A) (μm)	9.530

TABLE 3-7: *Intrusion Data Summary.*

3.3 Effect of Drying on Surface Area, Pore Volume and Pore Size Distribution Measurement

When a sample of the pre-swollen Ion-Exchanger was dried at 70 °C and 0.5 mmHg for 90 min, the bulk volume of the particles was reduced by about 50%. Closer examination of photographs taken through an optical microscope (micrographs) revealed that the particles tend to decrease in diameter by about 4% and also decrease in length by about 6%. They had suffered a change in dimensions but no distortion in shape from the drying process. The moisture content had simply been desorbed as described by several researchers [67, 68 and 69] in a physical process and the particle dimensions decreased proportionately.

Molecules of water are adsorbed onto cellulose adsorbents by hydrogen bonding, attaching the water molecules to the available hydroxyl groups of the substrate on the surfaces of the crystallites. Regenerated cellulose contains much greater numbers of available hydroxyl groups than in maximally swollen and mercerised cotton. Under 'normal' drying conditions when the temperature is moderate (below 120°C) the hydroxyl groups bind to each other causing the structure of the adsorbent (cellulose) [69] to pull together.

The adsorbed water molecules are really physically entrapped molecules that do not bond (chemically) or have any stoichiometric relation to the cellulose structure in which they are embedded. The water molecules are inclusion compounds embedded in the morphological and fine structure of the cellulose and do not enter the crystal lattice of the cellulose. However, as the water molecules are desorbed, some of the hydroxyl groups become permanently linked to one another and so cease to be available as potential sorbing points, hence much of the material's hygroscopicity is lost. This is why 'never-dried' regenerated cellulose film is so much preferred when it is desired to study cellulose in its most accessible and most reactive form.

In order to estimate the percentage volume change with drying, a centrifuge tube was filled with samples of the adsorbent up to the 1.5 ml mark (after centrifugation) and placed in an electric oven to dry, at 70°C, to a constant mass. The sample was then taken out and the new volume determined. The volume of the samples in every case had decreased to about 50% (or ~ 0.75 ml) of the original volume put into the centrifuge tubes. The weight also decreased by about 65% as expected (from the dry weight determination experiments in Section 3.2.5), showing that all the moisture adsorbed onto the adsorbent had been lost. Since the same drying process was employed before the BET adsorption experiments, these data on dimensional change are also valid for use in conjunction with the BET results.

In additon to the decreases in bulk volume and particle weight observed from the drying tests above, comparison of the results of mercury porosimetry (on fresh untreated) and nitrogen adsorption studies (on pre-dried adsorbents) shows that there is a practical collapse of the pores within the particles due to drying. This collapse resulted in a thousand-fold difference between the values of the total pore volume and average pore diameter determined from the two methods as expressed in Tables 3-5 to 3-7. The pore surface areas determined by either method are approximately equal, about 0.46 m^2/g in each case (Tables 3-4 and 3-7). This agrees with the explanation that the pore volume and diameter would decrease with drying along with the particle dimension, but the pore surface area should be unchanged. Since the prior drying stage is necessary for accurate results to be obtained from the nitrogen adsorption process, the parameters obtained from the study for calculating particle porosity need to be adjusted accordingly with those from the mercury porosimetry.

3.4 PROTEIN CONCENTRATION MEASUREMENTS

Two types of UV spectrometer or UV absorbance detectors have been used to measure the protein concentration in the solutions prepared. The SP8-400 UV/VIS spectrophotometer was used for isotherm measurements and the Waters 440 absorbance

detectors for stirred cell experiments. This is because the Waters 440 is attached to the stirred cell rig and so it is more convenient to measure random samples with the SP8-400. The mechanism of the measurement is briefly described below. The protein molecules in a protein solution through which an optical beam of a known wavelength (254 nm was used in this study) is passing, absorbs some of the transmitted light. The UV detector measures how much of the transmitted light has been absorbed, the absorbance (ABS), which is related to the protein concentration. In many cases, a linear relationship between the absorbance and the protein concentration is normally obtained up to a concentration of about 5 g/l as a calibration curve from a series of measurements from solutions of known protein concentration. The plot normally curves a little after this range. However, the plot of the absorbance versus the concentration for the linear region is usually extended to cover the desired experimental range. Figure 3-1 shows such a calibration curve for BSA solutions measured by the SP8-400 UV/VIS spectrophotometer for isotherm experiments. The concentration of a real solution may be found from the curve (Figure 3-1) when the UV detector gives its light absorbance reading. Figure 3-2 shows a sample calibration curve measured using the Water 440 detector for stirred cell. In the measurements, the absorbance of pure buffer solution, in which the protein solution was prepared, was measured and taken as the background value of the detector for calibration. During the experiments, the calibration curves were regularly checked.

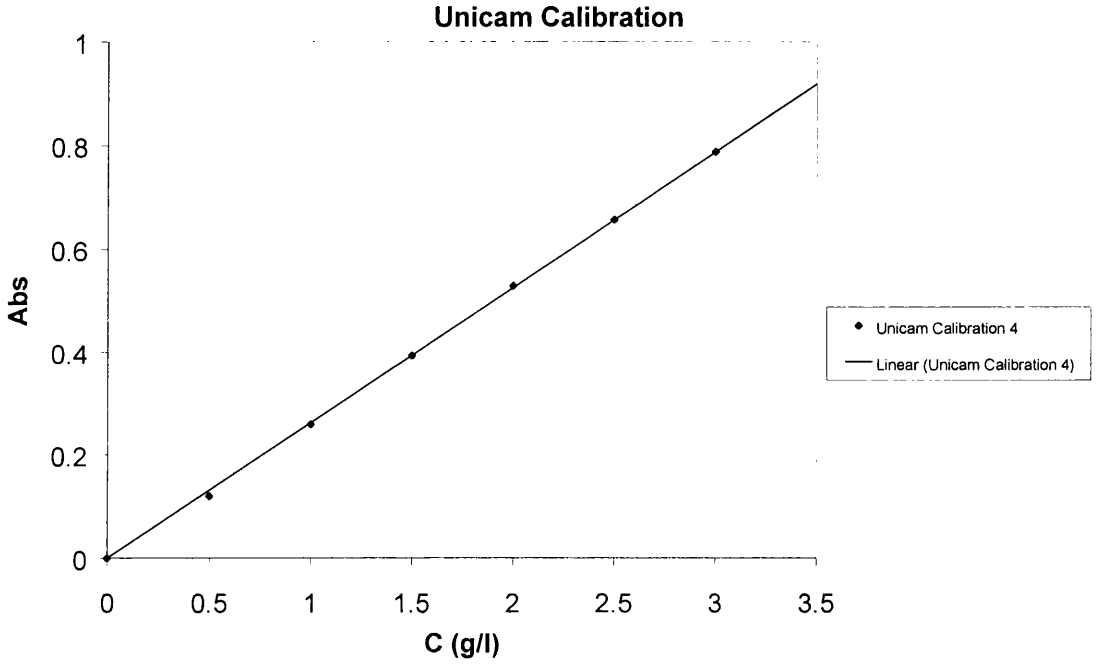

FIGURE 3-1: *Calibration curve of SP8-400 UV/VIS spectrophotometer, the relation of ABS and BSA concentration in 0.01 M Tris buffer.*

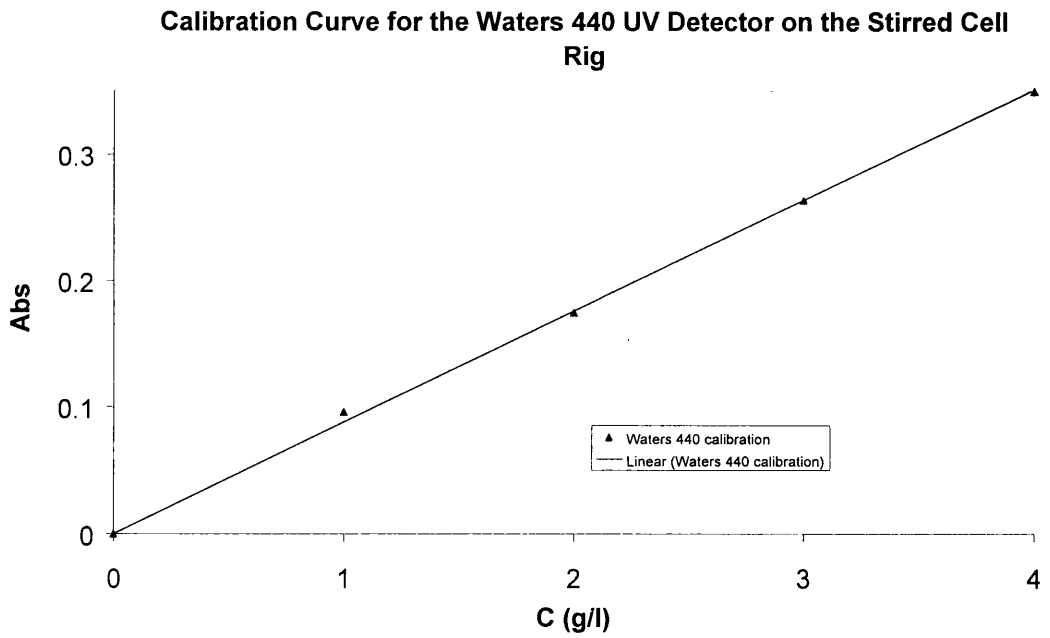

FIGURE 3-2: *Calibration curve of Waters 440 UV detector, the relation of ABS and BSA concentration in 0.01 M Tris buffer.*

3.5 ADSORPTION ISOTHERMS

3.5.1 Introduction

The adsorption isotherms are usually expressed as the amount of the adsorbate adsorbed on a unit mass of adsorbent as a function of adsorbate concentration at equilibrium. The isotherms are dependent on such properties of the adsorbate and adsorbent, as the polyelectrolyte features of the protein material and the surface textures of the adsorbent. They also depend on the conditions under which the adsorption equilibrium is achieved. Different equilibrium conditions will result in different isotherms. The isotherm study was conducted mainly for the purpose of determining the conditions under which reasonably high uptake adsorption can be achieved, as required in industrial operations when the Langmuir type isotherm is applied, as the Langmuir isotherm was one of the basic model development assumptions in Chapter 2. Experimentally, the isotherm of the protein systems was studied by mixing up a certain amount of adsorbent with a certain

volume of protein solution of known concentration at a constant temperature until the concentration of the supernatant solution ceased to change.

3.5.2 Experimental Procedure

The equilibrium isotherm for the adsorption of BSA onto the adsorbents has been determined in the following way.

1. Preparation of BSA Solution

Flaky crystalline BSA was put into a buffer solution in a volumetric flask and allowed to dissolve naturally at room temperature without any mechanical stirring in order to prevent any protein structure damage. The solution was then filtered to remove any visible undissolved materials using filter paper (BDH). The prepared BSA solutions of various protein concentrations were stored in a fridge at 4 °C and were used within 24 hours to reduce the risks of denaturing the proteins and contamination of the solution to a minimum. The concentration of the protein solution is given by the equation

$$C = \frac{M}{V} \times 1000 \tag{3.13}$$

where C is the protein concentration (g/l), M the mass of BSA (g) and V the volume of the liquid (ml).

2. Preparation of Adsorption Samples

To prepare samples for adsorption, a series of 0.4 g samples of the cellulose slurry (1:2) were placed into glass test tubes and a 10-g/l protein stock solution was prepared with 0.01 M Tris, 1.2 g/l sodium chloride and pH 7.5. Samples of the protein stock solution typically in the range 1.0 – 10 ml were added to the slurry in each test tube and diluted with 0.01 M buffer solution to produce 10 ml BSA solutions with concentrations between 1.0 – 10 g/l.

3. Adsorption Process

The sample tubes were then stoppered, inverted twice and put on an electric shaker at a frequency of 1400 Hz in a storeroom and left overnight at a constant temperature of 25 °C for adsorption to take place. Trial experiments were carried out to confirm that equilibrium was reached within 4 hours in most cases. In each isotherm experiment, three blank BSA samples (no adsorbent added) of known concentrations (usually in the range 1 – 3 g/l) were prepared and treated to the same condition as other isotherm samples to ensure that the pure BSA solution was not denatured (no concentration change and no precipitation) over the time course of the isotherm experiment.

4. Determination of the Isotherm

When the samples had attained equilibrium, about 2.5 ml of the sample was taken from each test tube for centrifugation. The samples were centrifuged at a speed of 10,000 rpm for 5 minutes to remove any fines, which may foul the detector. The BSA concentration of the clear solution abstracted after centrifuging was measured with the SP8-400 UV/VIS spectrophotometer as described in section 3.4. The following mass balance can be used to determine the amount of BSA adsorbed by a unit mass of solid particles

$$q^* = \frac{(C_O - C^*) \cdot V}{1000 \cdot W} \tag{3.14}$$

where C_o is the known initial concentration of the protein solution, V the volume of the sample and W the weight of the adsorbent. C^* is the protein concentration left in the liquid phase after the adsorption equilibrium was achieved and was measured by the UV detector. The isotherms were plotted as values of q^* versus values of C^*.

3.6 STIRRED CELL ADSORPTION EXPERIMENTS

3.6.1 Introduction

In the stirred cell (batch) adsorption experiments, the adsorbent particles are freely suspended in the protein solution in a large vessel relative to the size of the particles. The adsorption profile, the concentration of protein in the bulk solution as a function of

time, was monitored throughout the adsorption process. The experimental results were used to provide data for the theoretical model developed in Chapter 2. The apparatus and experimental procedures used for the stirred cell experiment are described in this section.

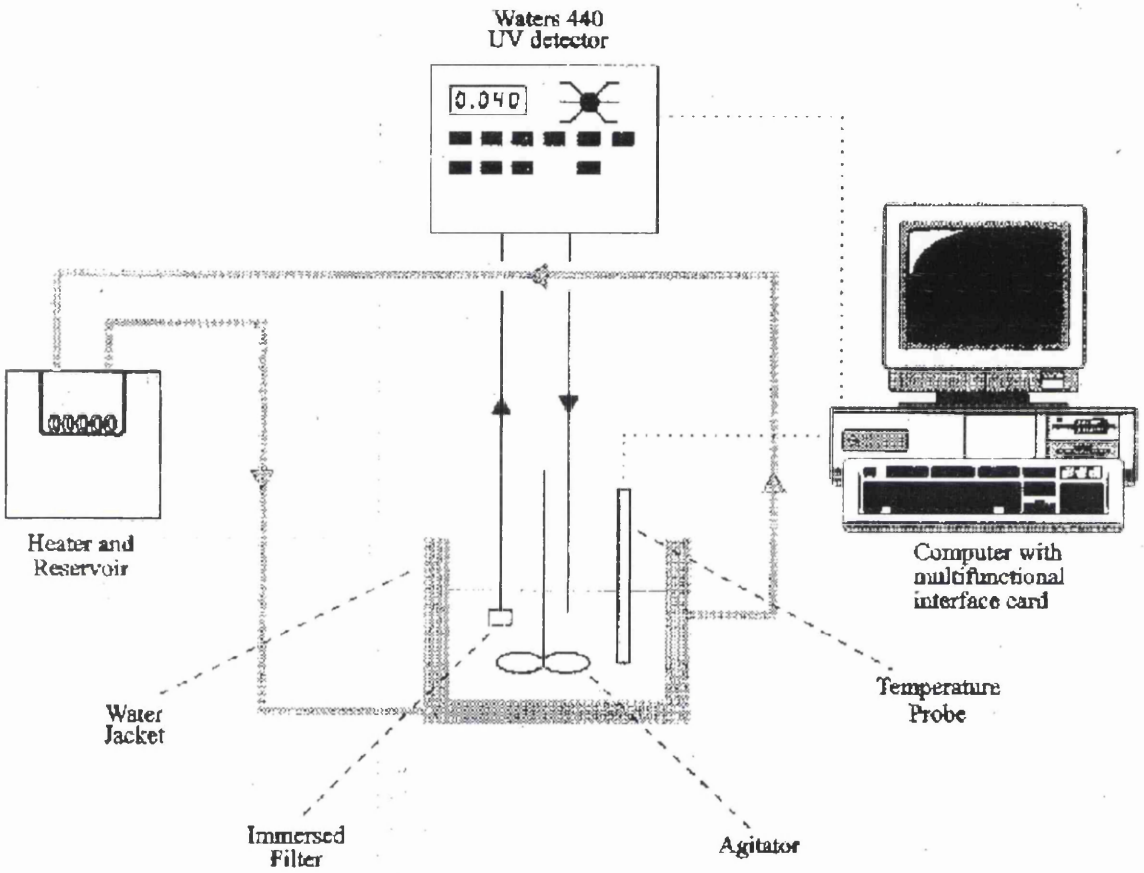

FIGURE 3-3: *The Purpose-Built Stirred Cell Adsorption Apparatus Set-Up.* [3]

3.6.2 Experimental Apparatus

A schematic representation of the set-up for the stirred cell adsorption experiment is shown in Figure 3-3. This apparatus was designed and constructed by a team of

researchers in the Chemical and Biological Process Engineering Department of the University of Wales Swansea [70], for studying protein adsorption and desorption, and has been used by other researchers for such studies [3, 18]. As the diagram shows, the device mainly consists of three units; a tank and stirrer, a protein concentration measuring unit, and a data acquisition and control unit.

1. Stirred Cell Unit

The stirred cell is a glass vessel of about 100 ml in volume, enclosed in a water jacket connected to a circulating water bath to control the temperature of the protein solution in the vessel. A thermocouple probe immersed in the solution measures the temperature. The temperature of the water bath was controlled to ±0.5 °C by a thermostat to keep the adsorption process in an isothermal condition. The adsorption occurred in the vessel where the adsorbent particles were freely suspended in the protein solution by means of agitation using a propeller stirrer (Lab-plant Ltd). The normal stirring speed used was 805 rpm.

2. Protein Concentration Measuring Unit

At the heart of the protein concentration measuring unit is a UV detector, which was fed from a sampling tube in the stirred cell, through a peristaltic pump. The sample tube with an internal diameter of 1.0 mm is made of silicone rubber of biological grade. The protein solution was circulated continuously from the stirred tank through the UV detector by means of the peristaltic pump. A small filter unit was fixed to the inlet of the sampling tube to prevent particles from entering the tube. The unit consists of a 13 mm diameter cellulose membrane filter of pore size 0.5 μm (Millipore, UK) which was supported by a plastic holder. The output of the UV detector (Waters 440 Absorbance detector) was connected to the data acquisition and control unit. The UV detector continuously measures the absorbance (ABS) of the protein solution passing through it. The ABS data were stored in a computer and converted into protein concentration by the calibration curve as shown in Figure 3-2.

3. Data Acquisition and Control

An IBM PC computer with a maths coprocessor and a multifunctional card has been used for the data acquisition and control in the experiments. The output from the UV detector, a voltage signal related to the absorbance of the protein solution, was recorded together with the sampling time by the computer in the form of an ASCII file. A program was developed [71] and used for controlling the start and termination of the experiment, setting the temperature of the water bath and recording the UV detector data as a function of time.

3.6.3 Experimental Procedures

The following procedure was adopted for conducting the stirred cell adsorption experiments.

(1) A zero point of the UV detector was set before the adsorption experiments by taking a stable reading of the background solution (buffer or water).

(2) 60 ml of the protein solution to be tested was loaded into the stirred tank. The protein concentration of the solution was known and this known value was taken as the initial value of the concentration for the adsorption process.

(3) The controlling program was started to set the temperature of the water bath (usually at 25 °C) and the stirrer and pump were turned on. Recording of the UV detector was started to provide the initial protein concentration value.

(4) After the temperature stabilised at 25 °C, the adsorbent material was loaded into the stirred cell. 0.2 g of the adsorbent particles (in slurry form) was added into the cell. For Ion D particles, it was found that since the particle needed to be pre-equilibrated before use and must not be dried, it is necessary to add the material in a slurry state. The samples were pre-equilibrated in the buffer as directed by the adsorbent manufacturer. The adsorbent was put into the tank either in slurry form, with an amount of buffer that made no difference to the adsorption results.

(5) The experiment was kept running until the adsorption process was close to equilibrium about 30 min in most cases or until there was no observable change in the UV reading within a reasonable time interval, usually about 15 minutes.

(6) Finally, the data usually in the form of absorbance (ABS) values against time in minutes were processed to obtain the protein concentration – time profile for the adsorption process. This requires reading off the equivalent concentration in g/l of the ABS values obtained from the stirred cell experiments from the calibration plot in Figure 3-2.

CHAPTER 4

MATERIAL SPECIFICATIONS AND ADSORPTION ISOTHERMS

4.1 INTRODUCTION

The measurements and experimental results of the specific properties and adsorption behaviour of the adsorbents used in this study are described in this Chapter. These include the particle size and size distribution of the adsorbents and the adsorption isotherms of the systems studied. The particle size was measured using a light microscope and the size distributions have been formulated into a mode that can be introduced into the numerical simulation models. The isotherm experiments were conducted using the methods described in Chapter 3 for each system. The main purpose of the isotherm study is to determine the Langmuir parameters q_m and K_D that are required in the process modelling. Other specifications of the materials, such as the porosity and density of the particles, the viscosity and density of the buffers, which are important parameters needed in the modelling process, are also presented.

4.2 ADSORBENT PARTICLE SIZE AND SIZE DISTRIBUTION

The particles used have a nominal average diameter of 30 μm, according to the manufacture, but possess a broad size distribution around this nominal size. This has a great bearing on the results obtained from modelling adsorption processes involving the adsorbent particles. The results of measurement of particle size and size distribution for different particles are presented in this section.

4.2.1 Size Distribution

The micrographs show that the adsorbent particles vary considerably in diameter both from particle to particle and along the length of a particle. The particle length ranges from about 40 μm to 600 μm. The measurement of a sample of individual particles also revealed that there are virtually no fines (i.e. particles of length < 10 μm), as is clear

from the micrographs in the Figures 2-1, 2-4 and 4-1. The assumption in modelling that that end effects can be neglected is therefore justified. The measured mean diameters and size distributions for the adsorbent particles are listed in Tables 4-1 and 4-2. A complete distribution of all the particles sampled in their size groups is given in Appendix A2.

	Total Diameter (μm)	Total Surface Area (μm^2)	d_{NL} (μm)	d_{NS} (μm)	d_{LS} (μm)
Express-Ion D	11,293.73	247,489.26	20.57	21.23	21.91

TABLE 4-1: *The Mean Diameters.*

Size Group (μm)	$f_{L,j}$ (μm)	$f_{s,j}$ (μm)	f_j (μm)	$d_{NL,j}$ (μm)	$d_{NS,j}$ (μm)	$d_{LS,j}$ (μm)
7 – 14.5	0.0658	0.0373	0.1111	12.1906	12.3096	12.4297
14.5 - 22	0.4888	0.4207	0.5392	18.6510	18.7536	18.8568
22 – 29.5	0.3430	0.3915	0.2842	24.8285	24.9203	25.0124
29.5 - 38	0.1024	0.1505	0.0656	32.1153	32.1573	32.1993

TABLE 4-2: *Particle size distribution calculated for Express-ion D.*

4.2.2 The Mean Diameters

In Chapter 2, a number of mean diameters defined for polydisperse particle systems have been given, such as the number-length mean diameter (d_{NL}), the number-surface mean diameter (d_{NS}), the number-volume mean diameter (d_{NV}), the surface-volume mean diameter (d_{SV}) and the length-surface mean diameter (d_{LS}). Their values were calculated from the size distribution data measured by the Image-analysis software MOCHA. The

mean diameters for the material are listed in Table 4-1, they were directly calculated from the micrographs obtained from the optical microscope.

The data (and micrographs) confirm that the Express-Ion D particles have varying cross-sectional diameters over their individual particle lengths, a factor used to classify the particles in groups, each of specified mean diameter, for modelling purposes. The data also reflect the absence of fine particles in the adsorbent material as indicated by the manufacturer. As a direct result of the small range of particle sizes within each size group, the different mean diameters calculated (Table 4-1) are fairly close [17].

FIGURE 4-1: *Sample micrograph showing a cross section of Express-Ion D particles.*

4.2.3 Development of the Particle Size Distribution

In Chapter 2, the particle size distribution for the model was developed by dividing the whole particle size range into a number of size groups. Each size group is characterised by a surface-mean diameter, denoted by $d_{NS,j}$ for group j, which can be derived and calculated from the measured distribution data as described below. The total surface area of particles in size group j may be either expressed as

$$S_j = \frac{\pi}{4} N_j d_{NS,j}^2 \tag{4.1}$$

or

$$S_j = \frac{\pi}{4} N d_{NS}^2 f_{s,j} \tag{4.2}$$

where N_j is the number of particles in size group j, $d_{NS,j}$ the number-surface mean diameter of the particles in group j, $f_{s,j}$ the surface distribution fraction of size group j, N the total particle number, and d_{NS} the number-surface mean diameter of all particles. From Equations 4.1 and 4.2, since $N_j = f_j N$, we have

$$f_{s,j}\, d_{NS}^2 = f_j\, d_{NS,j}^2 \tag{4.3}$$

or

$$d_{NS,j} = \left(\frac{f_{s,j}}{f_j} \right)^{\frac{1}{2}} d_{NS}$$

and $f_j = N_j/N$, the number distribution fraction. The values of $f_{s,j}$, $f_{L,j}$, f_j, and d_{NS} were all calculated from the cross sectional area and mean diameters measured by MOCHA shown in Appendix A2. The calculated values of d_{NS} for each group are given in Table 4-1 for the adsorbent used in this study. Similarly, from the length expressions, we get

$$f_{L,j} d_{NL} = f_j d_{NL,j} \tag{4.4}$$

or

$$d_{NL,j} = \left(\frac{f_{L,j}}{f_j} \right) d_{NL}$$

Dividing Equation 4.3 by Equation 4.4, the linear-surface mean diameter of particles in size group j is given by the following expression,

$$d_{LS,j} = \frac{d_{NS,j}^2}{d_{NL,j}} = \frac{f_{S,j}}{f_{L,j}} d_{LS} \tag{4.5}$$

where d_{LS} is the linear-surface mean diameter of all particles.

In practice, the whole size range of particles was divided into four groups (*i.e.* j = 1, 2, 3, 4) as a good compromise between computing time and accuracy [17]. The influence of the size group number on the simulation result will be presented in Chapter 5. A typical formulation of the particle size distribution for four size groups for Express-ion D adsorbent is shown in Table 4-1.

4.3 ADSORPTION ISOTHERMS

4.3.1 Introduction

Adsorption isotherms characterise the adsorption equilibrium state by describing the relation between the amounts of adsorbate (protein) adsorbed by unit weight of adsorbent and the concentration of adsorbate in the bulk liquid phase at equilibrium. For protein adsorption systems, at present, the isotherms have to be determined experimentally. The experimental apparatus and procedures used in this study have been described in Chapter 3. In this section, the experimental results for the BSA – Express-Ion D system will be presented. All isotherm experiments were carried out at a temperature of 25 °C. The effects of pH were researched while the effects of the buffer and salt concentration on the isotherms were investigated so that suitable conditions could be selected for obtaining

the Langmuir type isotherms with relatively high adsorption capacity for the system concerned. These conditions were then used for the adsorption experiments of the BSA – Express-Ion D system. These conditions were also used for the adsorption kinetic studies (simulation) in the stirred cell model.

4.3.2 Selection of Adsorption Conditions

Environmental factors, such as pH and salt concentration, have strong effects on adsorption isotherms [39, 72]. For protein-ion exchanger adsorption isotherms (e.g BSA – Express-Ion D), pH, buffer type and salt concentration are all important factors that have great influence on adsorption isotherms, while for protein-hydrophobic interaction (e.g Mb-HIC [17]), salt concentration alone is a major factor of concern. These influences will be discussed in this section. Together they provide a guideline for choosing a suitable environment for adsorption experiments.

1. Influence of pH on BSA – Express-Ion D Adsorption

In protein adsorption systems involving ion exchangers, the adsorption process mainly relies on the ionisation of protein molecules, and the ionisation is naturally sensitive to the pH of the medium. In general, at pH below or above the isoelectric point (pI), protein molecules are positively or negatively charged and can be readily adsorbed by ion exchangers. For cation exchangers (e.g. Whatman Express-ion C), protein molecules need to be positively charged, while for anion exchangers (e.g. Whatman Express-ion D) negatively charged protein is required. The determination of the optimum pH depends on achieving the maximum level of ionisation of the protein. Normally, the pH is chosen at a point below (for cation exchanger) or above (for anion exchanger) 1 – 2 units of the pI point of the protein. On the other hand, the pH also has a great effect on the adsorption capacity of ion exchangers. If the pH is taken to extreme values e.g. 4.0 for weak cationic Express-Ion C or about 9.5 for anionic Express-Ion D, the charge on the ion exchanger itself will be suppressed and their adsorption capacity will be lost. Therefore, the choice of ion exchangers according to the pI of the target protein should also be made with the optimum pH range of the adsorbent in mind.

The isotherm for the BSA - Express ion-D system at pH = 7.5 in 0.01 M Tris buffer is shown in Figure 4-4. The results of the isotherm experiments conducted at pH = 7.5 revealed a high enough adsorption capacity of Express-Ion D for BSA (pI = 4.8) to merit the adoption of this pH as the working value for this study.

Co, g/l	1	2	3	4	5	6	7
C*, g/l	0.13	0.21	0.80	1.51	2.33	3.17	4.00
q* g/g solid	0.11	0.15	0.29	0.35	0.38	0.39	0.40

TABLE 4-3: *The relationship between q* and C* for BSA adsorption on Express-Ion D at pH 7.5; buffer is 0.01 Tris +2 g/l NaCl.*

2. Influence of Buffers on BSA – Express-Ion D Adsorption

The buffer materials recommended for anionic exchangers (e.g. Express-Ion D) are acetate, phosphate and barbiturate, borate or Tris (hydroxymethyl)methylamine [Tris] . Whatman have tried and reported satisfactory results for the phosphate and Tris buffer in the literature for Express-Ion D. In the BSA – Express-Ion D adsorption isotherm experiments of this study, two concentrations of Tris buffer have been investigated. Their influence on the BSA adsorption isotherms is shown in Figure 4-2. The Langmuir parameters, q_m and K_D, obtained from the correlation of the experimental data to the Langmuir equation, are tabulated in Table 4-4.

The effects of buffer concentration (0.01 M and 0.02 M Tris) on the adsorption isotherm can be clearly observed from Table 4-4 and Figure 4-2. Less affinity (higher K_D value) and lower adsorption capacity (smaller q_m) were observed for higher buffer concentrations. A similar trend was reported by Li [17] in her work on Myoglobin.

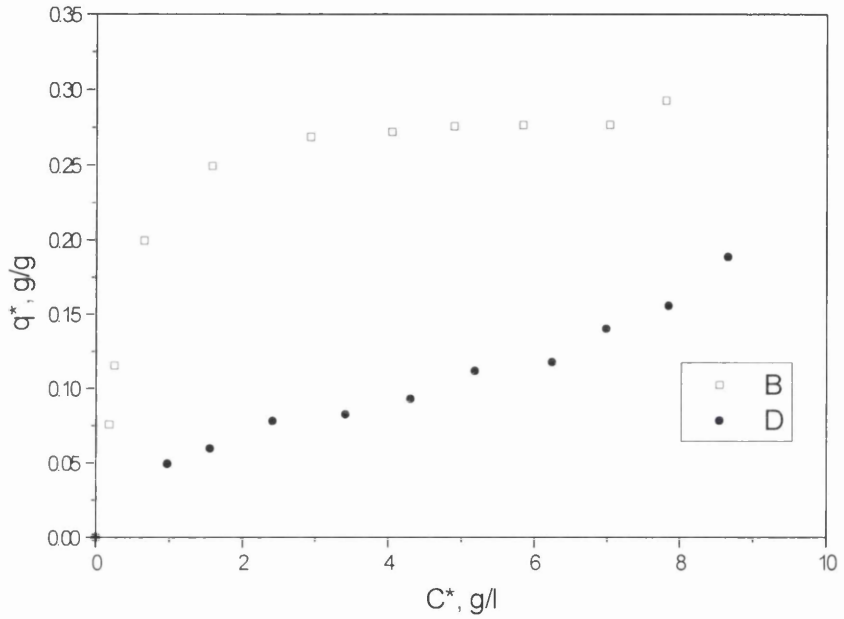

B = 0.01M Tris Buffer
D = 0.02M Tris Buffer

FIGURE 4-2: *Effect of Buffer concentration on BSA-ion D isotherms (5 g/l NaCl).*

The experimental data show that both these buffer concentrations are usable for the adsorption of BSA-Express ion-D systems. However, the higher concentration is not best suited to the present purpose of adsorption kinetics studies because of its high K_D value and low adsorption capacity, also as its isotherm did not fit the Langmuir equation well. Ideal conditions for testing model of adsorption kinetics are; a high capacity (q_m) to permit high relative precision of measurement, curved isotherm well-fitted by Langmuir equation (linear isotherms have the been assumed in the past), and K_D low enough to give strong isotherm curvature (stringent test of model) but high enough to allow a good number of liquid phase concentrations to be determined accurately in the range $0 < q < q_m$.

The 0.01 M buffer shows relatively high adsorption capacity and its isotherms fit the Langmuir equation form well. Tris (0.01 M, pH = 7.5 ± 0.1) was used as buffer for BSA – Express-Ion D adsorption in this study. 1.2 g/l NaCl was added to reduce the steepness of the initial part of the isotherm as a compromise between adsorption capacity and a good fit to the Langmuir equation.

Buffer	K_D, g/l	q_m, g/g
0.01 M Tris (hydroxymethyl)methylamine, pH=7.5	0.38978	0.30062
0.02 M Tris (hydroxymethyl)methylamine, pH=7.5	4.7294	0.18885

TABLE 4-4: *K_D and q_m for BSA – Express-ion D adsorption in different buffers.*

3. Influence of Salt Concentration on BSA – Express-Ion D adsorption

Addition of salt reduces the interaction between protein molecules and the ligands of ion exchanger (adsorbent) particles. Express-Ion D separations can be carried out quite effectively in saltless media, however trace salt quantities were added in this case to reduce the adsorption capacity and to obtain a better Langmuir fit.

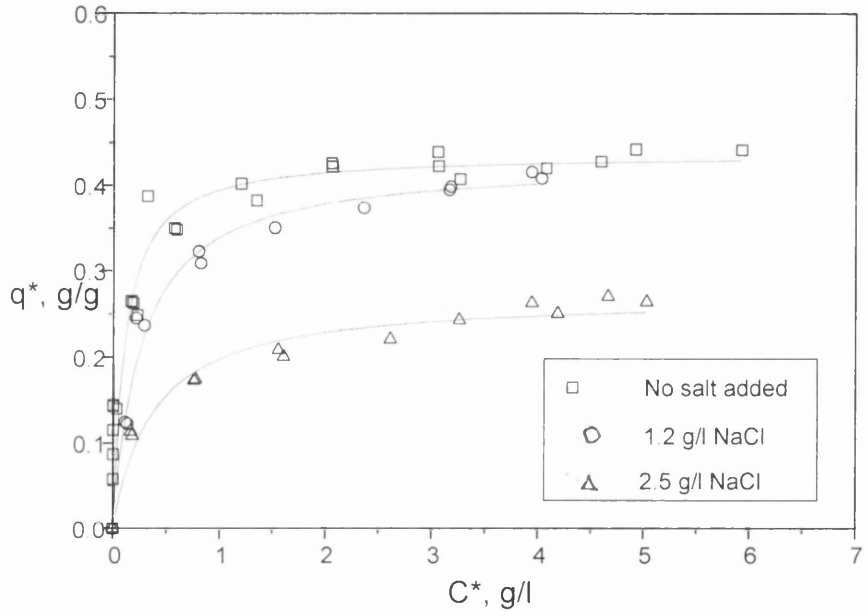

FIGURE 4-3: *Effect of salt concentration on BSA – Express-Ion D isotherms. Buffer is 0.01 M Tris, pH 7.5.*

Salt Concentration (g/l)	Co, g/l	C*, g/l	q* g/g solid
0.0	1	0.03	0.14
	2	0.17	0.26
	3	0.57	0.35
	4	1.35	0.38
	5	2.39	0.37
	6	3.06	0.42
	7	4.37	0.38
	8	4.93	0.44
	9	5.93	0.44
	10	6.51	0.50
1.2	1	0.11	0.12
	2	0.28	0.24
	3	0.81	0.29
	4	1.63	0.34
	5	2.36	0.37
	6	3.18	0.40
	7	3.95	0.44
2.5	1	0.17	0.11
	2	0.77	0.17
	3	1.61	0.19
	4	2.50	0.207
	5	3.21	0.25
	6	4.19	0.25
	7	5.03	0.27

TABLE 4-5: *The relationship between q* and C* for BSA adsorption on Express-Ion D at different salt concentrations; pH 7.5, buffer is 0.01M Tris.*

NaCl is the most widely used salt for ion exchange separations. This is because NaCl produces relatively high ''salting out'' or molar surface tension increment effects. Generally, as the concentration of salt increases, the maximum amount of protein bonded by the ion exchanger particles (maximum capacity) decreases due to competition between protein and salt ions for adsorption sites.

The determination of a suitable salt concentration for BSA-ion D adsorption was approached by analysing the isotherms obtained from adsorption experiments with different added salt concentration. NaCl concentrations of 0.02 M (1.2 g/l), and 0.04 M (2.5 g/l) were tested and compared to the results of saltless isotherm experiments. Figure 4-3 shows the isotherm curves of BSA adsorption on ion-D particles with different salt concentrations.

Less affinity (higher K_D value) and lower adsorption capacity (smaller q_m) were observed for higher salt concentrations. The results indicate that more BSA was adsorbed by Express-Ion D per gram of the dry adsorbent, under a lower NaCl concentration. The shape of the curves also vary with changing salt concentrations to reflect the decreasing interaction between the desired species. This again indicates that 0.01M Tris with 1.2 g/l NaCl is an ideal medium for the kinetic study, compromising between maximum adsorption capacity and best fit to a Langmuir equation on the one hand and an adequate range of liquid concentration for $0 < q < q_m$ on the other. This again is in direct agreement with the similar trend reported by Li [17] in their work on Myoglobin.

The experimental data show that while any of the three salt concentrations can be used for the adsorption of BSA – Express-Ion D systems, the high K_D value and low adsorption capacity of the higher concentration (2.5 g/l) medium is not as useful for the present purpose of adsorption kinetics studies as the 1.2 g/l solution; also its isotherm did not fit the Langmuir equation well. Although the saltless medium showed very high adsorption capacity and good K_D values, its isotherms are arguably more rectangular than they are of the Langmuir equation form. Since the Langmuir equation was assumed in

the development of the mathematical models, the medium with 1.2 g/l of NaCl was judged to be the most suitable for this study.

4.3.3 Determination of q_m and K_D

A Langmuir type of isotherm can be data-fitted in several different forms. A linearised form was chosen to determine the Langmuir parameters. The reason for this choice is that previous workers [3, 17, 18] have all shown this form to fit (marginally) better than the Langmuir curve form in the lower concentration region of interest as can be seen in Figure 4-4. We recall the Langmuir isotherm equation from Chapter 2 as,

$$q = \frac{q_m C}{C + K_D} \tag{4.6}$$

where q_m is the maximum capacity of the adsorbent corresponding to the complete filling of the pores, and K_D is the dissociation constant. These are the two important parameters characterising the isotherm and may be fitted using linear regression from the experimental data. Equation 4.6 can be converted to a linear form in terms of q_m and K_D as

$$\frac{C}{q} = \frac{K_d}{q_m} + \frac{1}{q_m} C \tag{4.7}$$

A plot of C/q versus C is a straight line of slope $1/q_m$ and intercept of K_D/q_m from which K_D and q_m are determined. Attempts were made to use other linear forms of Equation 4.7 but less accuracy was found [18]. A typical C/q versus C plot is shown in Figure 4-5 for BSA – Express-Ion-D system. The linear regression results in q_m = 0.422 g/g(solid), and K_D = 0.339 g/l while the plot of the original Langmuir equation gives q_m = 0.403 g/g(solid), and K_D = 0.288 g/l. The two isotherms differ little at low concentrations but there is a substantial difference at higher concentrations.

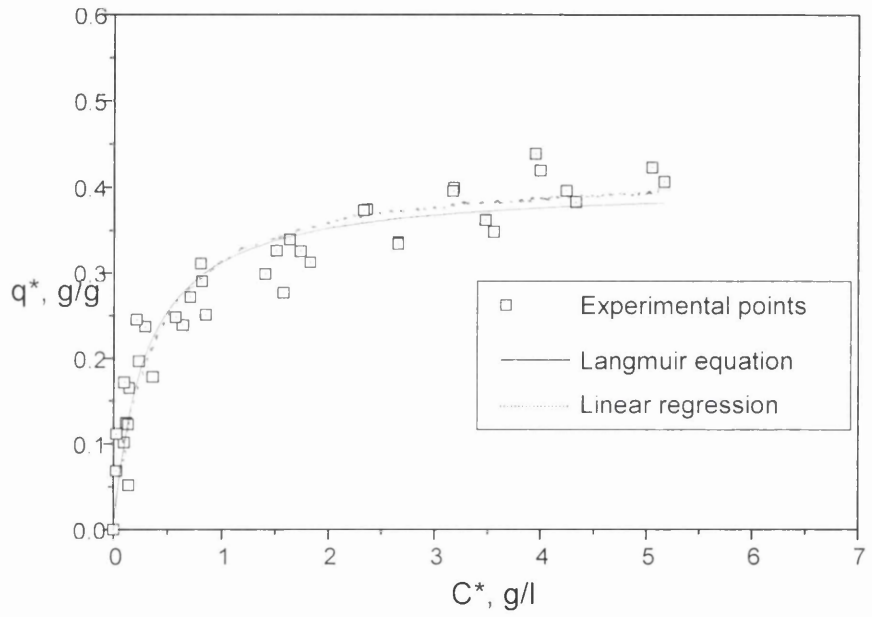

FIGURE 4-4: *Effect of the Langmuir form used on BSA-Express ion-D isotherms. 0.01 M Tris buffer, pH 7.5 and 1.2 g/l NaCl*

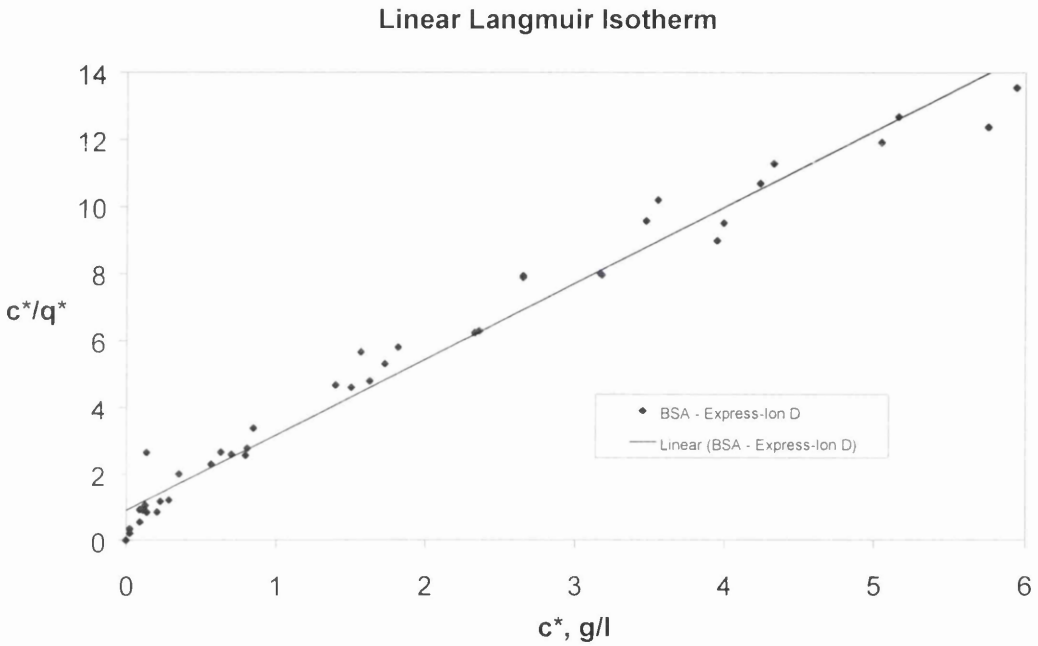

FIGURE 4-5: *Linear relationship between C*/q* vs. C* for BSA-Express ion-D.*

Figure 4-6 shows the effect of the range of points plotted on the shape of the isotherm and thus the value of the Langmuir parameters. The curve of the points up to and including 5.2 g/l has been chosen as a suitable compromise between the maximum adsorption capacity of the adsorbent and the effect of the rise in the isotherm after the region of interest (5.5 g/l) in this research.

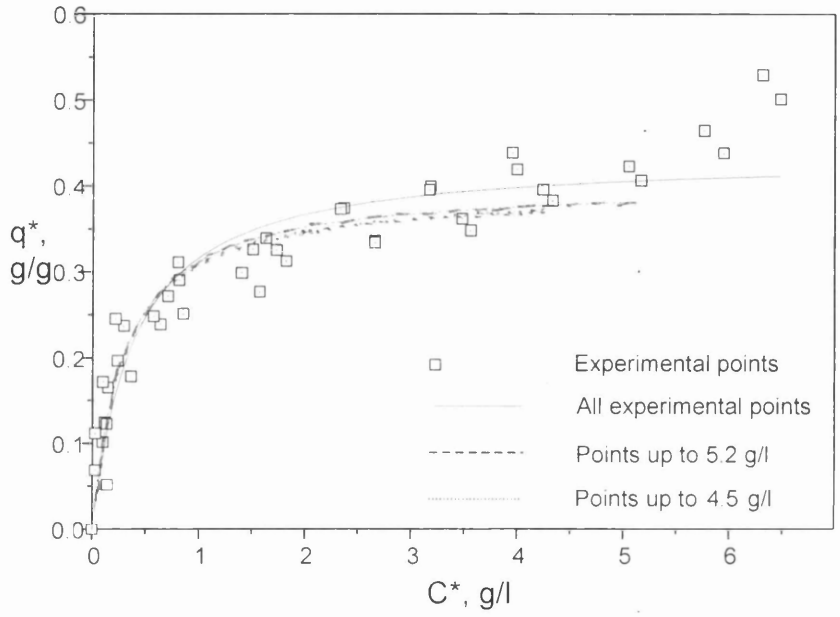

FIGURE 4-6: *Influence of the range of points plotted on BSA – Express-Ion-D isotherms*

A different isotherm or a combination of two or more forms would be required to completely cover the adsorption capacity of the adsorbents in this research. However, the concentration range used and the assumption of a Langmuir isotherm in the model development section of the work means that the middle isotherm (points up to 5.2 g/l) chosen would be sufficient for the purpose of model validation. It was necessary though to improve the fit of the simulated concentration-time profiles for the stirred cell adsorption at the lower protein concentrations 0.4 g/l, 0.77 g/l, and 1.0 g/l by employing

linear empirical fits to the equilibrium isotherm (Figure 4-5) within the ranges 0 – 0.4 g/l, 0 – 1.7 g/l, and 0 – 2.6 g/l respectively.

4.3.4 Isotherms for BSA-Express ion-D systems

The experimental isotherm plot for BSA-Express ion-D systems is illustrated in Figure 4-4, with buffer 0.01 M Tris at pH of 7.5 ± 0.1 and 1.2 g/l NaCl. The values of q_m and K_D determined from the linear regression and the direct plot are listed in Table 4-6. It can be seen that the isotherm is well fitted to the linearised Langmuir equation Equation 4-7. The data also show that the adsorption capacity of Express ion-D obtained is higher than that given by the manufacturer (0.37 g/g dry weight) for the batch used in 0.01 M phosphate buffer at pH 8.5 (in all cases).

Langmuir Form	K_D, g/l	q_m, g/g
Linear regression	0.33859	0.42198
Original Equation	0.28812	0.40327

TABLE 4-6: *Langmuir parameters for BSA-ion D system.*

4.4 DENSITY, POROSITY AND SURFACE AREA OF THE ADSORBENTS

The Solid density, ρ_s, of adsorbent particles was measured using a 25 ml density bottle as described in Section 3.2.7. The porosity of the particles can be calculated from the pore volume and the solid density of the material as;

$$\varepsilon = \frac{V_{PO}}{V_S + V_{PO}} = \frac{V_{PO}}{1/\rho_S + V_{PO}} \tag{4.8}$$

where V_{po} is the pore volume of a unit mass of particles, and V_s is the true solid volume of particles. The pore volume was measured by liquid nitrogen adsorption using the BET approach [53 and 73].

Property	Express ion-D
Nominal particle diameter, μm	20.570
Length-surface mean diameter, μm	21.910
BET surface area, S_w, m^2/g	0.455
Total pore volume V_{po}, cm^3/g	1.083
Mean pore diameter, d_η, μm (BJH)	9.530
Particle density, ρ_p, $10^6 g/ml$	0.446
True solid density, ρ_s, 10^6 g/ml	0.863
Porosity, ε	0.483
Surface density of BSA, mg/m^2	1.130
Protein concentrations, c_o, kg/m^3	0.4, 0.77, 1.0, 1.3, 2.0, 2.5
Diffusivity, D_e, $10^{-11} m^2/s \pm 11\%$	12.5, 5.46, 2.72, 2.72, 0.95, 0.95
Mass transfer coefficient, k_f, $10^{-5} m/s$	Variable

TABLE 4-7: *Adsorbent specifications.*

The method of Jones (Jones 1976) cited by Geoff Leaver in his work on large scale ion-exchange has been successfully used as a mean of cross-checking the value of the porosity determined from the BET equation above.

$$\varepsilon = \frac{q'_m NS_a Gd_r}{4M} \tag{4.9}$$

Where q'_m is the monolayer concentration of protein (kg/kg dry weight adsorbent) based on pore surface area (calculated from the protein adsorption isotherm), N is Avogadro's number, S_a is the surface area of adsorbent occupied by a protein molecule, M is the molecular weight of the protein (69000 g/mole by White et al 1973 – see [17]), d_r is the average pore diameter and G is the pseudo density of the adsorbent (kg dry weight/m^3 of swollen bulk volume). G and ε must be based on the same bulk volume in their denominators. For ε to be the porosity defined by Equation 4.8 then G must be based on (V_{po} + V_S) only, i.e. excluding extra-particle voidage. Similarly the numerator in G must be same as the denominator in q'_m. The latter equation (Equation 4.9) works as a check on Equation 4.8 because it uses the average pore diameter of the adsorbent instead of the total pore volume. The particle porosity was calculated as 0.448 when the maximum value of q'_m obtained from isotherm studies (0.44 kg/kg dry adsorbent) was used.

The results of the measurement of particle solid density, pore volume and BET surface area are listed in Table 4-7. The values of particle porosity are also given. The particle density ρ_p is calculated from the true density and the pore volume V_{po} as

$$\rho_P = \frac{1}{1/\rho_s + V_{PO}} \tag{4.10}$$

4.5 VISCOSITY AND DENSITY OF BUFFERS

The viscosity of the buffer solutions was measured using a Carri-Med rheometer (CS 100, AT Instruments, UK) available in the Department, and the density was measured using a density bottle of 25 ml. Both measurements were carried out at a temperature of 25 °C. The results are listed in Table 4-8.

Solution	Viscosity Ns/m^2 (Pa s)	Density Kg/m^3
0.01 M Tris pH 7.5 + 1.2 g/l NaCl	9.5×10^{-4}	1000

TABLE 4-8: *Viscosity and Density of Buffers.*

CHAPTER 5

STIRRED CELL: RESULTS AND DISCUSSION

5.1 INTRODUCTION

The results of the experiments and simulations conducted on the kinetics of BSA adsorption on Express-Ion exchanger D in the stirred cell mode of operation are presented in this Chapter. The methods, experimental set-up and procedures have been described in Chapter 3. The experimental data are interpreted in the form of protein concentration-time profiles of the bulk liquid phase measured during the adsorption process. The numerical simulations, using the polydisperse two-step model developed in Chapter 2, are fitted to the experimental data by adjusting the value of the effective pore diffusivity to match the experimental data in order to test the validity of the new model. The results of simulations using the two-step model for polydispersity are also compared to the simulation results obtained with the monodispersity model developed previously by the present author [50]. The main factors that may affect the simulation results, such as film mass transfer coefficient, the number of particle size groups adopted in the formulation of the particle size distribution data, and the equilibrium parameters, are also discussed.

5.2 ESTIMATION OF DIFFUSION COEFFICIENT IN FREE SOLUTION

The diffusion coefficient in free solution D_{AB} was estimated using the Geankoplis equation (Equation 2.109) described in Section 2.7.2. The calculated value for BSA (M_A = 66300) at 298 K is shown in Table 5.1 for the liquid solution used.

Solution	μ Ns/m^2 (Pa s)	D_{AB} m^2/s
0.01 M Tris pH 7.5 + 1.2 g/l NaCl	9.5×10^{-4}	7.19×10^{-10}

TABLE 5-1: *Diffusivity in Free Solution.*

5.3 PREDICTION OF LIQUID FILM MASS TRANSFER COEFFICIENT

The liquid film coefficient k_f in the stirred tank for the adsorbents was estimated using the correlation in Equation (2.101) Section 2.7.1. The result is detailed in Table 5.2 for the monodispersity model.

Medium	$k_f \times 10^{-5}$ (m/s)
Anion Exchange (Express-ion D)	5.19

TABLE 5-2: *Liquid Film Coefficient in Monodisperse Model for Express-Ion D.*

The values of k_f for the different particle size groups as used in the polydispersity model are shown in Table 5.3.

Medium	Size Groups ($M = 4$) (μm)	$k_f \times 10^{5}$ (m/s)
Anion Exchange (Express-ion D)	7 – 14.5	6.96
	14.5 – 22	5.37
	22 – 29.5	4.53
	29.5 – 38	3.90

TABLE 5-3: *Liquid Film Coefficient in Polydisperse Model for Express-Ion D.*

5.4 BSA ADSORPTION ON EXPRESS-ION D

5.4.1 Experimental Results

The experimental results for the adsorption of BSA on the adsorbent particles in the stirred cell mode are shown in Figures 5-1 and 5-2. The data are plotted as normalised

protein concentration (C/C_o) in the liquid phase against adsorption time. The profile so obtained is one of a decreasing concentration over the course of the adsorption. The experiments were carried out with different initial protein concentrations (C_o) as indicated in the figures. In the experiments, the values of the initial protein concentration tested were chosen according to the isotherm data. In principle, the range of the initial concentrations tested should cover the main parts of the isotherm curve, i.e. the initial, the curved and the flatter parts, in order to test the validity of the model and also determine the effect of isotherm on adsorption behaviour.

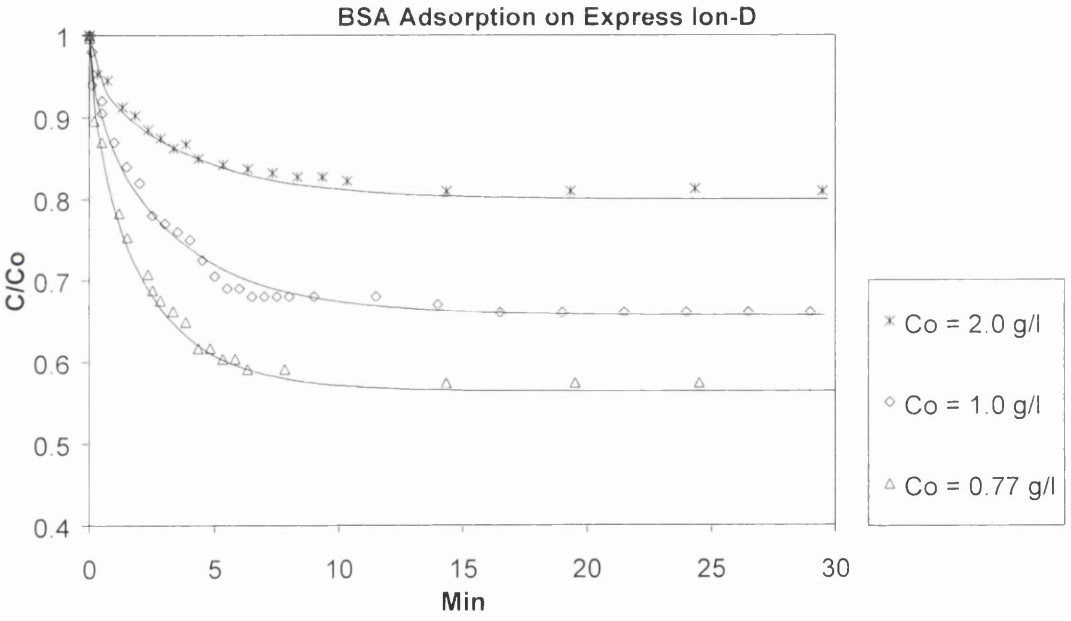

FIGURE 5-1 *Kinetics of BSA adsorption on Express-ion D, experimental data and theoretical simulations.*

The degree of equilibrium attainment, *E(t)*, may be defined as

$$E(t) = \frac{C_O - C(t)}{C_O - C_f} \times 100\% \qquad (5\text{-}1)$$

where $C(t)$ is the protein concentration in bulk liquid measured at time t, and C_f is the concentration when the adsorption equilibrium is reached and is independent of time.

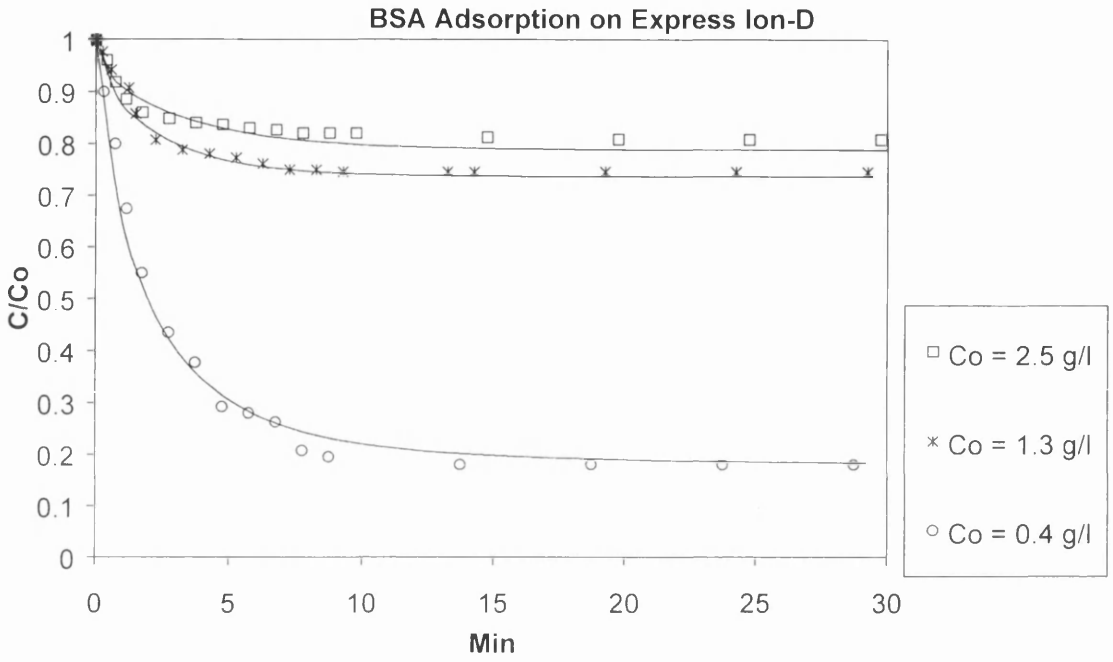

FIGURE 5-2 *Kinetics of BSA adsorption on Express-ion D, experimental data (points) and theoretical simulations (solid lines).*

The experimental results in Figures 5-1 and 5-2 show that the adsorption process reached 95% of its equilibrium attainment [i.e. $E(t=10\ \text{min})=95\%$] in less than 10 min for BSA – Express-Ion D (30 μm)(100% after 20 min), with an initial protein concentration of 0.4 g/l or more, compared with BSA – spherical silica-based PEI system which reached 50% (40 μm) and 80% (15 μm) equilibrium after 20 min respectively [18]. The degree of equilibrium obtained differs from one system to another according to the speed of the process characterised by the kinetic coefficients and may be used as a basis of a very simple, qualitative way of comparing the kinetics for different materials [18]. This comparison is being made since the protein involved in the two cases are the same and

the effect of the surface functional groups, which affect the rate of the surface reaction, is not included in two-step models for simulations.

The large difference in the adsorption rates between these two systems indicates that the cellulosic cylindrical Express-Ion D adsorbents possess a faster mass transfer rate than the spherical silica-based PEI adsorbents. It should be noted that Express-Ion D typically has pore sizes ten times larger than those for the silica based ion exchangers, and that pore structure may have bigger effect than adsorbent shape. The latter point is justified by the larger values of D_e obtained for Express-Ion D compared to silica based Bakerbond adsorbents (Table 6-1). The process of equilibrium attainment is fast for the present adsorption system compared with BSA – spherical silica-based PEI systems. It may be expected that at a fixed time the rod-like cellulosic Express-Ion D particles would reach about two times the degree of equilibrium of the 40 μm silica-based spherical PEI particles and 20% greater degree of equilibrium than the 15 μm PEI particles.

The adsorption process for BSA adsorption seems to proceed at the same rate regardless of the protein concentrations used on the adsorbent (Express-Ion D), Figures 5-1 and 5-2. Up to 85% of the equilibrium was reached in less than 5 min for for all the runs.

5.4.2 Numerical Simulation

Numerical simulation was carried out in the first instance using the previously developed model for monodisperse systems. The monodisperse system can be treated as a special case of the model with the size group number $M > 1$. The parameters required in the simulation were discussed in Chapter 2 (Section 2.7.1 and 2.8). The particle size distribution data can be found in Table 5-5. Four size groups were formulated for the adsorbent. The only unknown parameter is the effective pore diffusivity D_e, which is treated as a fittable parameter in the simulation where its value is varied until a reasonable fit between the simulation result and the experimental data is obtained. As a general rule, automatic fitting was not used though it could be incorporated in the algorithm. It proved more convenient and effective to assess the results visually and

alter values of D_e in steps. This procedure also provides an indication of the results to the sensitivity of the values of D_e in the simulation.

The stirred cell simulated curves at the lower protein concentrations 0.4 g/l, 0.77 g/l, and 1.0 g/l were greatly improved by linear empirical fits to the equilibrium isotherm (Figure 4-5) within the ranges 0 – 0.4 g/l, 0 – 1.7 g/l, and 0 – 2.6 g/l. The simulation results are shown in Figures 5-1 and 5-2 as solid lines along with the experimental data for Express-Ion D. The values of the effective pore diffusivity determined for each concentration and the value of the Langmuir parameter K_d used are tabulated in Table 5-4.

System	*Co* g/l	*t* (min) at *E(t)*=50%	K_d g/l	D_e, m^2/sec
Anion Exchanger (Express-ion D)	0.40	1.7	0.051	12.5×10^{-11}
	0.77	1.2	0.170	5.46×10^{-11}
	1.00	1.7	0.210	2.72×10^{-11}
	1.30	1.4	0.288	2.72×10^{-11}
	2.00	1.5	0.288	0.95×10^{-11}
	2.50	1.0	0.288	0.95×10^{-11}

Table 5-4: *Effective diffusivity determined for Express-ion D in stirred cell.*

The quality of fit between the theoretical and experimental profiles in Figures 5-1 and 5-2 is seen to vary with protein concentration. The experiments at various protein concentrations were generally fitted well by the model except the profile of the experiment at 0.77 g/l which agrees in shape with the experimental plot but fit rather less well in the later stages, showing less protein capacity than the experimental values. It can be seen from the concentration-time profiles that at least 80% of equilibrium was obtained within the first part of the plots in nearly all cases. The diffusion coefficient

has been estimated from the best fits to the initial part of the experimental data, giving the theoretical profiles shown.

5.5 DISCUSSION

5.5.1 Introduction

In macromolecule adsorption involving adsorbed species whose molecular diameter is not much smaller than the pore diameter, the pore diffusion rate, which is usually indicated by effective pore diffusivity, is greatly affected by the steric hindrance at the entrance to the pore and frictional resistance within the pores, as well as the pore size distribution and pore connectivity inside the adsorbent [17]. Due to a lack of understanding of pore diffusion mechanism, the real effective pore diffusivity cannot yet be theoretically predicted, but it can be determined by matching theoretical simulation to the experimental results as described above. The values of the effective pore diffusivity obtained may reflect the total restrictions to protein molecules diffusion inside pores, but their reliability is affected by a number of factors. These include the models adopted and the particle size and pore size distribution data obtained either from limited measurements or by assumptions. The protein diffusion inside the pores is affected by buffer type and salt concentration, and so is the effective diffusivity. In this section, these factors that influence the experimental and simulation results of BSA adsorption on Express-ion D systems will be further discussed.

5.5.2 Effect of Protein Concentration on Determination of Effective Diffusivity

The results from Table 5-4 show that the effective diffusivity depends strongly on the protein concentration. The results of the theoretical simulations indicate that the value of the effective diffusivity obtained for an initial protein concentration C_o = 2.5 g/l is much less than that obtained for an initial protein concentration Co = 0.4 g/l confirming the general trend that the effective diffusivity decreases with increasing protein concentration. The model assumption that the mass transfer parameters are independent of the adsorbate concentration was only satisfied within narrow bands of concentration, particularly in the middle and upper sections of the concentration range chosen.

Liapis [9] and Horstmann [31] assumed in their models that the mass transfer parameters were independent of concentration and found that the assumption was not justified experimentally. Similar results were reported by Hayek [18] in studying the kinetics of protein adsorption onto other spherical adsorbent particles of different sizes. Horstmann [31] studied the affinity adsorption of immunoglobulin G to protein A immobilised to agarose matrices and Hayek [18] studied the adsorption of BSA on particles of both derivatised polyethyleneimine (PEI) and HI-propyl silica-based adsorbents. Hayek [18] was able to detect a linear dependence of the effective diffusivity on the initial concentration.

Cussler [74] has noted that the concentration dependence of the diffusivity can vary greatly with pH and salt concentration. Under conditions of high electrolyte concentration and at the isoelectric point of the protein, where the protein has no net charge and the electrostatic effects are minimal, the diffusion coefficient has a value largely independent of changes in the solution. Under almost any other conditions such as high pH or absence of salt, the diffusion coefficient is strongly concentration-dependent, because of increased protein charge or increased electrostatic coupling. Hayek [18] studied the sensitivity of the concentration dependence of diffusion coefficient to solution conditions in stirred cell kinetics in detail. He successfully used the diffusion coefficient calculated as a function of average concentration to improve the fits of the theoretical profile to packed bed experimental results.

5.5.3 Effect of Particle Dispersity on Adsorption Profiles

The two-step theoretical (polydisperse) model developed in Chapter 2 included the assumption that the surface reaction rate was too fast and thus made an insignificant contribution to the overall resistance to the adsorption rate. The particles were considered to have a considerable size distribution formulated by dividing the whole range of sizes into a number of size groups and each group represented by a mean diameter. In this section, we examine the effectiveness in the simulations of applying the polydisperse model to BSA – Express-Ion D systems.

Figures 5-3 and 5-4 show the adsorption of BSA on Express-Ion D adsorbents with initial protein concentrations of 0.4g/l and 1.0 g/l respectively. The experimental data are shown as scattered points. First, the monodisperse model was used to fit theoretical results to the experimental data by adjusting the values of the effective diffusivity D_e. The uniform particles size chosen was that discussed in Section 4.2.1, d_{NS} = 21.23 μm. Trials with different values of D_e showed that the best fits were achieved with D_e = 12.5 × 10^{-11} m^2/sec for 0.4 g/l and D_e = 2.92 × 10^{-11} m^2/sec for 1.0 g/l. The results are shown in Figures 5-3 and 5-4 as dashed lines. The polydisperse model, d_{LS} = 21.91 μm, was then applied to the monodisperse cases using the size distribution data (by assuming four size groups i.e. M = 4) and the best fitted values of the effective pore diffusivity, 12.5 × 10^{-11} m^2/sec and 2.92 × 10^{-11} m^2/sec. The polydisperse simulation results are shown in the figures as solid lines.

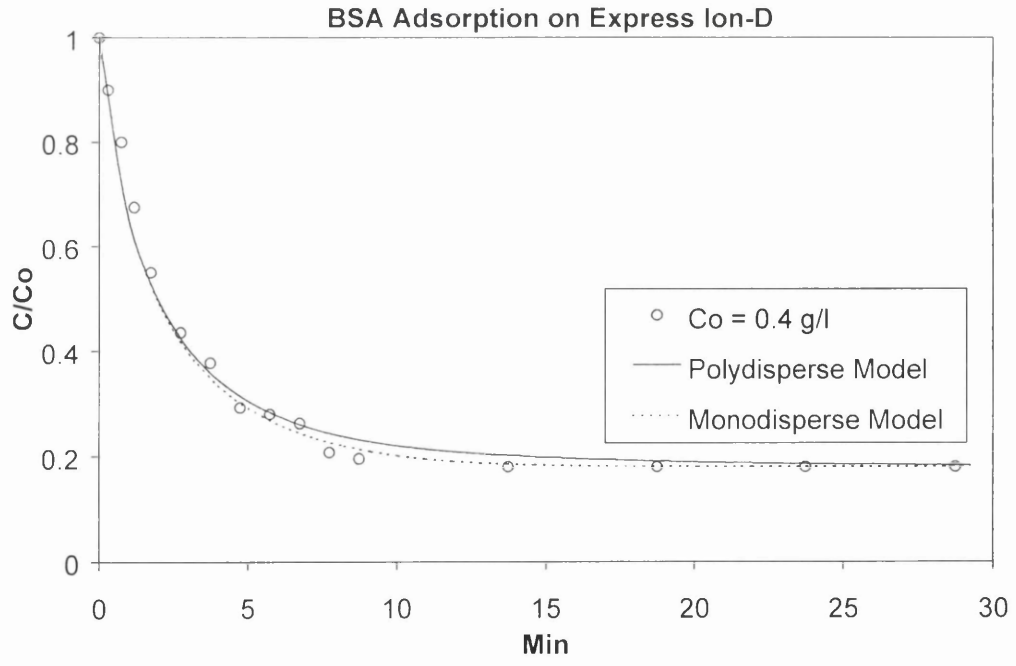

FIGURE 5-3 *Comparison of different models on simulation of BSA on Express-ion D adsorption. Initial protein concentration C_0 = 0.4 g/l.*

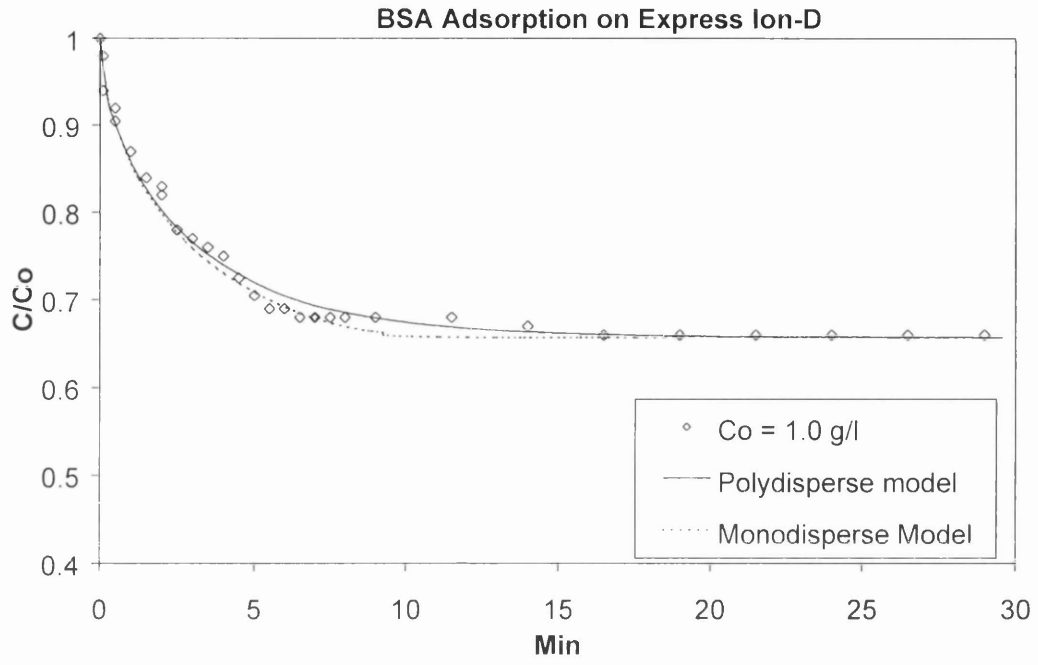

FIGURE 5-4 *Comparison of different models on simulation of BSA on Express-ion D adsorption. Initial protein concentration C_0 = 1.0 g/l.*

The application of a polydisperse model to the stirred cell simulation produced a slightly better fit to the experimental data compared with the monodisperse model. However, the monodispersity curves suggest faster adsorption kinetics than the polydispersity curves, a point better emphasized in the packed bed simulations (Figures 6-7 and 6-8). The implication of this is that a protein adsorption process using uniform particles would be faster than the same process using polydisperse particles of an equivalent mean diameter to the uniform particles.

A small lack of fit occurs in the latter stages at higher concentrations, regardless of dispersity, in some cases (Figures 5-1 and 5-2). This may be attributed to the assumption of a uniform pore size in the model. It is widely accepted that the wider pores fill up first (early stages of the adsorption curve) before the smaller pores (later stages). Pore

sizes have been shown to have a direct influence on the effective diffusivity [75] and the value of the effective pore diffusivity is greatly reduced in narrow pores. The effective diffusivity determined from modelling in the present case is only an average measure of the pore resistance since a uniform pore size was assumed. The current model does not consider the slow diffusion in long narrow pores in the interior of particles that dominate the process in the final stage where a lower effective diffusivity would be expected. This was shown by the slow approach to equilibrium from the experimental data at high concentrations (1.3 g/l, 2.0 g/l and 2.5 g/l).

5.5.4 Effect of Particle Size Group Number on Simulation

The number of the particle size groups used in the simulation is a compromise between the time needed for the solution/computational power and the accuracy of the simulation. This is because the greater the number of size groups used in the formulation of the particle size distribution, the longer the computational time required and the more accurate the simulation. The former becomes important in solving the packed-bed model where a much longer time is needed for a solution than that in the stirred cell model. Li [17] has shown, for a system with very wide size distribution, that the simulation results can be significantly improved by increasing the number of size groups used from one up to four (M=1, 2, 3, and 4 respectively), but when more than four groups were used, the simulation results showed little improvement. Typical results are presented in Figures 5-5 and 5-6 for BSA – Express-Ion D adsorption experiment at initial protein concentrations of 0.4 g/l and 1.0 g/l. The points are the experimental data, while the curves (dotted and solid lines) represent the simulation results with common effective diffusivities of $D_e = 12.5 \times 10^{-11}$ m^2/sec and $D_e = 2.72 \times 10^{-11}$ m^2/sec respectively, for comparison in each case in which M = 1, 2, 3, and 4 were taken in that order. The particle size groups are identified in Table 5-5.

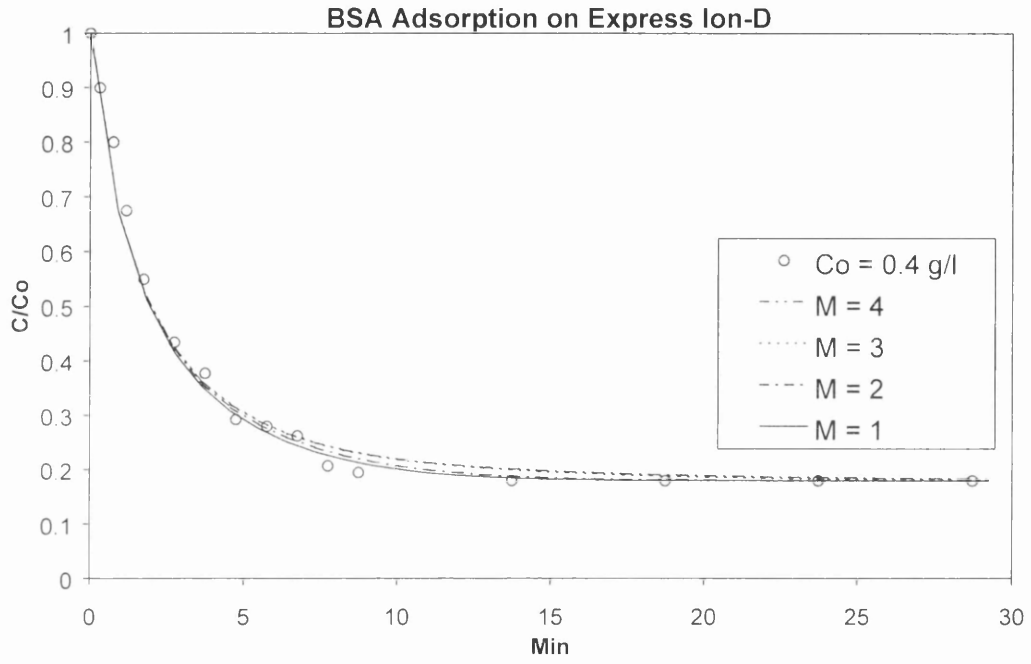

FIGURE 5-5 *Effect of particle size group number on simulation of BSA on Express-ion D adsorption.*

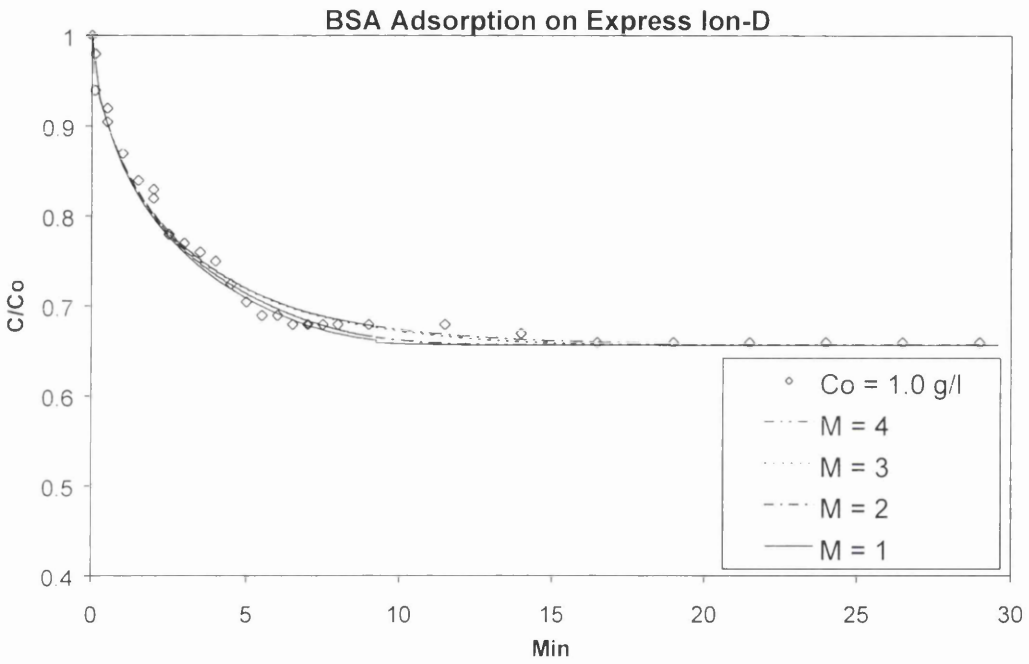

FIGURE 5-6 *Effect of particle size group number on simulation of BSA on Express-ion D adsorption.*

M	Size Range (μm)	d_{NS} (μm)
1	7 – 38	21.23
2	7 – 14.5	12.31
	14.5 – 38	22.09
3	7 – 14.5	12.31
	14.5 – 22	18.75
	22 – 38	26.43
4	7 – 14.5	12.31
	14.5 – 22	18.75
	22 – 29.5	24.92
	29.5 – 38	32.16

TABLE 5-5: *The mean diameters in size groups divided for Express-Ion D*

In the case of M = 1, the fit to the experimental data was mainly poor in the middle stages, but is not completely far off. The poor fit of the single size group fit is more pronounced in the higher concentration 1.0 g/l case. The closeness of the different size group plots clearly indicates that though there is a dispersity in the particle sizes, the particles do not deviate widely from a mean. This fact is also evident in the small differences between the number-linear, number-surface, and linear-surface mean diameters in Tables 4-1 and 4-2.

In the case of M = 2, the smallest size group was set out as one of the two size groups with a mean diameter of 12.3 μm, the rest forming another size group with a mean diameter of 22.1 μm. The simulation shows a quite similar result to that with M = 1, but a closer fit to the experimental points.

When M = 3 and 4 were taken, the fitted results show a great improvement, virtually indistinguishable, but generally appeared to be a near perfect fit to the experimental data in the case of M = 4 for C_0 = 1.0 g/l. The results of M = *3* and M = *4* confirmed the earlier assumption that creating six size groups (M = 6) would not further improve the fitting of the simulation, but would triple the computer time compared to the M = 4 case. So in this study, we took M = 4 as the optimum size group number for the adsorbent investigated. It would however be necessary to use a large size group number to

improve the fitting result in the case of particles possessing a much wider and flatter size distribution than that of both Express-Ion D particles and the silica-based CBX particles studied by Li [17], say 0.48 to 600 μm.

5.5.5 Effect of Film Mass Transfer Coefficient

The value of the mass transfer coefficient, k_f can be calculated using Equation 2.101. In simulation, different values of the mass transfer coefficient were used by assuming k_f/k_{fc} = 0.5, 1.0, 2.0, 5.0, respectively, where k_{fc} stands for the value predicted by Equation 2.101. Clearly, $k_f/k_{fc} < 1$ means exaggerating the effect of slow film mass transfer and vice versa. Figures 5-7 to 5-10 show the simulation results compared with the experimental data for BSA – Express-Ion D at C_0 = 0.4 g/l and 1.0 g/l correspondingly. The figures show clearly that the influence of the film mass transfer coefficient is significant (the profile varies significantly when k_f/k_{fc} changes) when $k_f/k_{fc} \sim 1$ but not when $k_f/k_{fc} \sim 5$. When k_f/k_{fc} = 5 – 10, the value of k_f is high enough for adsorption to be controlled only by the pore diffusion. This implies that the adsorption process is controlled by the liquid film mass transfer coefficient. Attempts have been made to improve the fit to the experimental data by changing k_f and D_e simultaneously. It was found however that the best fit was achieved at around k_f/k_{fc} = 1. A comparison of the results of the monodisperse plots, Figures 5-7 and 5-8, to the polydisperse cases, Figures 5-9 and 5-10 reveals that the effect of the liquid film mass transfer coefficient is independent of dispersity.

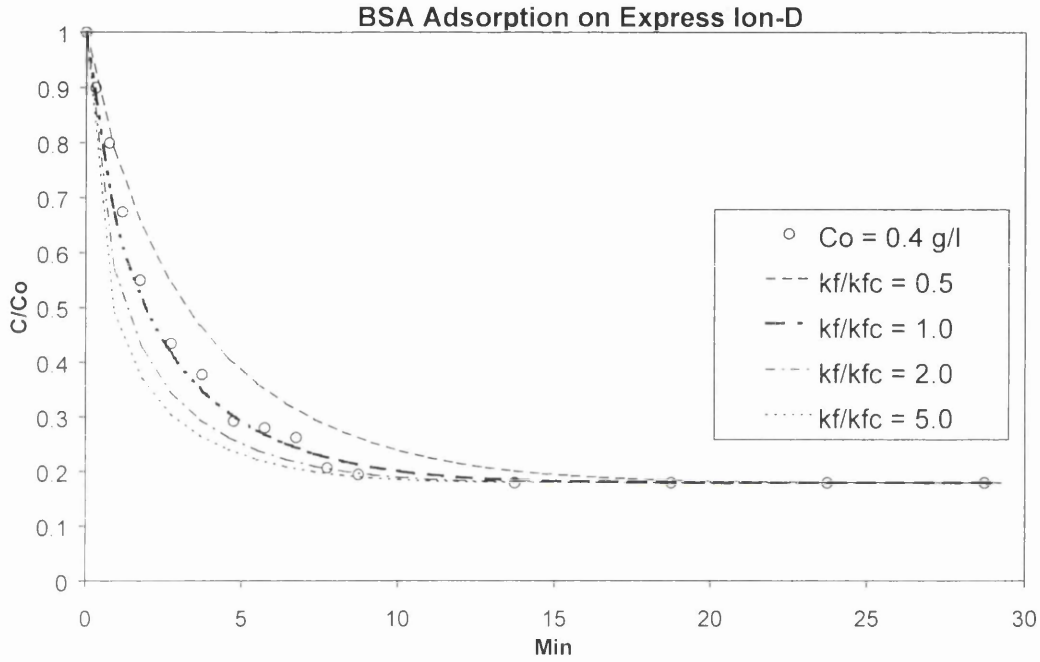

FIGURE 5-7 *Effect of film mass transfer coefficient on simulation of 0.4 g/l BSA on Express-Ion D adsorption (Monodisperse model).*

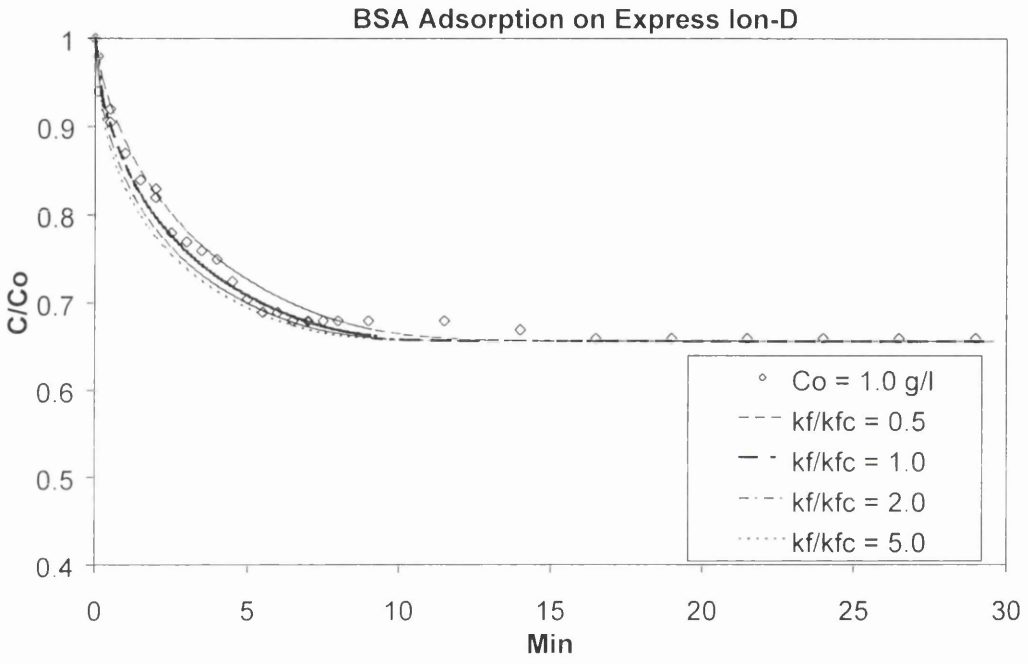

FIGURE 5-8 *Effect of film mass transfer coefficient on simulation of 1.0 g/l BSA on Express-Ion D adsorption (Monodisperse model).*

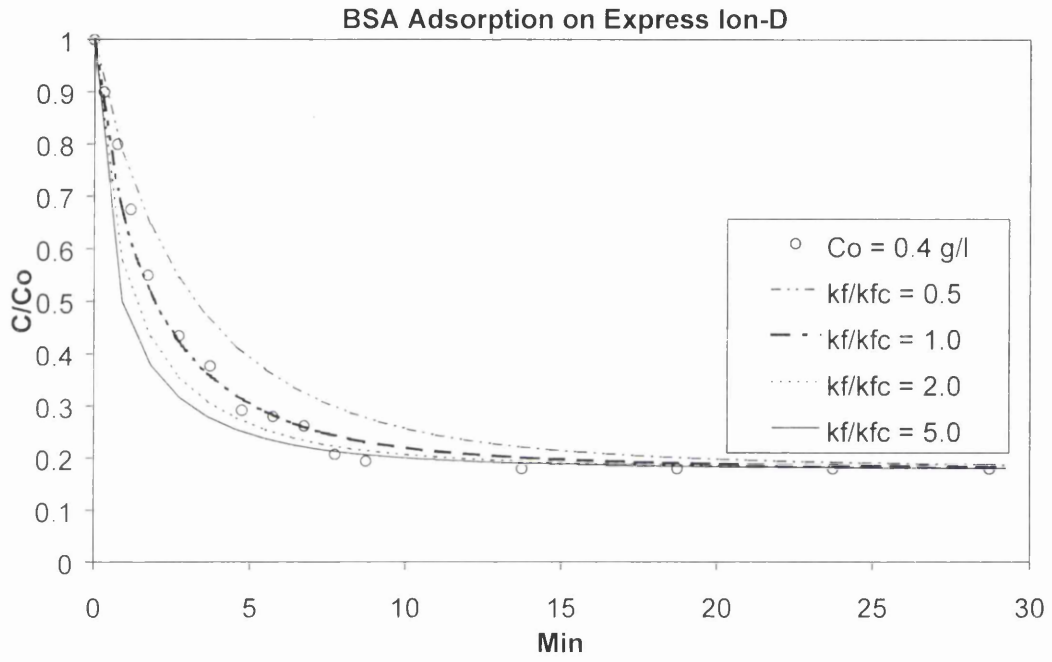

FIGURE 5-9 *Effect of film mass transfer coefficient on simulation of 0.4 g/l BSA on Express-Ion D adsorption (Polydisperse model).*

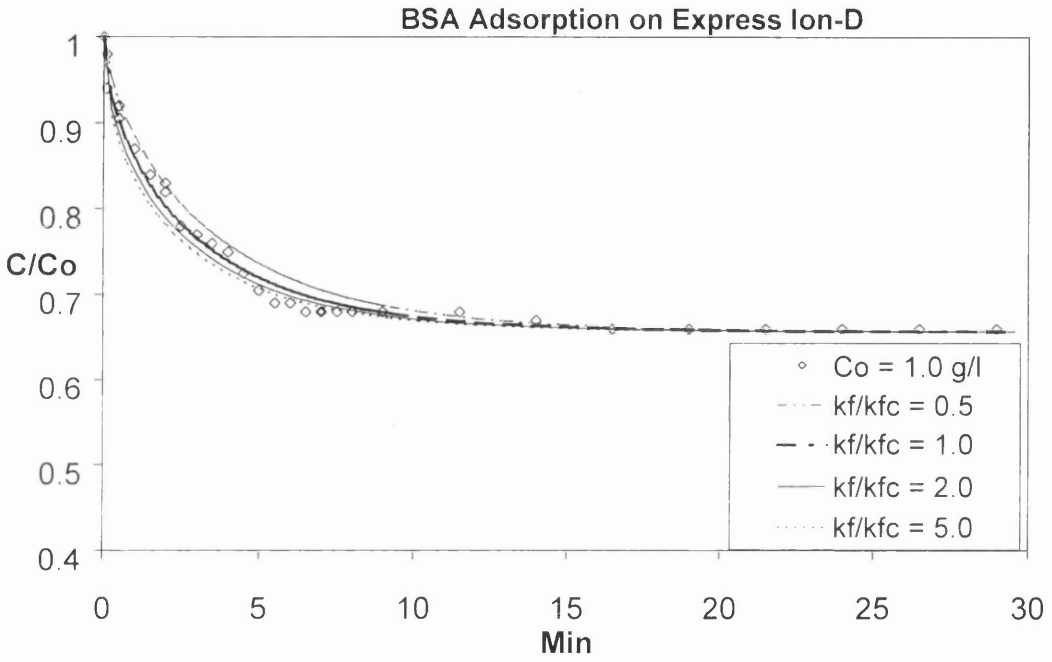

FIGURE 5-10 *Effect of film mass transfer coefficient on simulation of 1.0 g/l BSA on Express-Ion D adsorption (Polydisperse model).*

5.5.6 Effect of the Effective Pore Diffusivity.

The value of the effective pore diffusivity for each concentration-time plot was obtained by eye-fitting the simulated profiles to the corresponding experimental data as described in Section 5.4.2. The influence of effective pore diffusivity on packed bed simulations was studied at initial protein concentrations 0.4 g/l and 1.0 g/l. The values of pore effective diffusivity 12.5×10^{-11} m^2/s and 2.72×10^{-11} m^2/s gave the best fits to the respective systems. The effect of D_e on the adsorption process was investigated by alternately halving, doubling and multiplying the value of D_e by five. The results are shown in Figures 5-11 and 5-12.

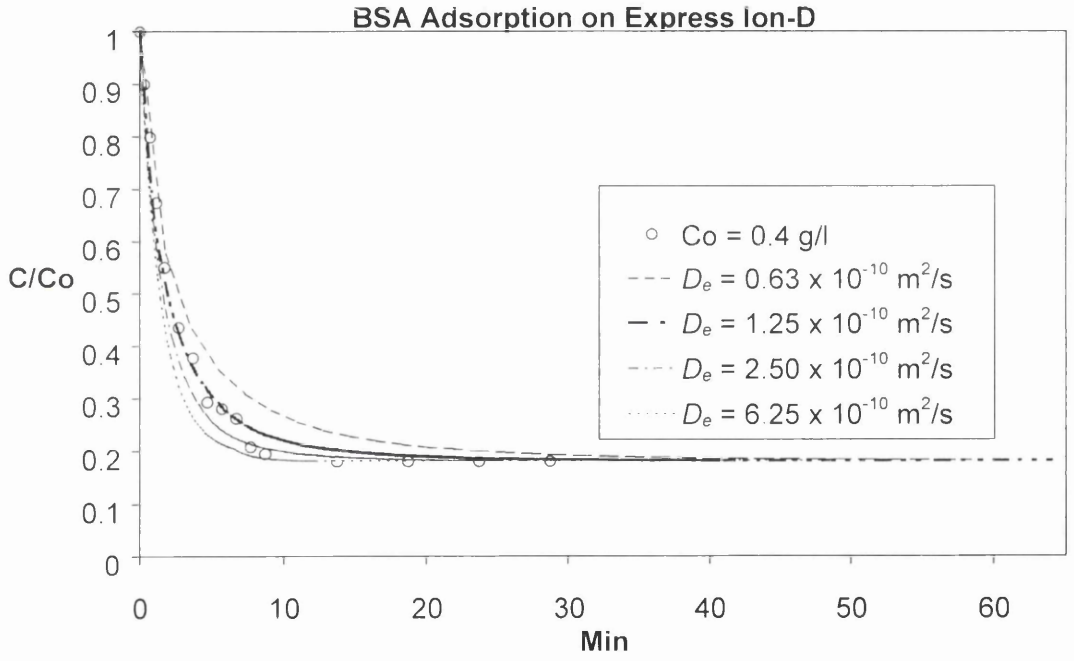

FIGURE 5-11: *Effect of the effective pore diffusivity D_e, on the simulation of 0.4 g/l BSA on Express-Ion D adsorption.*

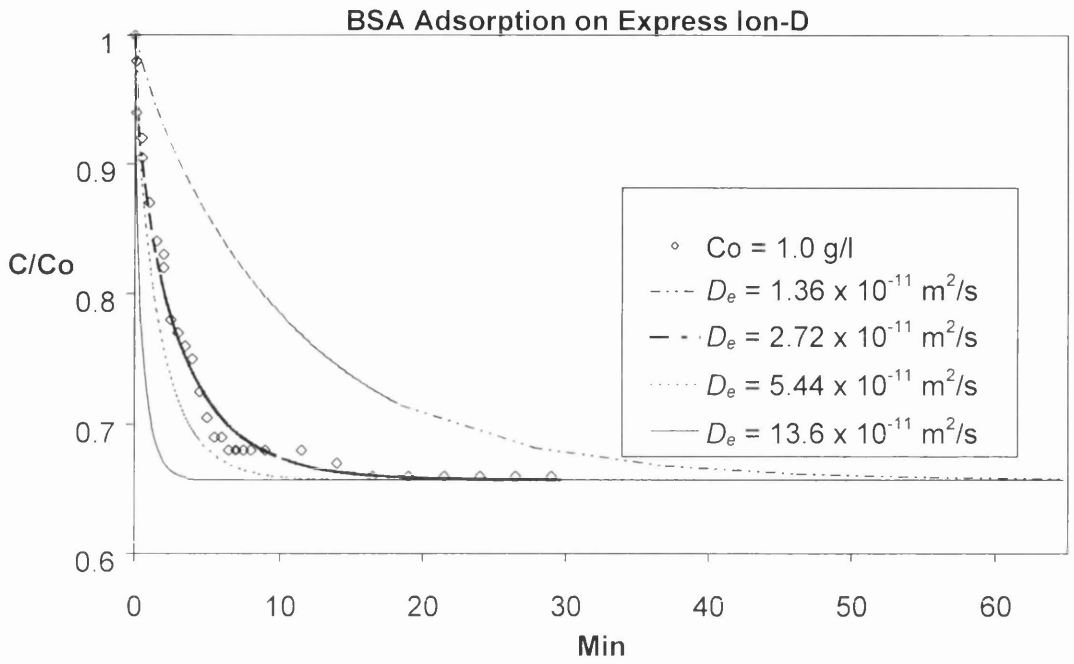

FIGURE 5-12: *Effect of the effective pore diffusivity D_e, on the simulation of 1.0 g/l BSA on Express-Ion D adsorption.*

The results show that the effective diffusivity is rate-controlling in the process, especially at higher protein concentrations. It can also be seen that the rate of adsorption increases with increasing D_e values and vice versa. The conclusion is that the resistance to diffusion through the liquid film and resistance to pore diffusion jointly control the rate of adsorption for the BSA – Express-Ion D system studied.

5.5.7 Effect of Stirring Rate on Adsorption

The effect of stirring rate on the adsorption process was studied by running the same adsorption experiment (same initial protein concentration) under different stirrer speeds ranging from 500 to 1500 rpm. The experiments followed the same pattern as the experiments conducted by Tang [71] using the same stirred cell rig. Stirrer speeds slower than 500 rpm cannot be obtained from the rig used. Figure 5-13 shows the

experimental results of the Express-Ion D adsorbent. The slowest stirring speed had the lowest rate of adsorption and the rate of adsorption increased with an increase in stirrer speed up to about 1000 rpm. Increases in the stirrer speed above 1000 rpm could not be studied as air bubbles begin to appear in the system at this speed. Beyond 1000 rpm the air bubbles make it impossible to accurately read the concentration values (the UV meter reading fluctuates constantly).

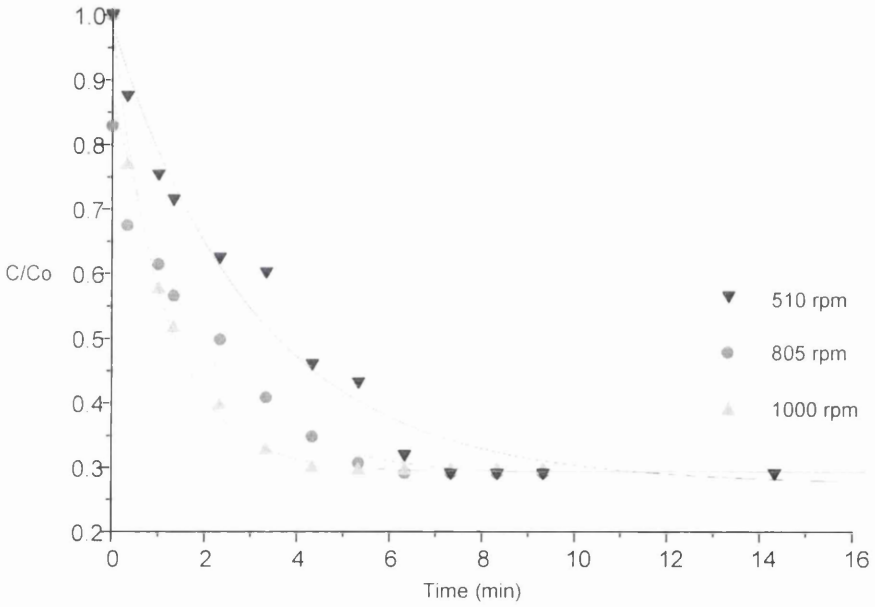

FIGURE 5-13 *Effect of Stirring Rate on the adsorption of BSA on Express-ion D.*

The reason for this effect of stirrer speed on the adsorption kinetics appears to be that the stirring in the tank affects the thickness of the boundary layer resisting mass transfer on the particle surface. As the stirring speed is increased, this thickness is reduced, thus enabling faster extra-particle mass transfer. As the stirrer speed increases, control of the overall kinetics passes exclusively to pore diffusion and further increases in the stirring rate would improve the adsorption kinetics less and less. Further increase in the stirrer

speed would have no effect on the kinetics but merely generate more air bubbles in the protein solutions. The results in the present work were obtained at a stirrer speed of 805 rpm.

5.5.8 Effect of the Equilibrium Parameters on Stirred Cell Simulations

The influence of the equilibrium parameters on the shape of the concentration-time profile was studied by varying one of the two parameters, q_m and K_d, at a time and keeping the other fixed. Figures 5-14 and 5-15 show the influence of increasing and reducing K_d by 50% on the Express-Ion D experiment with C_0 = 0.4 g/l and 1.0 g/l. The larger K_d values, i.e. smaller initial slope of the isotherm, seem to worsen the fit of the late stages of the adsorption profile and also disturbs the fit of the initial region. This is theoretically explained in terms of a lower initial slope of the equilibrium isotherm leading to a lower final solid concentration, that is less uptake of protein; thus the profile with smaller K_d lies below that with the larger K_d.

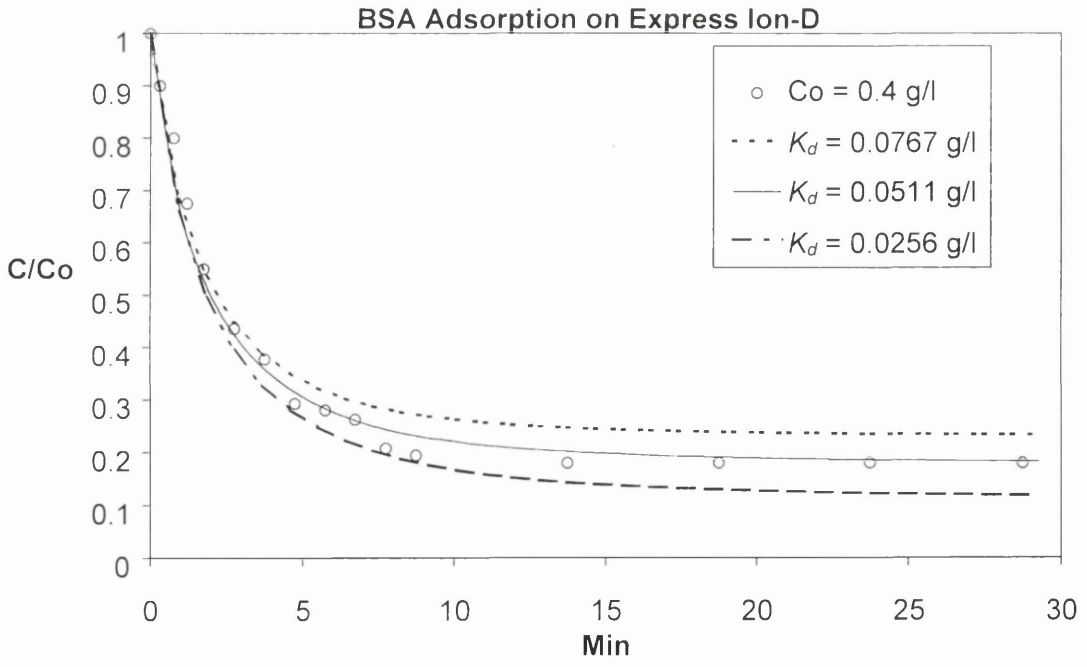

FIGURE 5-14 *Effect of Equilibrium Parameter K_d on the adsorption of BSA on Express-Ion D.*

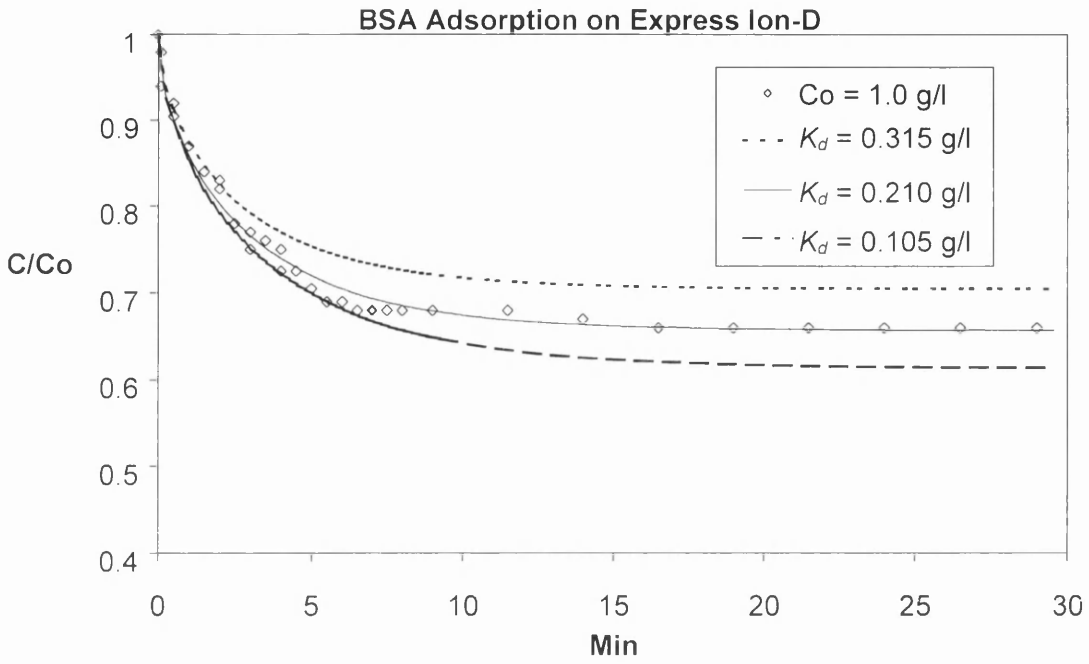

FIGURE 5-15 *Effect of Equilibrium Parameter K_d on the adsorption of BSA on Express-Ion D.*

However, the shape of the equilibrium isotherm contradicts the suggestion of a higher K_d because the equilibrium plot (Figure 4-4) requires a smaller K_d if the fit of the initial part of the isotherm is to be improved. The effect of a 50% smaller K_d than that of the equilibrium isotherm on the concentration-time profile (Figures 5-14 and 5-15) results in a greater uptake of protein by the solid (adsorbent) and the curve lies below that with the original K_d. The overall fit of the concentration-time profile can be improved with altered K_d values and restored closer to the experimental points by combining a slightly reduced K_d with a smaller diffusivity. Since different combinations of parameters can give the same fit, it is important to determine the equilibrium parameters accurately before estimating the diffusivity from the fit.

The influence of a 10% larger and smaller q_m than that of the equilibrium isotherm is illustrated in Figures 5.16 and 5-17 for the same experiments at 0.4 g/l and 1.0 g/l initial protein concentration. The influence of q_m, at these starting concentrations where the

final solid concentration is well below the maximum capacity q_m, is similar to the influence of K_d in terms of the change to the initial slope of the isotherm. The larger q_m has a steeper slope and thus higher uptake of protein and vice versa for the smaller q_m.

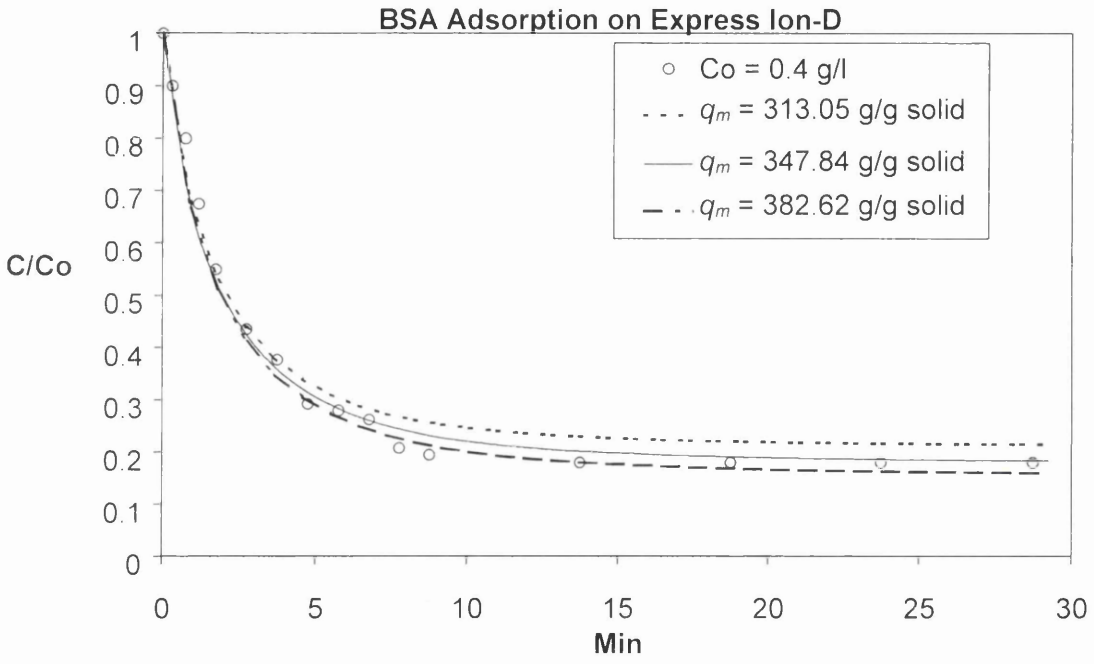

FIGURE 5-16 *Effect of Equilibrium Parameter q_m on the adsorption of BSA on Express-Ion D.*

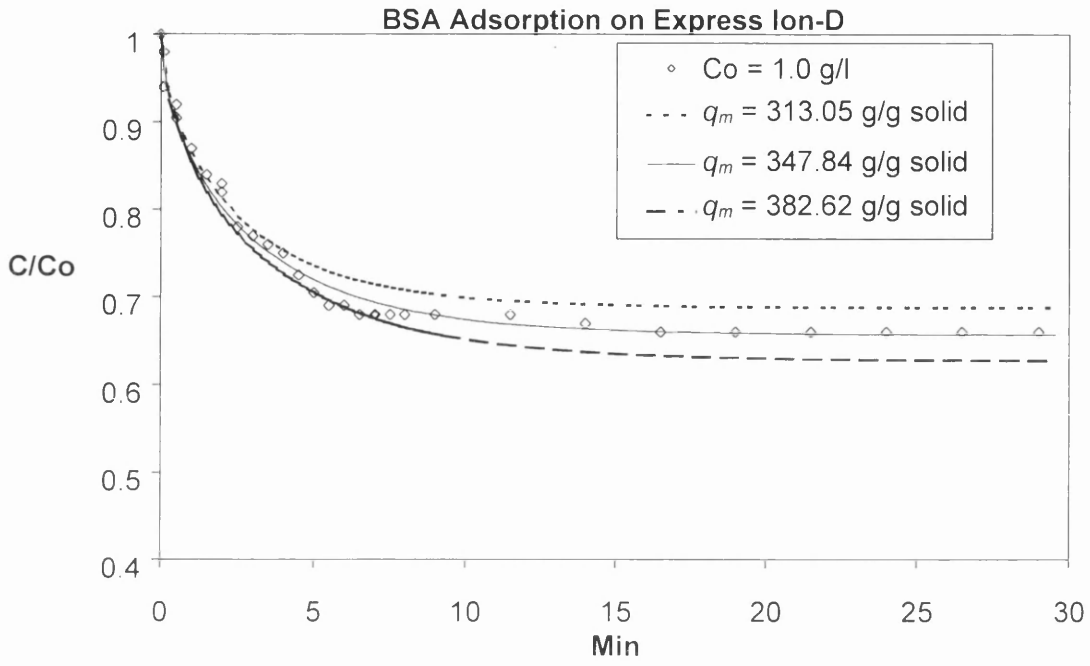

FIGURE 5-17 *Effect of Equilibrium Parameter q_m on the adsorption of BSA on Express-Ion D.*

The influence of K_d diminishes as the operating range of concentration C_0 (or C_f) rises. Thus for the other experiments of higher initial concentration the effect of K_d is smaller than we have seen for the 0.4 g/l and1.0 g/l experiment. The arbitrarily assumed changes in K_d (50%) and q_m (10%) are relatively large in comparison with the experimental precision of ± 5% and ± 1%, respectively. Hence the shifts in the fits seen in Figures 5-14 to 5-17 imply that the theoretical fits adopted are fairly insensitive to the value of K_d and q_m at concentrations greater than 1.0 g/l.

CHAPTER 6

PACKED BED: MODEL PREDICTIONS

6.1 INTRODUCTION

In the last Chapter, the experimental and simulation results for the stirred cell operation were presented, and the values of the effective pore diffusivity were derived by matching the simulation results to the experimental data. The adsorption profiles obtained were a good fit to the experimental results and provide a good source for the estimation of the pore effective diffusivity for the system being studied. The values of the effective diffusivity obtained were used to study the effects on the model of the main factors that may affect the simulation results. We were able to show that the calculated value of the film mass transfer coefficient gave the best fit to the experimental data, the number of particle size groups adopted in the formulation of the particle size distribution data does influence the accuracy of the simulation, and that the margins of error in the values of the equilibrium parameters used in the simulations are small enough not to have significantly affected the value of the effective pore diffusivity obtained.

The objective of this research was to develop kinetic models which allow prediction of the theoretical profiles for the adsorption of protein on cylindrical adsorbents under stirred cell and packed bed operation. In the absence of experimental data for the latter, theoretical profiles using hypothetical particles, modeled after the particles studied by previous workers Hayek and Li [17, 18], have been used to make predictions for the model developed for cylindrical particles in Chapter 2. The results of the simulations are presented in this chapter.

The anion exchange and hydrophobic interaction systems studied by Bassam Hayek [18], and the cation exchange CBX and hydrophobic HIC interactions studied by QiangYi Li

[17] (all Bakerbond silica-based adsorbents) have all been simulated. Firstly, the theoretical curves they obtained for spherical particles were reproduced to test the accuracy of the original computer program in its implementation on the system used for this present work. The program written for cylindrical particles was then implemented. The systems predicted involved the adsorption of bovine serum albumin (BSA) on cylindrical particles C/HIC 40, C/HIC 15, C/PEI 40 and C/PEI 15, and the adsorption of Myoglobin (Mb) on cylindrical particles C/CBX 40, C/CBX 15, C/HIC 40 and C/CHIC 15. The acronyms C/HIC, C/PEI and C/CBX denote hypothetical cylindrical particles created for predictive purposes with the characteristics reported for spherical hydrophobic interaction (Hi-propyl, HIC), cation exchanger CBX adsorbents [17] and anion exchange (polyethyleneimine, PEI) forms of the adsorbents [18]. The acronyms HIC, PEI and CBX denote the spherical particles. The numbers 40, 20 and 15 indicate the nominal diameter of the particle in μm.

The theoretical breakthrough profiles are discussed for each system studied. The sensitivity of the model to the various kinetic parameters involved in the process is also discussed. The effect of particle geometry is examined by comparing the model data obtained from the spherical and the simulated cylindrical adsorbents. Also presented in this Chapter are the simulation results of the packed bed desorption.

6.2 Model Validation

Mathematical models such as the packed bed model constructed in Chapter 2 require validation before they can be used for process prediction. The best method of model validation is to compare its predictions to experimental data. In the absence of experimental data for cylindrical particles in a packed bed at this time, as earlier mentioned, the computer program written for the solution of the ordinary differential equations that simulate the adsorption process for cylindrical particles was first modified to reproduce the results obtained for the process of adsorption using spherical particles in a packed bed.

The present model includes the effect of experimental delays that occur in the flow line of packed-bed equipment, as reported by previous workers [3, 17, 18 and 25]. The program modified for spherical particles was tested using data for four theoretical concentration profiles each, obtained from the works of Li [17] and Hayek [18], (Table 6-1). The theoretical profiles were obtained by these authors by curve-fitting experimental profiles using the effective pore diffusivity as the adjustable parameter [17, 18] and were taken as the target profiles for the present model validation. The present models gave excellent agreement to the theoretical curves, in every case, when the same diffusivities estimated by the workers were used. Figures 6-1 to 6-4 show the profiles obtained for all four particles considered.

The data in Table 6-1 for Bakerbond adsorbents were then employed in the subsequent predictive tests for the packed bed cylindrical particle model of Chapter 2. The data for Express-Ion D have been included in Table 6-1 for comparison. The major focus in these predictive tests is on the effect of particle geometry on the adsorption processes observed by Hayek and Li. Therefore, the bed voidage (ε_b) and film mass transfer coefficient (k_f) for Bakerbond adsorbents were assumed the same for the hypothetical cylindrical particles as for real spherical particles, despite likely difference due to shape of particles.

Property	Bakerbond								Whatman
	Anion exchange (PEI) (Hayek)		Hydrophobic interaction (Hi-propyl) (Hayek)		Cation exchange (CBX) (Li)		Hydrophobic interaction (Hi-propyl HIC) (Li)		Express-Ion D (Onugha)
Nominal particle diameter, μm	40	15	40	15	40	15	40	15	30
Volume-surface mean diameter, μm	41.9	18.0	41.9	18.0	42.4	11.2	42.8	17.6	-
Linear-surface mean diameter, μm	-	-	-	-	-	-	-	-	21.9
BET surface area, S_w, m^2/g	268	98	285	98	213	45.9	285	55.44	0.46
Mean pore diameter, d_η, nm	21.8	27.3	20.6	27.3	21.2	31.3	20.6	27.7	9.5
Particle density, ρ_p, $10^6 g/m^3$	0.506	0.811	0.507	0.800	0.483	1.032	0.503	0.995	0.446
True solid density, ρ, $10^6 g/m^3$	1.945	1.938	1.960	1.880	1.933	1.89	1.94	1.860	0.863
Particle porosity, ε	0.74	0.58	0.74	0.57	0.749	0.467	0.739	0.48	0.483
Bed porosity, ε_b	0.35	0.35	0.35	0.35	0.327	0.327	0.327	0.327	-
Surface density of BSA, mg/m^2	1.13	1.40	0.55	0.34	N/A	N/A	N/A	N/A	1.13
Protein	BSA	BSA	BSA	BSA	Mb	Mb	Mb	Mb	BSA
Protein concentrations, c_o, kg/m^3	0.77	1.38	0.96	1.43	4.5	2.5	2.0	4.0	1.3
Diffusivity, D_e, $10^{-11} m^2/s \pm 11\%$	0.146	0.142	0.028	0.029	9.0	2.0	2.0	2.0	2.72
Mass transfer coefficient, k_f, $10^{-5} m/s$	1.57	2.07	1.28	1.65	variable	variable	variable	variable	variable

TABLE 6-1: *Physical properties of adsorbents, protein concentrations, and diffusivity.*

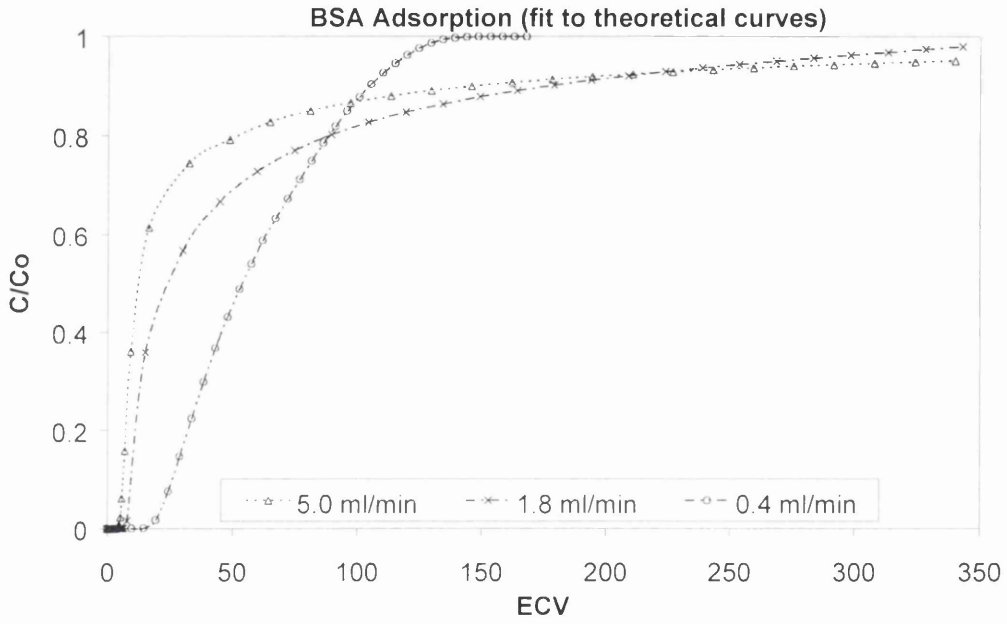

FIGURE 6-1: *Theoretical profiles (shown by curves) for BSA on spherical 40 μm silica-based PEI particles compared with Hayek's theoretical profiles (shown by data-points).*

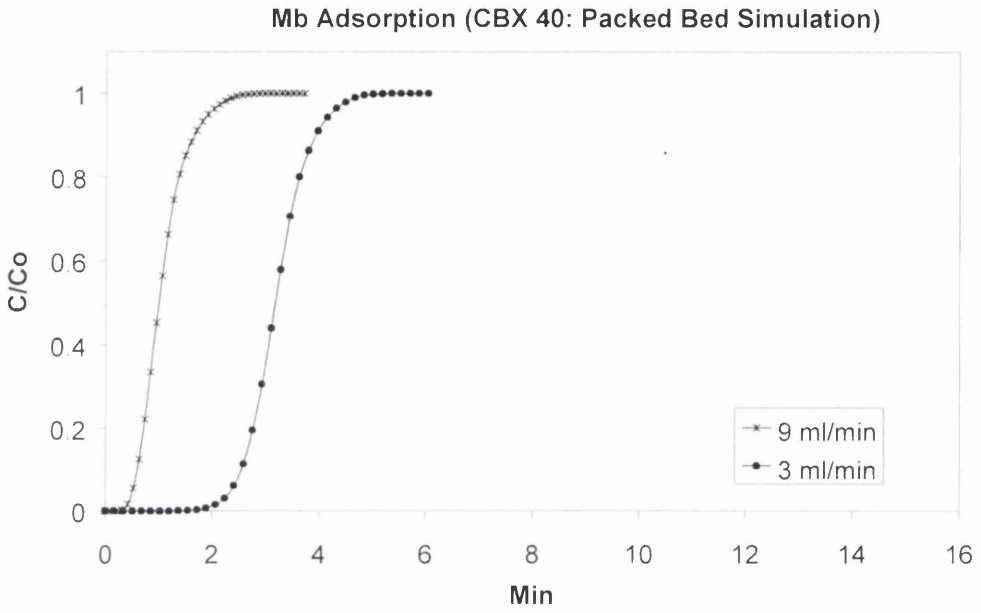

FIGURE 6-2: *Theoretical profiles (shown by curves) for Mb on spherical 40 μm silica-based CBX particles compared with Li's theoretical profiles (shown by data-points).*

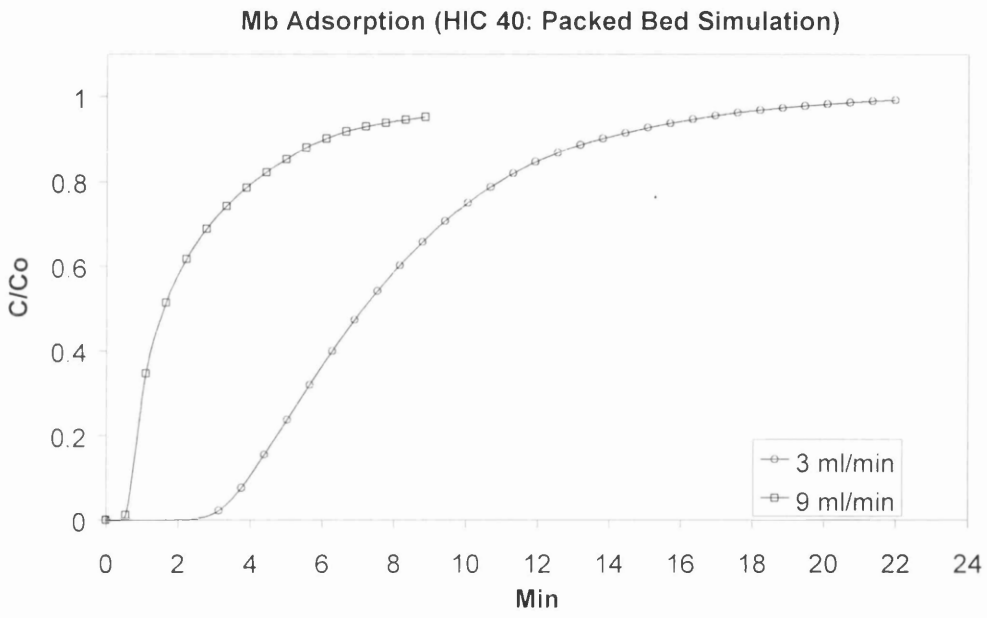

FIGURE 6-3: *Theoretical profiles (shown by curves) for Mb on spherical 40 μm silica-based HIC particles compared with Li's theoretical profiles (shown by data-points).*

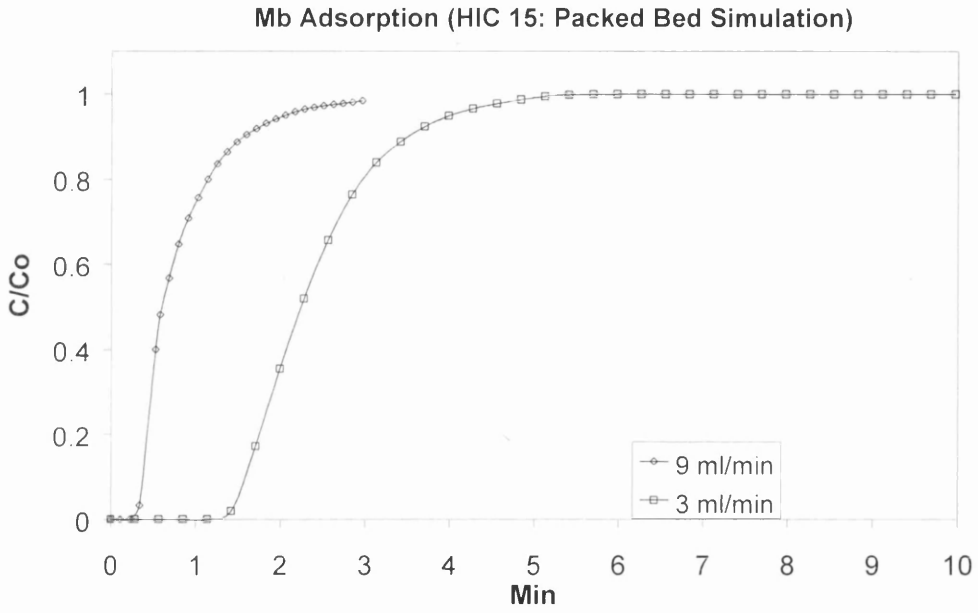

FIGURE 6-4: *Theoretical profiles (shown by curves) for Mb on spherical 15 μm silica-based HIC particles compared with Li's theoretical profiles (shown by data-points).*

6.3 SENSITIVITY OF THE PACKED BED MODEL PREDICTIONS TO PARAMETERS.

6.3.1 Introduction

The shapes and the position of the breakthrough curves for packed bed adsorption are not only affected by their adsorption isotherms but also by the mass transfer characteristics of the system. The factors that affect the isotherms, such as the buffer type, concentration and pH, will indirectly have an influence on the breakthrough curves. The breakthrough curves are affected because any change in those factors would result in alteration of the isotherm parameters, K_D and q_m, which would in turn affect the theoretical modelling of the packed bed adsorption [18, 31]. The mass transfer parameters, film mass transfer coefficient and pore diffusion coefficient, have a direct influence on the breakthrough characteristics of the adsorption system; these can be studied by theoretical simulation. We will consider the effect of the film mass transfer coefficient and effective pore diffusivity to determine whether they are jointly or either one singularly rate determining. The extent to which the size distribution of a system of cylindrical particles in a packed bed influences the theoretical simulation of the adsorption of protein onto it will be considered. The efficacy of the newly developed two-step polydisperse model on the prediction of the breakthrough curves will also be shown in comparison with the monodisperse one.

6.3.2 Influence of the Liquid Film Mass Transfer Coefficient (k_f).

In the simulations presented above, the liquid film mass transfer coefficients used were calculated using Equation 2.108 for cylindrical particles as described in Section 2.7.2. In this section, we will examine the influence of the film mass transfer coefficient on the simulation results and the shapes of the breakthrough curves. A typical simulation result is presented in Figure 6-5 for the 40 μm C/CBX system at a flowrate of 3 ml/min and protein feed concentration of 4 g/l.

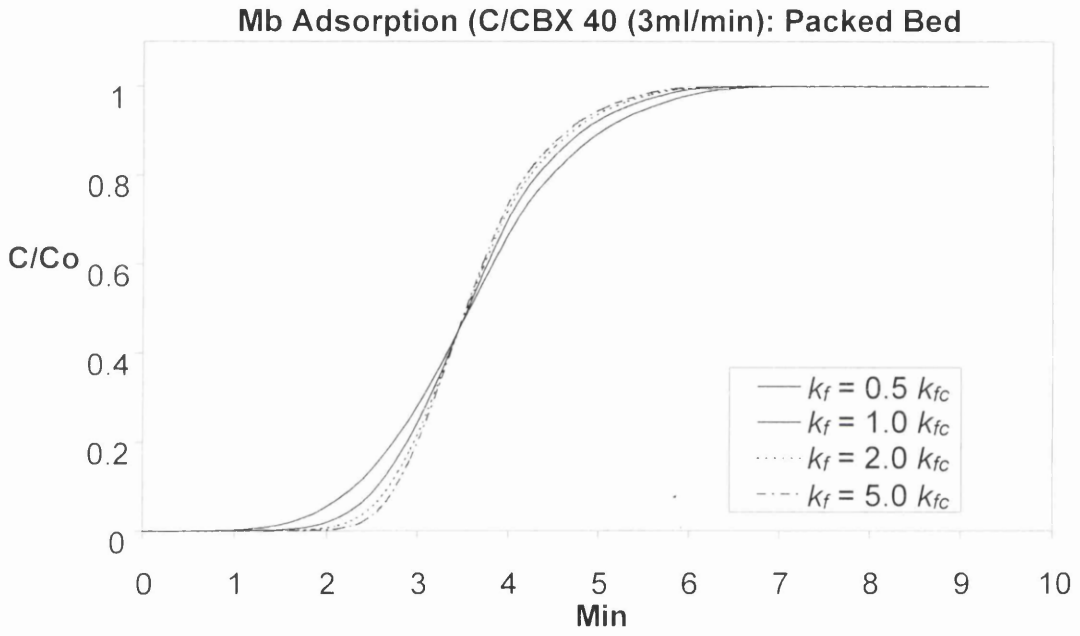

FIGURE 6-5: *Effect of film mass transfer coefficient (k_f/k_{fc}) on the packed bed simulation of Myoglobin (Mb) on polydisperse C/CBX 40. k_{fc} is particle size dependent for polydisperse model and is calculated automatically using size data.*

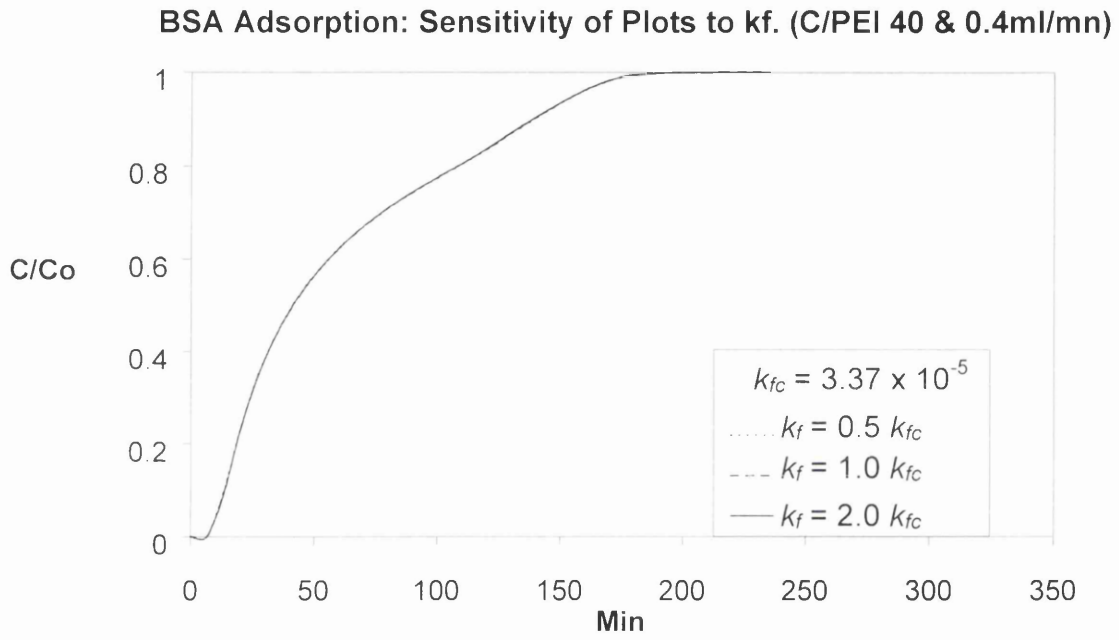

FIGURE 6-6: *Effect of film mass transfer coefficient (k_f/k_{fc}) on the packed bed simulation of BSA on monodisperse C/PEI 40 .*

The values of k_f examined were in the range of k_f/k_{fc} = 0.5 – 5.0, where k_{fc} is the value of k_f calculated using Equation 2.108 (a single value for the monodisperse model and different values depending on the particle size in the polydisperse model). The same value of the effective pore diffusivity (9×10^{-11} m^2/sec) was used for all the cases in Figure 6.5. The result indicates that smaller k_f led to an earlier start of breakthrough and slower approach to equilibrium and vice versa, which is the expected result. The simulation results for the effect of the mass transfer coefficient show that the shape of the adsorption process is moderately sensitive to the variations of k_f. This indicates that film mass transfer is relatively important to the whole adsorption process for the Mb systems studied. This finding is in complete contrast to the results obtained with adsorption systems using BSA in Figure 6-6, where the same plot is obtained for all values of k_f.

6.3.3 Effect of Particle Dispersity on Breakthrough Curves

Simulation results of the two different models, the polydisperse two-step model and the monodisperese two-step model developed in Chapter 2, were studied for the effect of size distribution on the breakthrough curves. Typical results are shown in Figures 6-7 and 6-8 for C/HIC 40 μm and C/CBX 40 μm particles, respectively. The solid lines were produced by the polydisperse model with four particle size groups, group number M = 4, and effective pore diffusivity of 9×10^{-11} m^2/sec. The dotted lines were results of the monodisperse model assuming a mean particle diameter (d_{NS}) of 20 μm, and an effective pore diffusivity of 7×10^{-11} m^2/sec.

Research with spherical particles has shown that a polydisperse model tends to give much better fits to experimental data than a monodisperse model for particles with a wide size distribution [17]. The rate of protein adsorption is affected by particle size and size distribution too. Smaller particles adsorb protein molecules faster than larger particles because of the shorter diffusion distances inside the pores and relatively greater film mass transfer coefficient.

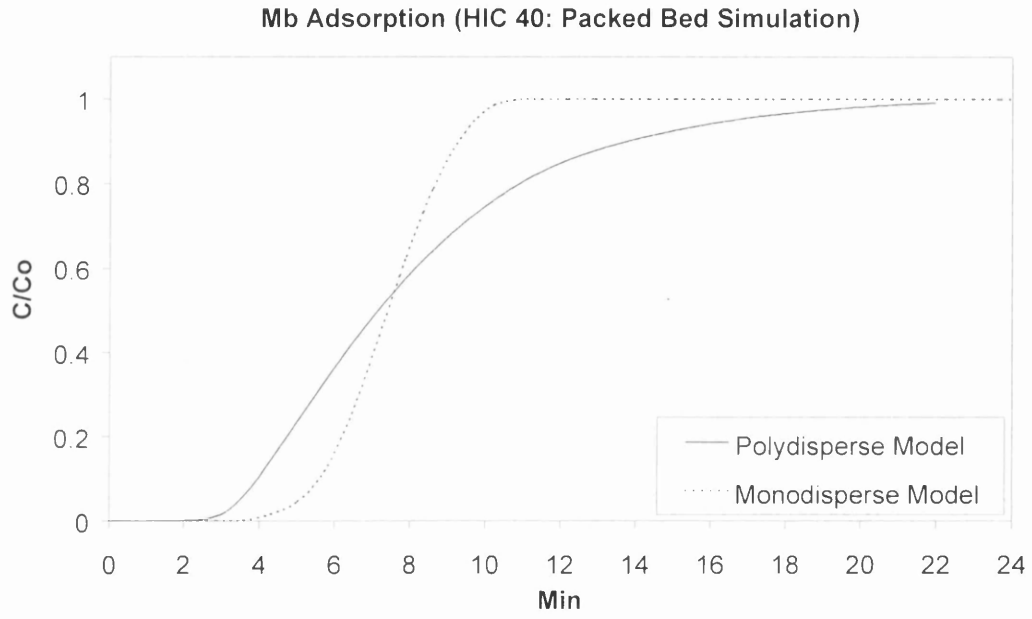

FIGURE 6-7: *Comparison of monodisperse and polydisperse models on the packed bed simulation of Mb on C/HIC 40 μm.*

The faster rate of adsorption is seen in the simulation result using the monodisperse model, as a lower rate of concentration increase at the beginning of breakthrough and the faster approach to equilibrium compared to the profile for the polydisperse model which should more accurately represent the experiment data. This behaviour could be related to the fact that a uniform mean particle diameter that could not allow for the fast mass transfer occurring in the smaller particles below the mean size and the slow mass transfer in the larger particles above the mean size was assumed for the monodisperse model.

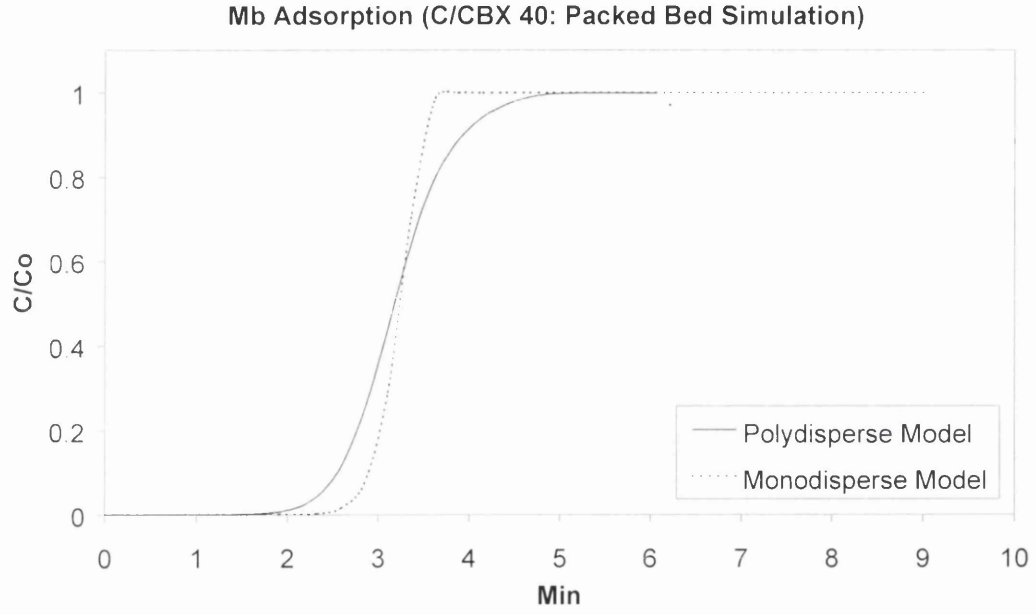

FIGURE 6-8: *Comparison of monodisperse and polydisperse models on the packed bed simulation of Myoglobin (Mb) on C/CBX 40 μm.*

6.3.4 Sensitivity of the Model to the Effective Pore Diffusivity.

The form of the effective diffusion coefficient expressed in the present model combines the diffusivity in free solution with the effects of the hydrodynamic and electrostatic hindrance to protein diffusion (hindered diffusion), and the resistance to diffusion due to

the path length and pore shape (tortuosity). The reason for combining the hindered diffusion and the tortuosity into one effective diffusivity is that they are difficult to predict for materials with pore structures as complex as those examined here [12].

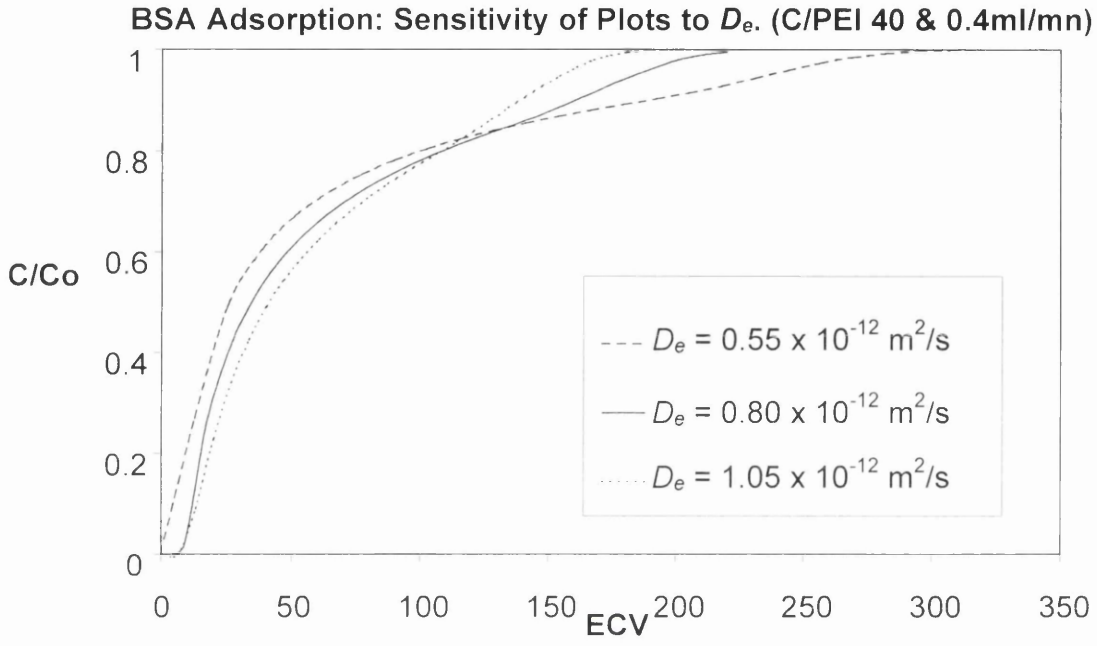

FIGURE 6-9: *Effect of the effective pore diffusivity D_e, on the packed bed simulation of BSA on C/PEI 40 μm system.*

The influence of effective pore diffusivity on packed bed simulations was studied on C/PEI 40 μm and C/CBX 40 μm particles. The values of pore effective diffusivity 0.08 × 10^{-11} m^2/s and 9 × 10^{-11} m^2/s for C/PEI 40 μm and C/CBX 40 μm systems, respectively taken from stirred cell experiments [17, 18] gave the best fit to the relevant packed bed simulations. By alternately increasing and decreasing D_e by 30% in the case of anionic PEI and by doubling and halving it in the case of cationic CBX, we investigated the effect of D_e on the adsorption process. The results are shown in Figures 6-9 and 6-10 for C/PEI 40 μm and C/CBX 40 μm respectively. The larger D_e results in a later start of

breakthrough and an earlier completion than the breakthrough profile for the smaller diffusivity.

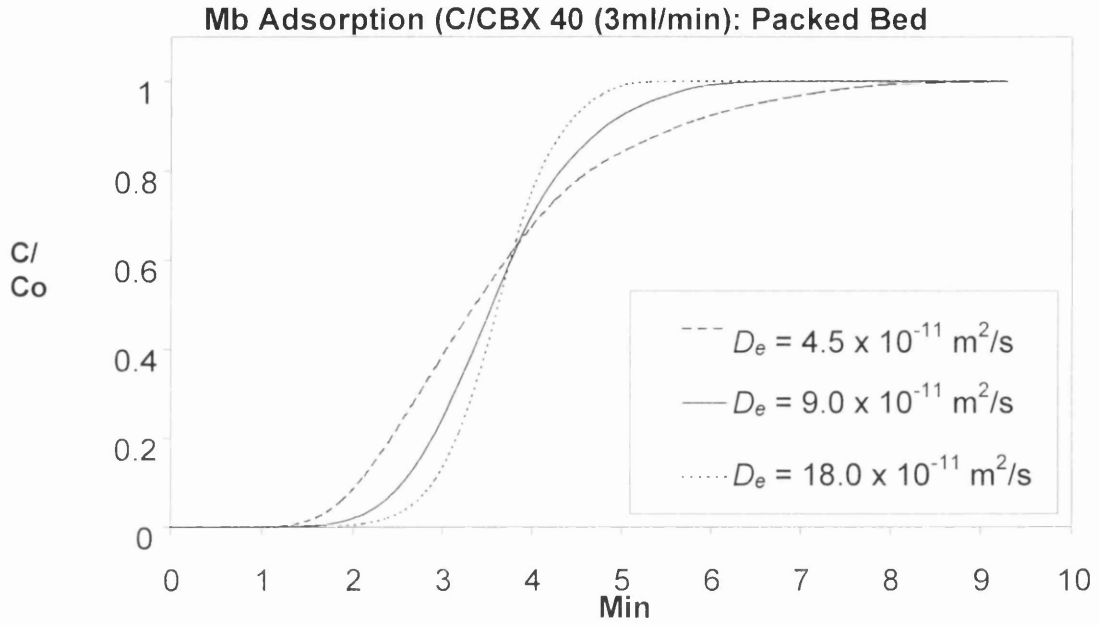

FIGURE 6-10: *Effect of the effective pore diffusivity D_e, on the packed bed simulation of Mb on C/CBX 40 μm system.*

In the study of Mb adsorption on Bakerbond CBX and BSA on anionic PEI particles [3], the effective pore diffusivity of BSA was smaller than that of Myoglobin. Pore diffusion strongly dominated the whole adsorption process in the case of BSA. Breakthrough curves were more sensitive to the change of D_e than the change of k_f. A change of D_e by 30%, for example, gave significant change in breakthrough the curve (Figure 6-9), while a 50% difference in k_f produced practically no change to the profile (Figure 6-6). This indicates that the resistance from the film mass transfer can be neglected in the case of BSA on a wide pore ion exchanger (Bakerbond PEI, average pore diameter 21.8 μm).

In such systems as that in Figure 6-6, a one step model, involving only the pore diffusion resistance, would be sufficient for describing the adsorption process of BSA reasonably

well. In contrast to BSA, the pore diffusion of Myoglobin system is (generally) much faster, as indicated by the higher value of D_e. Still the influence of the mass transfer coefficient can be clearly seen in Figure 6-5, making the Mb polydisperse systems jointly dominated by both pore diffusion and film mass transfer.

An increase in the diffusion coefficient will increase the rate of protein diffusion and vice versa, which is observed as generally faster kinetics. The concentration profiles in Figures 6-9 and 6-10 depict this. The present model predicts an inverse proportionality between the pore diffusion coefficient and the adsorption time conforming to the expected trend for packed bed operations.

6.3.5 Sensitivity of the Model to the Number of Bed Sections.

The number of bed sections assumed in the execution of the packed bed model can substantially alter the theoretical adsorption profile. Increasing or decreasing the number of bed sections basically increases or decreases the number of elements in the solution to the adsorption equations. It was observed in the present study that the simulation results for a system with very wide size distribution, such as Bakerbond silica-based adsorbents, can be significantly improved by increasing the number of bed sections used from five up to twenty (N_x = 5, 10, 15, and 20 respectively).

When more than twenty bed sections were used, the simulation results showed little improvement, suggesting that there is an optimum value for N_x as in the case with the number of particle size groups. Also, although it is the case that the greater the number of bed sections in the solution the better the accuracy of the model, it was noted that the time required for the solution increased too. Therefore the number of bed sections used in the simulation is a compromise between the time needed for the solution/computational power and the accuracy of the simulation. A typical result is presented in Figure 6-11 for Mb on C/CBX. So in this study, N_x = 20 was taken as the optimum number of bed sections for the adsorbents investigated.

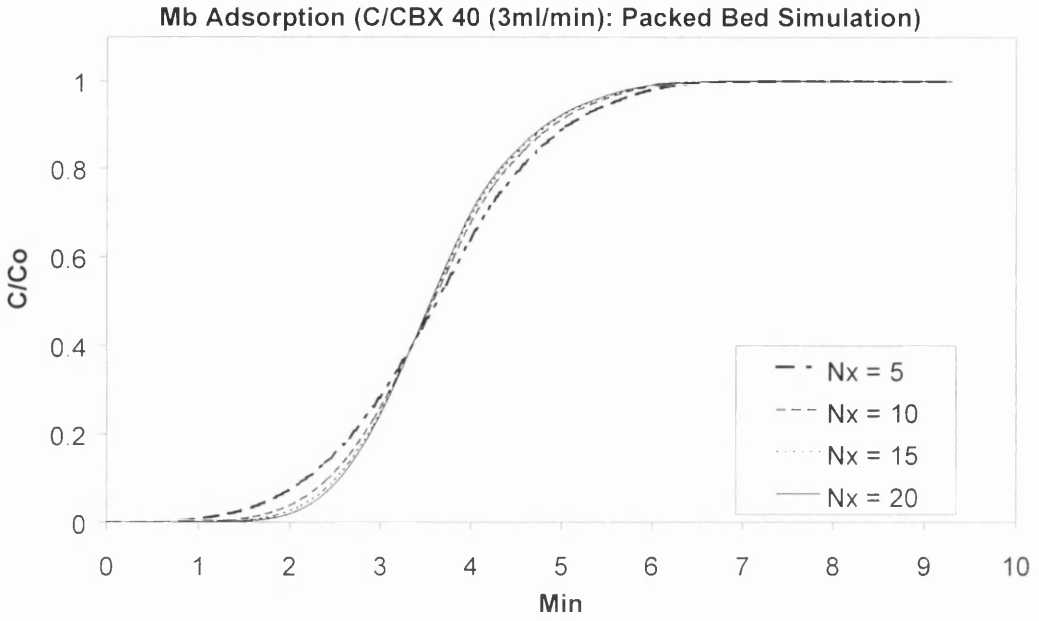

FIGURE 6-11: *Effect of the number of bed section N_x, on the packed bed simulation of Mb on C/CBX 40 μm system.*

Similar results have been obtained for spherical particles by Li [17] and Hayek [18] who showed that there is practically no need to use more than twenty bed sections in the theoretically profiles for packed bed experiments involving polydisperse particles.

6.3.6 Sensitivity of the Model to the Effect of Delay and Mixing in the Flow Line.

The contribution of the delay and mixing in the flow line to the adsorption profile was explained in Section 2.6.5. The concentration profile for the packed bed model is distorted by the spreading process that occurs due to mixing in the valves, pump and fittings on the flow line. These create an effect equivalent to a non-sharp concentration step at the column inlet. The computer program developed for the solution of the packed model presented in this chapter allows for a non-sharp inlet profile.

The theoretical adsorption profile for a system without considering the effect of delay and mixing would typically breakthrough earlier than the experimental profile and finish sooner than the experimental plot too. It in effect suggests less protein capacity for the adsorbents and greater throughput than can be truly obtained. The results of the theoretical simulation of the adsorption of Mb on C/CBX 40 μm with and without the delay and mixing effect are shown in Figure 6-12.

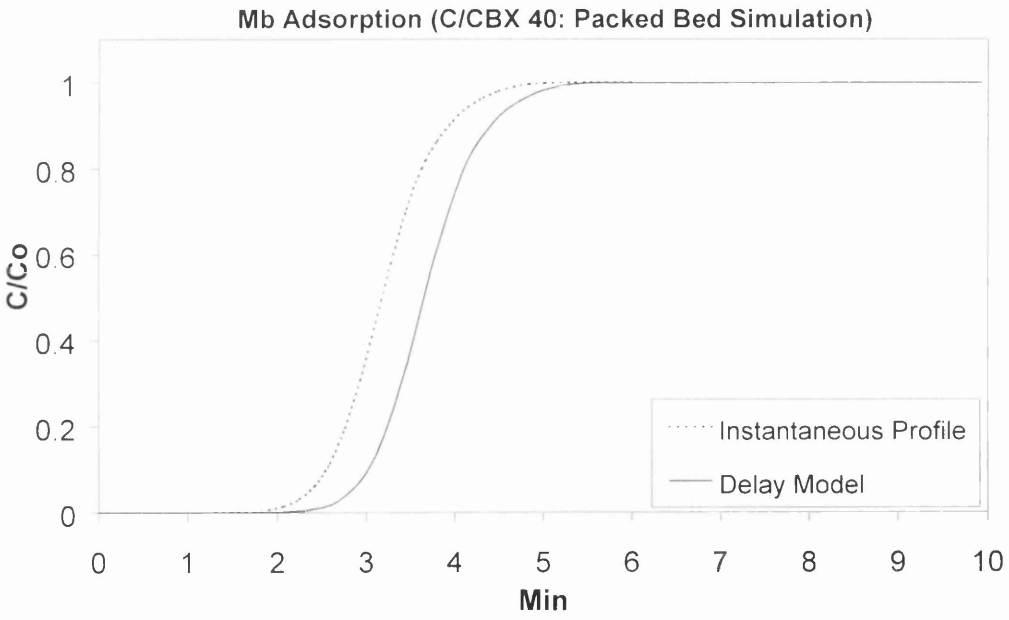

FIGURE 6-12: *Effect of the delay and mixing on the packed bed simulation of Mb on C/CBX 40 μm system.*

6.4 DESORPTION RESULTS

The packed bed model for the desorption process is basically the same as that for adsorption. The only variations are in the specifications for the initial and boundary conditions, as mentioned in Chapter 2 (Section 2.9.3). The two-step polydisperse model was used in the simulations. The modification of the inlet step to a non-sharp concentration profile caused by the mixing chamber effect, which was discussed in Chapter 2 for the adsorption case, was also applied in desorption modelling.

The simulated breakthrough curves for the desorption processes considered are plotted in Figure 6-13 and 6-14. The values of the effective pore diffusion coefficient adopted in the desorption simulations were the same as those used in the adsorption profiles (Table 6-2).

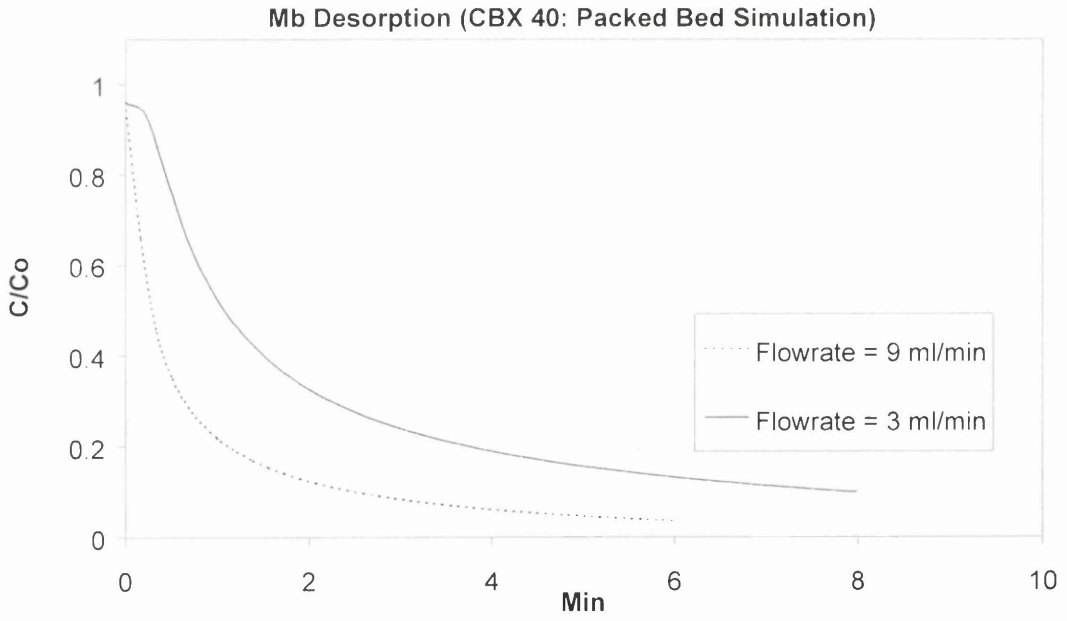

FIGURE 6-13: *Theoretical simulations of the desorption of Mb on CBX 40 μm.*

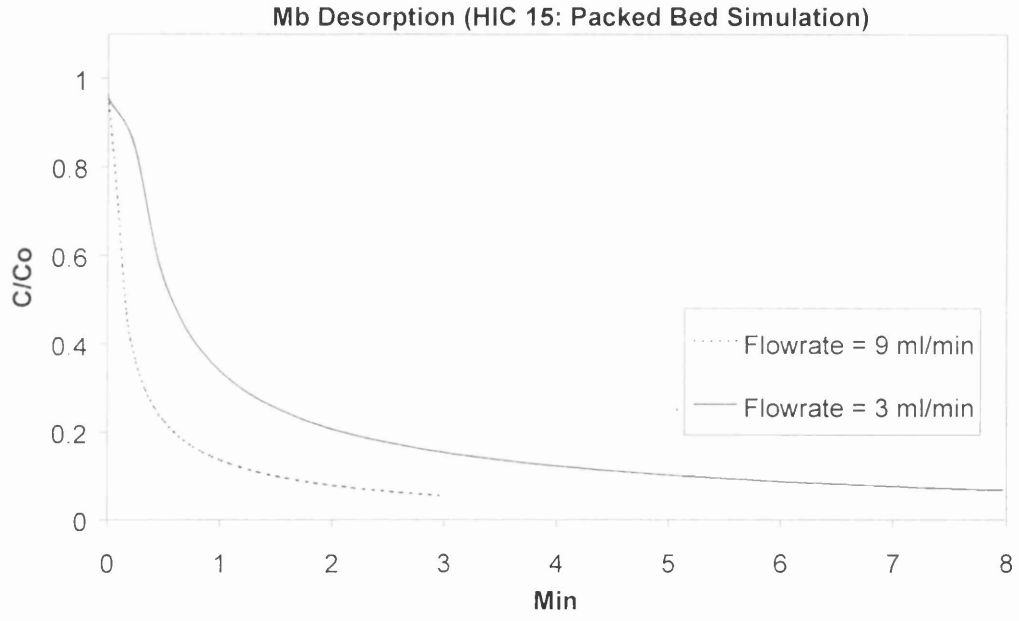

FIGURE 6-14: *Theoretical simulations of the desorption of Mb on HIC 15 μm.*

System	C/C_o at $t = 0$	C_o (g/l)	Flowrate, ml/min	D_e (m^2/s)
CBX 40	0.960	4.0	3.0	9.0×10^{-11}
	0.962		9.0	
HIC 15	0.955	4.0	3.0	1.50×10^{-11}
	0.963		9.0	

TABLE 6-2: *Desorption Parameters*

6.5 COMPARISON OF SPHERICAL AND CYLINDRICAL PACKED BED RESULTS

The theoretical profiles for the comparison of the spherical and cylindrical packed bed models have been plotted in terms of dimensionless concentration as in all the previous cases in this present work. In addition, the results are now shown against the number of empty column volume equivalents (ECV) delivered. When the breakthrough curves for different flowrates are plotted in terms of ECV, the effect of the mobile phase velocity on the rate of transport of protein along the bed is eliminated. This leaves the kinetic (and thermodynamic) effects, if significant, to control the shape of the curves.

The theoretical adsorption profiles fitted to the experimental results for the spherical particles studied by Li and Hayek [17, 18] are plotted next to the equivalent, hypothetical, cylindrical particles having the same diameter as the spheres. The results are shown in Figures 6-15 to 6-18.

As shown in Figures 6-15 to 6-17, for the adsorption step, the profiles for the spherical particles consistently breakthrough later than those for the cylindrical particles and finish earlier. That is, the spherical particles curves are steeper than the cylindrical curves, implying faster kinetics. The justification is that the protein adsorption process for a spherical particle can be thought of as taking place in three spatial dimensions while the process occurs in only two dimensions for a cylindrical particle, where there are no end

effects (infinite length). An assembly of spheres of the same diameter as a long cylinder has a greater surface area and more diffusion paths to the center. However, even though this comparison is at the same diameter, cylindrical particles offer advantages of lower pressure drop at the same diameter, or lower diameter at the same pressure drop than the spherical particles, in which case the kinetics would actually be faster not slower for a bed of cylindrical particles.

The curves cross each other before the beds are saturated in each case so that the area above the curves is equal for both the spherical and the cylindrical plots. This shows that the particle/bed capacity is the same in each case since only the particle geometry has been altered between the models for both particles in each case.

The result of the comparison of the spherical and cylindrical packed bed desorption models is given in Figure 6-18. The cylindrical profile for the desorption step lies just below the spherical profile. The cylindrical particles curve is slightly steeper at the start implying marginally faster desorption kinetics for the same particle characteristics, equilibrium parameters and particle diameter. However, the spherical profiles eventually meet the cylindrical curves and they cross before equilibrium because both profiles have the same value of q_m.

The difference between the spherical and cylindrical curves is much smaller in desorption than in adsorption, which is characteristic of a strong influence from a Langmuir isotherm curvature [34]. A Langmuir isotherm gives self-sharpening breakthrough curves in adsorption and diffuse curves in desorption. The slope of the isotherm (dq/dc) at a fixed concentration is proportional to the net retention volume (V_N) [40], such that dq/dc, and hence V_N, decreases with increasing concentration.

$$V_N \quad \alpha \quad \frac{dq}{dc}$$

The concentration at the start of desorption in the experiment is sufficiently well up the isotherm to give a near-zero slope dq/dc. If the breakthrough curves were governed

entirely by the isotherm and not by the kinetics, ECV̇ would be proportional to dq/dc at each concentration and a near-zero value of ECV would be observed when breakthrough begins. The desorption plot thus confirms that the breakthrough curves are strongly influenced by the isotherm and not only by the kinetics.

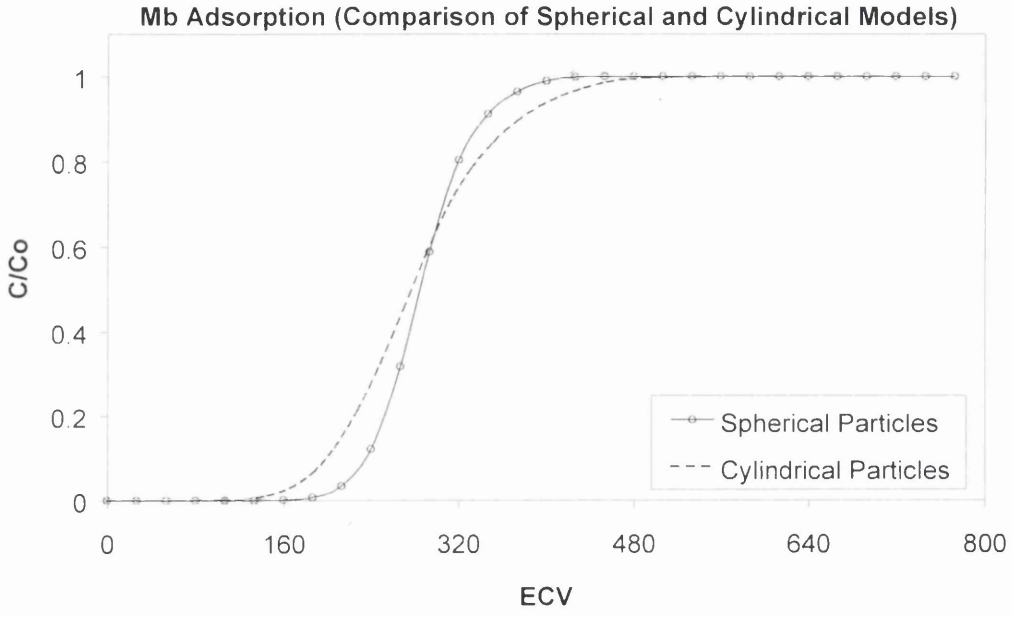

FIGURE 6-15: *Comparison of 40 μm CBX spherical and cylindrical (C/CBX) particles' adsorption kinetics. Protein is Myoglobin (Mb) and the flowrate is 3 ml/min.*

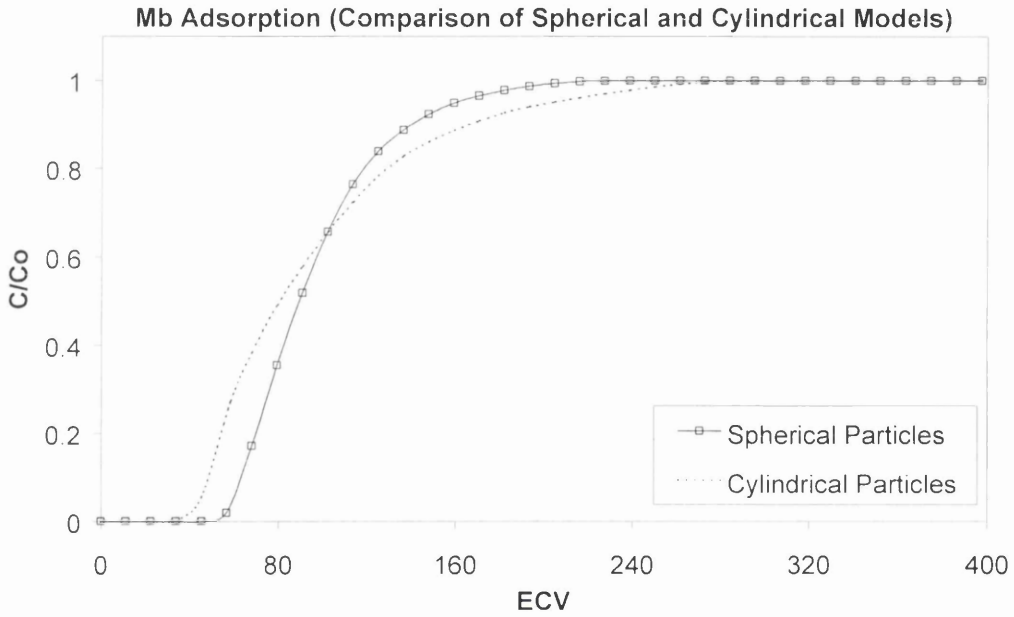

FIGURE 6-16: *Comparison of 15μm HIC spherical and cylindrical (C/HIC) particles' adsorption kinetics. Protein is Myoglobin (Mb) and the flowrate is 3 ml/min.*

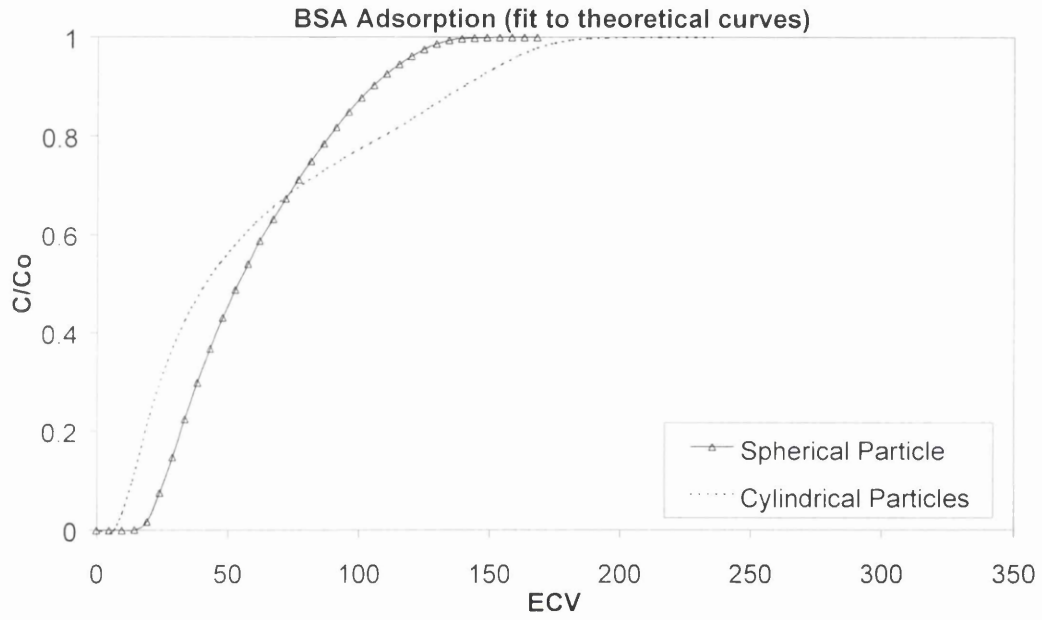

FIGURE 6-17: *Comparison of 40 μm PEI spherical and cylindrical (C/PEI) particles' adsorption kinetics. Protein is BS and the flowrate is 0.4 ml/min.*

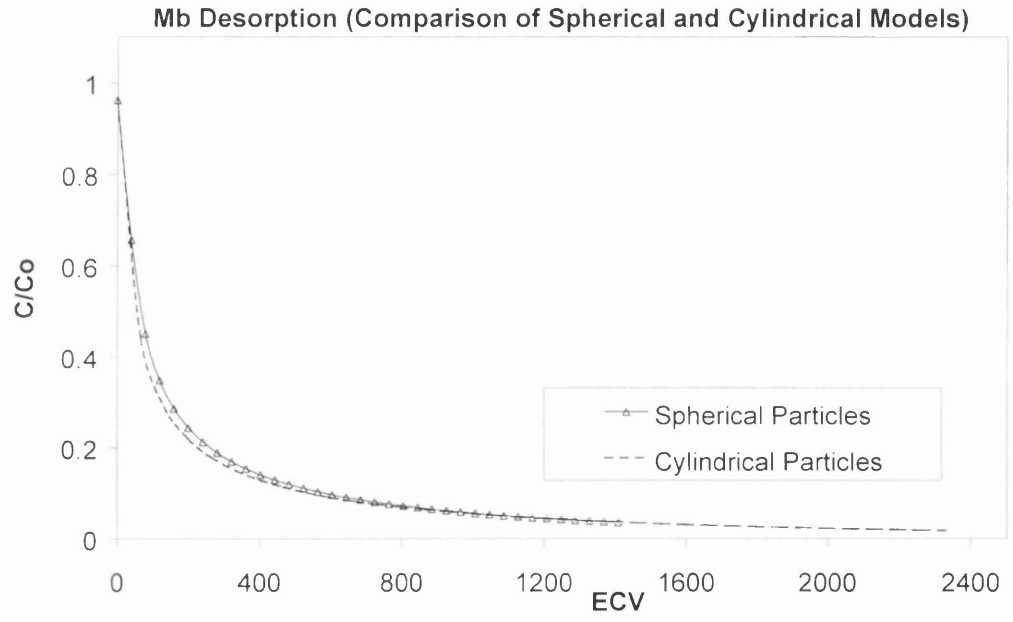

FIGURE 6-18: *Comparison of 40 μm CBX spherical and cylindrical (C/CBX) particles' adsorption kinetics in desorption mode. Protein is BSA and the flowrate is 9.0 ml/min.*

CHAPTER 7

CONCLUSIONS AND RECOMMENDATIONS

7.1 INTRODUCTION

The aim of this research has been to study, theoretically and experimentally, the kinetics of macromolecule adsorption onto porous adsorbents that are fibrous or formed of rod-shaped particles. Bovine Serum Albumin (BSA) was used as a representative macromolecule of average molecular weight, about 67,000. The adsorbent studied was Whatman Express-Ion D, which consists of rod-shaped particles of reconstituted cellulose with a nominal particle diameter of 30 μm. Express-Ion D is a weak anion exchanger that normally binds negatively charged proteins at pH above their pI. The adsorption process in stirred cell mode was both experimentally studied and numerically simulated, while the packed bed model was used for a numerical explanation of the effect of parameter variation, using other workers' experimental data in the simulation. The main objectives of the study were to establish the theoretical models for description of the adsorption kinetics of protein molecules on cylindrical (porous and semi-rigid) particles, to validate the models (for the stirred cell mode), and to investigate the influence of process parameters on the adsorption rate. A number of conclusions may be drawn from the study.

7.2 CHARACTERISATION OF MATERIALS AND ADSORPTION EQUILIBRIUM

The particle size measurements show that Express-Ion D is polydisperse and has a considerable size distribution around the nominal diameter. The length of the rod-like particles ranges from 40 μm to 600 μm, and their diameters, both from particle to particle and across the length of a particle, range from 7 μm to 40 μm. The measurements also show that there are virtually no fines present in the sample (i.e. particles less than < 10 μm in length). The particle size distribution was formulated by dividing the whole size range into four size groups. Each size group is characterised by a number-

surface mean diameter, which was derived and calculated from the measured distribution data. The formulated particle size distribution has been successfully introduced into the models and shown to be effective in improving the theoretical simulation results.

Langmuir adsorption isotherms showing a relatively high adsorption capacity for the BSA – Express-Ion D system were obtained by selecting proper pH, buffer and salt concentration. It was demonstrated that the adsorption capacity is influenced by environmental factors, such as pH, buffer and salt concentration. The experimental results show that the adsorption capacity q_m of the semi-rigid, cellulose based adsorbent Express-Ion D is quite high compared to the silica-based adsorbents Whatman Partsil BioPrep [3] and Bakerbond cation exchanger CBX, and anion exchanger PEI [18], per dry gram of adsorbent used. High adsorption capacities have been gained using 0.01M Tris buffer at a pH of 7.5 ± 0.2, with no sodium chloride (NaCl) added. The adsorption capacity decreases with increasing salt content, but the saltless isotherm was very nearly rectangular with only a small range of concentration over which the changing capacity could be studied. The adsorption capacity of the adsorbent was greatly reduced at the other extreme of high salt concentrations. A suitable buffer for the system studied was found to be 0.01M Tris at pH 7.5 with 1.2 g/l NaCl added.

7.3 Modelling and Numerical Simulation

The process of protein adsorption on porous adsorbents occurs in three stages: transport of protein molecules from the bulk fluid to the external particle surface described by a liquid film coefficient k_f; intraparticle diffusion characterized by an effective pore diffusivity D_e; and interaction between the protein molecules and the adsorbent (surface reaction). Three two-step models have been developed to simulate the process described above; they are two-step models because the resistance to surface reaction (the third step) is neglected. First, a polydisperse stirred cell model improving on the monodisperse model constructed in a previous study and reviewed in Chapter 2. Secondly, both a monodisperse and polydisperse model for adsorption and desorption in packed bed mode of operation were then built.

The effective diffusivity was adopted in the models as the single fittable parameter, in the case of the stirred cell to match theoretical plots to the experimental data. The quality of the fit was satisfactory, and the simulation was much improved using the polydisperse models. The fitted effective pore diffusivity was found to depend strongly on protein concentration but could be treated satisfactorily as independent of the protein concentration over small concentration bands.

The packed bed model, in computer-program form, was first validated by checking that a variant of it for spherical models predicted the same concentration-time profiles as the similar spherical particle models developed and experimentally tested by previous workers [17, 18], when data from those works and their fitted diffusion coefficients were employed in the new model. The data and diffusion coefficients were then applied to each equivalent (hypothetical) cylindrical particle system to predict the breakthrough curves and the effect of process parameters.

By taking account of the particle size distribution in the models, the influence of the assumption of a number of particle size groups on the adsorption kinetics has been investigated theoretically. In the improved (polydisperse) two-step model, the column inlet concentration profile has been taken into account in the packed bed mode, while the mixing chamber effect in the sampling line was included in the simulation results in the stirred cell mode. Experimental results by previous researchers show that these effects need to be incorporated in simulations.

The simulations also show that for the system studied, the surface reaction rate is fast enough for the surface reaction step to be neglected, so that the two-step model can provide a proper description of the adsorption process.

7.4 INFLUENCE OF PROCESS PARAMETERS

The influence of several parameters on the adsorption kinetics has been investigated by experiment and by simulation. The parameters include the pH of buffer, buffer type and salt concentration, particle size distribution, the effective diffusivity, and the film mass transfer coefficient.

The results of the stirred cell experiments show that at a fixed time the adsorption process for BSA – Express-Ion D (30 μm) would reach about two times the degree of equilibrium of the BSA – 40 μm PEI (spherical, silica-based particles) system and a 20% greater degree of equilibrium than the BSA - 15 μm PEI system. The concentration-time curves predicted by the packed bed models constructed for cylindrical particles were compared with the results from the models for spherical particles. The results showed that the process was mostly slower with the cylindrical particles of the same diameter. However, other workers have argued that cylindrical adsorbents are more mechanically stable than spherical adsorbents down to small particle diameters. Cylindrical particles therefore have a clear advantage for increased throughputs since the rate of adsorption, which controls the throughputs, may be very sensitive to liquid velocity and, especially, particle diameter and surface area [16, 17 and 18]. Fibrous polymers such as Express Ion D are believed to be mechanically equivalent to bead-like particles five-times their diameter thus giving much improved kinetics over the bead-like particles at the same pressure drop.

By examining the influence of the extra-particle mass transfer coefficient on the adsorption profile obtained (and predicted in the case of packed bed) it has been concluded that the intra-particle (pore) diffusion would be jointly rate controlling with the film mass transfer coefficient in the adsorption process for the systems investigated. The pore diffusion would be more dominant at higher protein concentrations, while the film mass transfer coefficient would be more dominant at lower protein concentrations. The resistance to the adsorption process by the surface reaction can be neglected.

7.5 GENERAL REMARKS AND FUTURE WORK

The completed study of protein (BSA) adsorption on cylindrical rigid porous adsorbents (Whatman Express-Ion D adsorbents) includes two major aspects: theoretical modeling and experimental verification. The introduction of particle size distributions into the theoretical modeling has shown a slight improvement in the simulation results. The comparison of the simulation results between the spherical and cylindrical models has provided general identification and understanding of the rate differences in their adsorption processes. It has been found that the particle size distribution data have a great effect on the determination of the pore diffusivity. Since the pore length is related to the particle size, a precise and accurate description of the pore diffusion relies on understanding the pore structure, the pore length and pore size distribution. A previous study [3] with the subject of pore structure as its basis yielded unsatisfactory results proving that more work needs to be done to improve the understanding of the contribution of pore structure to the determination of pore diffusion.

Besides the improvement of theoretical simulation modeling, the experimental work on adsorption isotherms and stirred tank adsorption operations has provided detailed information on the adsorbent, Whatman Express-Ion D, as potential adsorbent for purification of BSA and similar proteins. It is an example of a semi-rigid, high performance cellulose-based adsorbent that provides an alternative route to protein separations at high throughputs compared with rigid silica-based adsorbents. Data such as those obtained here, together with exhaustive packed bed tests, can be used in conjunction with the theoretical models in the design and optimisation of improved protein separation.

7.6 RECOMMENDATIONS

The main recommendation at this stage would be to validate the findings of the packed bed model experimentally using cylindrical particle types and two or more proteins, and adsorbent particle sizes. Further work on this model could also include its experimental

validation to make it suitable for industrial application. The stirred cell model could be tested experimentally against either another cylindrical particle, particle size or protein.

It is hoped that attempts would be made at solving the model using newer more powerful computers would speed up the simulation times for the packed bed experiments. This would enable effects such as that of having more than six size groups of a polydisperse model to be studied for adsorbents with very wide particle size ranges.

Finally, the model could also be developed for use with other industrially significant chromatographic systems such as soft gels and perfusion chromatographic adsorbents.

References

1. Weatherly, L. R. *Engineering Processes for Bioseparations.* Butterworth-Heinemann Ltd., 1994.

2. Robyt, J. F. and B. J. White. *Biochemical Techniques – Theory and Practice.* Brooks/Cole 1987.

3. Ashmead, S. R.: *The Kinetics of Protein Adsorption on Porous Particles.* PhD Thesis University of Wales Swansea (1999).

4. Katz, E. D. *High Performance Liquid Chromatography: Principles and Methods in Biotechnology.* Wiley & Sons 1996.

5. Chang, C. and A. M. Lenhoff: *J. Chromatog.* A, 827 281-293 (1998). Comparison of Protein Adsorption Isotherms and Uptake Rates in Preparative Cation-Exchange Materials.

6. Fernandez, M. A. and G. Carta: *J. Chromatog.* A, 746 (1996) 169-183. Characterization of Protein Adsorption by Composite Silica-polyacrylamide gel anion exchangers I. Equilibrium and Mass Transfer in Agitated Contactors.

7. Guan-Sajonz, H., P. Sajonz, G. Zhong, and G. Guiochon: *Biotechnol. Prog.* 12 (1996) 380-386. Study of the Mass Transfer Kinetics of BSA on a TSK-GEL DEAE-5PW Anion Exchanger in a Wide Concentration Range.

8. Leonard, M.: *J. Chromatog.* B, 699 (1997) 3-27. New Packing Materials for Protein Chromatography.

9. McCoy, M. A. and A. I. Liapis: *J. Chromatog.* 548 25-60 (1991). Evaluation of Kinetic Models for Biospecific Adsorption and its Implications for Finite Bath and Column Performance.

10. Nash, D. C. and H. A. Chase: *J. Chromatog.* A, 807 (1998) 185-207. Comparison of Diffusion and Diffusion-Convection Matrices for use in Ion-Exchange Separations of Proteins.

11. Tongta, A., A. I. Liapis, D. J. Siehr: *J. Chromatog.* A, 686 (1994) 21-29. Equilibrium and Kinetic Parameters of the Adsorption of α-chymotrypsinogen A onto Hydrophobic Porous Adsorbent Particles.

12. Weaver, L. E. Jr., and G. Carta: *Biotechnol. Prog.* (1996), 12, 342-355. Protein Adsorption on Cation Exchangers: Comparison of Macroporous and Gel-Composite Media.

13. Andrade, J.D. *Principles of Protein Adsorption.* Surface and Interfacial Aspects of Biochemical Polymers, ed. J.D. Andrade, Vol. 2, p.1. (1985). Plenum Press, New York.

14. Horbett, T. A. and J. L. Brash: In Proteins at Interfaces: Physicochemical and Biochemical Studies. *ACS Symp. Series* 343. (1987) Proteins at Interfaces: Current Issues and Future Prospects.

15. Norde, W.: *Adv. Colloid Interface Sci.* 25. 267 (1986). Adsorption of Proteins from Solution at the Solid-Liquid Interface.

16. Petruzzelli, D., A. Kalinitchev, V. S. Soldatov and G. Tiravanti: *Ind. Eng. Chem. Res.* 34 (1995) 2618-2624. Chloride/Sulfate Ion Exchange Kinetics on Fibrous Resins: Two Independent Models for Diffusion Control.

17. Li, Qiang Yi: *Kinetics of Macromolecule Adsorption on Porous Rigid Particles.* PhD Thesis University of Wales Swansea (1997).

18. Hayek, B. O.: *Kinetics of Protein Adsorption on Rigid Particles.* PhD Thesis University of Wales Swansea (1994).

19. Wikström, P. and P. O. Larsson: *J. Chromatog.* 388(1) (1987) 123-134. Affinity Fibre – A New Support for Rapid Enzyme Purification by High Performance Liquid Affinity Chromatography.

20. Beaver, R. P.: *J. Chrom. Sci.*, September 1988. Dependence of Performance on Fibre Uniformity in Aligned Fibre Column HPLC.

21. Rao, P. S., T. Murugesan, M. Surianarayan and K. V. Raghavan: *Chem. Eng. Sci.* 50 (1995) 890 – 897

22. Kaczmarski, K., D. Antos, H. Sajonz, P. Sajonz, and G. Guiochon: *J. Chromatog.* A, 925 (2001) (1-2) 1-17. Comparative Modeling of Breakthrough Curves of Bovine Serum Albumin in Anion-Exchange Chromatography.

23. Graham, E. E. and C. F. Fook: *A I Chem. Eng. J.* 28 (1982). Rate of Protein-Absorption and Desorption on cellulosic Ion Exchangers.

24. Tsou, H. S. and E. E. Graham: *A I Chem Eng. J.* 31 (1985). Prediction of Adsorption and Desorption of Protein on Dextran based Ion-Exchange Resin.

25. Arnold, F.H., H. W. Blanch and C.R. Wilkie: *Chem Eng. J.* 30 B25-36 (1985). Analysis of Affinity Separations II: The Characterisation of Affinity Columns by Pulse Techniques.

26. Schneider, P. and J. M. Smith: *A I Chem Eng. J.* 14 762-771 (1968). Adsorption Rate Constants from Chromatography.

27. Venkatesh Natarajan, B. W. Bequette and S. M. Cramer: *Journal of Chromatography A*, 876 (2000) 51–62. Optimization of Ion-Exchange Displacement Separations, I: Validation of an Iterative Scheme and its use as a Methods Development Tool.

28. Leaver, G., J. A. Howell and J. R. Conder: *J. Chromatog.* 590 101-112 (1992). Adsorption Kinetics of Albumin on a Cross-linked Cellulose Chromatographic Ion-Exchanger.

29. Hayek, B. O.: *A New Method for Studying the Adsorption Kinetics of Proteins.* MSc Thesis University of Wales Swansea (1991).

30. Fernandez, M. A., W. S. Laughinghouse and G. Carta: *J. Chromatog.* A, 746 (1996) 185-198. Characterization of Protein Adsorption by Composite Silica-polyacrylamide gel anion exchangers II. Mass Transfer in Packed Columns and Predictability of Breakthrough behaviour.

31. Horstmann, B. J. and H. A. Chase: *Chem. Eng. Res. Des.* 67 (1989) 243. Modelling the Affinity Adsorption of Immunoglobulin G to Protein A Immobilised to Agarose Matrices.

32. Skidmore, G. L., B. J. Horstmann and H. A. Chase: *J. Chromatog.* 498 (1990) 113-128. Modelling Single-Component Protein Adsorption to the Cation Exchanger S Sepharose FF.

33. Conder, J. R. and B. O. Hayek: *Biochem. Eng. J.* 6 (2000) 215-223. Adsorption Kinetics and Equilibra of Bovine Serum Albumin on Rigid Ion-Exchange and Hydrophobic Interaction Chromatography Matrices in a Stirred cell.

34. Conder, J. R. and B. O. Hayek: *Biochem. Eng. J.* 6 (2000) 225-232. Adsorption and Desorption Kinetics of Bovine Serum Albumin in Ion-Exchange and Hydrophobic Interaction Chromatography on Silica Matrices.

35. Liapis, A. I.: *J. Biotechnol.* (1989) 143-160. Theoretical Aspects of Affinity Chromatography.

36. Van Deemter, J., F. Zuiderwerg, and A. Klinkenberg: *Chem. Eng. Sci.* 5 (1956) 271.

37. Do, D. D. and R. G. Rice: *Chem. Eng. Sci.*, Vol 45, No. 5, (1990) 1419-1421. Applicability of the External-Diffusion Model in Adsorption Studies.

38. Skidmore, G. L., and H. A. Chase: *J. Chromatog.* 505 (1990) 329-347. Two-Component Protein Adsorption to the Cation Exchanger S Sepharose FF.

39. Leaver, G.: *Large Scale Ion-Exchange Chromatography of Animal Blood Proteins.* PhD Thesis University of Wales Swansea (March 1984).

40. Conder, J. R., and C. L. Young: *Physicochemical Measurement by Gas Chromatography.* JohnWiley & Sons Ltd, 1979

41. Heeter, G. A. and A. I. Liapis: *J. Chromatog.* A, 796 (1998) 157-164. Frontal Chromatography of Proteins; Effect of Axial Dispersion on Column Performance.

42. Baily, J. E. and D. F. Ollis: *Biological Engineering Fundamentals.* 2nd ed. McGraw-Hill, 1986.

43. Foster, D. F.: *Virus Removal by Resinous Sorbents.* PhD Thesis University of Illinois (August 1974).

44. Hagel, L., *in Aqueous Size Exclusion Chromatography* (ed. P Dublin), Elsevier.

45. Barrett, E. P., L. G. Joyner and P. P. Halenda: *J. Am. Chem. Soc.,* 73 (1951) 373. The Determination of Pore Volume and Area Distributions in Porous Substances I: Computations from Nitrogen Isotherms.

46. Wheeler, A.: *Presentations at Catalysis Symposia,* Gibson Island (June 1945 and 1946) A. A. A. S. Conferences.

47. Dullen, F. A. L., *Porous Media: Fluid Transport and Pore Structure,* 2nd Ed. Academic Press, 1992. (page 8).

48. Conder, J. R., B. O. Hayek and Q. Li: Concentration Profiles and Kinetics for Faster Biomolecule Separations, in Ion Exchange Developments and Applications (proceedings of the International Conference IEX '96, Cambridge, 14-19 July, 1996), J. A. Greig, editor. Royal Society of Chemistry/Society of Chemical Industry, London, 1996. p. 506-515.

49. Arve, B. H.: *The Modelling and Analysis of Multicomponent, Multivalent Biospecific Adsorption.* PhD Thesis, University of Missouri-Rolla, Rolla, Missouri, U.S.A. (1986).

50. Onugha, L. C.: *Protein Adsorption Kinetics on Porous Cylindrical Particles in a Stirred Cell.* MSc Thesis University of Wales Swansea (2000).

51. Cantor, R. C. and P. R. Schimmel: *Biophysical Chemistry Part II. Techniques for the Study of Biological Structure and Function.* (1980). Freeman.

52. Pålsson, E., A. Smeds, A. Petersson, and P. O. Larsson: *J. Chromatog.* A, 840 (1) 39-50 (1990). Faster Isolation of Recombinant Factor VII SQ with a Super porous Agarose Matrix.

53. Allen, T., *Particle Size Measurement.* 4th ed. Chapman and Hall, 1990.

54. Arve, B. H. and A. I. Liapis: *Biotechnol. Bioeng.* 32, 616-627 (1988). Biospecific Adsorption in Fixed and Periodic Countercurrent Beds.

55. Geankoplis, C. J. *Transport Processes and Unit Operations*, 2nd Ed. Boston: Allyn and Bacon Inc. 1983.

56. Grzegorczyk, D. S. and G. Carta: *Chem. Eng. Sci.* 51 (1996) 819. Adsorption of Amino Acids on Porous Polymeric Adsorbents – II. Intraparticle Mass Transfer.

57. Sherwood, T. K., R. L. Pigford and C. R. Wilkie, *Mass Transfer.* New York: McGraw-Hill, 1975.

58. Treybal, R. E. *Mass Transfer Operations*, 3rd ed. McGraw-Hill, 1981.

59. Wakao, N. T. Oshima and S. Yagi: *Chem. Eng. Jap.* 22, (1958) 780. Mass Transfer from Packed Beds of Particles to a Fluid.

60. Foo, S. C. and R. G. Rice: *A I Chem. J.* 21 (16) (1975) 1149-1158. On the Prediction of Ultimate separation in Parametric Pumps.

61. Polson, A: *J. Phys. Colloid Chem.* 54 (1950) 649.

62. Causserand, C., Y. Kara and P. Aimar: *J. Membrane Sc.* 186 (2001) 165 – 181. Protein Fractionation using Selective Adsorption on Clay Surface before Filtration.

63. Bowen, W. R. and P. M. Williams: *Biotechnol. Bioeng.*, 50 (1996) 125. Dynamic Ultrafiltration Model for Proteins: A Colloidal Interaction Approach.

64. Cohn, E. J., L. E. Strong, W. L. Hughes, D. J. Mulford, J. N. Ashworth, M. Melin, and H. L. Taylor: *J. Am. Chem. Soc.*, 68 (1946) 459. Preparation and Properties of Serum and Plasma proteins IV. A System for the Separation into Fractions of the Protein and Lipoproptein Components of Biological Tissues and Fluids.

65. Edwards, W. G.: *Physicochemical Studies of Cellulosic Ion Exchangers.* PhD Thesis. University of Wales Swansea (1978).

66. Tabor, D.: *Gases, liquids and solids: and other states of matter*, 3rd ed. Cambridge University Press, 1991.

67. Honeyman, J., *Recent Advances in the Chemistry of Cellulose and Starch*, Heywood & Company Ltd., London 2000.

68. Ott, E., H.M. Spurlin and M.W. Grafflin: *Cellulose and cellulose derivatives.* 2nd completely rev. and augm. ed. Interscience Publishers, New York, 1954.

69. Bikales, N. M. and L. Segal: *Cellulose and cellulose derivatives. Parts 4 and 5.* Wiley-Interscience, New York [Chichester], 1971.

70. Tang, L. X., M. G. Jones, R. W. Lovitt and J. R. Conder: *Computer Automation of an Analyser for Study of Protein Adsorption/Desorption Processes.* Dep. of Chem. Eng., University of Wales Swansea.

71. Tang, L. X.: SERC Research Project Report, Dep. of Chem. Eng., University of Wales Swansea. 1992.

72. Norde, W. and J. Lyklema: *J. Colloids and Interface Science*, 66 (1978) 257. The Adsorption of Human Plasma Albumin and Bovine Puncreas Ribonuclease at Negatively Charged Polystyrene Surfaces I: Adsorption Isotherm, Effect of Charge, Ionic Strength, and Temperature.

73. Orr, C. and J. M. Dalaville.: *Fine Particle Measurement.* MacMillan, New York, 1959.

74. Cussler, E. L. *Diffusion: Mass Transfer in Fluid Systems.* 2nd ed. Cambridge University press, 1997.

75. Deen, W. M.: *AICHE J.*, 33, 1409 (1987). Hindered Transport of Large Molecules in Liquid-Filled Pores.

76. Elwing, H., S. Welin, A. Askendal and I. Lundström: *J. Colloid Interface Sci.* 123, (1988) 306. Adsorption of Fibrinogen as a Measure of the Distribution of Methyl Groups on Silicon Surfaces.

77. Membrez, J., P. P. Infelta, and A. Renken: *Chem. Eng. Sci.* 51 (1996) 44-89. Use of the Laplace Transform Technique for Simple Kinetic Parameter Evaluation: Application to the Adsorption of a Protein on Porous Beads.

78. Heeter, G. A. and A. I. Liapis: *J. Chromatog.* A 776 (1997) 3-13. Model Discrimination and Estimation of the Intraparticle Mass Transfer Parameters for the Adsorption of Bovine Serum Albumin onto Porous Adsorbent Particles by the use of Experimental Frontal Analysis Data.

79. Conder, J. R., G. Leaver, and J. A. Howell: *I. Chem. E. Symp. Ser.* 118, 1-15 (1990). Adsorption Isotherms of Albumin on a Cross-Linked Cellulose Chromatographic Ion-Exchanger.

80. Bin Daina, M. M.: *Fouling and Regeneration of Silica Adsorbents for Protein Separation*. MSc Dissertation University of Wales Swansea (1999).

81. Chapra, S. C. and R. P. Canale: *Numerical Methods for Engineers*. 3rd ed. WCB/McGraw Hill International Editions, 1998.

82. Coulson, J. M., and J. F. *Richardson. Chemical Engineering Volume Three*. 2nd ed. Oxford Pergamon Press 1975.

83. Coulson, J. M., and J. F. *Richardson. Chemical Engineering Volume Two*. 5th ed. Oxford Pergamon Press 1991.

84. Kanekanian, A. D. A. and M. J. Lewis: *Developments in Food Proteins*. Vol. 4, (1986). Protein Isolation Using Ion-Exchangers.

85. McCabe, W. L., J. C. Smith and P. Harriott, *Unit Operations of Chemical Engineering*. 4th ed., New York: McGraw-Hill, 1985.

86. Smith, G. D., *Numerical Solution of Partial Differential Equations: Finite Difference Methods*, 2nd Ed. Oxford: Clarendon Press, 1978.

87. Tswett, M., *Ber. Deut. Botan. Ges*, 24, p.384.

88. Walsh, G. and D. Headon: *Protein Biotechnology*. Wiley & Sons, 1994.

APPENDIX A

APPENDIX A1

DETERMINATION OF THE VOIDAGE REDUCTION IN A COLUMN OF CLOSE-PACKED FIBROUS PARTICLES

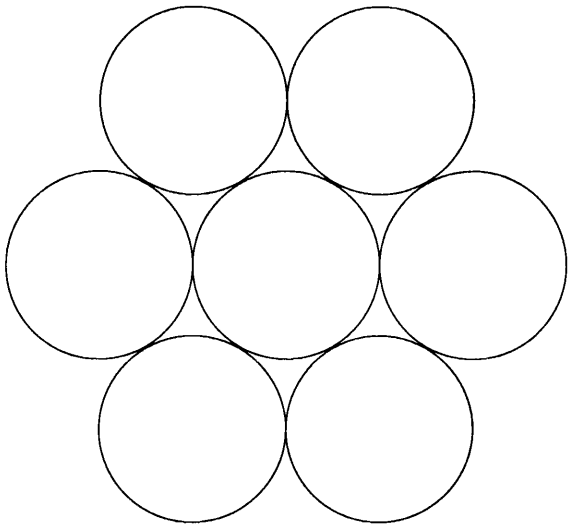

FIGURE A1-1: *Bundle of close-packed fibres.*

Let us assume a bundle of hexagonally close-packed fibrous particles aligned parallel to each other and to the axis of the column. The space (voidage) around a particle surrounded by six others approximates a hexagon as in Figure A1-2. The hexagon so formed can be divided into six triangles from which the voidage around the particle, and thus column voidage, can be calculated as follows.

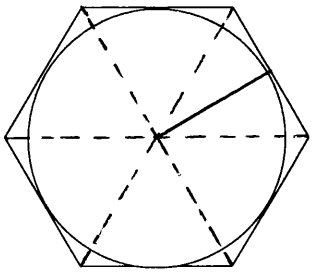

FIGURE A1-2: *The space around a single cylinder.*

Area of Hexagon = 6 × area of the triangle

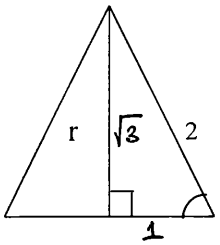

$$= \quad 6 \times \frac{r}{\sqrt{3}} \times r$$

$$= \quad 2 \times \sqrt{3} \times r^2$$

Area of circle $= \quad \pi r^2$

Therefore,

Circle / Hexagon $= \quad \dfrac{\pi r^2}{2\sqrt{3}\, r^2}$

$$= \quad \frac{\pi}{2\sqrt{3}}$$

$$= \quad 0.907$$

Therefore, voidage $\varepsilon_b = 1 - 0.907$

$= 0.093$

APPENDIX A2

COMPLETE DISTRIBUTION OF ALL PARTICLES SAMPLED IN THEIR SIZE GROUPS

Mean Diameter	Classes	% under	Surface	Classes	% under	Surface
20.5714544	7 - 14.5			7 - 14.5		
Total Diameter	13.51461	61	182.6446281	10.36523114		107.4380165
11293.72847	7.329325		53.71900826	7.820295697		61.15702479
	8.576346	f_j	73.55371901	9.663768921		93.38842975
d_{NL}	8.131156	0.1111	66.11570248	14.20045396		201.6528926
20.5714544	10.60173		112.3966942	13.11109555		171.9008264
	10.64064	$f_{L,j}$	113.2231405	11.39087644		129.7520661
Total Surface Area	10.16395	0.044595	103.3057851	10.16394535		103.3057851
152938.843	13.0162		169.4214876	11.09686874		123.1404959
	10.64064	$f_{s,j}$	113.2231405	10.94690416		119.8347107
d_{NS}	12.36497	0.041274	152.892562	13.51460795		182.6446281
16.69062993	10.98459		120.661157	12.85648693		165.2892562
	13.1111	$d_{NL,j}$	171.9008264	11.64204407		135.5371901
d_{LS}	13.75704	8.256524	189.2561983	11.64204407		135.5371901
13.54192669	13.75704		189.2561983	12.92060946		166.9421488
	13.66663	$d_{NS,j}$	186.7768595	12.23056732		149.5867769
	12.85649	10.17311	165.2892562	13.63636364		185.9504132
	14.11289		199.1735537	12.92060946		166.9421488
	14.22952	$d_{LS,j}$	202.4793388	13.11109555		171.9008264
	11.49919	12.5346	132.231405	13.11109555		171.9008264
	14.20045		201.6528926	13.63636364		185.9504132
	10.04124		100.8264463			
	13.66663		186.7768595	Total Length		Total Surface
	13.23656		175.2066116	503.6479538		6312.396694
	13.84686		191.7355372			
	13.0162		169.4214876			
	11.39088		129.7520661	Avg Length		
	11.39088		129.7520661	12.28409643		
	14.11289		199.1735537			
	10.64064		113.2231405			
	14.22952		202.4793388			
	12.19673		148.7603306			
	12.19673		148.7603306			
	14.11289		199.1735537			
	13.51461		182.6446281			
	12.23057		149.5867769			
	12.92061		166.9421488			
	13.51461		182.6446281			
	14.20045		201.6528926			
	12.85649		165.2892562			
	12.23057		149.5867769			
	10.9469		119.8347107			

Classes 14.5 - 22	% under	Surface	Classes 14.5 - 22	% under	Surface
16.76281	296	280.9917	17.48671		305.7851
15.45455		238.843	18.2725		333.8843
15.04813	f_j	226.4463	15.69334		246.281
14.68681	0.5392	215.7025	15.69334		246.281
15.53455		241.3223	18.40769		338.843
16.38887	$f_{L,j}$	268.595	20.42928		417.3554
15.53455	0.062368	241.3223	17.90701		320.6612
18.98238		360.3306	21.14492		447.1074
19.58242	$f_{s,j}$	383.4711	20.02065		400.8264
20.12359	0.080127	404.9587	20.42928		417.3554
19.85485		394.2149	15.48126		239.6694
18.40769	$d_{NL,j}$	338.843	19.4554		378.5124
18.40769	2.37961	338.843	18.71933		350.4132
16.38887		268.595	16.38887		268.595
17.55746	$d_{NS,j}$	308.2645	17.46307		304.9587
18.40769	6.495419	338.843	21.30068		453.719
18.74139		351.2397	20.92884		438.0165
18.74139	$d_{LS,j}$	351.2397	20.18509		407.438
17.55746	17.72999	308.2645	17.65135		311.5702
19.26329		371.0744	17.48671		305.7851
20.12359		404.9587	16.38887		268.595
18.74139		351.2397	14.54545		211.5702
17.90701		320.6612	14.54545		211.5702
19.93792		397.5207	15.45455		238.843
18.74139		351.2397	15.45455		238.843
18.40769		338.843	16.46434		271.0744
17.55746		308.2645	15.56113		242.1488
15.87659		252.0661	21.96917		482.6446
15.45455		238.843	20.77029		431.405
16.71343		279.3388	17.90701		320.6612
16.71343		279.3388	16.71343		279.3388
17.55746		308.2645	19.11254		365.2893
18.74139		351.2397	21.96917		482.6446
17.90701		320.6612	19.51901		380.9917
17.90701		320.6612	19.66664		386.7769
16.71343		279.3388	18.18182		330.5785
17.55746		308.2645	18.2951		334.7107
17.55746		308.2645	14.65865		214.876
16.71343		279.3388	16.91007		285.9504
16.10913		259.5041	19.17729		367.7686

Classes 14.5 - 22	% under	Surface	Classes 14.5 - 22	% under	Surface
19.17729		367.7686	20.90909		437.1901
18.2951		334.7107	18.20453		331.405
19.11254		365.2893	19.11254		365.2893
19.11254		365.2893	20.02065		400.8264
19.95863		398.3471	19.11254		365.2893
19.51901		380.9917	19.11254		365.2893
20.32789		413.2231	21.89381		479.3388
17.48671		305.7851	20.90909		437.1901
16.26231		264.4628	18.18182		330.5785
17.08027		291.7355	17.29663		299.1736
16.68869		278.5124	14.57384		212.3967
17.48671		305.7851	16.38887		268.595
18.71933		350.4132	20		400
20.42928		417.3554	20.02065		400.8264
19.51901		380.9917	19.17729		367.7686
21.98798		483.4711	19.17729		367.7686
20.02065		400.8264	19.11254		365.2893
21.30068		453.719	17.90701		320.6612
18.18182		330.5785	16.71343		279.3388
18.91696		357.8512	14.79893		219.0083
19.66664		386.7769	15.53455		241.3223
21.98798		483.4711	14.99311		224.7934
20.42928		417.3554	14.37399		206.6116
17.93008		321.4876	16.10913		259.5041
20.42928		417.3554	17.55746		308.2645
19.66664		386.7769	18.74139		351.2397
20.73046		429.7521	16.26231		264.4628
21.30068		453.719	16.08346		258.6777
20.02065		400.8264	19.66664		386.7769
20.57038		423.1405	19.95863		398.3471
20.57038		423.1405	21.20346		449.5868
16.38887		268.595	21.89381		479.3388
19.11254		365.2893	20.73046		429.7521
18.2725		333.8843	18.65299		347.9339
15.56113		242.1488	17.65135		311.5702
17.29663		299.1736	18.04494		325.6198
20		400	17.36816		301.6529
20.92884		438.0165	18.04494		325.6198
18.18182		330.5785	16.38887		268.595
21.81818		476.0331	16.68869		278.5124

Classes 14.5 - 22	% under	Surface	Classes 14.5 - 22	% under	Surface
16.26231		264.4628	17.36816		301.6529
21.30068		453.719	17.15269		294.2149
18.91696		357.8512	17.65135		311.5702
18.11351		328.0992	18.40769		338.843
20.51003		420.6612	19.4554		378.5124
20.73046		429.7521	17.65135		311.5702
19.85485		394.2149	19.28473		371.9008
20.73046		429.7521	18.91696		357.8512
19.58242		383.4711	18.04494		325.6198
17.90701		320.6612	18.18182		330.5785
15.87659		252.0661	16.76281		280.9917
18.2951		334.7107	18.65299		347.9339
18.74139		351.2397	21.45532		460.3306
20.32789		413.2231	19.66664		386.7769
17.55746		308.2645	18.71933		350.4132
20.77029		431.405	18.71933		350.4132
20.98799		440.4959	19.17729		367.7686
18.74139		351.2397	18.71933		350.4132
18.2951		334.7107	20.73046		429.7521
18.65299		347.9339	21.45532		460.3306
17.99908		323.9669	21.96917		482.6446
21.22294		450.4132	20.18509		407.438
21.6852		470.2479	21.20346		449.5868
21.96917		482.6446	19.95863		398.3471
21.96917		482.6446	21.14492		447.1074
17.93008		321.4876	21.28127		452.8926
20.92884		438.0165	20.51003		420.6612
16.91007		285.9504	18.40769		338.843
16.1859		261.9835	16.98322		288.4298
17.65135		311.5702	15.53455		241.3223
17.15269		294.2149	18.74139		351.2397
17.46307		304.9587	21.22294		450.4132
18.65299		347.9339	21.22294		450.4132
19.28473		371.9008	21.39746		457.8512
20.61052		424.7934	21.39746		457.8512
18.65299		347.9339	21.98798		483.4711
17.46307		304.9587	17.48671		305.7851
16.38887		268.595	16.76281		280.9917
19.4554		378.5124	16.10913		259.5041
18.04494		325.6198	15.23914		232.2314

Classes 14.5 - 22	% under	Surface	Classes 14.5 - 22	% under	Surface
21.98798		483.4711	16.1859		261.9835
21.96917		482.6446	21.20346		449.5868
21.96917		482.6446	17.90701		320.6612
20.73046		429.7521	19.51901		380.9917
19.26329		371.0744	19.93792		397.5207
16.26231		264.4628	19.58242		383.4711
16.98322		288.4298	21.60884		466.9421
20.51003		420.6612	21.81818		476.0331
20.51003		420.6612	20		400
21.22294		450.4132	20		400
19.43414		377.686	20.92884		438.0165
19.62458		385.124	18.38523		338.0165
19.32754		373.5537	18.54189		343.8017
21.22294		450.4132	21.60884		466.9421
19.66664		386.7769	17.93008		321.4876
16.38887		268.595	21.6852		470.2479
14.68681		215.7025			
17.90701		320.6612	**Total Length**		**Total Surf**
19.93792		397.5207	704.3647		12489.26
21.5514		464.4628			
21.20346		449.5868	**Avg Length**		
21.22294		450.4132	17.60912		
21.89381		479.3388			
20.57038		423.1405			
19.32754		373.5537			
20.61052		424.7934			
18.04494		325.6198			
18.65299		347.9339			
18.04494		325.6198			
14.9102		222.314			
16.08346		258.6777			
18.74139		351.2397			
18.18182		330.5785			
17.24879		297.5207			
16.38887		268.595			
14.9102		222.314			
15.64059		244.6281			
14.9102		222.314			
17.08027		291.7355			
17.15269		294.2149			

Classes 22 - 29.5	% under	Surface	Classes 22.0 - 29.5	% under	Surface
22.99838	156	528.9256	22.45289		504.1322
25.01239		625.6198	24.00069		576.0331
25.32434	f_j	641.3223	24.81335		615.7025
26.0324	0.2842	677.686	26.86052		721.4876
23.63636		558.6777	25.61637		656.1983
23.30183	$f_{L,j}$	542.9752	24.0179		576.8595
22.79988	0	519.8347	26.36364		695.0413
23.91445		571.9008	24.54545		602.4793
25.71297	$f_{s,j}$	661.157	23.63636		558.6777
26.92199	0	724.7934	22.74545		517.3554
26.61324		708.2645	23.63636		558.6777
25.60023	$d_{NL,j}$	655.3719	27.28787		744.6281
28.70482	0	823.9669	28.18182		794.2149
22.13781		490.0826	26.42626		698.3471
23.28409	$d_{NS,j}$	542.1488	27.82769		774.3802
24.20641	0	585.9504	27.82769		774.3802
22.36068		500	27.70864		767.7686
22.45289	$d_{LS,j}$	504.1322	28.93424		837.1901
24.72995	#DIV/0!	611.5702	28.99131		840.4959
24.15515		583.4711	27.82769		774.3802
22.78175		519.0083	26.42626		698.3471
22.94442		526.4463	24.00069		576.0331
22.19374		492.562	22.72727		516.5289
24.00069		576.0331	22.45289		504.1322
23.58386		556.1983	23.70619		561.9835
25.20986		635.5372	26.84513		720.6612
26.86052		721.4876	22.36068		500
22.78175		519.0083	25.01239		625.6198
22.45289		504.1322	22.50803		506.6116
22.78175		519.0083	22.50803		506.6116
23.23079		539.6694	23.79319		566.1157
22.78175		519.0083	22.00676		484.2975
23.58386		556.1983	23.79319		566.1157
24.0179		576.8595	23.86255		569.4215
22.36068		500	27.02922		730.5785
22.79988		519.8347	25.07839		628.9256
23.17736		537.1901	23.17736		537.1901
22.45289		504.1322	23.14168		535.5372
23.28409		542.1488	22.48967		505.7851
22.58135		509.9174	22.48967		505.7851

Classes 22.0 - 29.5	% under	Surface	Classes 22.0 - 29.5	% under	Surface
25.14421		632.2314	25.47077		648.7603
24.72995		611.5702	27.82769		774.3802
24.56228		603.3058	28.74798		826.4463
27.12079		735.5372	28.53155		814.0496
27.27273		743.8017	25.27534		638.843
27.82769		774.3802	26.55106		704.9587
28.00531		784.2975	24.00069		576.0331
28.31348		801.6529	24.47802		599.1736
27.70864		767.7686	26.0324		677.686
26.42626		698.3471	28.87705		833.8843
24.00069		576.0331	22.28664		496.6942
23.46089		550.4132	23.37265		546.281
22.78175		519.0083	23.91445		571.9008
23.17736		537.1901	22.28664		496.6942
23.63636		558.6777	22.50803		506.6116
24.47802		599.1736	22.58135		509.9174
23.46089		550.4132	22.00676		484.2975
22.50803		506.6116	22.36068		500
25.07839		628.9256	22.79988		519.8347
24.46113		598.3471	22.45289		504.1322
22.58135		509.9174	22.45289		504.1322
23.14168		535.5372	23.86255		569.4215
23.86255		569.4215	23.01634		529.7521
23.86255		569.4215	23.70619		561.9835
24.56228		603.3058	22.72727		516.5289
22.00676		484.2975	23.63636		558.6777
26.00064		676.0331	22.58135		509.9174
26.55106		704.9587	29.44388		866.9421
28.24041		797.5207	29.21847		853.719
22.58135		509.9174	29.21847		853.719
23.79319		566.1157	29.10511		847.1074
25.7451		662.8099	28.19648		795.0413
24.46113		598.3471	28.19648		795.0413
25.07839		628.9256	26.42626		698.3471
26.36364		695.0413	27.28787		744.6281
27.70864		767.7686	28.19648		795.0413
28.00531		784.2975			
26.73717		714.876	**Total Length**		**Total Surf**
28.74798		826.4463	0		0
28.54603		814.876			
			Avg Length		
			#DIV/0!		

Classes	% under	Surface
29.5 - 38		
30.88234	36	953.719
30.27423		916.5289
30.38323	f_j	923.1405
31.81818	0.0656	1012.397
33.64865		1132.231
29.59786	$f_{L,j}$	876.0331
30.88234	0.102371	953.719
29.7788		886.7769
29.6815	$f_{s,j}$	880.9917
31.55737	0.154421	995.8678
32.16692		1034.711
31.50495	$d_{NL,j}$	992.562
34.80762	32.11531	1211.57
31.66195		1002.479
34.16053	$d_{NS,j}$	1166.942
33.74675	32.15728	1138.843
31.30759		980.1653
31.34716	$d_{LS,j}$	982.6446
32.52463	32.1993	1057.851
32.52463		1057.851
32.52463		1057.851
29.98622		899.1736
31.97365		1022.314
31.12226		968.595
30.96252		958.6777
33.74675		1138.843
34.84321		1214.05
34.55741		1194.215
30.92246		956.1983
30.92246		956.1983
30.05505		903.3058
32.77774		1074.38
37.66973		1419.008
33.34022		1111.57
33.63636		1131.405
32.85329		1079.339
Total Length		**Total Surf**
1156.151		37242.15
Avg Length		
32.11531		

APPENDIX A3

PARTICLE SIZE DATA: NUMBER, LINEAR AND SURFACE DISTRIBUTIONS

Size Range	$f_{L,j}$	$f_{s,j}$	f_j	$d_{NL,j}$	$d_{NS,j}$	$d_{LS,j}$
7 - 14.5	0.065844	0.037344	0.1111	12.19064	12.30958	12.42968
14.5 - 22	0.488829	0.420664	0.5392	18.65104	18.75361	18.85675
22 - 29.5	0.342955	0.391512	0.2842	24.82846	24.92026	25.01239
29.5 - 38	0.102371	0.15048	0.0656	32.11531	32.15728	32.1993

TABLE A3-1: *Full Particle Size Range.*

Size Range	$f_{L,j}$	$f_{s,j}$	f_j	$d_{NL,j}$	$d_{NS,j}$	$d_{LS,j}$
7 - 14.5	0.065844	0.037344	0.1111	12.19064	12.30958	12.42968
14.5 - 22	0.488829	0.420664	0.5392	18.65104	18.75361	18.85675
22 - 38	0.445326	0.541992	0.3498	26.19475	26.08947	25.98461

TABLE A3-2: *Particle Size Distribution for Three Size Groups.*

Size Range	$f_{L,j}$	$f_{s,j}$	f_j	$d_{NL,j}$	$d_{NS,j}$	$d_{LS,j}$
7 - 14.5	0.065844	0.037344	0.1111	12.19064	12.30958	12.42968
14.5 - 38	0.934155	0.962656	0.889	20.96979	21.81039	22.68468

TABLE A3-3: *Particle Size Distribution for Two Size Groups.*

APPENDIX B

APPENDIX B1

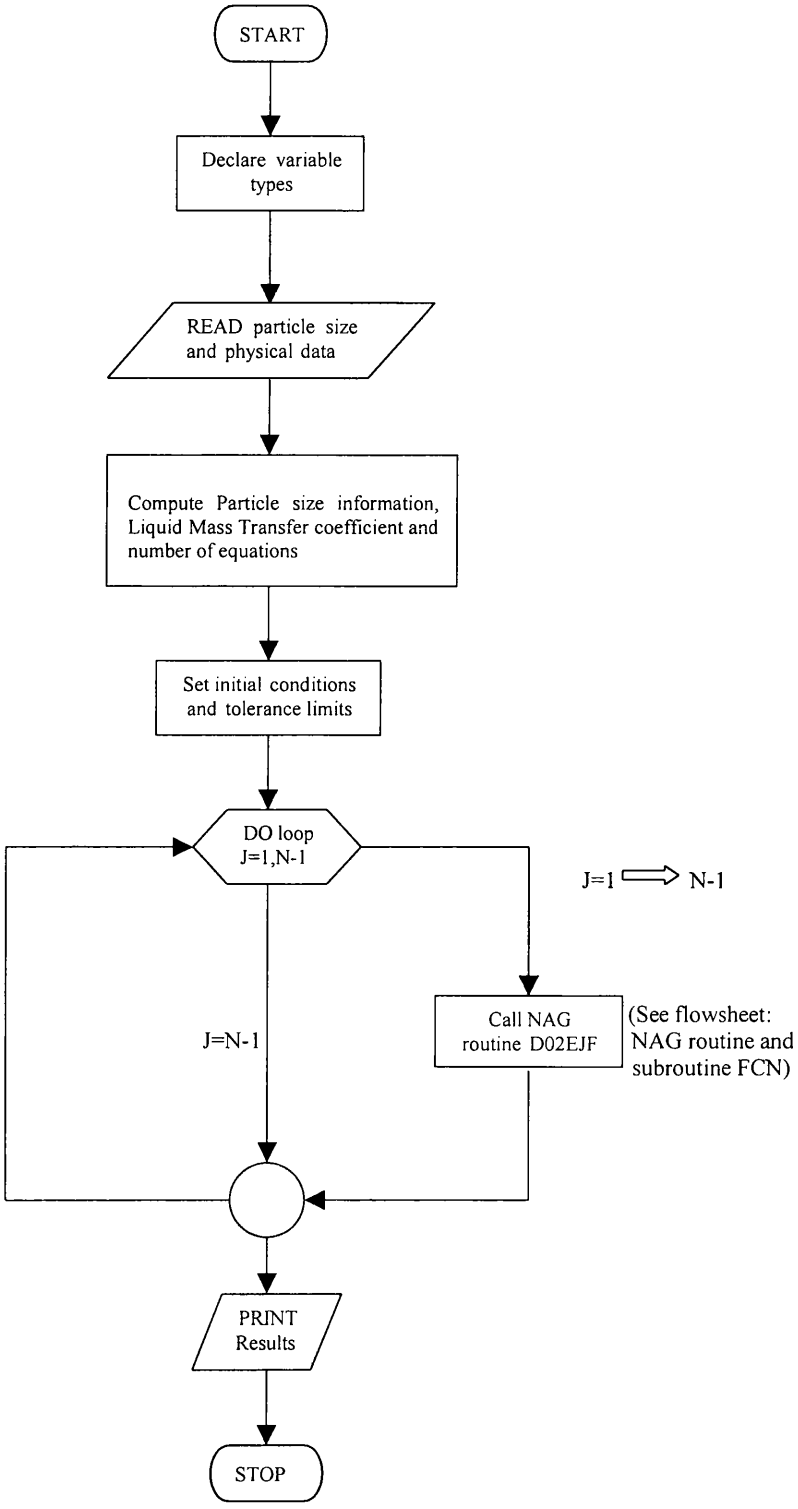

FIGURE B1-1: *Flow sheet of the main program for the stirred cell model*

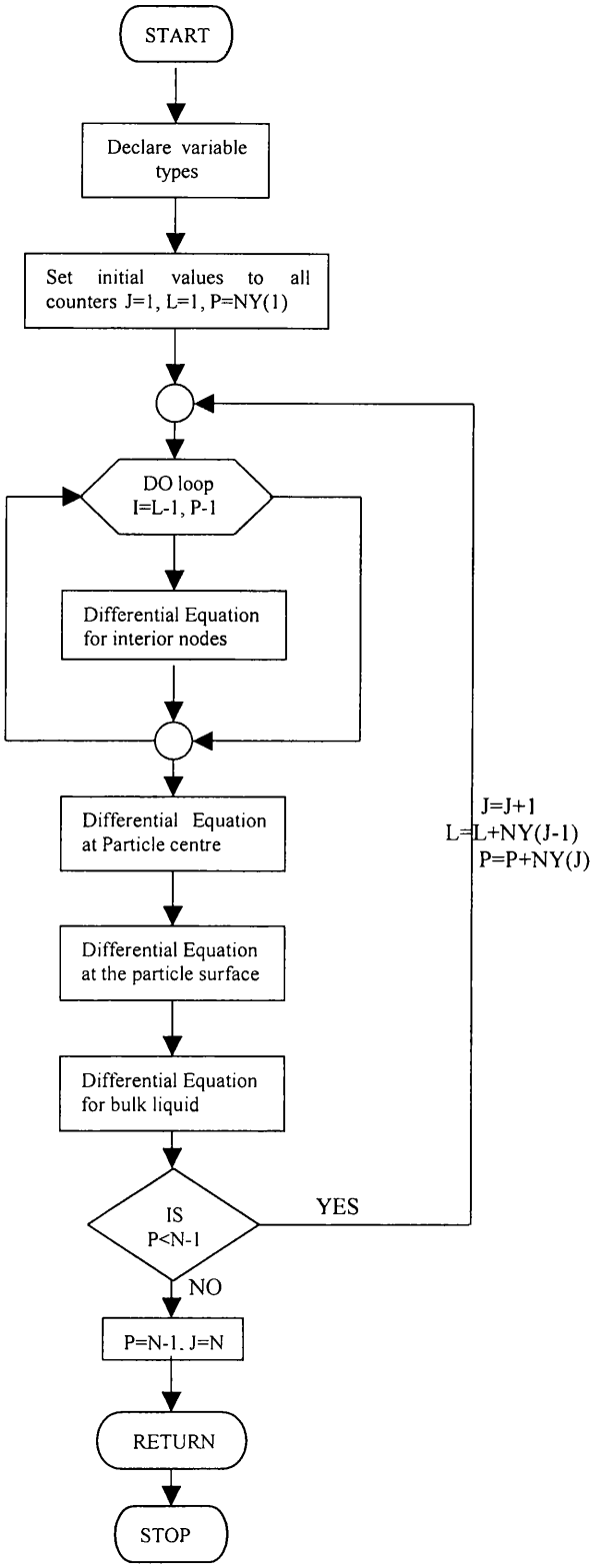

FIGURE B1-2: *Flow sheet of the subroutine FCN for solving the stirred tank model.*

(B1-2) DEFINITION OF THE TERMS USED IN THE COMPUTER CODING OF THE STIRRED CELL MODEL

ATOL	Tolerance limits
CKF	Liquid film mass transfer coefficient
CKD	Langmuir coefficient
CO	Initial concentration
DIF	Effective diffusivity
D0	Parameter for calculating CKF
E	Porosity
FDIL	Number-Linear distribution fraction
G	Reciprocal of time constant for delay in sample loop
H	Step size
I, J, L, P	Counters
ID	Number of particle size groups
K	Maximum number of time steps (used to calculate H)
N	Number of equations/points
QM	Langmuir coefficient
R	Particle radius
RDIL	Number-Linear mean diameter
RDIS	Number-Surface mean diameter
RS	Parameter for calculating CKF
RLRS	Linear-Surface mean diameter
TM	Time
TOL	Tolerance limit
VAL	Ratio of total volume of solid/volume of liquid
X	Dimensionless Time
XEND	Time limit

```
C================== CHUKA4B.FOR ==============================C
C                                                              C
C==============================================================C
C=== THIS PROGRAM USES THE NAG SUBROUTINE DO2EJF TO SOLVE SYSTEM  ===C
C== OF ORDINARY DIFFERENTIAL EQUATIONS FOR STIRRED CELL ADSORPTION.==C
C==== THE MODEL ACCOUNTS FOR POLYDISPERSITY IN PARTICLE SIZE.  ======C
C==== THE EQUATIONS ARE STIFF.  THE PARTICLES ARE CYLINDRICAL.  ======C
C==============================================================
C
C                      Contents: - Main Program                C
C                      - Solution Subroutine FCN               C
C                      - Output Subroutine 'OUTPUT'            C
C============================================================== C
C                                                              C
C======================= MAIN PROGRAM ========================C
C====================  Defining all Variables  ================C

      OPTIONS (CHECK)

      INTEGER M,N,IW
      INTEGER K,ID,NY(32)
      INTEGER I,IFAIL,J

      PARAMETER (M=200)
      PARAMETER (IW=(24+2*M)*2*M+100)

      DOUBLE PRECISION H,XEND
      DOUBLE PRECISION TOL,X,TM
      DOUBLE PRECISION W(IW),Y(M)
      DOUBLE PRECISION CO,DIF,QM,CKD,E,R,RS,B,DR
     1 ,CKF(32),SH(32),DZ(32),DZSQ(32),DUM2(32)
     2 ,DUM4(32),DUM5,RDIL(32),FDIL(32),RDIS(32),RLRS(32),RLS(32)

      EXTERNAL D02EJW
      EXTERNAL D02EJF,D02EJY,FCN,OUTPUT
      INTRINSIC REAL,INT

C===    Setting up memory locations    ======================C

      COMMON XEND,H,K
      COMMON/CONSTANTS/DIF,QM,CKD,E,VAL,R,B,CO,ID,RS,N
      COMMON/DISTRIBUTION/RDIL
      COMMON/DISTRI/FDIL
```

```
      COMMON/DDZZ/DZ
      COMMON/DZSQZ/DZSQ
      COMMON/DUM/DUM4
      COMMON/NYY/NY
      COMMON/CK/DUM2
      COMMON/SHI/SH
      COMMON/RLRS/RLRS

      CHARACTER*14 FNAME1
      CHARACTER*14 FNAME2
      CHARACTER*14 FNAME3
      OPEN(UNIT=4,FILE='SCExD04B.DAT',STATUS='OLD')
      READ(4,001) FNAME1,FNAME2,FNAME3
001   FORMAT(A14)
      OPEN(UNIT=5,FILE=FNAME1,STATUS='OLD')
      OPEN(UNIT=6,FILE=FNAME2,STATUS='OLD')
      OPEN(UNIT=7,FILE=FNAME3,STATUS='OLD')

      READ(5,*) DIF,D0,XEND,K,CO,QM,CKD,E,VAL,R
     1 ,TOL,RS,DR
      READ(6,*) ID,(RDIL(I),I=1,ID),(RDIS(I),I=1,ID)
     1 ,(FDIL(I),I=1,ID)
```

C=== Calculating all particle size related parameters ==C

```
      B=QM*CKD*(1-E)/E
      DUM5=R*R/DIF

      N=0
      DO 002 I=1,ID
      RDIL(I)=RDIL(I)/2.0
      RDIS(I)=RDIS(I)/2.0
      RLRS(I)=(RDIS(I)/RDIL(I))**2
      RLS(I)=RDIS(I)**2/RDIL(I)
      CKF(I)=(D0/RLS(I)+RS)
      SH(I)=(1.0*CKF(I))*R/(DIF*E)
      NY(I)=2+INT(RDIS(I)/DR)
      IF (RDIL(I).LT.10E-6) THEN
      NY(I)=5
      ELSE
      ENDIF
      DZ(I)=RDIL(I)/R/REAL(NY(I)-1)
      DZSQ(I)=DZ(I)*DZ(I)
      DUM2(I)=2.0*SH(I)*VAL*E
      DUM4(I)=2.0*SH(I)*DZ(I)
      N=N+NY(I)
002   CONTINUE
      N=N+1
```

C=== Setting all initial conditions ==========C

```
      X=0.0E0
      DO 003 J=1,N-1
      Y(J)=0.0E0
003   CONTINUE
      Y(N)=1.0

      H=(XEND-X)/REAL(K+1)
C-----Tolerance limit
      IFAIL=0

C===     Calling NAG routine D02EJF     ======================C

      GOTO 004

      CALL D02EJF(X,XEND,N,Y,FCN,D02EJY,TOL,'D',OUTPUT,D02EJW,W,
     1 IW,IFAIL)

004   CONTINUE

      TM=X*DUM5/60

C-----Checking main program performance
      PRINT*, 'IFAIL,TOL,IW',IFAIL,TOL,IW
      PRINT*, 'R',R
      PRINT*, 'DIF',DIF
      PRINT*, 'N',N
      PRINT*, 'H',H
      PRINT*, 'CO',CO
      PRINT*, 'CKF(1,2)',(CKF(I),I=1,2)
      PRINT*, 'CKF(3,4)',(CKF(I),I=3,4)
      PRINT*, 'SH(1,2)',(SH(I),I=1,2)
      PRINT*, 'SH(3,4)',(SH(I),I=3,4)
      PRINT*, 'X',X
      PRINT*, 'TM',TM
      PRINT*, 'Y(N)',Y(N)

      STOP
      END
C==============    END OF MAIN PROGRAM     ====================C
C                                                              C
C================ SOLUTION SUBROUTINE FCN =====================C

      SUBROUTINE FCN(X,Y,F)

      INTEGER M,N,P,I,J,ID,NY(32)
      PARAMETER (M=200)

      DOUBLE PRECISION B,DIF,CKD,E,VAL,QM,CO
      DOUBLE PRECISION F(M),Y(M),DUM3,DUM8,RS,Q,S,X
      DOUBLE PRECISION RDIL(32),FDIL(32),DZ(32)
     1 ,DZSQ(32),DUM4(32),DUM2(32),SH(32),RLRS(32)
```

```
      COMMON/CONSTANTS/DIF,QM,CKD,E,VAL,R,B,CO,ID,RS,N
      COMMON/DISTRIBUTION/RDIL
      COMMON/DISTRI/FDIL
      COMMON/DDZZ/DZ
      COMMON/DZSQZ/DZSQ
      COMMON/DUM/DUM4
      COMMON/NYY/NY
      COMMON/CK/DUM2
      COMMON/SHI/SH
      COMMON/RLRS/RLRS

      Q(S)=(CO**2)*((CKD/CO+S)**2)/((CO**2)*(CKD/CO+S)**2+B)

C-----Setting up counters
      L=1
      P=NY(1)
      J=1
      FFR=0.0

C===    Ordinary differential equations to be solved    ======C

005   DO 006 I=L+1,P-1
      DUM3=I-L
C-----Equation for interior nodes of particles
      F(I)=Q(Y(I))*((DUM3+0.5)*Y(I+1)/(DUM3)-2.0*Y(I)+(DUM3-0.5)
     1 *Y(I-1)/DUM3)/DZSQ(J)/RLRS(J)

006   CONTINUE

C-----Equation for centre of particles
      F(L)=4.0*Q(Y(L))*(Y(L+1)-Y(L))/DZSQ(J)/RLRS(J)

      DUM3=P-L
      DUM8=(DUM3+0.5)/DUM3
C-----Equation for surface of particles
      F(P)=Q(Y(P))*(DUM4(J)*DUM8*Y(N)
     1 +(-2.0-DUM4(J)*DUM8)*Y(P)+2.0*Y(P-1))/DZSQ(J)/RLRS(J)

C-----Equation for the bulk liquid
      FFR=FFR+DUM2(J)*FDIL(J)*(Y(N)-Y(P))
C-----Checking subroutine performance
      PRINT*, 'X,Y(N)',X,Y(N)

      IF(P.LT.N-1)THEN
      J=J+1
      L=L+NY(J-1)
      P=P+NY(J)
      GOTO 005
      ENDIF
```

```
      F(N)=-FFR

      RETURN
      END
C============== END OF SOLUTION SUBROUTINE 'FCN' ================C
C                                                                 C
C=============  OUTPUT SUBROUTINE 'OUTPUT'  ====================C

      SUBROUTINE OUTPUT(X,Y)

      INTEGER M,N
      INTEGER I,NY(32)
      PARAMETER (M=200,N=29)

      DOUBLE PRECISION X,Y(N),H,XEND
      DOUBLE PRECISION B,DIF,CKD,E,R,VAL,QM,CO,RS
      DOUBLE PRECISION RDIL(32),FDIL(32),SH(32)
     1 ,DZ(32),DZSQ(32),DUM4(32),DUM2(32),RLRS(32)

      COMMON XEND,H,I
      COMMON/CONSTANTS/DIF,QM,CKD,E,VAL,R,B,CO,ID,RS,N
      COMMON/DISTRIBUTION/RDIL
      COMMON/DISTRI/FDIL
      COMMON/DDZZ/DZ
      COMMON/DZSQZ/DZSQ
      COMMON/DUM/DUM4
      COMMON/NYY/NY
      COMMON/CK/DUM2
      COMMON/SHI/SH
      COMMON/RLRS/RLRS
C-----Writing intermediate solution at desired point
      WRITE(7,007) X,Y(N)
C-----Next point at which 'output' is to be called
      X=XEND-REAL(I)*H
      I=I-1

      RETURN
007   FORMAT(3X,F10.3,2X,F8.4)
      END
C============== END OF OUTPUT SUBROUTINE 'OUTPUT' ================C
C                                                                 C
C============================== END ==============================C
```

APPENDIX B2

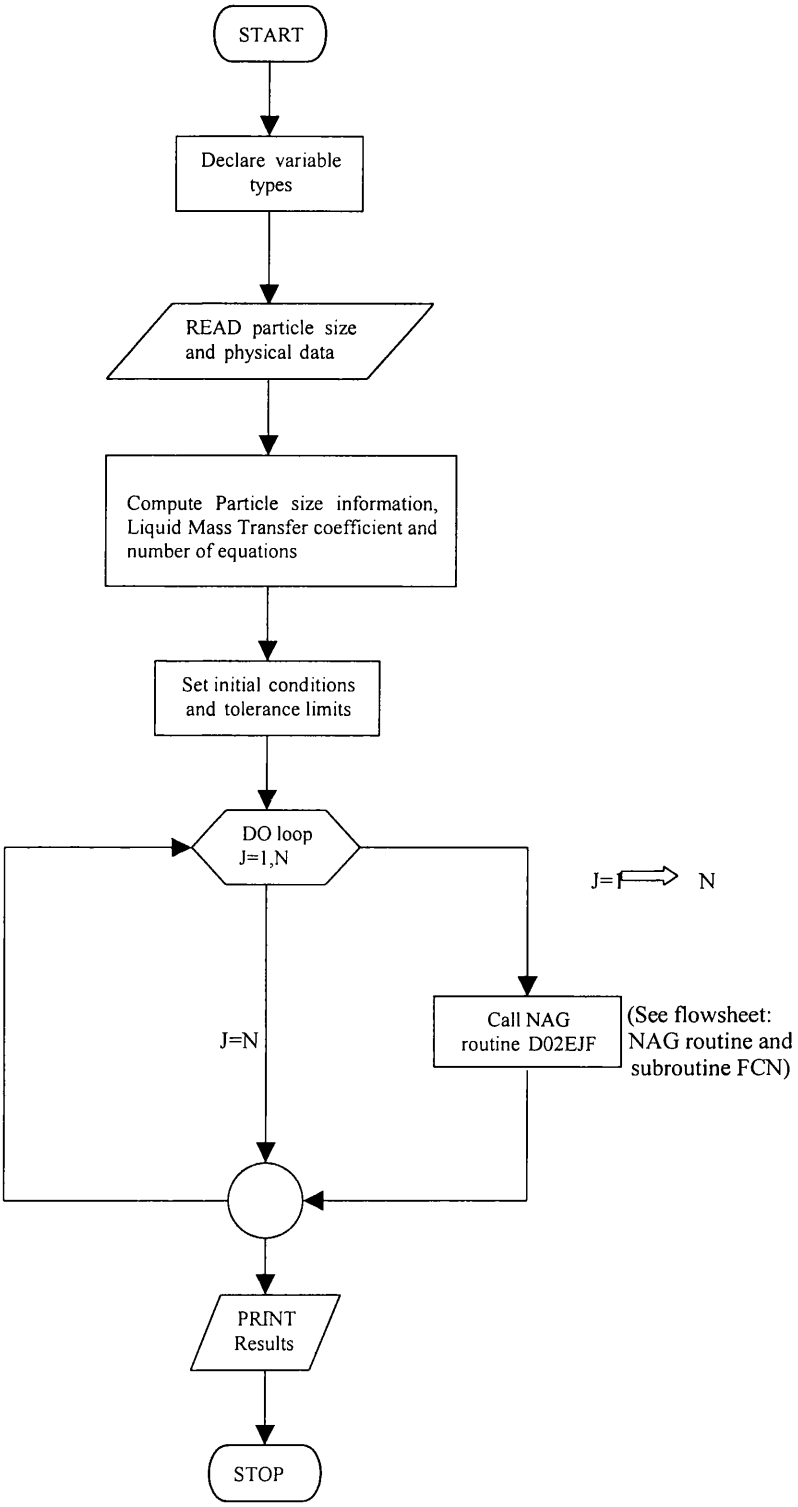

FIGURE B2-1: *Flow sheet of the main program for the Packed bed model*

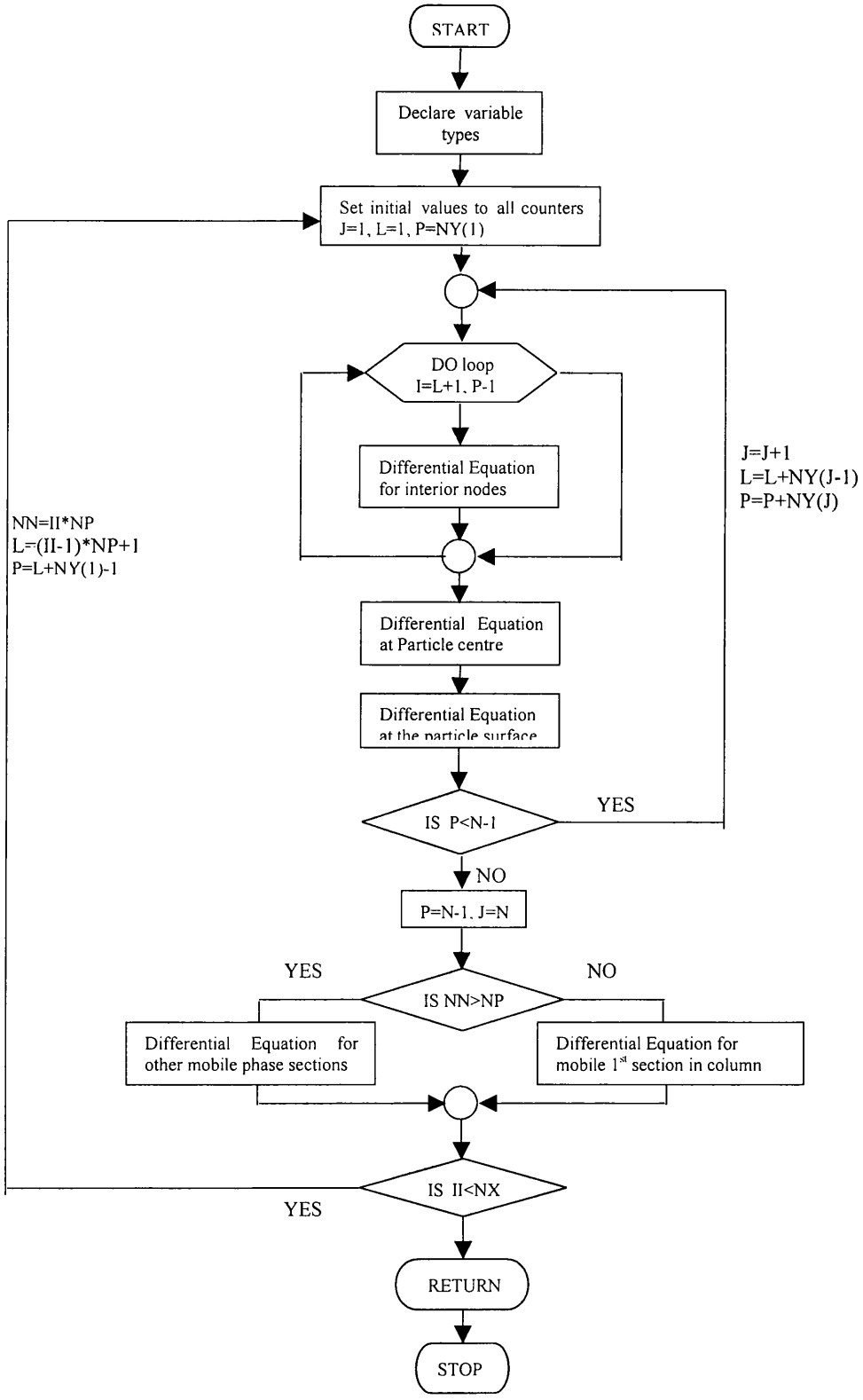

FIGURE B2-2: *Flow sheet of the subroutine FCN for solving the packed bed model.*

(B1-2) DEFINITION OF THE TERMS USED IN THE COMPUTER CODING OF THE STIRRED CELL MODEL

ATOL	Tolerance limits
CKF	Liquid film mass transfer coefficient
CKD	Langmuir coefficient
CLN	Column length
CO	Initial concentration
DIF	Effective diffusivity
DH	Distance between sections in the bed
D0	Parameter for calculating CKF
E	Porosity
EB	Bed void fraction
FDIL	Number-Linear distribution fraction
G	Reciprocal of time constant for delay in sample loop
H	Step size
I, J, L, NN, P	Counters
ID	Number of particle size groups
K	Maximum number of time steps (used to calculate H)
N	Number of equations/points
NX	Number of sections in the bed
QM	Langmuir coefficient
R	Particle radius
RDIL	Number-Linear mean diameter
RDIS	Number-Surface mean diameter
RS	Parameter for calculating CKF
RLRS	Linear-Surface mean diameter
TM	Time
TOL	Tolerance limit
U	Intergranular velocity
US	Superficial flow velocity

VAL	Ratio of total volume of solid/volume of liquid
X	Dimensionless time
XEND	Time limit

```
C======================= CHUKA5B.FOR ============================C
C                                                                 C
C=================================================================C
C==== THIS PROGRAM USES THE NAG SUBROUTINE DO2EJF TO SOLVE SYSTEM ==C
C=== OF ORDINARY DIFFERENTIAL EQUATIONS FOR PACKED BED ADSORPTION. ==C
C====   THE MODEL ACCOUNTS FOR POLYDISPERSITY IN PARTICLE SIZE.   ====C
C===    THE EQUATIONS ARE STIFF. THE PARTICLES ARE CYLINDRICAL.   ====C
C=================================================================C
C                        Contents: - Main Program                 C
C                                  - Solution Subroutine FCN      C
C                                  - Output Subroutine 'OUTPUT'   C
C=================================================================C
C                                                                 C
C======================= MAIN PROGRAM ============================C
C===================== Defining all Variables ====================C

      OPTIONS (CHECK)

      INTEGER M,N,IW
      INTEGER K,ID,NY(32)
      INTEGER I,IFAIL,J

      PARAMETER (M=1200)
      PARAMETER (IW=(24+2*M)*2*M+100)

      DOUBLE PRECISION H,XEND,D0,ff
      DOUBLE PRECISION TOL,X,TM
      DOUBLE PRECISION W(IW),Y(M)
      DOUBLE PRECISION CO,DIF,QM,CKD,E,R,RS,B,DR,G
     1 ,CKF(32),SH(32),DZ(32),DZSQ(32),DUM1,DUM2(32)
     2 ,DUM4(32),DUM5,RDIL(32),FDIL(32),RDIS(32),RLRS(32),RLS(32)

      EXTERNAL D02EJW
      EXTERNAL D02EJF,D02EJY,FCN,OUTPUT
      INTRINSIC REAL,INT

C===    Setting up memory locations          ======================C

      COMMON XEND,H,K
      COMMON/CONSTANTS/DIF,QM,CKD,E,R,B,CO,ID,RS,N,NP,NX,DUM1,DUM5,G
      COMMON/DISTRIBUTION/RDIL
      COMMON/DISTRI/FDIL
      COMMON/DDZZ/DZ
```

```
      COMMON/DZSQZ/DZSQ
      COMMON/DUM/DUM4
      COMMON/NYY/NY
      COMMON/CK/DUM2
      COMMON/SHI/SH
      COMMON/RLRS/RLRS

      CHARACTER*13 FNAME1
      CHARACTER*13 FNAME2
      CHARACTER*13 FNAME3
      OPEN(UNIT=4,FILE='PBExD10.DAT',STATUS='OLD')
      READ(4,001) FNAME1,FNAME2,FNAME3
001   FORMAT(A13)
      OPEN(UNIT=5,FILE=FNAME1,STATUS='OLD')
      OPEN(UNIT=6,FILE=FNAME2,STATUS='OLD')
      OPEN(UNIT=7,FILE=FNAME3,STATUS='OLD')

      READ(5,*) DIF,D0,XEND,K,CO,QM,CKD,E,EB,R,CLN,US,NX
     1 ,TOL,RS,G,DR,ff
      READ(6,*) ID,(RDIL(I),I=1,ID),(RDIS(I),I=1,ID)
     1 ,(FDIL(I),I=1,ID)

C===  Calculating all particle size related parameters  ==C

      B=QM*CKD*(1-E)/E
      U=US/EB
      DH=1/REAL(NX)
      DUM1=U*R*R/(CLN*DIF*DH)
      DUM5=R*R/DIF
      NP=0

      DO 002 I=1,ID
      RDIL(I)=RDIL(I)/2.0
      RDIS(I)=RDIS(I)/2.0
      RLRS(I)=(RDIS(I)/RDIL(I))**2
      RLS(I)=RDIS(I)**2/RDIL(I)
      CKF(I)=ff*0.5*D0*(2.0+RS*(US*RLS(I)*2.0)**0.5/D0**0.333)/RLS(I)
      SH(I)=(1.0*CKF(I))*R/(DIF*E)
      NY(I)=2+INT(RDIL(I)/DR)
      IF (RDIL(I).LT.10E-6) THEN
      NY(I)=5
      ELSE
      ENDIF
      DZ(I)=RDIL(I)/R/REAL(NY(I)-1)
      DZSQ(I)=DZ(I)*DZ(I)
      DUM2(I)=2.0*E*SH(I)*FDIL(I)*(1-EB)/EB
      DUM4(I)=2.0*SH(I)*DZ(I)
      NP=NP+NY(I)
002   CONTINUE

      NP=NP+1
```

```
      N=NP*NX

C===  Setting all initial conditions  ==================C

      X=0.0E0
      DO 003 J=1,N
      Y(J)=0.0E0
003   CONTINUE

      H=(XEND-X)/REAL(K+1)
C-----Tolerance limit
      IFAIL=0

C===  Calling NAG routine D02EJF  ====================C

      GOTO 004

      CALL D02EJF(X,XEND,N,Y,FCN,D02EJY,TOL,'R',OUTPUT,D02EJW,W,
     1 IW,IFAIL)

004   CONTINUE

      FLRT=US*1000.0
      TM=X*DUM5/60
      ECV=TM*FLRT/0.83
C-----Checking main program performance
      PRINT*, 'IFAIL,TOL,IW',IFAIL,TOL,IW
      PRINT*, 'R',R
      PRINT*, 'FLRT',FLRT
      PRINT*, 'DIF',DIF
      PRINT*, 'N',N
      PRINT*, 'H',H
      PRINT*, 'NP',NP
      PRINT*, 'CO',CO
      PRINT*, 'CKF(1,2)',(CKF(I),I=1,2)
      PRINT*, 'CKF(3,4)',(CKF(I),I=3,4)
      PRINT*, 'SH(1,2)',(SH(I),I=1,2)
      PRINT*, 'SH(3,4)',(SH(I),I=3,4)
      PRINT*, 'X',X
      PRINT*, 'TM',TM
      PRINT*, 'ECV',ECV
      PRINT*, 'Y(N)',Y(N)

      STOP
      END
C============  END OF MAIN PROGRAM  ========================C
C                                                           C
C============  SOLUTION SUBROUTINE FCN  ====================C

      SUBROUTINE FCN(X,Y,F)
```

```
      INTEGER M,N,P,I,J,ID,NY(32)
      PARAMETER (M=1200)

      DOUBLE PRECISION B,DIF,CKD,E,QM,CO,R,DUM1,DUM5,G
      DOUBLE PRECISION F(M),Y(M),DUM3,DUM8,RS,Q,S,X
      DOUBLE PRECISION RDIL(32),FDIL(32),DZ(32)
     1 ,DZSQ(32),DUM2(32),DUM4(32),SH(32),RLRS(32)

      COMMON/CONSTANTS/DIF,QM,CKD,E,R,B,CO,ID,RS,N,NP,NX,DUM1,DUM5,G
      COMMON/DISTRIBUTION/RDIL
      COMMON/DISTRI/FDIL
      COMMON/DDZZ/DZ
      COMMON/DZSQZ/DZSQ
      COMMON/DUM/DUM4
      COMMON/NYY/NY
      COMMON/CK/DUM2
      COMMON/SHI/SH
      COMMON/RLRS/RLRS

      Q(S)=(CO**2)*((CKD/CO+S)**2)/((CO**2)*(CKD/CO+S)**2+B)
C-----Allowing for delay and mixing effect
      TM=X*DUM5/60
      CC0=1.0-EXP(-G*TM)
      CC0=1.0
C-----Setting up counters
      L=1
      II=1
      P=NY(1)
      NN=NP
005   J=1

      FFR=0.0

C===    Ordinary differential equations to be solved    ======C
C-----Equation for interior nodes of particles
006   DO 007 I=L+1,P-1

      DUM3=I-L
      DUM6=(DUM3+0.5)/DUM3
      DUM7=(DUM3-0.5)/DUM3
      F(I)=Q(Y(I))*(DUM6*Y(I+1)-2.0*Y(I)+DUM7
     1 *Y(I-1))/DZSQ(J)/RLRS(J)

007   CONTINUE
C-----Equation for centre of particles
      F(L)=4.0*Q(Y(L))*(Y(L+1)-Y(L))/DZSQ(J)/RLRS(J)
C-----Equation for surface of particles
      DUM3=(P-L)
      DUM8=(DUM3+0.5)/DUM3
      F(P)=Q(Y(P))*(DUM4(J)*DUM8*Y(NN)
     1 +(-2.0-DUM4(J)*DUM8)*Y(P)+2.0*Y(P-1))/DZSQ(J)/RLRS(J)
```

```
      FFR=FFR+DUM2(J)*(Y(NN)-Y(P))

      IF(P.LT.NN-1)THEN
      J=J+1
      L=L+NY(J-1)
      P=P+NY(J)
      GOTO 006
      ELSE
      ENDIF
C-----Equation for the mobile phase of other sections
      IF(NN.GT.NP)THEN
      F(NN)=DUM1*(Y(NN-NP)-Y(NN))-FFR
C-----Equation for the mobile phase of the first section
      ELSE
      F(NN)=DUM1*(CC0-Y(NN))-FFR
      ENDIF
C-----Checking subroutine performance

      TM=TM/60

      PRINT*, 'CC0,TM,Y(N)',CC0,TM,Y(N)

      IF(II.LT.NX)THEN
      II=II+1
      NN=II*NP
      L=(II-1)*NP+1
      P=L+NY(1)-1
      GOTO 005
      ELSE

      RETURN
      ENDIF
      END
C============== END OF SOLUTION SUBROUTINE  FCN ==================C
C                                                                  C
C============== OUTPUT SUBROUTINE 'OUTPUT' ======================C

      SUBROUTINE OUTPUT(X,Y)

      INTEGER M,N
      INTEGER I,NY(32)
      PARAMETER (M=1200,N=580)

      DOUBLE PRECISION X,Y(N),H,XEND
      DOUBLE PRECISION B,DIF,CKD,E,R,QM,CO,RS,DUM1
      DOUBLE PRECISION RDIL(32),FDIL(32),DZ(32),DUM5,G
     1 ,DZSQ(32),DUM2(32),DUM4(32),SH(32),RLRS(32)

      INTRINSIC REAL
```

```
      COMMON XEND,H,I
      COMMON/CONSTANTS/DIF,QM,CKD,E,R,B,CO,ID,RS,N,NP,NX,DUM1,DUM5,G
      COMMON/DISTRIBUTION/RDIL
      COMMON/DISTRI/FDIL
      COMMON/DDZZ/DZ
      COMMON/DZSQZ/DZSQ
      COMMON/DUM/DUM4
      COMMON/NYY/NY
      COMMON/CK/DUM2
      COMMON/SHI/SH
      COMMON/RLRS/RLRS
C-----Writing intermediate solutions at desired point
      WRITE(7,008) X,Y(N)
C-----Next point at which 'output' is to be called
      X=XEND-REAL(I)*H
      I=I-1

      RETURN
008   FORMAT(3X,F10.3,2X,F8.4)
      END
C============== END OF OUTPUT SUBROUTINE 'OUTPUT' ==============C
C                                                                C
C============================== END ==============================C
```

APPENDIX B3

```
C======================= CHUKA6B.FOR ============================C
C                                                                  C
C==================================================================C
C=== THIS PROGRAM USES THE NAG SUBROUTINE DO2EJF TO SOLVE SYSTEM ===C
C=== OF ORDINARY DIFFERENTIAL EQUATIONS FOR PACKED BED DESORPTION. ==C
C===      THE MODEL ACCOUNTS FOR POLYDISPERSITY IN PARTICLE SIZE.  ===C
C====== THE EQUATIONS ARE STIFF. THE PARTICLES ARE CYLINDRICAL.  =====C
C==================================================================C
C                          Contents: - Main Program                C
C                          - Solution Subroutine FCN               C
C                          - Output Subroutine 'OUTPUT'            C
C ============================== ================================C
C                                                                  C
C======================= MAIN PROGRAM ============================C
C====================== Defining all Variables ====================C

      OPTIONS (CHECK)

      INTEGER M,N,IW
      INTEGER K,ID,NY(32)
      INTEGER I,IFAIL,J

      PARAMETER (M=1200)
      PARAMETER (IW=(24+2*M)*2*M+100)

      DOUBLE PRECISION H,XEND,D0,ff
      DOUBLE PRECISION TOL,X,TM
      DOUBLE PRECISION W(IW),Y(M)
      DOUBLE PRECISION CO,DIF,QM,CKD,E,R,RS,B,DR,G
     1 ,CKF(32),SH(32),DZ(32),DZSQ(32),DUM1,DUM2(32)
     2 ,DUM4(32),DUM5,RDIS(32),FDIL(32),RDISV(32),RSRV(32),RSV(32)

      EXTERNAL D02EJW
      EXTERNAL D02EJF,D02EJY,FCN,OUTPUT
      INTRINSIC REAL,INT

C===     Setting up memory locations      ======================C

      COMMON XEND,H,K
      COMMON/CONSTANTS/DIF,QM,CKD,E,R,B,CO,ID,RS,N,NP,NX,DUM1,DUM5,G
```

```
      COMMON/DISTRIBUTION/RDIS
      COMMON/DISTRI/FDIL
      COMMON/DDZZ/DZ
      COMMON/DZSQZ/DZSQ
      COMMON/DUM/DUM4
      COMMON/NYY/NY
      COMMON/CK/DUM2
      COMMON/SHI/SH
      COMMON/RSRV/RSRV

      CHARACTER*13 FNAME1
      CHARACTER*13 FNAME2
      CHARACTER*13 FNAME3
      OPEN(UNIT=4,FILE='PBCBX40I.DAT',STATUS='OLD')
      READ(4,001) FNAME1,FNAME2,FNAME3
001   FORMAT(A13)
      OPEN(UNIT=5,FILE=FNAME1,STATUS='OLD')
      OPEN(UNIT=6,FILE=FNAME2,STATUS='OLD')
      OPEN(UNIT=7,FILE=FNAME3,STATUS='NEW')

      READ(5,*) DIF,D0,XEND,K,CO,QM,CKD,E,EB,R,CLN,US,NX
     1 ,TOL,RS,G,DR,ff
      READ(6,*) ID,(RDIS(I),I=1,ID),(RDISV(I),I=1,ID)
     1 ,(FDIL(I),I=1,ID)

C===    Calculating all particle size related parameters      ==C

      B=QM*CKD*(1-E)/E
      U=US/EB
      DH=1/REAL(NX)
      DUM1=U*R*R/(CLN*DIF*DH)
      DUM5=R*R/DIF
      NP=0

      DO 002 I=1,ID
      RDIS(I)=RDIS(I)/2.0
      RDISV(I)=RDISV(I)/2.0
      RSRV(I)=(RDISV(I)/RDIS(I))**2
      RSV(I)=RDISV(I)**3/RDIS(I)**2
      CKF(I)=ff*0.5*D0*(2.0+RS*(US*RSV(I)*2.0)**0.5/D0**0.333)/RSV(I)
      SH(I)=(1.0*CKF(I))*R/(DIF*E)
      NY(I)=2+INT(RDIS(I)/DR)
      IF (RDIS(I).LT.10E-6) THEN
      NY(I)=5
      ELSE
      ENDIF
      DZ(I)=RDIS(I)/R/REAL(NY(I)-1)
      DZSQ(I)=DZ(I)*DZ(I)
      DUM2(I)=2.0*E*SH(I)*FDIL(I)*(1-EB)/EB
      DUM4(I)=2.0*SH(I)*DZ(I)
      NP=NP+NY(I)
```

```
002  CONTINUE

     NP=NP+1
     N=NP*NX

C===     Setting all initial conditions     ====================C

     X=0.0E0
     DO 003 J=1,N
     Y(J)=0.962
003  CONTINUE

     H=(XEND-X)/REAL(K+1)
C-----Tolerance limit
     IFAIL=-1

C===     Calling NAG routine D02EJF     ========================C

     GOTO 004

     CALL D02EJF(X,XEND,N,Y,FCN,D02EJY,TOL,'R',OUTPUT,D02EJW,W,
    1 IW,IFAIL)

004  CONTINUE

     FLRT=US*1000.0
     TM=X*DUM5/60
     ECV=TM*FLRT/0.83
C-----Checking main program performance
     PRINT*, 'IFAIL,TOL,IW',IFAIL,TOL,IW
     PRINT*, 'R',R
     PRINT*, 'FLRT',FLRT
     PRINT*, 'DIF',DIF
     PRINT*, 'N',N
     PRINT*, 'H',H
     PRINT*, 'NP',NP
     PRINT*, 'CO',CO
     PRINT*, 'CKF(1,2)',(CKF(I),I=1,2)
     PRINT*, 'CKF(3,4)',(CKF(I),I=3,4)
     PRINT*, 'SH(1,2)',(SH(I),I=1,2)
     PRINT*, 'SH(3,4)',(SH(I),I=3,4)
     PRINT*, 'X',X
     PRINT*, 'TM',TM
     PRINT*, 'ECV',ECV
     PRINT*, 'Y(N)',Y(N)

     STOP
     END
C============== END OF MAIN PROGRAM ============================C
C                                                               C
C                                                               C
```

```
C============== SOLUTION SUBROUTINE FCN ======================C

      SUBROUTINE FCN(X,Y,F)

      INTEGER M,N,P,I,J,ID,NY(32)
      PARAMETER (M=1200)

      DOUBLE PRECISION B,DIF,CKD,E,QM,CO,R,DUM1,DUM5,G
      DOUBLE PRECISION F(M),Y(M),DUM3,DUM8,RS,Q,S,X
      DOUBLE PRECISION RDIS(32),FDIL(32),DZ(32)
     1 ,DZSQ(32),DUM2(32),DUM4(32),SH(32),RSRV(32)

      COMMON/CONSTANTS/DIF,QM,CKD,E,R,B,CO,ID,RS,N,NP,NX,DUM1,DUM5,G
      COMMON/DISTRIBUTION/RDIS
      COMMON/DISTRI/FDIL
      COMMON/DDZZ/DZ
      COMMON/DZSQZ/DZSQ
      COMMON/DUM/DUM4
      COMMON/NYY/NY
      COMMON/CK/DUM2
      COMMON/SHI/SH
      COMMON/RSRV/RSRV

      Q(S)=(CO**2)*((CKD/CO+S)**2)/((CO**2)*(CKD/CO+S)**2+B)
C-----Allowing for delay and mixing effect
      TM=X*DUM5
      CC0=EXP(-G*TM)
      CC0=0.0
C-----Setting up counters
      L=1
      II=1
      P=NY(1)
      NN=NP
005   J=1

      FFR=0.0

C===     Ordinary differential equations to be solved      ======C
C-----Equation for interior nodes of particles
006   DO 007 I=L+1,P-1

      DUM3=I-L
      DUM6=(DUM3+0.5)/DUM3
      DUM7=(DUM3-0.5)/DUM3
      F(I)=Q(Y(I))*(DUM6*Y(I+1)-2.0*Y(I)+DUM7
     1 *Y(I-1))/DZSQ(J)/RSRV(J)

007   CONTINUE
C-----Equation for centre of particles
      F(L)=4.0*Q(Y(L))*(Y(L+1)-Y(L))/DZSQ(J)/RSRV(J)
```

```
C-----Equation for surface of particles
      DUM3=(P-L)
      DUM8=(DUM3+0.5)/DUM3
      F(P)=Q(Y(P))*(DUM4(J)*DUM8*Y(NN)
     1 +(-2.0-DUM4(J)*DUM8)*Y(P)+2.0*Y(P-1))/DZSQ(J)/RSRV(J)

      FFR=FFR+DUM2(J)*(Y(NN)-Y(P))

      IF(P.LT.NN-1)THEN
      J=J+1
      L=L+NY(J-1)
      P=P+NY(J)
      GOTO 006
      ELSE
      ENDIF
C-----Equation for the mobile phase of other sections
      IF(NN.GT.NP)THEN
      F(NN)=DUM1*(Y(NN-NP)-Y(NN))-FFR
C-----Equation for the mobile phase of the first section
      ELSE
      F(NN)=DUM1*(CC0-Y(NN))-FFR
      ENDIF
C-----Checking subroutine performance
      PRINT*, 'CC0,X,Y(N)',CC0,X,Y(N)

      IF(II.LT.NX)THEN
      II=II+1
      NN=II*NP
      L=(II-1)*NP+1
      P=L+NY(1)-1
      GOTO 005
      ELSE

      RETURN
      ENDIF
      END
C============== END OF SOLUTION SUBROUTINE  FCN ================C
C                                                               C
C============== OUTPUT SUBROUTINE 'OUTPUT' ====================C

      SUBROUTINE OUTPUT(X,Y)

      INTEGER M,N
      INTEGER I,NY(32)
      PARAMETER (M=1200,N=1140)

      DOUBLE PRECISION X,Y(N),H,XEND
      DOUBLE PRECISION B,DIF,CKD,E,R,QM,CO,RS,DUM1
      DOUBLE PRECISION RDIS(32),FDIL(32),DZ(32),DUM5,G
     1 ,DZSQ(32),DUM2(32),DUM4(32),SH(32),RSRV(32)
```

```
      INTRINSIC REAL

      COMMON XEND,H,I
      COMMON/CONSTANTS/DIF,QM,CKD,E,R,B,CO,ID,RS,N,NP,NX,DUM1,DUM5,G
      COMMON/DISTRIBUTION/RDIS
      COMMON/DISTRI/FDIL
      COMMON/DDZZ/DZ
      COMMON/DZSQZ/DZSQ
      COMMON/DUM/DUM4
      COMMON/NYY/NY
      COMMON/CK/DUM2
      COMMON/SHI/SH
      COMMON/RSRV/RSRV
C-----Writing intermediate solutions at desired point
      WRITE(7,008) X,Y(N)
C-----Next point at which 'output' is to be called
      X=XEND-REAL(I)*H
      I=I-1

      RETURN
008   FORMAT(3X,F10.3,2X,F8.4)
      END
C============== END OF OUTPUT SUBROUTINE 'OUTPUT' ==============C
C                                                               C
C============================== END ============================C
```

APPENDIX B4

C/PEI 40			C/PEI 15		
Dimensionless Time X	Real time Minutes (min)	Concentration C/C_o (g/l)	Dimensionless Time X	Real time Minutes (min)	Concentration C/C_o (g/l)
0	0	1	0	0	1
0.52	1.56	0.91	0.51	0.95	0.92
1.05	3.13	0.88	1.02	1.91	0.89
1.58	4.70	0.86	1.52	2.86	0.87
2.11	6.27	0.84	2.03	3.82	0.86
2.64	7.84	0.83	2.54	4.77	0.85
3.17	9.41	0.82	3.05	5.73	0.84
3.70	10.98	0.81	3.56	6.69	0.83
4.23	12.54	0.80	4.07	7.64	0.82
4.76	14.11	0.79	4.58	8.60	0.81
5.29	15.68	0.78	5.09	9.55	0.81
5.82	17.25	0.78	5.60	10.51	0.80
6.35	18.82	0.77	6.11	11.47	0.80
6.88	20.39	0.77	6.62	12.42	0.79
7.41	21.96	0.76	7.13	13.38	0.79
7.94	23.52	0.76	7.64	14.33	0.79
8.47	25.09	0.76	8.15	15.29	0.78
9	26.66	0.75	8.66	16.25	0.78
9.52	28.23	0.75	9.17	17.20	0.78
10.05	29.80	0.75	9.68	18.16	0.77
10.58	31.37	0.75	10.16	19.11	0.77
11.11	32.94	0.74	10.76	20.07	0.77
11.64	34.50	0.74	11.26	21.03	0.77
12.17	36.07	0.74	11.72	21.98	0.76
12.70	37.64	0.74	12.23	22.94	0.76
13.23	39.21	0.74	12.74	23.89	0.76
13.76	40.78	0.74	13.25	24.85	0.76
14.29	42.35	0.73	13.76	25.80	0.76
14.82	43.92	0.73	14.27	26.76	0.76
15.35	45.49	0.73	14.78	27.72	0.76
15.88	47.05	0.73	15.29	28.67	0.75
16.41	48.62	0.73	15.80	29.63	0.75
16.94	50.19	0.73	16.31	30.58	0.75
17.47	51.76	0.73	16.82	31.54	0.75
18	53.33	0.73	17.33	32.49	0.75
18.52	54.90	0.73	17.84	33.45	0.75
19.05	56.47	0.73	18.35	34.41	0.75
19.58	58.03	0.73	18.86	35.36	0.75
20.11	59.60	0.73	19.37	36.32	0.75
20.64	61.17	0.73	19.88	37.27	0.75
21.17	62.74	0.73	20.39	38.23	0.75
21.70	64.31	0.73	20.90	39.19	0.75
22.23	65.88	0.73	21.41	40.14	0.75
22.76	67.45	0.73	21.92	41.10	0.75
23.29	69.01	0.73	22.43	42.05	0.75
23.82	70.58	0.73	22.94	43.01	0.75
24.35	72.15	0.73	23.45	43.97	0.75
24.88	73.72	0.73	23.96	44.92	0.75
25.41	75.29	0.73	24.47	45.88	0.75
25.94	76.86	0.73	24.98	46.83	0.75
26.47	78.43	0.73	25.49	47.79	0.75
27	80	0.73	26	48.75	0.75

TABLE B4-1: *Values of changing Bovine Serum Albumin (BSA) concentration with time obtained from the program of equations for two particle radii C/PEI 40 and C/PEI 15.*

C/HIC 40			C/HIC 15		
Dimensionless Time X	Real Time Minutes (min)	Concentration C/C_o (g/l)	Dimensionless Time X	Real Time Minutes (min)	Concentration C/C_o (g/l)
0	0	1	0	0	1
0.45	0.73	0.88	0.68	0.42	0.85
0.90	1.47	0.84	1.37	0.84	0.80
1.35	2.21	0.81	2.05	1.26	0.77
1.80	2.95	0.79	2.74	1.68	0.74
2.25	3.68	0.77	3.43	2.10	0.72
2.70	4.42	0.75	4.11	2.52	0.70
3.15	5.16	0.74	4.80	2.94	0.68
3.60	5.90	0.72	5.49	3.36	0.67
4.05	6.64	0.71	6.17	3.78	0.65
4.51	7.37	0.70	6.86	4.20	0.64
4.96	8.11	0.69	7.54	4.62	0.63
5.41	8.85	0.68	8.23	5.04	0.62
5.86	9.59	0.68	8.92	5.46	0.61
6.31	10.32	0.67	9.60	5.88	0.61
6.76	11.06	0.66	10.29	6.30	0.60
7.21	11.80	0.65	10.98	6.72	0.59
7.66	12.54	0.65	11.66	7.14	0.58
8.11	13.28	0.64	12.35	7.56	0.58
8.56	14.01	0.64	13.03	7.98	0.57
9.02	14.75	0.63	13.72	8.40	0.57
9.47	15.49	0.63	14.41	8.83	0.56
9.92	16.23	0.62	15.09	9.25	0.56
10.37	16.97	0.62	15.78	9.67	0.55
10.82	17.70	0.62	16.47	10.09	0.55
11.27	18.44	0.61	17.15	10.51	0.55
11.72	19.18	0.61	17.84	10.93	0.54
12.17	19.91	0.60	18.52	11.35	0.54
12.62	20.65	0.60	19.21	11.77	0.54
13.07	21.39	0.60	19.90	12.19	0.53
13.52	22.13	0.59	20.58	12.61	0.53
13.98	22.87	0.59	21.27	13.03	0.53
14.43	23.60	0.59	21.96	13.45	0.53
14.88	24.34	0.59	22.64	13.87	0.52
15.33	25.08	0.58	23.33	14.29	0.52
15.78	25.82	0.58	24.02	14.71	0.52
16.23	26.56	0.58	24.70	15.13	0.52
16.68	27.29	0.58	25.39	15.55	0.52
17.13	28.03	0.58	26.07	15.97	0.52
17.58	28.77	0.57	26.76	16.40	0.51
18.03	29.51	0.57	27.45	16.82	0.51
18.49	30.24	0.57	28.13	17.24	0.51
18.94	30.98	0.57	28.82	17.66	0.51
19.39	31.72	0.57	29.51	18.08	0.51
19.84	32.46	0.57	30.19	18.50	0.51
20.29	33.20	0.57	30.88	18.92	0.51
20.74	33.93	0.56	31.56	19.34	0.51
21.19	34.67	0.56	32.25	19.76	0.51
21.64	35.41	0.56	32.94	20.18	0.51
22.09	36.15	0.56	33.62	20.60	0.51
22.54	36.88	0.56	34.31	21.02	0.51
23	37.62	0.56	35	21.44	0.51

TABLE B4-2: *Values of changing BSA concentration with time obtained from the program of equations for two particle radii C/HIC 40 and C/HIC 15.*

Sample: 000-018 Cellulose
Operator: rm
Submitter: Swansea
File Name: C:\DEMO3000\DATA\000-018.SMP

Started: 10/8/2001 11:16:30AM Analysis Adsorptive: N2
Completed: 10/8/2001 3:48:15PM Analysis Bath: 77.35 K
Report Time: 10/8/2001 5:06:32PM Sample Weight: 0.6140 g
Warm Freespace: 6.5799 cm^3 MEASURED Cold Freespace: 20.2645 cm^3
Equil. Interval: 15 secs Low Pressure Dose: None
Sample Density: 1.000 g/cm^3 Automatic Degas: No

Summary Report

Area

Single Point Surface Area at P/Po 0.17971225 :	0.3156	m^2/g
BET Surface Area:	0.3979	m^2/g
BJH Adsorption Cumulative Surface Area of pores between 1.700000 and 300.000000 nm Diameter:	0.4289	m^2/g
BJH Desorption Cumulative Surface Area of pores between 1.700000 and 300.000000 nm Diameter:	0.4591	m^2/g

Volume

Single Point Adsorption Total Pore Volume of pores less than 148.6052 nm Diameter at P/Po 0.98680588:	0.000788	cm^3/g
BJH Adsorption Cumulative Pore Volume of pores between 1.700000 and 300.000000 nm Diameter:	0.001066	cm^3/g
BJH Desorption Cumulative Pore Volume of pores between 1.700000 and 300.000000 nm Diameter:	0.001065	cm^3/g

Pore Size

Adsorption Average Pore Diameter (4V/A by BET):	7.9180	nm
BJH Adsorption Average Pore Diameter (4V/A):	9.9385	nm
BJH Desorption Average Pore Diameter (4V/A):	9.2760	nm